Growth, Characterisation and Electronic Applications of Amorphous Hydrogenated Carbon

Shashi Paul

November 2000

A thesis
submitted for the degree of Doctor of Philosophy
at the De Montfort Univeristy

Dedication

A violet by a mossy stone
Half hidden from the eye!
--Fair as a star, when only one
Is shining in the sky.

From "She Dwelt Among Untrodden Ways"
by William Wordsworth

To my wife and best friend, Dalia.

Declaration

I declare that no part of this thesis has been accepted, or is currently being submitted, for any degree or diploma or certificate or any other qualification in this University or elsewhere.

This thesis is the result of my own work unless otherwise stated.

Acknowledgements

I would like to express my deepest gratitude to my research supervisor, Dr. Frank Clough, for his guidance, support and constant encouragement. I am also indebted to him for proofreading the draft of my thesis. His suggestions and criticisms were most helpful.

My heartfelt thanks are due to my wife Dalia, for reviewing my thesis and for proofreading the draft. I express my thanks to her, for academic as well as emotional support.

I am thankful to Prof. W.I. Milne, Dr. J. Robertson and Prof. G.A.J. Amaratunga of Cambridge University for their valuable comments and also to my Cambridge colleague Dr. M. Chhowalla for some insightful discussions.

I would like to thank Dr S.C Deane, Dr R.B Wehrspohn and Dr M.J Powell of Philips Research Laboratory, Redhill, Surrey, UK, for insightful discussions during their visit to DMU. Their comments and criticisms helped my research significantly.

I would like to acknowledge the help of A. Zimmerman, I. Hayward and I. Wilcock of Renishaw plc for allowing me to use their Raman Spectroscope, the data from which has been presented in my thesis.

I gratefully acknowledge the help and co-operation of Mr.P.J. Taylor of the Emerging Tech. Res. Centre in De Montford University (DMU), Leicester, for setting up various instruments for my work. Without his help, much of my doctoral work would not have been possible. I also thank Prof. S. N. E Madathil and Dr. M.M De Souza for allowing me to use electrical meters.

I am very grateful to the Electrical Engineering Department of DMU for awarding me the bursary that made my stay and work in DMU possible.

ABSTRACT

Growth, Characterisation and Electronic Applications of Amorphous Hydrogenated Carbon

Shashi Paul
De Montfort University
November, 2000.

My thesis proposes solutions to a number of riddles associated with the material, hydrogenated amorphous carbon, (a-C:H). This material has lately generated interest in the electronic engineering community, owing to some remarkable properties. The characterisation of amorphous carbon films, grown by radio frequency plasma enhanced chemical vapour deposition has been reported. The coexistence of multiple phases in the same a-C:H film manifests itself in the inconsistent electrical behaviour of different parts of the film, thus rendering it difficult to predict the nature of films. For the first time, in this thesis, a reliable prediction of Schottky contact formation on a-C:H films is reported. A novel and simple development on a Scanning Electron Microscope, configured to study the electrical properties of the grown a-C:H films, has been reported. Since device performance is crucially linked to the density of states in the film, a study of the same was undertaken in my doctoral research. I present a mathematical formalism to estimate the density of states in a-C:H. The most commonly used metal, (aluminium), for contact formation on a-C:H films, has been concluded to be the least suitable. On the basis of the study presented in this thesis, copper and chromium are judged to be the best alternatives. The resilience of a-C:H/Si heterostructures under high voltages (upto 900 V) has been reported in this thesis for the first time. The performance of a-C:H grown at room temperature on GaAs, has been studied and concluded to be satisfactory on the basis of good adherence and low leakage currents. Such a structure was motivated by the applicability in Metal Insulator Semiconductor Field Effect Transistors, (MISFET).

TABLE OF CONTENTS

CHAPTER 0

Overview of Thesis

My Ph.D. research involved the study of diamond like carbon (DLC); a material with extremely interesting properties though not particularly well understood. These unique mechanical, optical, chemical and electrical properties of diamond-like carbon) have generated intense interest over recent the years and inspired me to undertake an invesitgation of the growth, characterisation and study of DLC films.

There were no prior investigations of the growth of amorphous hydrogenated carbon (a-C:H) in the Emerging Technologies Research Centre at De Montfort University in Leicester. Therefore my first goal was to produce device quality a-C:H films and achieve uniform and reproducible properties over a large substrate area by the technique of radio frequency plasma-enhanced chemical vapour deposition (rf-PECVD). These goals motivated us to develop an elegant and simple way, which could be utilised to optimise film properties for implementation in large area electronics. This method takes into account, the thickness, refractive index and resistivity of the grown films. We had to assure ourselves about the high quality of the films before proceeding to perform analyses of the same. These films were investigated using FTIR, SEM, micro-Raman analysis, ellipsometry, UV spectroscopy, *I-V* and *C-V* techniques. DLC films were grown from the gas mixture of CH_4/Ar. The effect of DC

self-bias voltages on the film properties of DLC films is investigated extensively during my research.

DC self-bias was concluded to be a key parameter that influences various properties of the films. This is in line with work already published.

0.1 Some Important outcomes of my thesis

Diamond-like carbon presented quite a few challenges when I started my graduate study, namley, the formation of schottky contacts, a proper understanding of the density of states, interaction with metals that are employed to form contacts with amorphous carbon films, uniformity of the film properties over large substrate areas, etc. These issues needed to be addressed before we could embark upon the task of utilising DLC as an electronic grade material. Not much is published on the density of states in a-C:H. But density of states is a key parameter that influences the realisation of any device out of amorphous carbon. It is a generally held belief that the formation of a Schottky contact on DLC is not possible. However, there is no work published on the subject of behaviour of metallic contacts formed on amorphous carbon. In my Ph.D research we attempted to understand such issues and tried to resolve them.

It was believed that Schottky contacts are not possible on diamond-like carbon due to a conducting superficial layer on the DLC. We investigated this problem thoroughly and *realised that (for the first time) Schottky contacts are possible to a-C:H when the contact area is less than 1 μm* [1]. To improve the predictability of the Schottky contacts, we

deposited DLC on metal strips and found that there is a pronounced probability of forming contacts near the edge of the metal strip [2].

One of the most important by-products of my doctoral thesis is a mathematical formulation that we developed, to estimate the density of states in a-C:H. The methodology is simple and easily calculable. When I started my research, the density of states in a-C:H films was poorly understood. Various methods had been employed by other workers to deduce the density of states. Our investigations show that capacitance measurements on MIS structure is an appropriate way to deduce the density of states. In this regard, we have developed an analytical formalism, which agrees well the experimental data [3].

Diamond-like carbon can be deposited by rf-PECVD at room temperature. Therefore, metal-semiconductor-metal (MSM)switches can be fabricated at room temperature on inexpensive plastic substrates. We have extensively investigated the properties of MSM devices by *I-V* and *C-V-f* measurement. Our *I-V* investigation revealed that the conduction mechanism in our DLC films is of Poole-Frenkel type [4].

The reliability of metal contacts to a-C:H is important. In view of this, we have investigated the behaviour of various contact metals with a-C:H. This investigation shows *that Al is not a good metal to use, to make contacts on a-C:H films, while Cu and Cr are quite stable as a metal contact to a-C:H* [5]. This investigation shows the importance of the selection of the metal that is to be used to form contacts to a-C:H. This investigation was carried out for the first time on a-C:H films.

Diamond-like carbon films have high breakdown strength. We have exploited this property to use a-C:H to manufacture high breakdown diodes. We have manufactured a-C:H/Si diodes which can withstand upto ~900 V, for the first time [6,7].

A-C:H is a low-k material and therefore can be used as an interlayer dielectric material. We have thoroughly investigated the use of a-C:H in order to justify its use as a low-k material [8,9].

We have also developed a technique which can be used to investigate (using the combination of a micro tip and a scanning electron microscope) the in-homogeneity in the material [8].

We have also found that quartz is the best substrate for deposition of a-C:H, to collect IR spectrum in the wavenumber range of 2400 cm^{-1} and 3500 cm^{-1} [10].

0.1 Organisation of my thesis

Chapter 1 introduces the different allotropic forms of carbon.

Chapter 2 deals with various characterisation techniques used in investigating the amorphous hydrogenated carbon deposited in our lab.

A detailed introduction to amorphous hydrogenated carbon and the comparison with other allotropes of carbon is presented in Chapter 3. This chapter also covers issues such as plasma enhanced chemical processes and achievement of the optimum growth conditions.

In PECVD systems, the DC self-bias voltage is the key parameter in determining film properties. Chapter 4 examines the effect of DC-self bias on bandgap, resistivity, refractive index, hydrogen concentration of the film, defects in the films and other structural information.

The information on the DOS will help to determine the behaviour of devices based on a-C:H. Chapter 5 examines the various structures suitable for determining density of states and the relevant development of the theory to find DOS from such structures.

A new experimental method to make submicron metal contacts on any material using SEM and sub-micron metal tips has also been successfully developed for the first time. This novel instrument was used to investigate the variation of the electrical properties of DLC in the submicron regions. Detailed instrumentation will be discussed in Chapter 6.

In Chapter 7, electrical properties of MSM devices are examined. In addition, the formation of Schottky diodes and reliability tests for MSM devices for different metal contacts have also been discussed in the chapter.

Amorphous hydrogenated carbon can be deposited at room temperature and depending upon the growth conditions it can have high resistivity (in insulator range) and very low dielectric constant. These properties of a-C:H encouraged workers to use it for the inter-layer low-k dielectric material for VLSI/ULSI. Chapter 8 examines the use of a-C:H as a low-k material [11].

Deposition of gate insulator in the arsenic based compound semiconductors (such as GaAs, AlGaAs), always causes stoichiometric changes in these materials. The deposition of any

material above 350° C results in the segregation of As at the surface of the semiconductor, which deteriorates the MISFET properties. A-C:H can be deposited at room temperature and hence the effect of temperature on arsenic segregation can be eliminated. Chapter 9 investigates the use a-C: H as a gate insulator in arsenic based compound semiconductors.

Chapter 10 examines the effect of DC self bias on the properties of a-C:H/Si heterostructures. The electrical characteristics of p-n junctions are fundamental to the electronics industry. Rectification, isolation, amplification and switching are key operations that involve the use of p-n junctions in electronic circuits. Therefore, fabrication of p-n junction diodes is an appropriate starting point in the development of a semiconductor technology based on amorphous carbon.

Chapter 11 is the conclusive chapter of my thesis; a summary of the results we have obtained is mentioned in it, along with suggestions for future work to understand DLC properties and to exploit this material in the electronics industry.

0.2 Work Published/Present

1. Schottky barrier formation on r.f-plasma enhanced chemical vapour deposited hydrogenated amorphous carbon, S. Paul and F.J Clough, *Diamond and Related Materials*, 1998, Vol .7, pp.1734-1738.
2. Schottky Contacts on Amorphous Carbon: a More Reliable Approach. S.Paul and F.J Clough, submitted to *Applied Physics Letters* (accepted).

3. Determination of Density of States in a-C:H from MIS structures, S.Paul and F.J Clough (submitted to Physical Review B),

4. Metal/diamond-like carbon/metal switches for active matrix flat panel displays - current status and optimisation, F.J. Clough, S. Paul, S. Egret, J. Robertson, and W.I. Milne, *Recent Research development in Applied Physics*, 1999, Vol.2, pp.163-176, (Invited).

5. Capacitance-time investigation of Metal/a-C:H/Si structure – a Reliability test of the metal contacts, S.Paul and F.J Clough, (submitted to *Microelectronic Reliability*).

6. High Reverse Breakdown a-C:H/Si Diodes Manufactured by rf-PECVD, S.Paul and F.J Clough, *Materials Research Society Proceeding*, 2000, Vol. 593, pp.427-432

7. Thickness Dependent Reverse Breakdown Voltage of a-C:H/Si diodes, S.Paul and F.J Clough, Submitted to *Electron Device Letters* (IEEE)

8. A novel technique to investigate the in-homogeneity in material- An arrangement of micro-tip and scanning electron microscope, S.Paul and F.J Clough, (to be submitted)

9. Substrate Sensitivity of the adhesion and material properties of r.f-PECVD amorphous carbon, S. Paul and F.J Clough, Materials *Research Society Proceeding* , 2000, Vol. 558, pp.149-154.

10. Selection of substrate for Infrared Investigation in diamond-like carbon, S.Paul and F.J Clough, (submitted to Thin Solid Films B).

11. Diamond-like Carbon a low –k material – Issues related to its deposition on metal strips, S.Paul and F.J Clough, (to be submitted to *J. Vac. Sci. and Tech. B*)

12. Effect of DC-Self bias on rectification factor of DLC/Si heterostructures grown by PECVD, S. Paul and F.J Clough (presented at the Chelsea Conference, March 29-30, 1999, held at Imperial College, London).

13. Schottky Barrier Formation in Amorphous Carbon Metal-Semiconductor-Metal Structures, S. Paul, F.J Clough, IOP Annual Congress on Diamond and Diamond Like Carbon Growth at Low Pressures :Fundamentals to Applications, 17 - 19 March, 1998, Brighton, UK.

CHAPTER 1

Carbon Allotropes and Diamond-like carbon

1. 1 Introduction

Our world occupies a unique niche in the Universe in regard to the ubiquitous display of life herein; the very essence of life being Carbon. Carbon is one of the most fascinating of all the elements that nature offers. It not only manifests itself as the raw material of all living things, but also surrounds us in terms of every-day paraphernalia. More interestingly, multiple forms or allotropes mark this omnipresence of carbon. Allotropes range from the mundane ash to the laboratory-manufactured bucky-balls and nano-tubes, [1,2,3]; these synthetically generated forms being recent development in the field of carbon science. While some allotropes are crystalline, others are amorphous. In general, there is an amazingly large range of structure and property across all the allotropes. For example, diamond is a high bandgap, semiconducting material while graphite has metal-like electrical properties. Thus it appears that the interesting question to address is the reason for this extreme versatility exhibited by carbon. The answer lies in the electronic structure of the carbon atom, with four electrons in the last shell and an atomic number of 6. This favours the carbon atom to form three kinds of hybridisations, namely, sp^3, sp^2 and sp^1. A comprehensive discussion of the details regarding these hybridised states will be found later in Chapter 3. The diametrically opposite properties of some of the different allotropes are explained on the basis of the differences in the hybridisation states and the crystal structures of these forms.

1. 2 Examples of some Allotropes of Carbon

Detailed discussions on the features of some allotropes of carbon are included in this section; these are, diamond, graphite, polycrystalline diamond and diamond-like carbon.

1.2.1 Diamond

Diamond is a pure form carbon. Diamond has high hardness and some very interesting optical properties, which result from the compact arrangement of the carbon atoms in its rigid, tightly bonded structure. *Fig.-1.1 shows the crystal structure of diamond. The* occurrence of diamond suggests that it forms in nature, under highly intemperate conditions, i.e. extremely high pressure and temperature (Fig.-1.2).

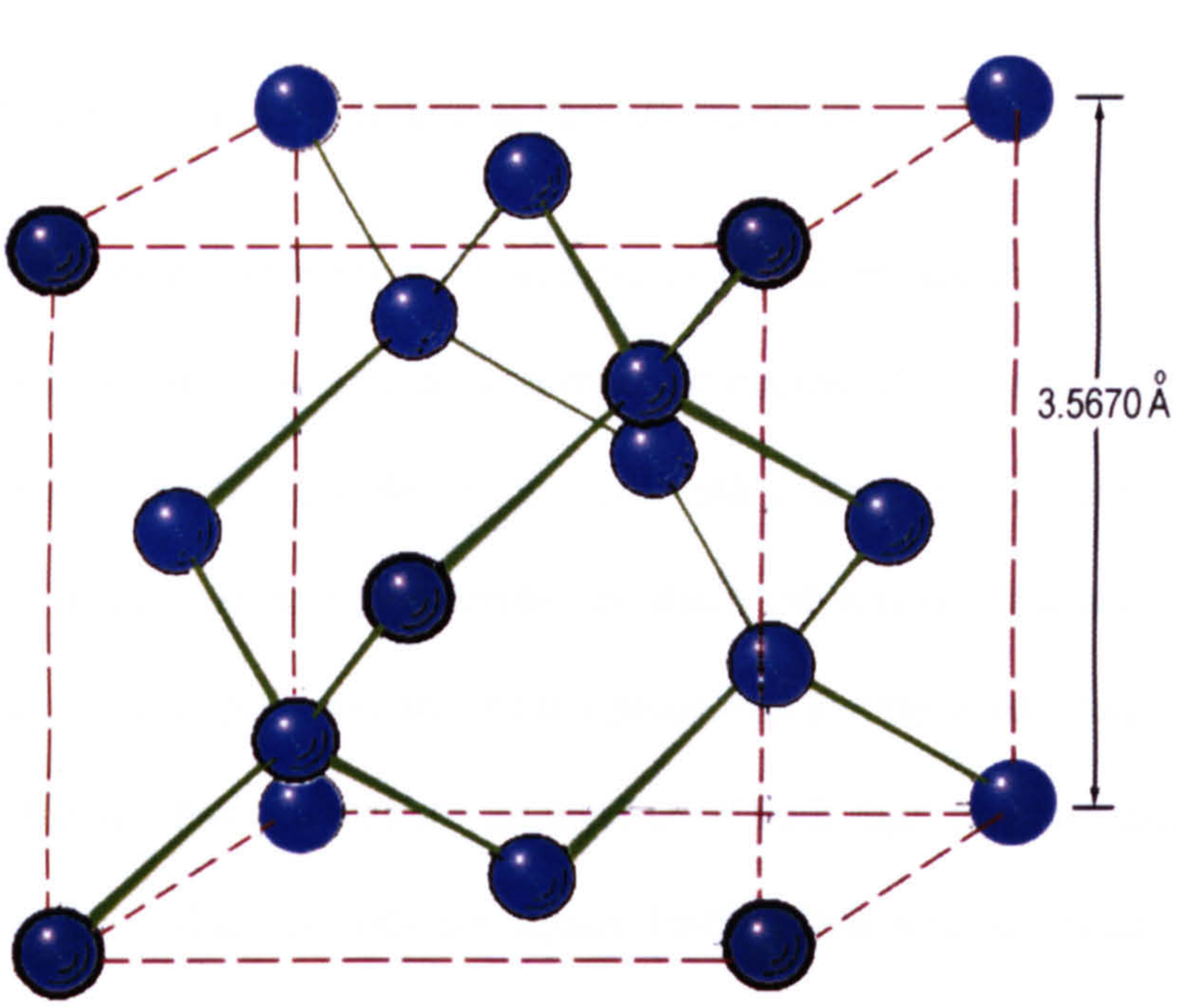

Fig.-1.1 Crystal structure of diamond

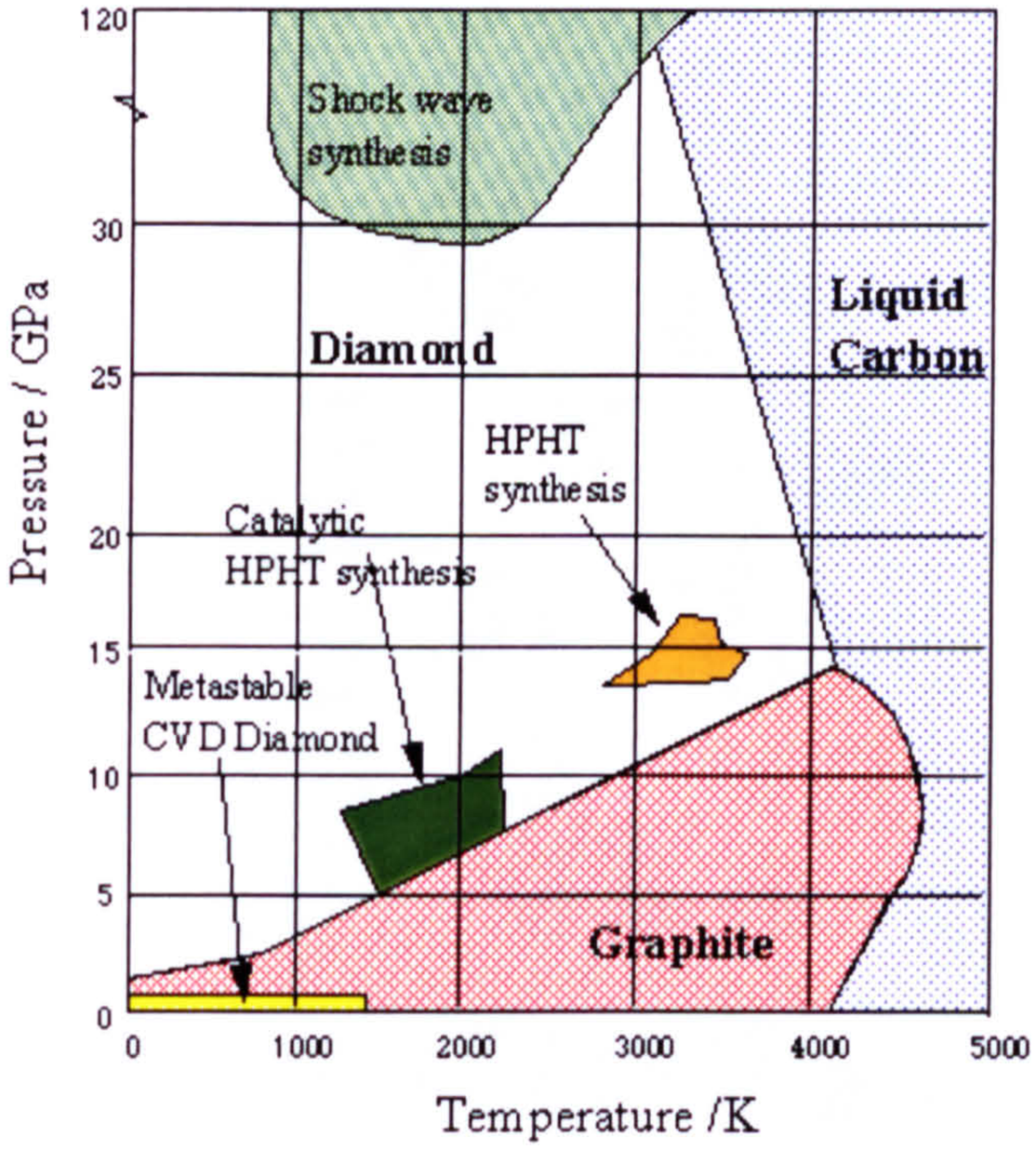

Fig.-1.2 Phase diagram for carbon at various pressures .

There were many attempts to synthesise diamond artificially, primarily by dissolving carbon in molten iron. Inspite of a number of claims of successful synthesis of artificial diamond around the last decade of the nineteenth century, none were considered credible. The race to mimic nature and manufacture diamond was to continue till 1955, when the General Electric Company announced the successful synthesis of diamond. The key to the success of the GE process was the attainment of both high pressure and high temperature (5000°F and 1.5 million pounds per square inch). This was achieved in special heat and pressure-resistant chambers (under1000 ton of press). However, this technique produces only small diamond crystals (Fig.-1.3).

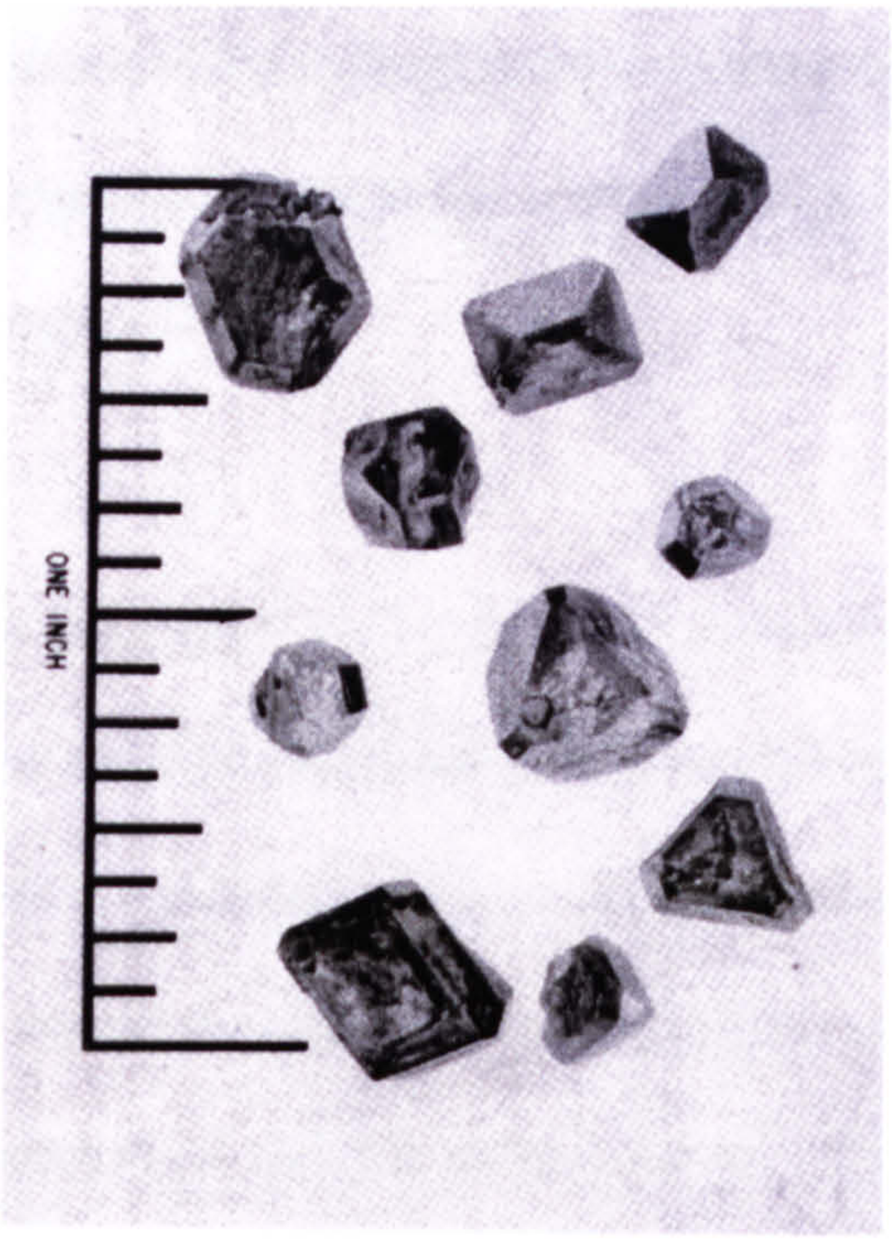

Fig.-1.3 Diamond crystal produced by General Electric company in 1955. The size of crystal is quite small.

The cost of manufacturing such gems is so high that the small crystal size renders the product incompetetive in the market in natural stones, at least for the present. However, the appeal of diamond certainly surpasses ornamentation. In fact, diamond has some very interesting properties, which render its industrial applicability high. Some such properties are high thermal conductivity, high badgap and the feature that devices made from diamond are very stable at high temperatures. The unique properties of diamond led many electronic industries to want to develop a way to achieve diamond in the form of thin films or even as large crystals. But most of the attempts were futile. A fruitful by-product of this curiosity to

grow a single crystal of diamond led to the discovery of many other forms of carbon which possess diamond-like properties; amorphous carbon, tetrahedral carbon, polycrystalline diamond being such examples [4,5,6].

1.2.2 Graphite

Graphite is an another allotropic form of carbon, which is commonly available in nature. Graphite has a crystalline structure composed of triagonally bonded sp^2 carbon atoms. Its structure is such that three σ-bonds are created in a planar direction, with the fourth electron forming a π-bond in the normal direction. The π-bond is very weak in nature, which results in overlapping of the conduction and the valence bands. This makes graphite a good conductor of electricity.

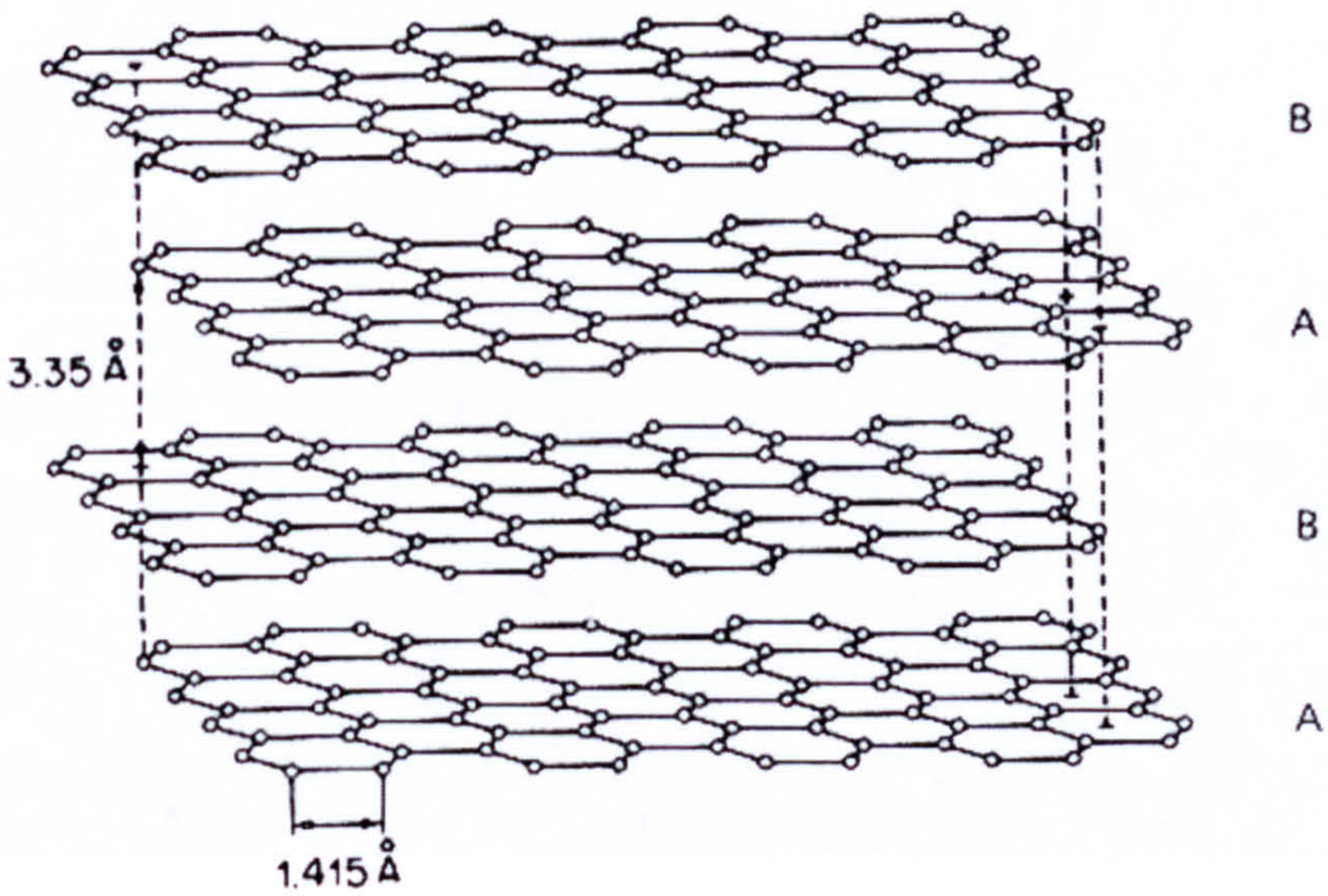

Fig.-1.4 Crystal structure of graphite.

1.2.3 Polycrystalline diamond

This material was an outcome of the efforts exerted to industrially manufacture single crystals of diamond. There are a number of techniques which are being used presently to grow polycrystalline diamond. These techniques include high temperature PECVD [6], laser ablation [7], rf induction thermal plasma [8], DC discharge assisted CVD [9], hot filament and combustion flame growth [10]. A mixture of hydrocarbon gases (CH_4, C_2H_2, C_6H_6) and hydrogen is used to grow polycrystalline diamond. A high quality of poly-crystalline diamond films can be obtained by pre-seeding the substrate with diamond powder or metal powder.

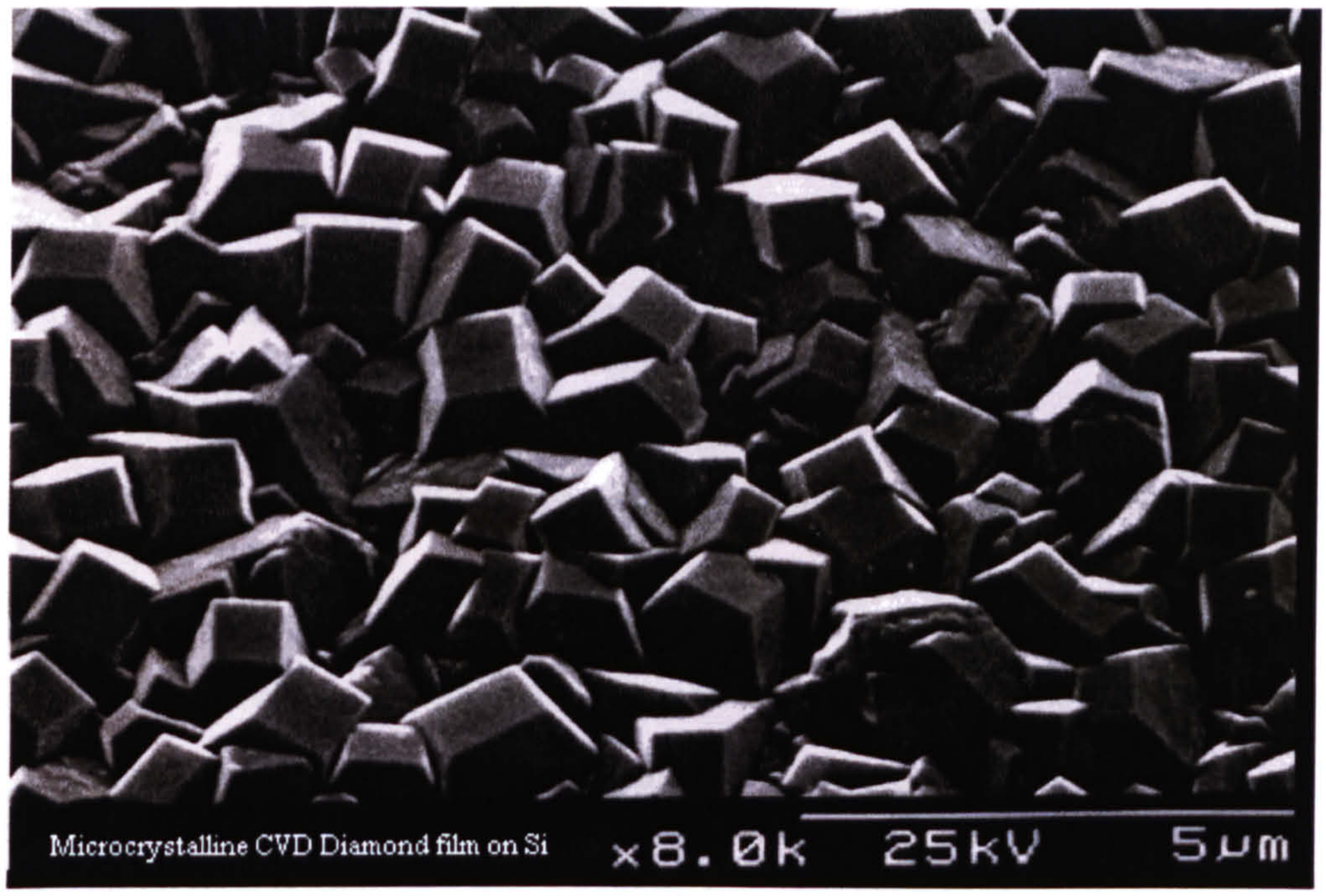

Fig.-1.5 Microcrystalline diamond film on Si substrate deposited by chemical vapour deposition.

The aforesaid techniques involve high temperature growth (700 -1200^{0}C) and this makes it difficult to integrate the films with other materials.

1.2.4 Diamond-like carbon

In recent years, there have been numerous developments in the field of diamond-like carbon [11,12,13,14]. The interest in diamond like carbon is encouraged by the properties of diamond. Diamond surpasses all other known materials as far as a number of physical properties are concerned, such as, the highest values of atomic density, bulk modulus, hardness, thermal conductivity, breakdown field and inertness to the environment. There are a number of names given to diamond-like carbon such as, tetrahedral carbon, amorphous carbon, fluorinated amorphous carbon, hydrogenated amorphous carbon and hydrogenated tetrahedral carbon. DLC films are amorphous in nature, but some nanocrystalline and nanocluster inclusions of different carbon forms have been reported in the amorphous matrix [15,16].

The higher the sp^3 constituent of the film, the more closely does the film resemble the properties of diamond. The fraction of the sp^3 phase in the film is mainly determined by the growth conditions and the techniques that one has used to deposit the film [17,18,19]. The amount of sp^3 bonding and hydrogen in any DLC film depends on the deposition process used and can be represented by a ternary phase diagram [17], (Fig.-1.6).

Amorphous hydrogenated carbon (a-C:H) is an interesting material to investigate. This is

due to its unique and beneficial properties. The material is hard, extremely chemically inert and electrically speaking, its resistivity can be varied from insulating to semiconducting [20,21,22]. Furthermore, its badgap can be adjusted for the desired application [21,22]. Thin a-C:H films are used as protective anti-reflection coatings [23] e.g. on glass plates in bar-code laser scanners and protective, wear and corrosion reducing coatings. Currently, investigations are also underway, on the possible utilisation of a-C:H in microelectronics [24,25,26] and lithography [27].

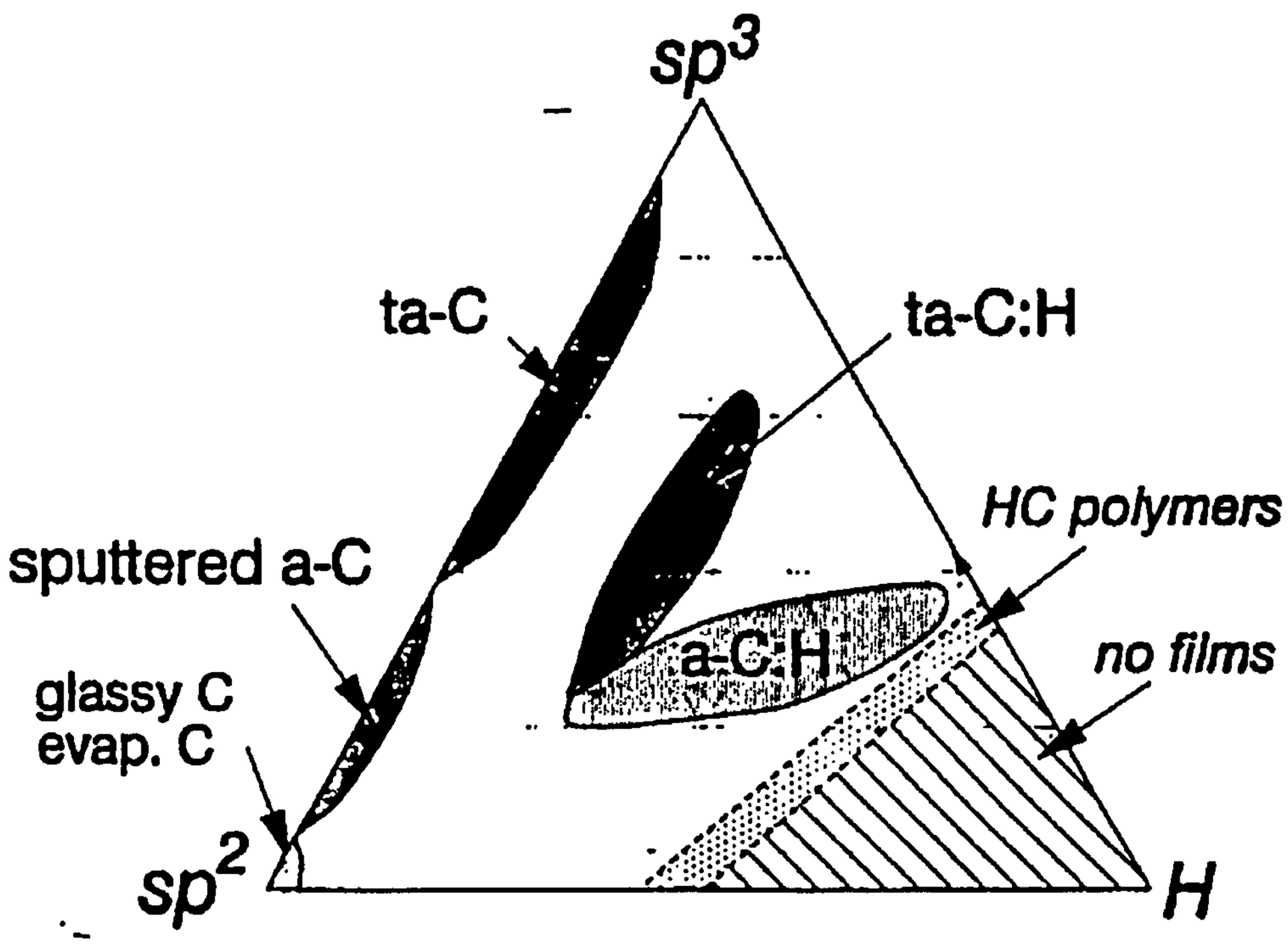

Fig.-1.6 A phase diagram of sp^3, sp^2 bonding and hydrogen contents of various forms of diamond like carbon [17].

Various techniques are used to deposit a-C:H film, one of which is Chemical Vapour Deposition (CVD). Examples of this technique are RF parallel plate plasma deposition

(RF-PECVD) [28] and Hot Wire deposition (HW-CVD) [29]. A general feature of the most common techniques is that the transport of the active particles towards a substrate is determined by diffusion. In the RF-PECVD technique the transport of particles towards the substrate is determined by direct transport.

Even though there is a lot of interest in developing diamond-like carbon for various electronic as well as mechanical applications, not all studies agree in the obtained results. In Silva et al [30], it is mentioned that to develop DLC for future applications, unification of the properties of DLC is important. Presently, the properties of diamond-like carbon vary from one laboratory to another. One reason for this inconsistency could be the precise fraction of the constituents, sp^2 and sp^3. The field of diamond-like carbon appeals strongly to the curious mind since there is still a plethora of puzzles to be unravelled.

References

1. J. Baggott, *New Scientist*, **131**, 34 (1991).

2. M.Chhowalla, R.A.Aharonov, C.JKiely, I.Alexandrou, and G.A.J.Amaratunga, *Philosophical Magazine Letters*, **75**, 329 (1997).

3. J.Hone, M.C.Laguno, N.M.Nemes, A.T. Johnson, J.E. Fischer, D.A. Walters, M.J. Casavant, J. Chmidt, R.E. Smalley, *Appl. Phys. Lett.*, **77**, 666 (2000)

4. S.Aisenverg and Chabot, *J.Appl. Phys.*, **42**, 2953 (1971).

5. D.R.McKenzie, *Rep. Prog. Phys.*, **59**, 1611 (1996).

6. M.Kamo, Y.Sato, S.Matsumoto, and N.Setaka, *J.Cryst. Growth*, **62**, 642 (1983)

7. J.A Martin, L.Vazquez, P.Bernard, F.Comin, S.Ferrer, *Appl. Phys. Lett.*, **57**, 1742 (1990).

8. S.Masumoto, M.Hino, and T.Kobayashi, *Appl. Phys. Lett.*, **51**, 737 (1987).

9. K.Suzuki, A.Sawabe, H.Yasuda and T.Inuzuka, *Appl. Phys. Lett.*, **50**, 728 (1987).

10. Y.Hirose, and Y.Terasawa, *Jpn. J. Appl. Phys.*, **25**, L519 (1986).

11. J.Robertson, *Adv. Phys.*, **35**, 317 (1986).

12. Y.Lifshitz, *Diamond Relat. Mater.*, **5**, 388 (1996).

13. S.R.P. Silva, G.A.J. Amaratunga, C.P.Constantinue, *J. Appl. Phys.*, **72**, 1149 (1992).

14. D.R. McKenzie, D.Muller, B.A.Pailthorpe, *Phys. Rev. Lett.*, **67**, 773 (1991).

15. S.R.P Silva and G.A.J. Amaratunga, *J. Mater Sci.*, **29**, 5962 (1994).

16. Ph. Komninou, G.Nouet, P.Patsalas, Th. Kehagias, M.Gioti, S.Logothetidis, Th. Karakostas, *Diamond Relat. Mat.*, **9**, 703 (2000).

17. J.Robertson, Proceedings of the Ist International Specialist meeting on Amorphous Carbon (SMAC'97), Published by World Scientific Publishing Co. Pte. Ltd., Singapore., 32, 1997.

18. J.Roberson, *Prog. Solid State Chem.*, **21**, 199 (1991).

19. P.J. Fallon, V.S. Veerasamy, C.A. Davis, J.Robertson, G.A.J. Amaratunga, W.I.Milne, J.Koskinen, *Phys. Rev. B*, **B48**, 4777 (1993).

20. F.J Clough, S.Paul, S.Egret, W.I.Milne and J.Robertson, *Recent Adv. In Physics*, 2, (1999).

21. E.Ohta, Y.Kimura, H. Kondo, M.Takahashi, K.Kameyama, K.Yamada, I.V.Fujimura,

22nd Int. Conf. Sol. Stat. Devices and Materials (SSDM), 589 (1990).

22. S.Egret, J.Robertson, W.I. Milne, F.JClough, *Diamond Relat. Mater.*, **6**, 879 (1997).

23. B. Bhushan, Tribology and Mechanics of Magnetic Storage Devices, second ed., Springer, New York, 1996.

24. J.P.Sulivan, T.A.Friedmann, C.A. Apblett, M.P.Siegal, N.Missert, M.L.Lovejoy, P.B.Mirkarimi, and K.F.McCarty, *MRS Synp. Proc.*, **381**, 273 (1995)

25. A.Grill, V.Patel, C.Jahnes, *J. Of the Electrochem. Soceity*, **145**, 1649 (1998).

26. K.Endo, *European Patent Application*, **EP 0 701 283 A2**, (1995).

27. R. Rank, H. Brückl, J. Kretz, I. Mönch, and G. Reiss, *Vacuum*, **48**, 467 (1997)

28. W.Zhu, B.R.Stoner, B.E.Williams, J.T. Glass, *Proc. of the IEEE*, **79**, 621 (1991).

29. F.G Celii, P.E. Pehrsson, H.T Wang and J.E Butler, *Appl. Phys. Letts*, **57**, 2043 (1988).

30. S.R.P.Silva, Invited talk on amorphous carbon, in the *Chelsea Conference, March 29-30, 1999*, held at Imperial College, London, UK.

CHAPTER 2

Experimental Characterisation Techniques for Diamond-like carbon

The nano-scale structure of amorphous carbon is characterised by multiple phases, [1,2,3,4]. Hence diamond-like carbon films often exhibit apparently inconsistent structural and electronic properties. This calls for careful interpretation of the results of investigation of a-C:H films. Prior to the deposition of the films, knowledge of resistivity, hydrogen concentration, energy gap, density of states, etc. can be employed, to improve film quality. Utilisation of a-C:H films in devices pre-empts thorough understanding of various material properties and the influence that growth parameters can exercise on these properties. This chapter focuses on the basic techniques employed in our investigation of a-C:H films.

2. 1 Ellipsometry

Ellipsometry is a sensitive optical technique used for determining the properties of surfaces and thin films, [5,6]. If linearly polarised light of a known orientation is reflected at oblique incidence from a surface, the reflected light is elliptically polarised. The shape and orientation of the ellipse depend on the angle of incidence, the direction of the polarisation of the incident light, and the reflection properties of the surface. We can measure the polarisation of reflected light with a quarter-wave plate followed by an analyser; the orientations of the quarter-wave plate and the analyser are varied until no light passes though the analyser. From these orientations and the direction of polarisation

of the incident light we can calculate the relative phase and amplitude change, introduced by reflection from the surface.

An ellipsometer measures the changes in the polarisation state of light when light is reflected from a sample. If the sample properties exhibit any variation (for example the thickness of a thin film deposited on a substrate may not be a constant across the film) then the reflection properties of the sample will also change. By measuring these changes in the reflection properties we can deduce the actual change in the film's thickness.

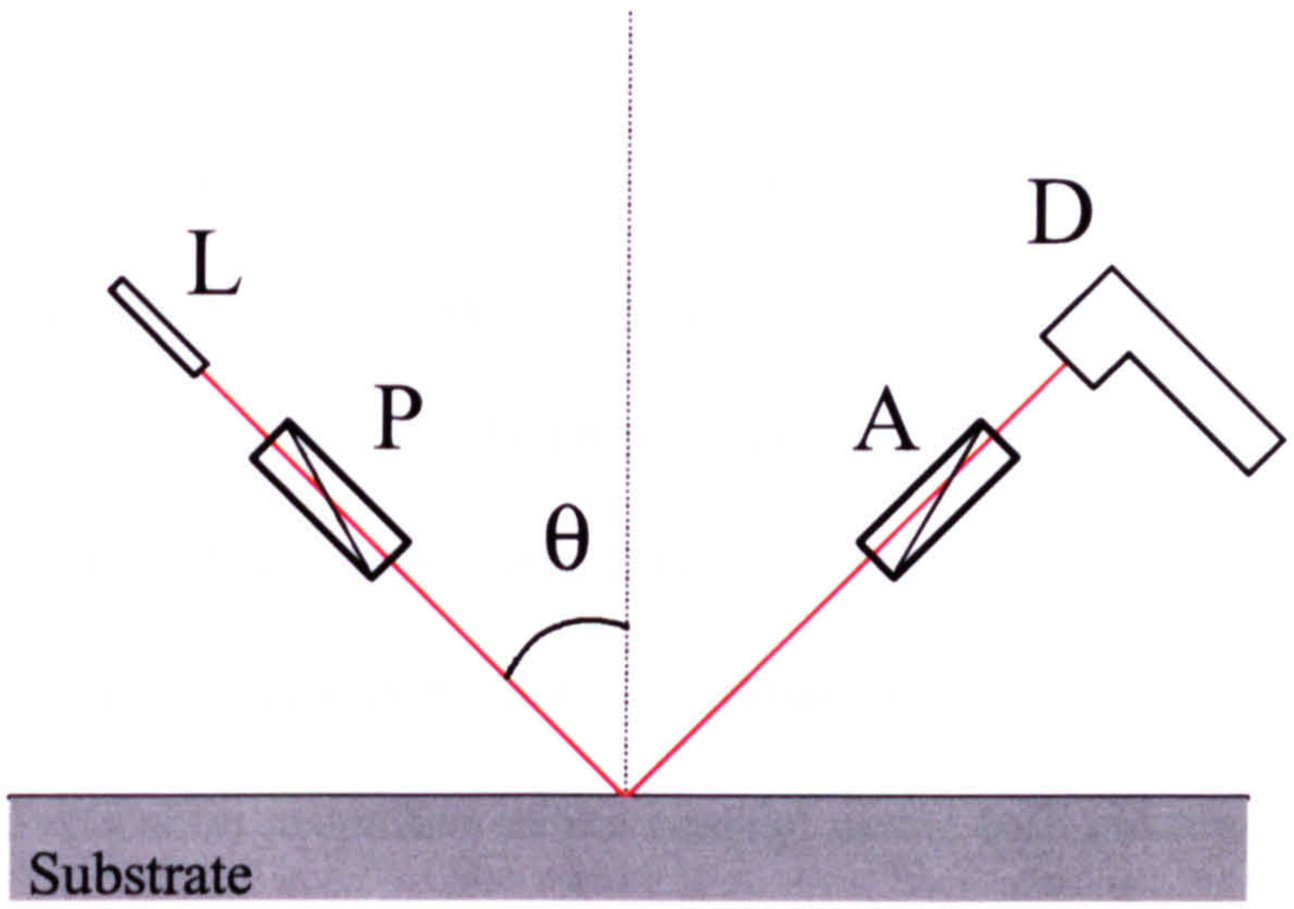

Fig.-2.1 A schematic diagram of a nulling ellipsometer. L: the light source; P: the polarising prism; A: the analyser prism; D: the light detector.

The most important application of Ellipsometry is to study thin films. In the context of Ellipsometry, a "thin" film is one that ranges from essentially zero thickness to several thousand Angstroms, although this range can be extended in some cases. If a film is thin enough to produce an interference pattern, it will probably be a good ellipsometric sample. The sensitivity of an ellipsometer is such that a change in film thickness of a few

Angstroms is quite easy to detect. Fig.-2.1 is a schematic diagram of a nulling ellipsometer, in which **L** is the light source, **P** the polarising prism, **Q** the quarter-wave plate compensator, **S** the sample under study, **A** the analyser prism and **D** is the light detector. Here **L** represents an unpolarised monochromatic light source that is highly collimated with a small beam divergence. A low power Helium-Neon laser serves to generate such a beam.

When we make a null measurement we get two numbers: the angular settings of the polariser and analyser at null, (P and A). We can therefore compute two characteristics of the sample from these two numbers, e.g. the index of refraction and optical absorption of a clean optically absorbing sample. If we have a transparent film on a known substrate we can deduce the index of refraction and the thickness of the film. If on the other hand, our sample constitutes a thin, optically absorbing film of unknown refractive index and thickness, placed on a known substrate, there are three unknown parameters which together determine the reflection properties of the sample; under such circumstances, we cannot determine both the refractive index and film thickness from a single measurement. This is sometimes called the fundamental problem of Ellipsometry.

We used a Rudolph ellipsometer (Model AutoEL-3) for the measurement of refractive index (R.I) and thickness. R.I can reflect the properties of the film and suggest the optical density of the film. We used R.I as a key parameter to optimise the properties of our films.

2. 2 Infrared Spectroscopy:

Infrared spectroscopy is a technique used to detect and characterise the vibrations of molecules, [7,8]. This technique is useful in obtaining information about sp^3, sp^2 and sp^1 hybridised C-H bonds in amorphous carbon.

Table-2.1 Various IR peaks observed in the diamond-like carbon films [9].

Wave Number (cm^{-1})	Corresponding vibrational bond(s)
3420	unassigned
3308	$-C\equiv C-H$ sp^1
3080	CH_2 (olefinic) sp^2
3010	CH (olefinic) sp^2
2960	CH_3
2360±30	O = C = O
1592	C = C aromatic stretch sp^2
1568	C = C aromatic stretch sp^2
1493	C = C aromatic stretch sp^2
1430	- CH_3 or $>CH_2$
1352	amorphous carbon
1280	CH or CH_2 (out-of-plane) sp^3/sp^2
1205	C - H aromatic ring (out-of-plane)
1167	nanocrystalline/amorphous diamond
1064	C - H aromatic ring (out-of-plane)
990	- $CH = CH_2$
780	C - H aromatic ring (out-of-plane)

It has been concluded by a number of workers that a finite amount of hydrogen is always present in the films, [10,11,12,13]. This is due to the hydrocarbon source that is used to deposit the a-C:H films; the existing hydrogen influences the optical gap and electrical properties of the deposited films. Therefore, it is crucially important to estimate the fraction of hydrogen in the films to prepare the film for electronic applications. It should

be noted that only the bonded molecules are IR active and therefore it is not possible to measure the absolute amount of the hydrogen content by IR analysis only. The different peaks present in DLC films have been tabulated in Table-2.1, [9]. The peak values mentioned in this table can be used to assign the different types of bonds present in our films.

2. 3 Raman Spectroscopy:

Raman spectroscopy has been widely used for the analysis of carbon allotropes, [14,15,16,17]. This is a non-destructive technique, requires no special specimen preparation and can be made confocal so that an area as small as 1x1 μm^2 can be sampled. Different materials, (such as diamond, graphite, buckminsterfullerene, amorphous carbon and graphite), leave unique signatures in their respective Raman spectra. The locations of the Raman features in the spectra of some allotropes of carbon are mentioned in Table-2.2. It is quite clear from this table that the spectrum of each allotrope is a blueprint of the material. Thus Raman analysis is a tool to identify the material at hand.

The basic principle of Raman spectroscopy is shown in Fig.-2.2. The sample is excited with laser light; this causes the molecules in it to start vibrating and scatter light, both elastically, (Raleigh scattering) as well as inelastically, (Raman Scattering). The Raleigh scattered light is 10^8 times stronger in intensity than the Raman Scattered light. With the use of proper filters one can eliminate the Raleigh scattering component. The remaining Raman signatures can be further resolved into individual components, using a spectrometer.

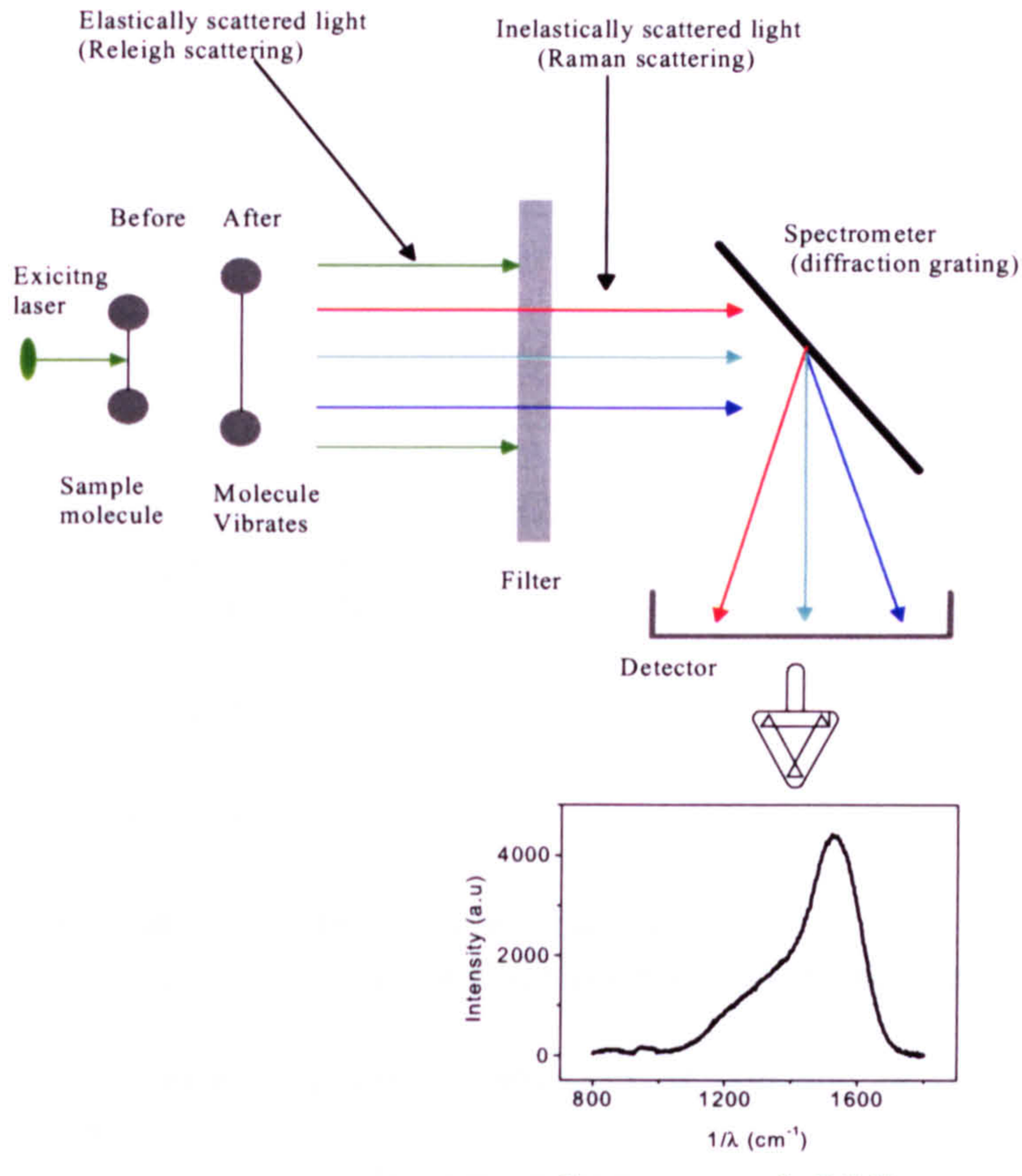

Fig.-2.2 Schematic diagram representing Raman spectroscopy.

In diamond-like carbon, attention is focussed on the region of the spectrum, around the wavenumber of 1450 cm^{-1}, where a typical Raman spectrum of amorphous carbon shows two peaks [18,19]. The first peak (D) is called the "disorder peak" as it arises from amorphous or disorder of carbon. The "G" peak is similar to that observed in the Raman spectrum of microcrystalline graphite. The D peak is approximately at a wavenumber of 1350 cm^{-1} and the G peak is around 1580 cm^{-1}. The analysis of the relative intensities of the two peaks and of their exact positions can be used to gain insight into the type of hybridisation, stress and sp^3/sp^2 ratio [20,21].

Table-2.2 Raman features assigned to constituents, which may be present in a-C:H [ref. 12 and references therein]

Raman Feature (cm^{-1})	**Peak assigned to:**
1180	Nano-crystalline diamond [22] Hexagonal diamond [23] or sp^3-rich phase [24]
1305	Hexagonal diamond [25]
1332	Cubic Diamond
1350	D peak of microcrystalline graphite or alternating ring stretched vibration in condensed benzene rings[14]
1490	Semicircle ring stretch vibration of benzene or condensed benzene rings or in the case of a-C:H, contribution form C-H vibrations at 1500 cm^{-1} or contribution from the phonon density of states in finite-sized crystals[14]
1580	G peak of graphite or sp^2 stretch vibration in benzene or condensed benzene rings or sp^2 stretch vibration of olefinic/conjugated chains[14]

We used Renishaw Raman Spectrometer (Model No. System 2000) for the analysis of amorphous carbon films deposited in our laboratory. Micro-Raman measurements were carried out using the 514.5 nm line of an Ar ion laser with a 2 μm spot size.

2. 4 Ultra-violet spectroscopy

The DC self-bias voltage at which the films were deposited, controls the electrical and optical properties of the a-C:H films. Information about the optical bandgap of the films can be obtained by using ultra-violet transmission spectroscopy [26,27,28]. A UV-visible

spectrophotometer in the range of 180-900nm was used to study the optical properties. The films were deposited on quartz substrates for UV analysis. The absorption coefficient, α, can be determined from the following equation [9]:

$$I = I_o \exp(-\alpha d) \tag{2.1}$$

Here I is the transmitted intensity, I_o is a constant and d is the thickness of the a-C:H film. The transmitted intensity can be calibrated against a quartz substrate by placing the quartz substrate in the sample holder. The "Tauc-intercept", (which is also called the Tauc-gap) is a commonly used tool for estimating bandgap in amorphous semiconductor materials; it is obtained by plotting $(\alpha h\nu)^{1/2}$ against $h\nu$ [9].

2. 5 Electron Spin Resonance

Electron spin resonance spectroscopy and related magnetic resonance spectroscopy techniques are powerful in studying the micro-structure of paramagnetic centres, their interactions with the lattice and their mutual interactions, [29,30,31,32]. The terms, "Electron Spin Resonance" (ESR) or "Electron Paramagnetic Resonance" (EPR) indicate a technique which takes advantage of the Zeeman effect to investigate the density of states near the Fermi level and the local structure in the neighbourhood of the ESR active centres. ESR is active when the total spin of the quasi-particles that occupy it, is non-zero. The common cases are those in which the total spin is either 1/2 or 1. The reversal of spin of these unpaired electrons in an applied magnetic field is recorded. The magnitude of the energy change is quite small. The ESR spectrometer therefore operates at microwave frequencies. In practise, spectra are obtained by varying the magnetic field

at a constant frequency. Absorption of energy associated with the spin transition occurs at the resonant condition [32]:

$$\Delta E = h\nu = g\beta_e H \tag{2.2}$$

where β_e is a constant, the Bohr Megneton ($\beta_e = eh/4\pi mc$) and H is the strength of applied magentic field. The factor g, the gyromagnetic ratio, has a value of 2.0023 for a free electron, [32] but varies significantly for paramagentic ions in the solid state. The local induced field comes from the orbital motion of electrons; spin-orbit coupling mixes J, L and S and shifts g, the shift can can be towards $g<2$ or $g>2$. g is thus characteristic of different electronic structures and is also known as the Landé splitting factor.

2. 6 Electron Energy Loss Spectroscopy

The chemical composition in the material can also by analysed by Electron Energy Loss Spectroscopy, (EELS), [33,34,35]. EELS is a technique associated with analytical electron microscopy. It can be used for elemental analysis, (for light elements such as nitrogen and carbon) and for studying energy levels in the surface of solids. In the EELS technique, a monochromatic incident beam of electrons is used to ionise the inner shell of an atom in the sample. These ionisations are a preface to the generation of X-rays. The electrons that are responsible for these ionisations suffer an energy loss as a consequence. An EELS spectrum is a plot of the intensity of these electrons against energy loss. An intense peak occurs at zero energy loss. This peak corresponds to the electrons that are either scattered inelastically or those that do not interact with a sample. The other peaks in the EELS spectrum correspond to the electrons responsible for inner shell ionisations. The peaks are usually weak and broad and the spectra increase in complexity with

increasing atomic number. EELS is a particularly useful technique for analysing light atoms, such as, carbon. Carbon has many allotropes, each with a different electronic structure. Consequently, energy losses vary across the whole range of the carbon allotropes. Thus, depending upon the energy loss and its intensity, one can approximate the phase of carbon in the DLC. This technique can also be used to estimate the sp^2/sp^3 ratio in DLC [34].

2. 7 Scanning Electron Microscopy

Scanning Electron Microscopy (SEM) is an extremely versatile technique capable of providing vital information over a wide range of magnification [36,37]. SEM complements optical microscopes for studying texture, topography and surface features of powders or solid pieces; features up to tens of micrometers in size can been seen and, because of the depth of focus of the SEM instruments, the resulting pictures have a definite three-dimensional quality. In our investigation, we used a Leica S430 scanning electron microscope. This is a 30 KeV instrument that is fully controlled from within a WINDOWS environment. A full set of detectors, including the secondary emission electron detector, backscatter electron detector and cathode-luminescence detector are fitted in addition to a transmission adapter. Images are included with descriptions of these detectors for direct comparison of the information that may be obtained by careful selection of the detector. Energy dispersive X-rays may be used for qualitative chemical analysis of samples. The microscope operates at very low accelerating voltages and beam currents and gives good resolution (upto 4 nm) on un-coated specimens.

In our work, SEM was used to determine the quality of the a-C:H films deposited on Si, Glass and metal-coated glass and silicon substrates. Devices such as diodes and MSM

structures have also been investigated with an SEM, both prior to and after the electrical measurements. This investigation helped us to understand the behaviour of metals on the surface of a-C:H after the imposition of electrical stress. This study is vital in selecting the desired contact material for a-C:H.

2. 8 Electrical Measurements:

It is important to know the electrical behaviour of the material that is subsequently employed in device fabrication. The resistivity and the conduction mechanism responsible for the semiconducting behaviour and the resistivity of the material are important factors to clarify, in order to realise the desired properties of the device. The electrical behaviour and test structures used in the measurements will be discussed in the subsequent chapters. We used various instruments, (an LCR HP, picoammter, high voltage source), to measure the electrical behaviour of test structures. I-V data was used to deduce the conduction mechanism in the a-C:H films and to estimate the resistivity. Capacitance-voltage-frequency, (*C-V-f*) measurement was used for testing the reliability of the devices and also to estimate the resisitivity. *C-V-f* data was also used to deduce the density of states in the a-C:H film deposited at different growth conditions.

References:

1. M. Weider, S.Sattel, T. Gressen, K. Jung, H. Ehrhardt, V.Veerswamy and J.Robertson, *Phys. Rev.*, **B53,** 1594 (1996)

2. M. Chhowalla, J.Robertson, C.W.Chen, S.R.P Silva, C.A.Davis, G.A.J Amaratunga and W.I Milne, *J. Appl. Phys.*, **81(1)**, 139 (1997).

3. S.R.P. Silva, G.A.J. Amaratunga, *J.Mater. Sci.*, **29**, 4962 (1994).

4. Y.Ando, X.Zhao, H.Kataura, Y.Achiba, K.Kaneto, M.Tsuruta, S.Uemura, and S.IiJima, *Diamond Relat. Mater.*, **9**, 847 (2000).

5. M.Elias, L. Zajickova, V. Bursikova, J. Janca, M. Lorenc, *Diamond Relat. Mater.*, **9**, 553 (2000).

6. S. Xu, L.K Cheah, and B.K Tay, *Thin Solid Films*, **312** (1-2), 1998.

7. P.H. Williams, I.Fleming, in spectroscopic methods in organic chemistry, McGrawHill London, 1980.

8. B. Dischler, A. Bubenzer, P. Koidl, *Appl. Phys. Lett.*, **42**, 636 (1983).

9. S.R.P Silva, *Ph.D Thesis*, Dept. of Engineering, Cambridge Univeristy, 1993.

10. S.R.P. Silva, G.A.J.Amaratunga, C.P.Constantinou, J.Appl.Phys., **72**, 1149 (1992).

11. L. Martinu, A.Raveh, D. Boutard, S.Houle, D.Poitras, N.Vella, and M.R.Wertheimer, *Diamond and Related Materials*, **2**, 673 (1993),

12. M. Weiler, S. Sattrl, T. Giessen, K. Jung, H. Ehrhardt, V.S.Veerasamy, and J.Robertson, *Phys. Rev. B*, **53**, 1594 (1996).

13. D. Sunil, V.D.Vankar, K.L,Chopra, *J.Appl. Phys.*, **69**, 3719 (1991).

14. J. Schwan, S.Ulrich, V.Batori, H.Ehrardt and S.R.P.Silva, *J. Appl. Phys.*, **80(1)**, 440 (1996).

15. K.W.R Gilkes, H.S Sands, D.N Batchelder, J. Robertson, and W.I Milne, *Appl. Phys. Lett.*, **70**, 1980 (1997).

16. Appl. Phys. Lett., **59**, 779(1991).

17. L. Nistor, V. Buschman, V. Ralchenko, G.Dinca, I. Vlasov, J. Van Landuyt, H. Fuess, *Diamond Relat. Mater.*, **9**, 269 (2000).

18. R. Shuker and R. Gammon, *Phys. Rev. Lett.*, **25**, 222 (1970)

19. F. Li and J.S, Lannin, *Phys. Rev.*, B39, 6220 (1989).

20. A.V Stanishevsky, L.Y. Khriacchtchev, *Diamond Relat. Mater.*, **5**, 1355 (1996).

21. S. Prawer, and K.W Nugent, *Proceeding of the Ist International Specialist Meeting on Amorphous Carbon (SMAC'97)*, eds., S.R.P. Silva, J. Robertson, W.I. Milne, G.A.J Amaratunga, World Scientific Publishing Co. Pte Ltd., pp.199, 1997.

22. W. Yarbrough and R. Rey, in *Diamond and Related Materials*, edited by A. Badzian, M. Geis, and G. Johnson (Materials Research Society, Pittsburgh 1988), extended abstract Vol.. **EA-15**, p.33.

23. S.R.P. Silva, G.Amaratunga, E.Salje, and K. Knowels, *J. Mater. Res.*, **29**, 4962 (1994)

24. R. Schroder, R. Nemanich, and J. Glass, *Phys. Rev.*, **B41**, 3738 (1990).

25. D. Knight and W. White, *J. Mater. Res.*, **4**, 385 (1989)

26. R. Tauc, Grigorovici, and A. Vancu, Phys. Status Solidi, 15, 627 (1966)

27. R.A Street, Hydrogenated Amorphous Silicon (Cambridge University Press, Cambridge, 1991).

28. J.P Xanthakis, *Diamond and Relat. Mater.*, **9**, 1369 (2000).

29. J. Robertson, *Diamond and Relat. Mater.*, 6, 212 (1997).

30. J.H. Van Vleck, *Phys. Rev. B*, **74**, 1168 (1948).

31. G. Fusco, A. Tagliaffero, W.I. Milne, M. Fanciulli, *Diamond and Relat. Mater*, **3**, 844 (1994).

32. C.P. Pole, *Electron Spin Resonance*, John-Wiley, London, 1983.

33. N-H. Cho, K. M. Krishnan, D. K. Veirs, M. D. Rubin, C. B. Hopper, and B. Bhushan, *J. Mater. Res*, **5**, 2543 (1990).

34. G. M Pharr, D. L Callahan, S. D McAdams, T.Y Tsui S. Anders, A. Anders, J. W. Ager III, I. G. Brown, S.R.P.Silva and J. Robertson, *Appl. Phys. Lett.*, **68**, 779 (1996).

35. S.Ravi, P.Silva, S.Xu, B.X.Tay, H.S.Tan and W.I.Milne, *Appl. Phys. Lett.*, **69**, 491

(1996).

36. V. R. M. Rao and W. C. Nixon , *J. Vac. Sci. Technol*, **61**, 1861 (1971).

37. T. J. Aton, S. S. Mahant-Shetti, R. J. Gale, M. H. Bennett-Lilley, M. G. Harward, C. A. Pico, and T. L. Weaver, *J. Vac. Sci. Technol,* B **8**, 2041 (1990).

CHAPTER 3

Diamond-like carbon and its growth by the PECVD technique

3.1 Introduction

As science evolves, individual branches of study appear to progress towards greater specialisation. Paradoxically though, it is also true that such specialisation is often accompanied by greater overlap among the different disciplines. A notable example in this context is the relationship of the element carbon with multiple scientific fields, such as physics, chemistry, biology and engineering. In fact carbon is such a versatile element (from the point of view of life sciences and suitability in industrial applications) that it merits its own private branch of science. Carbon science and engineering is a vast field; we would like to confine ourselves to the discussion of those forms of carbon (and their properties) that have a direct bearing to the field of electronics.

The basic reason for the remarkable versatility shown by carbon is the ability of the element to undergo hybridisation; exhibiting sp^3, sp^2 and sp^1 types of bonding, depending on ambient conditions. Fig.-3.1 illustrates these three bond types. In the sp^3 configuration, (see Fig.-3.1(c)) all four atoms produce a strong σ-bond with the adjacent atoms. In the sp^2 (see Fig.-3.1(b)) case three of the electrons are assigned to the trigonally directed sp^2 hybrids which form σ-bonds and the fourth electron lies in a p orbital, normal to the σ bonding plane. This fourth electron forms weak π bonds with adjacent p orbitals. The sp^1 state (Fig.-3.1(a)) is characterised by two of the four electrons in a σ bond configuration and the other two electrons are left in orthogonal orbitals to produce π

bonds. The capacity of carbon to form these three types of hybridisations results in a number of allotropes, both crystalline and non-crystalline. We have discussed a few of these allotropes in Chapter 1.

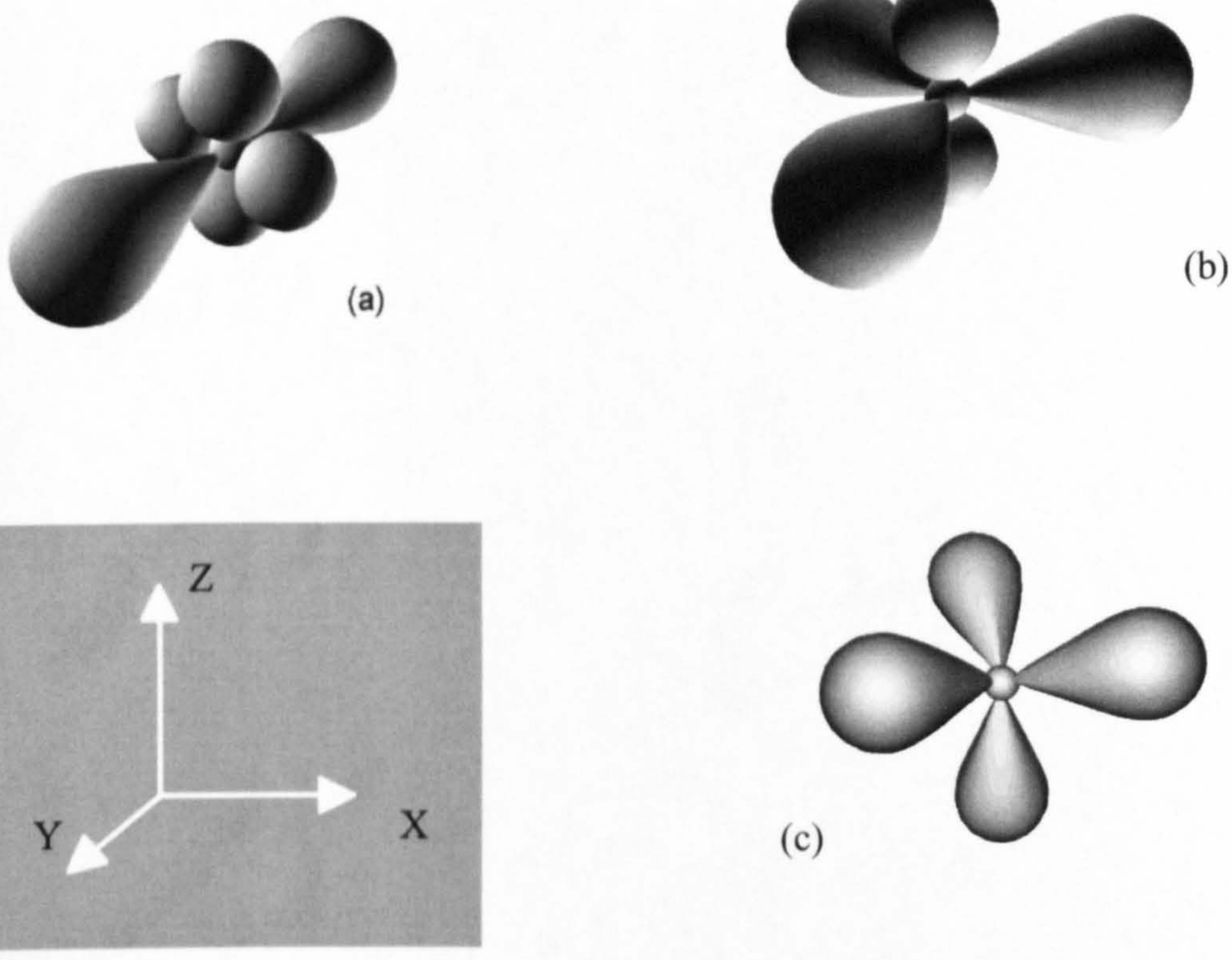

Fig.-3. 1 Carbon exhibits three types of hybridisation (a) sp^1, (b) sp^2 and (c) sp^3.

The forms of carbon differ from each other in physical as well as electronic properties, [1,2,3]. As discussed in Chapter-2, the features of Raman spectra serves as a thumb print of an allotrope, [4,5,6]. It is evident from these spectra that allotropes of carbon have

different structures. The various properties of the allotropes of carbon are tabulated in Table-3.1.

Table –3.1 Properties of various forms of carbon [1,28].

Allotropes	**Density (g cm^{-3})**	**Hard-ness (GPa)**	**% of sp^3**	**% of H**	**Bandgap (eV)**	**Resis-tivity (Ωcm)**
Diamond	3.515	100	100	0	5.5	10^{18}
Graphite	2.262	10-20	0	0	-0.04	$4x10^{-5}$
Ion beam a-C	3.0	100	90±5	≈ 9	1.5 – 3.5	~ 10^2
Hard a-C:H	1.6 – 2.2	10-20	30 - 60	20-40	0.8 – 1.7	10^6 - 10^9
Soft a-C:H	0.9 – 1.6	< 5	50 – 80	40 – 65	1.6-4.0	10^9 - 10^{15}

Over the last few decades it has become clear that non-crystalline carbon [1,2,7] exists in various forms. Examples of the sp^2 rich varieties of amorphous carbon are glassy carbon and evaporated carbon [8, 9]. Glassy carbon is formed by pyrolysis and its structure consists of convoluted graphitic layers. It has considerable medium-range order. As its name suggests, evaporated amorphous carbon is formed by evaporation; it exhibits much greater disorder in the arrangement of sp^2 sites than glassy carbon.

In recent years, interest has grown in those forms of carbon which contain a high percentage of sp^3 bonding. These materials, often known as diamond-like carbon (DLC),

have a wider band gap, high atomic density, high hardness, chemical inertness and high smoothness [1, 2, 7].

In view of the very desirable characteristics of this material, I endeavoured to grow a-C:H films with the intention of studying its material properties aimed at its use in electronic devices.

DLC can be deposited by various techniques, such as, ion beam deposition (IBD) [10], ion beam assisted deposition [11], laser plasmas, radio frequency (RF) discharge plasma enhanced chemical vapour deposition (rf-PECVD) [12] and the electron cyclotron resonance (ECR) plasma technique [13].

The rf-PECVD technique offers a key advantage in depositing DLC on a large area substrate at room temperature and also allows compatibility with large area plastic substrates [12]. The rf-PECVD has the following advantages apart from the low temperature deposition:

- conformal deposition
- low pinhole density
- excellent uniformity

Diamond-like carbon is currently a relatively immature electronic material and it is important to fully understand the relationship between the deposition process and film properties. The amorphous carbon films can be subdivided into two main forms: hydrogenated and un-hydrogenated.

In this chapter I will be discussing the various growth conditions that affect the deposition of hydrogenated amorphous carbon (a-C:H) by the technique of RF-PECVD.

In the following sections the technicalities of the PECVD system and the parameters involved in the process of growing these films will be discussed.

3.2 Introduction to PECVD deposition system

The plasma process is also known as low-pressure, cold-plasma, nonequilibrium plasma process, or the glow discharge process. Some techniques based on the concept of the plasma-assisted process include approaches such as plasma-assisted chemical vapour deposition, (PACVD), plasma-enhanced chemical vapour deposition, (PECVD), ionitriding and plasma etching [14, 15, 16]. These processes may be used for production in advanced microelectronics and in the manufacture of present and future generations of large-scale integrated circuits.

Plasma chemistry takes place under nonequilibrium conditions; and the reactions can occur while gaseous precursors are exposed in the reaction chamber, which remains at a relatively low temperature (40°C – 80°C) [16]. Thus, this is a cold-plasma deposition process. The phenomenon is similar to that which occurs in a fluorescent bulb. Cold plasma is a very complex system and is not fully understood yet. However, present knowledge of chemistry and physics can be employed to achieve the desired properties of the deposited material by adjusting the growth conditions. Cold plasma is generally excited and sustained electrically by direct current (DC) [17], radio frequency (RF) [18, 19], or microwave (MW) power [20, 21], applied to a gas or a mixture of gases that are confined in the space between two electrodes. In the DC plasma process, conducting electrodes are required. The deposition of dielectric films by the use of DC discharge technique is not possible. This is because the electrodes exposed to the plasma, gradually

become covered with the insulating material that is being deposited. Therefore, soon after a DC discharge has been initiated, it will quickly extinguish as electrons and negatively charged ions accumulate on the surface of the insulating material that covers the anode and recombine with the available ions. The cathode is also covered with positively charged ions.

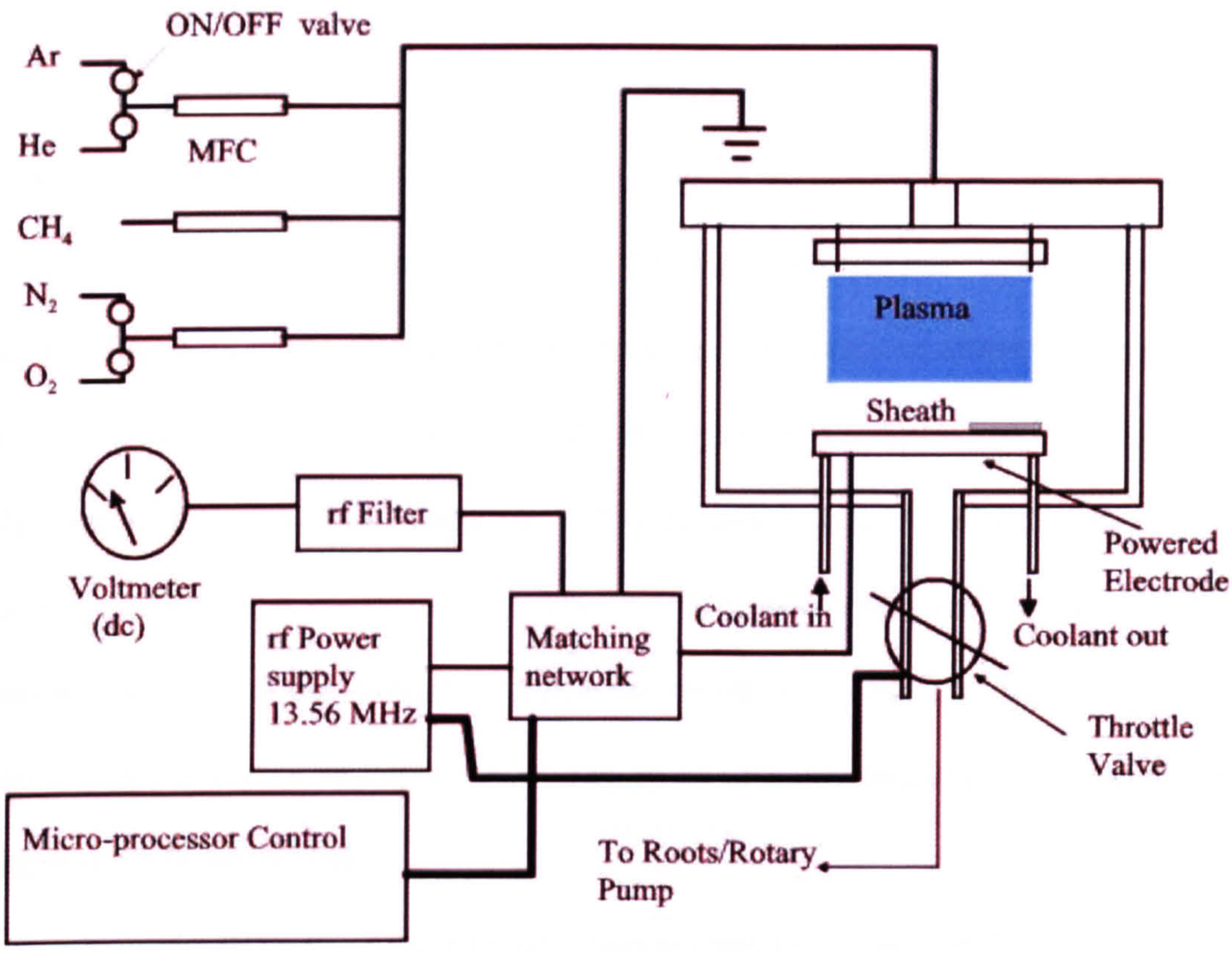

Fig.-3. 2 Schematic diagram of a PECVD reactor used for the deposition of a-C:H films.

The solution to this problem is the use of an alternating current (ac) plasma. When an alternating electric field is applied between the two electrodes of the discharge chamber, each electrode acts alternately as cathode and anode. When the breakdown potential is surpassed on each half of the ac cycle, a temporary DC glow discharge is sustained. But at low frequencies, it is not possible to sustain such a temporary DC discharge. When the frequency of the applied electric field is higher than the critical frequency, (the critical frequency is defined as the reciprocal of the time taken by the positively charged ion to move between the two electrodes) [14,16], the ions with instantaneous positions at the anode cannot reach the cathode, before the field is reversed. At this frequency, the distance travelled by the ions during a half-cycle of the electric field becomes smaller than the thickness of the plasma sheath. At such a frequency or above, the positive space charge is partly retained between the two half cycles of the alternating electrical field and helps the re-initiation of the discharge. This results in a potential difference across the plasma sheath, that is similar to DC bias superimposed across the electrodes. The bias generated by such a mechanism is called the self-bias. Generally, high frequency ac is used to achieve such a situation. A typical value of radio frequency used in the PECVD system is 13.56 MHz [16].

A schematic diagram of the PECVD system used to deposit DLC in our laboratory is shown in the Fig.-3.2. The system consists of the vacuum chamber with rf electrodes and a high speed roots/rotory pump system. The lower electrode also serves as a substrate holder. Impedance matching of the output from the rf generator and the glow discharge system is achieved by an automatic power-matching unit. The lower electrode

becomes negatively biased (V_b) with respect to the plasma, which is basically due to the higher mobility of electrons as compared to ions. V_b is measured by a voltmeter. The flow of gases (Ar, He, CH_4) are regulated by individual mass flow controllers (MFCs). The pressure in the deposition chamber during the deposition of DLC is measured by a capacitance manometer. Typically, the lower electrode is kept at room temperature by circulating water, the temperature of which is controlled by the chiller.

3.3 Parameters that control the properties of films deposited by PECVD

There are a number of parameters which control the film properties and growth rate [22, 23, 24], for examples, RF- power, chamber pressure, substrate temperature, reactor geometry, pumping speed and precursor flow rates. The rf frequency can be omitted in this discussion about the free parameters, since this is fixed in our reactor. The geometry of the reactor, especially the surface areas of the upper and lower electrodes, affect ion energies and hence the properties of the deposited film. We have not altered the area of the electrodes during whole investigation, so we can omit consideration of reactor geometry from the following discussion. The pumping speed normally remains constant and this can also be disregarded from our list of growth-determining parameters.

The rf-power can be fine tuned; however, the net power coupled into the system is not uniquely correlated with the deposition process since there may be substantial losses in the matching unit. The self-bias voltage, (V_b) on the other hand is a more meaningful parameter . This is because V_b gives the average sheath potential within which the ions forming the film are accelerated. Also, the energy of the ions depends on the mean free path i.e. on the pressure. The substrate temperature is not changed in this work and

therefore self-bias and pressure are the key deposition parameters which determine the properties of films, in our experimental set-up.

3.3.1 DC Self -bias

The value of self-bias depends on various factors, such as, electrode area, the gases, pressure and rf power. It has been seen in the PECVD system that the dc self-bias (V_b) can be expressed as [25]:

$$V_b \propto \left(\frac{P_{rf}}{p}\right)^{\frac{1}{2}} \qquad \ldots\ldots \quad 3.1$$

where, p is the chamber pressure and P_{rf} is the RF power applied across the electrodes.

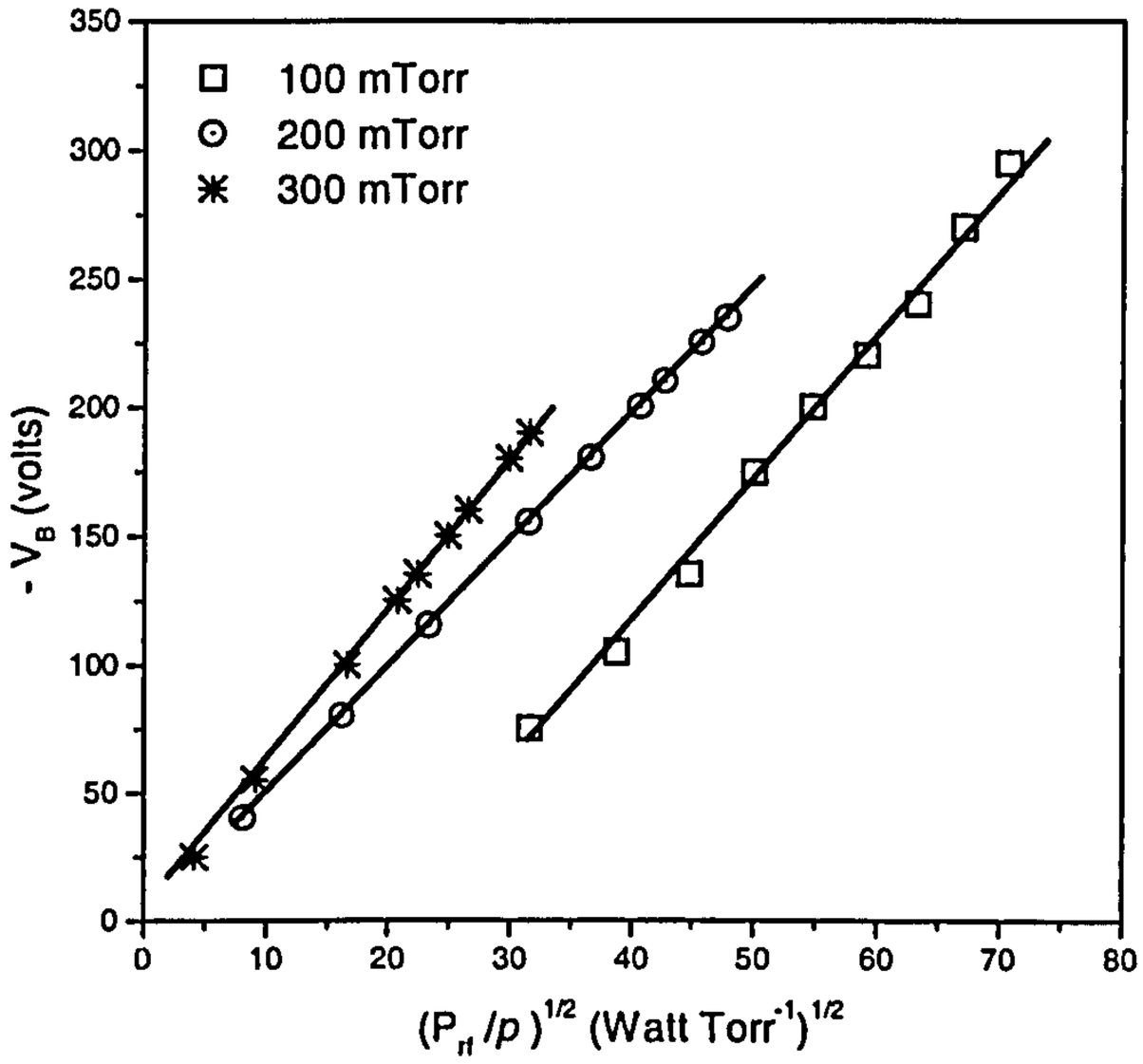

Fig.-3. 3 Variation of dc self bias with rf power applied across the electrodes, at three different pressures.

The value of the self-bias is dependent on the RF power applied to the electrode and the pressure in the reactor. It increases with increasing power and decreasing pressure. If we plot V_b against $(P_{rf} / p)^{1/2}$, a linear relation is expected. The plot for our system is shown in Fig-3.3 at three different values of pressure. It is evident from the plot that the expected linearity is followed very closely in our system. This offers confidence at the outset. These characteristics were measured with methane and argon as the gases were fed into the chamber at flow rates of 10 sccm and 100 sccm, respectively.

3.3.2 Average Ions Energy consideration

The properties of amorphous carbon films are mainly dependent on the ion energies that participate in the deposition process [26]. The ion energies in the rf-PECVD system are determined by the DC self-bias voltage that develops across the sheath space and the inelastic collisions that occur in the acceleration process across the sheath. These parameters (DC-bias and nature of inelastic collisions) are controlled by the chamber pressure, nature of the used gases, and the fraction of the rf-power that is coupled into the chamber. The empirical relation between the average ion energy and the DC-bias measured across the ion sheath at a given pressure is, according to Bubenzer [27]:

$$E = K\left(\frac{V_B}{p^{0.5}}\right) \qquad \text{..... 3.2}$$

Where E is the average energy of the ions, V_B the dc bias measured across the ions sheath and p is the pressure in units of μbar and K is constant.

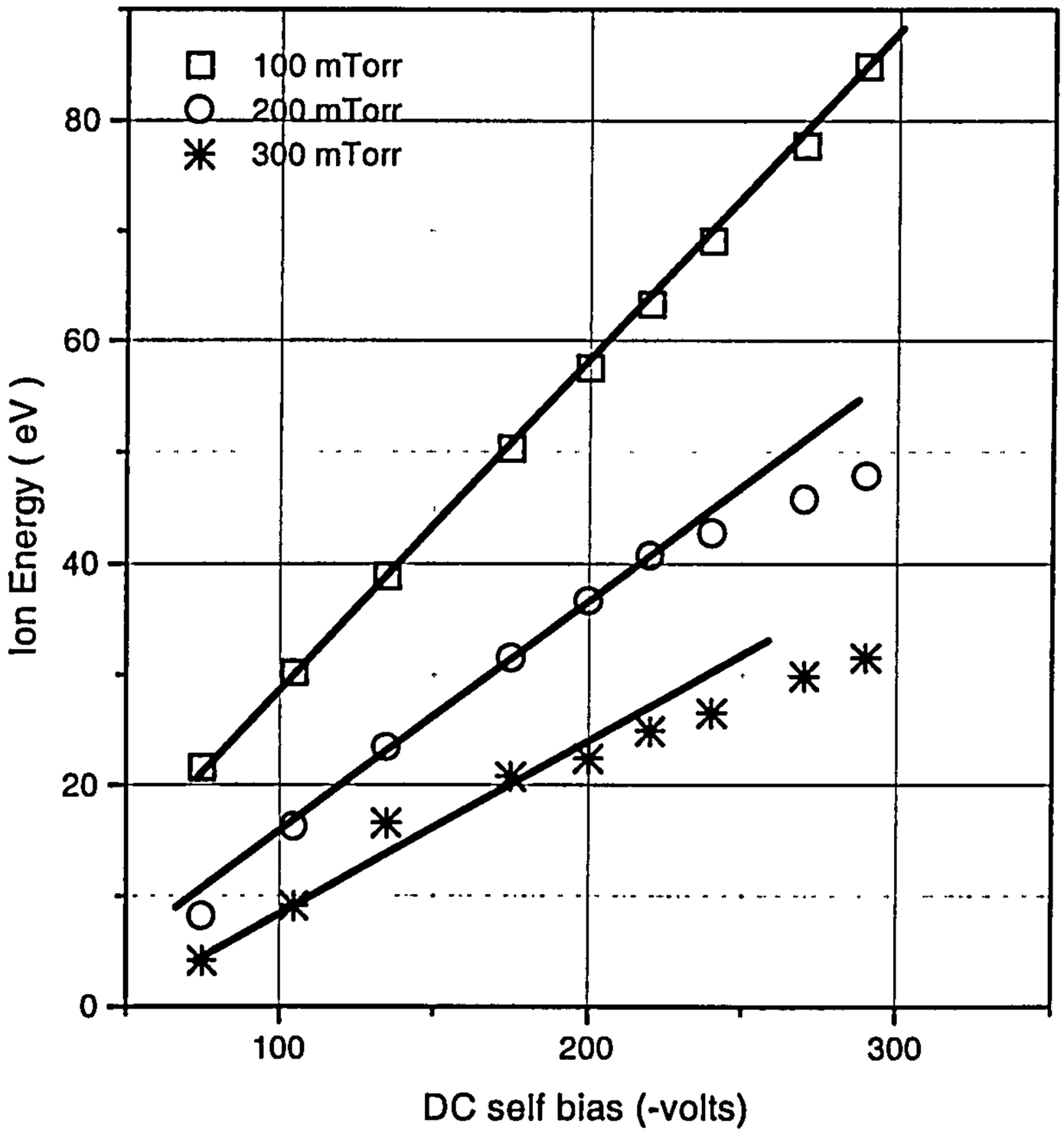

Fig. –3.4 Variation in the average ion energy with rf power at three different pressures.

Ion energy is an important quantity because it is closely related to properties of the deposited film. The energy is not directly accessible. However, some conclusions on the average energy of ions impinging on the substrate can drawn be from the dependence of the deposition temperature (rise of the substrate temperature due to the dissipation of ion energy) and growth rate on bias and pressure. We have calculated the average ion energy,

(with K = 3.3, [28]), using Eqn.(3.2) at three different pressures; 100 mTorr, 200 mTorr and 300 mTorr. The variation in the average ion energy with changes in the DC self -bias is shown in the Fig.-3.4. It is quite evident from Fig.-3.4 that the ranges of ion energies achieved for a given change in the RF power is different at different pressures. The range of ion energies, corresponding to a change in the imposed DC self-bias from -70 V to –295 V at, 100 mTorr, 200 mTorr and 300 mTorr, are 21-85 eV, 8-48 eV, and 4-31 eV. These results are in good agreement with the theory of rf-plasma [16]; one expects ion energy to increase as the chamber pressure falls. The ion-energy vs DC self bias follows the relationship given in Eq.3.2 for pressure 100 mTorr. It does not follow the aforesaid relationship at higher values of DC self bias for pressures 200 mTorr and 300 mTorr. This may be due to the accumulation of charge at a higher pressure that causes the average ion energy to deviate from theory (Equ.-3.2). The properties of diamond-like carbon are functions of ion energy. Therefore, to prepare a film with the desired electronic properties, a proper band of energies has to be selected. In other words, it is very important to optimise the film properties. Thus, the deposition of a "good" film requires knowledge of the change brought about in ion energy by the rf –power, in the chamber where the a-C:H is to be deposited.

There are a number of models mentioned in the literature which suggest different windows of ion energies that give rise to the required properties of a-C:H films. Robertson [29] predicted the ion energies should be centred around 60 eV, Koidl et. al [26] experimentally found an energy range of 40-80 eV, Lifshitz et. al. [30] proposed an ion energy range of 50-100 eV and McKenzie et al. [31] suggested an ion energy

distribution centred around 40 eV for optimum sp^3 bonding in a-C:H on the basis of their empirical observations. Thus the conclusion drawn on the basis of all these models is that the peak of the favourable ion energy window is centred around 50 eV for deposition of a-C:H.

3.3.3 Selection of growth conditions for uniform resistivity, thickness and refractive index:

The nature of plasma deposition is such that it is difficult to get exact uniformity in film properties when the substrates are placed at different locations in the PECVD chamber. Different laboratories engaged in DLC deposition may have different ways of optimising the various properties of DLC. The industrial application of diamond-like carbon requires require high deposition rate over large areas and uniformity in the layer thickness to better than $\pm$ 5%. The choice of growth conditions will play a vital role in achieving such requirements. The in-homogeneity in the film properties generally arises from the electric field non-uniformity in the PECVD reactor. However, powder contamination of plasma (or dusty plasma) [32,33,34], gas depletion [16] and substrate and electrode topology can also produce significant variations in the film properties. Dusty plasma should not be allowed to participate in the film growth. Dusty plasma have been the focus of intense research in the past decade [33,34,35,36,37]; as a branch of physics, it finds applicability in the industrial processing of materials and as well in astrophysics. "*Dusty Plasmas*" are normal plasmas that contain sub-micron or micron sized dust particles in addition to ions and free electrons. The dust grains become electrically charged due to

the interaction with the plasma, causing them to act as a third charged plasma species. The industrial community has encouraged the study of dusty plasma. This is because, dust may be present in the plasma reactor, creating a source of contamination, thus harming the yield. Therefore it is important to reduce or completely stop the incorporation of such particles in the material.

There are a few reports on the dusty nature of carbon related plasma[38,39]. Burden et al [38] have carried the investigation of formation of dusty plasma in amorphous carbon PECVD chamber. In this report, the chamber pressure was kept to 250 mTorr and methane gas was used to investigate the nature of the plasma. The investigation shows that brown coloured dust was formed adjacent to the chamber wall. Analysis of the dust shows that it is made up of a nano-tubes, etc, while the material deposited on the substrate (which was kept at the bottom electrode) was amorphous in nature (amorphous carbon). The pressure at which we deposited (100 mTorr) the films is lower than that of the Burden et al [38]. Therefore mean free path (which inversely proportional to the chamber pressure) of the species (ions, electron, etc.) is larger than the plasma conditions reported in [38]. This reduces the chances of interaction of species in the gas phase and this helps to reduce the dust formation in our chamber. Burden et al have also hypothesised that the formation of dust is in the gas phase, though we have not come across any work to support this hypothesis.

Seebock et al [37] show that the electrode heating together with proper gas flow can be used to avoid incorporation of dust particles into the growing film. In this investigation temperature of the lower electrode was raised to 80°C and then they suggested that

lighter particles are driven upward by thermophoresis and may be trapped at the sheath edge, while, a strong downward-directed gas flow (feeding gas through the upper electrode) prohibits the trapping of particles at the lower sheath boundary. The situation in our reactor is quite similar to this investigation. It has been shown by Silva [28] that, although the temperature of the lower electrode is kept constant at 20° C by passing the coolant through it, (via a feedback controlled system), the surface temperature of the electrode varies in the range of 80-150° C, depending upon the rf power coupled to the plasma. The rise in the temperature is probably due to ion bombardment and plasma heating [40]. The rise in the temperature will play a similar role as reported by Seebock et al [37] to drive lighter particles upward. Also, the high pumping speed of the pump will not let any segregation or accumulation of particles near the lower sheath boundary. Thus both these processes reduce the chances of incorporation of dusty plasma in the growing film.

After the deposition of a-C:H films, the inner walls of our chamber were carefully examined. It has seen in our reactor chamber that there is a formation of a very thin yellowish layer at the upper electrode and the walls of the chamber, while the lower electrode was found free from any such deposition. Such indication suggests that there is no incorporation of dust in the film deposited. To further confirm this, surfaces of the a-C:H films were examined with an SEM and the investigation show that films are smooth and free from dust particles or grains. Therefore, we can strongly say that there is hardly any inclusion of particulates due to dusty plasma and measured properties of the solely of a-C:H nature.

Nevertheless, over a wide range of operating parameters any electric field inhomogeneity must be avoided for uniform deposition over a large area. To use DLC for large area electronics, one should check for consistency in the film properties by growing films at a number of locations, over the large area of the lower electrode. A number of combinations of flow rates of methane and argon were scanned to achieve the films, which were found to have desired properties (I.R, thickness and resistivity). However, these properties could not be guaranteed to be uniform over the entire area of the bottom plate under similar growth conditions. After reaching this point, we carried out the following experiment to achieve uniformity in R.I, resistivity and thickness.

To extract the optimum growth conditions, (conditions corresponding to nearly uniform properties in the deposited films), we placed the substrates (as already mentioned), at three different positions in the chamber, namely, at the centre, position-1 and position-2. Position-1 and position-2 are 5" away from the centre in diametrically opposite directions. The three positions were chosen to be co-linear.

It is important to check for symmetry, if any, in the properties of the films grown at the three different positions. The various growth conditions under which the films were deposited are listed in Table-3.2. These films were investigated using ellipsometery and electrical measurements. In the preliminary investigation, we measured the Refractive Index (R.I), thickness and resistivity (ρ). A comparison of resistivities of the films deposited under the same growth conditions was made at an electric field of1 $MVcm^{-1}$.

Table-3.2 Set of growth conditions used to optimise the a-C:H films

RUN No.	**CH_4 Flow Rate (sccm)**	**Ar Flow Rate (sccm)**	**Chamber pressure (mTorr)**	**DC-Self bias (Volts)**	**Growth time (minutes)**
61	10	68	100	-160	25
62	10	140	100	-160	25
63	5	68	100	-160	25
64	20	68	100	-160	25
65	20	140	100	-160	25
67	**10**	**100**	**100**	**-160**	**25**

The R.I, thickness and resistivity (measured at five different locations of each sample) of the films grown at the three different positions, during the runs mentioned in Table-3.2 are displayed in bar-chart form, in Fig.-3.5. It is clear from Fig.-3.5 that there is a large spatial variation in the film properties grown under the same growth conditions. The thicknesses and R.I of films deposited at different locations in RUN 62 are very similar. However, the resistivity of the film deposited at the centre of the reactor, during this run, is 3 orders of magnitude higher than for the films grown at position-1 and position-2. The values of resistivity and R.I are quite similar for all three films during RUN-64. The only difference is in the thickness. Films deposited in RUN-61, RUN-63 and RUN-65 do not show much overlap in the properties. This investigation showed that even when the dc-self bias is maintained as a constant for all the depositions, flow

dynamics and molar concentration play a major role in determining consistency of the film properties.

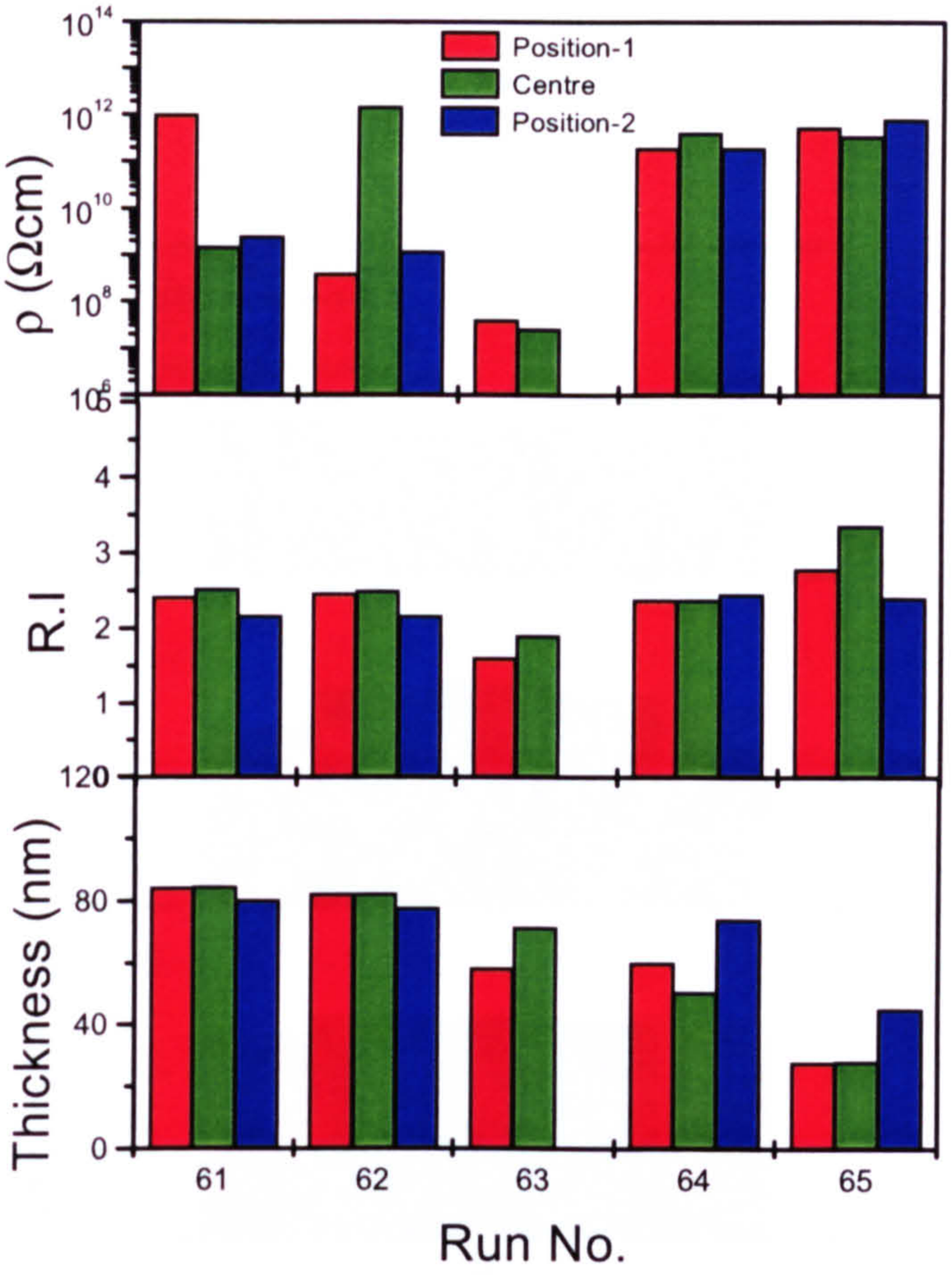

Fig.-3.5 Variation in the resistivity, thickness, and R.I of the a-C:H films deposited at three different positions, (position-1, position-2 and centre of the reactor), under different growth conditions.

This study directed work towards specific flow rates for methane and argon, namely 10 sccm and 100 sccm respectively. It can be observed from Table-3.2 that during run

number 67 the flow rates match the values mentioned above. Films grown at the three different positions, with these flow rates showed encouraging consistency over the different material properties. To make a thorough check, we proceeded to carry out run number 67 again, but this time with the substrates placed at five different locations, Right postion-1, Right position –2 , Centre, Left position – 1 and Left position-2.

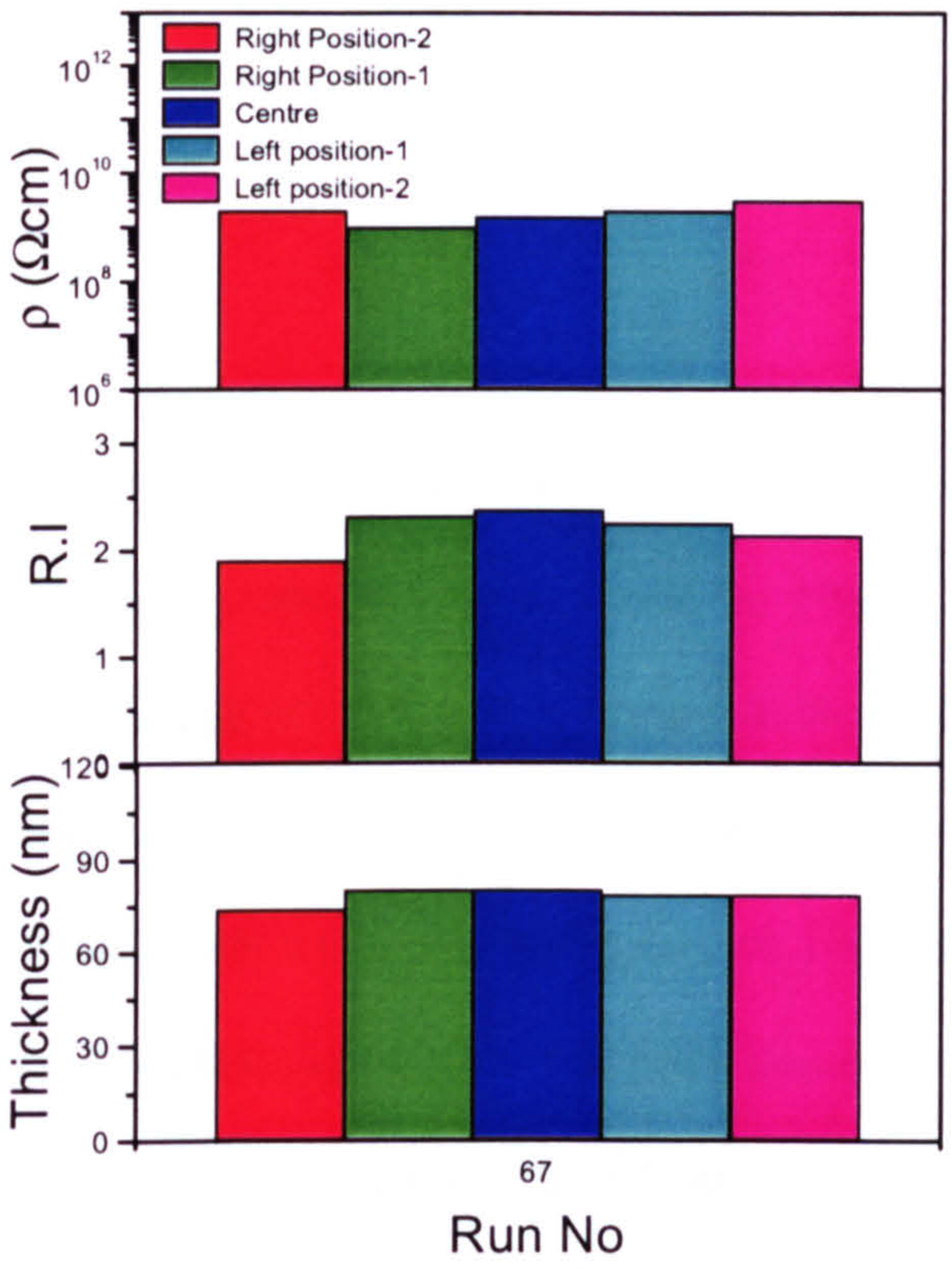

Fig.-3.6 Variation of resistivity, R.I and thickness, when substrates were placed at five different locations under same growth conditions and flow rates of 10sccm and 100 sccm for methane and argon respectively.

The film properties corresponding to this run are shown in the Fig,-3.6. It is quite clear from the bar chart that the properties of the films at the five different positions, deposited during this run, are quite similar.

We have also investigated the change uniformity of the thickness under same similar growth conditions at a given values of DC self bias. The films were quite uniform at three different locations and there is hardly any change in the film thickness under same growth conditions at given values of DC self bias voltage.

Summary

The investigation carried out in this chapter helped us to obtain uniform film properties over a large area in the deposition chamber. This is a very simple empirical approach, which we developed in the laboratory by considering three parameters, namely, thickness, R.I and resistivity. In this way, one can obtain uniform properties of the film on large substrates. This is an important step to prepare DLC for large area electronics, where the size of the substrates can be $1ft^2$. We have also seen that at a pressure of 100 mTorr we can obtain maximum variation in the ion energy and consequently in the properties of the films deposited under dc self bias voltage. We have typically deposited a-C:H from a mixture of 100 sccm of Ar and 10 sccm of CH_4 at a pressure of 100 mTorr and at room temperature by varying the DC self-bias voltage. These growth conditions were maintained, (unless otherwise stated), throughout our investigations. Now, it vital to understand film properties in greater details to realise devices out of a-C:H. The next

chapter is dedicated to a study of the detailed properties of the films deposited in our laboratory.

References

1. J.Robertson, *Adv. Phys*, **35**, 317 (1986).
2. K.JClay, S.P.Speakman, N.A.Morrison, N.Tomozeiu, W.I.Milne, A.Kapoor, *Diamond Relat. Mater.*, **7**, 1100 (1998).
3. J.Walker, *Rep. Prog. Phys.*, **42**, 1605 (1979).
4. K.W.R.Gilkes, H.S.Sands, D.N.batchelder, J.Robertson, and W.I.Milne, *Appl. Phys. Lett.*, **70**, 1980 (1997).
5. Y.Ando, X.Zhao, H.Kataura, Y.Achiba, K.Kaneto, M.Tsuruta, S.Uemura, and S.IiJima, *Diamond Relat. Mater.*, **9**, 847 (2000).
6. J.Y.Feng, N.G.Shang, X.S.Sun, I.Bello, C.S.Lee, and S.T.Lee, *Diamond Relat. Mater.*, **9**, 872 (2000).
7. D.R.Mckenzie, *Rep. Prog.Phys.*, **59**, 1611 (1996).
8. D.P Uskokovic, S.K Milonjic, D.I Rakovic, *Materials Science Forum*, **282-2**, 239 (1998).
9. U. Falke, A.K Weber, J. Ullmann, Microsc. Microanalysis. Macrostr., **6(1)**, 113 (1995).
10. X.He, W.Li, and H.Li, J. Vac. Sci. Technol. A **11** (6), 2964 (1993).

11. X.He, W.Li, and H.Li, J. Vac. Sci. Technol. A **14** (4), 2039 (1996).

12. H.Vora and T.J. Moravec, *J. Appl. Phys.*, **53**, 6151 (1981).

13. K.C. Park, J.H. Moon, J. Jang, and M.H. Oh, *Appl. Phys. Lett.*, **68**, 3594 (1996).

14. F.F Chen, *Introduction of Plasma Physics and Controlled Fusion*, 2nd ed., New York: Plenum Press, 1984.

15. I.B. Chapman, *Glow Discharge Processes: Sputtering and Plasma Etching*, New York: John Wiley & Sons, 1980.

16. J.A. Thornton, and A.S. Penfold, *Thin Film Processes*, eds. J.L. Vosson, and W.Kern, New York: Academic Press, 1978.

17. J.K Lee, K.Y Eun, H.B Chae, and Y.J Baik, *Diamond Relat. Mater.*, **9**, 364 (2000).

18. L. Holland and S.M. Ojha, *Thin Solid Films*, **38**, L17 (1976).

19. W.Zhu, B.R Stoner, B.E.Williams, and J.T Glass, *Proc. of the IEEE*, **79**, 621, (1991).

20. S.R.P Silva, G.A.J.Amaratunga, and C.P.Constantinou, *J. Appl. Phys.*, **72**, 1149 (1992).

21. H.S. Butler and G.S Kino, *Phys. Fluids*, **6**, 1364 (1963).

22. J.C. Angus, P. Koidl, S.Domitz, *Plasma Deposited Thin Films*, CRC Press, Boca Raton, FL, 1986.

23. R.O.Dillon, J.A. Woollam, V.Katkanat, *Phys.Rev. B*, **29**, 3482 (1984).

24. B.Dischler, A. Bubenzer, P. Kiodl, *Solid State Commun.*, **48**, 10 (1983).

25. T. Catherine, *In Diamond and Diamond-like Films and Coating, NATO-ASI Series B: Physics*, eds., R.E Clasing, L.L. Horton, J.C Angus, and P. Koidl, **Vol. 226**, p.193, New York: Plenum Press, 1991.

26. P. Koidl, C.Wild, B.Dischler, J. Wagner and M. Ramsteiner, *Mat. Sci. Forum*, **52&53**, 41 (1989).

27. A. Bubenzer, B.Sischler, G. Brandt, P.Koidl, *J. Appl. Phys.*, **54**, 4590 (1983).

28. S.R.P Silva, Ph.D Thesis, Dept. Of Engineering Cambridge University, 1993.

29. J. Robertson, Phil. Trans. R. Sco. Lond. A, 342, 277 (1993).

30. Y. Lifshitz, S.R. Kasi, J.W. Rabalais, and W. Eckstein, Phys. Rev. B, 41, 10468 (1990).

31. D.R Mckenzie, D. Muller and B.A Pailthorpe, Phys. Rev. Lett, 67, 773 (1991).

32. M. Rosenberg, *J. Vac. Sci. Technol. A*, **14(2)**, 631 (1996).

33. J H Chu, Ji-Bin Du and Lin I, J. *Phys. D: Appl. Phys.* **27**, 296 (1994).

34. Y.Watanabe, *Plasma Phys. Control. Fusion,* **39**, A59 (1997).

35. S Raoux, D Cheung, M Fodor, W.N Taylor and K Fairbairn, *Plasma Sources Sci.Technol.*, **6**, 405 (1997).

36. A Bouchoule and L Boufendi, *Plasma Sources Sci.Technol.*, **3**, 292 (1994).

37. R J Seebock, W Bohme, W E Kohler, M Romheld and S Veprek, *Plasma Sources Sci.Technol.*, **3**, 359(1994).

38. A.P Burden and S.R.P Silva, *Appl. Phys. Lett.*, **73**, 3082 (1998).

39. A.P Burden, J.V Anguita and S.R.P Silva, Thin Solid Films, **332**, 252 (1998).

40. A.E Wendt and W.N.G., *J. Appl. Phys.*, **71**, 4718 (1992).

CHAPTER-4

Experimental Characterisation of Hydrogenated Amorphous Carbon Films

The last chapter, (Chapter-3) was devoted to a discussion of the achievement of uniformity of different properties, (thickness, resistivity and refractive index, R.I) of a-C:H films, deposited over a large area of the lower electrode in our PECVD reactor. This chapter focuses on the influence exerted by the DC self-bias voltage on these and a few other properties of the a-C:H films, (such as, growth rate, hydrogen composition, structure of the film, bandgap, surface morphology and defects).

To understand the effect of the self-bias on the aforesaid properties, we need to compare a-C:H films deposited under different values of the DC bias. Such a comparison is meaningful only if any other parameter that has a bearing on the film properties, is maintained a constant. Film thickness is such a parameter; hence the thickness of the films must roughly be the same for any such comparison to be reliable. After consulting available literature, it is understood that generally, consideration of film thickness is ignored while comparing corresponding properties of different films [1,2]. The first section of this chapter deals with the scheme adopted to achieve roughly the same thickness of a-C:H films deposited at different bias voltages.

Deposition of amorphous carbon by PECVD is a non-equilibrium process, characterised by the interaction of energetic ions with the surface of the growing film[3]. The meta-stable

structure of amorphous carbon most likely originates from the thermal and pressure spikes, produced by the impinging energetic species, at the growth surface [4]. The rate at which ions strike the growing surface and their energy at impact, are important factors which determine the growth of films deposited under different DC bias. The explanation of the bias dependence is relatively simple and has been discussed by various workers [5,6,7].

Firstly, the bias dependent growth of a-C:H is considered. The deposition rate of a-C:H decreases with increasing DC self-bias. It has been reported that the growth of a-C:H films takes place through the interaction between the substrate surface and a physio-absored hydrocarbon layer [3]. There is always a competition between the growth and etching processes on the surface of the growing film. The etch rate is primarily a function of ion energy. Higher the energy, higher is the etch rate. Therefore, an increase in the DC self-bias causes an increase in the etch rate, which subsequently decelerates growth. Thus a film that is deposited at a higher bias has a lower growth rate. However, it is not merely the quantity of the deposited material that is affected by changes in the self-bias; the quality of the film too undergoes a change, depending on the value of the bias. The ion energy is higher at a higher bias; consequently the softer parts of the film can be etched away relatively easily when the ions strike the growing surface with a higher energy. This implies that the films deposited at a higher bias are harder, as characterised by a higher percentage of sp^3-like network; this is due to the removal of the softer portions (sp^2-like) of the film at higher DC bias voltages. It is obvious that a greater percentage of the softer parts of the film will be etched away if the film is subjected to the etching process for a longer time, i.e. the growth time increases, (as long as

the bias is high enough to induce an effective etching process). This explains the time dependence of the growth of a-C:H films. Thus we expect the film properties to be functions of growth time and DC self-bias, in general.

4.1 Film Thickness as a Function of Deposition Time

To optimise the thickness of a-C:H films, for a particular device application, it is important to know the growth rate of the film, under a set of given growth conditions. To establish this, we deposited films at five different DC bias, (-75 V, -135 V, -200 V, -240 V, -295 V), for growth times of 5, 10, 20, 40 and 60 minutes. The films were deposited from the gas mixture of CH_4 (10 sccm) and Ar (100 sccm), at room temperature and a chamber pressure of 100 mTorr. The outcome of this experiment is plotted in Fig.-4.1 (A), which shows variation in thickness with change in deposition time, as a function of DC self-bias. Fig.-4.1 (B) shows the growth rate plotted against growth time.

The growth rate plot in the Fig.-4.1 is calculated by using the following formula:

$$Growth\ \ rate = \frac{d}{t} \qquad \ldots\ldots\ldots\ 4.1$$

Here d is the thickness of the deposited material in time t.

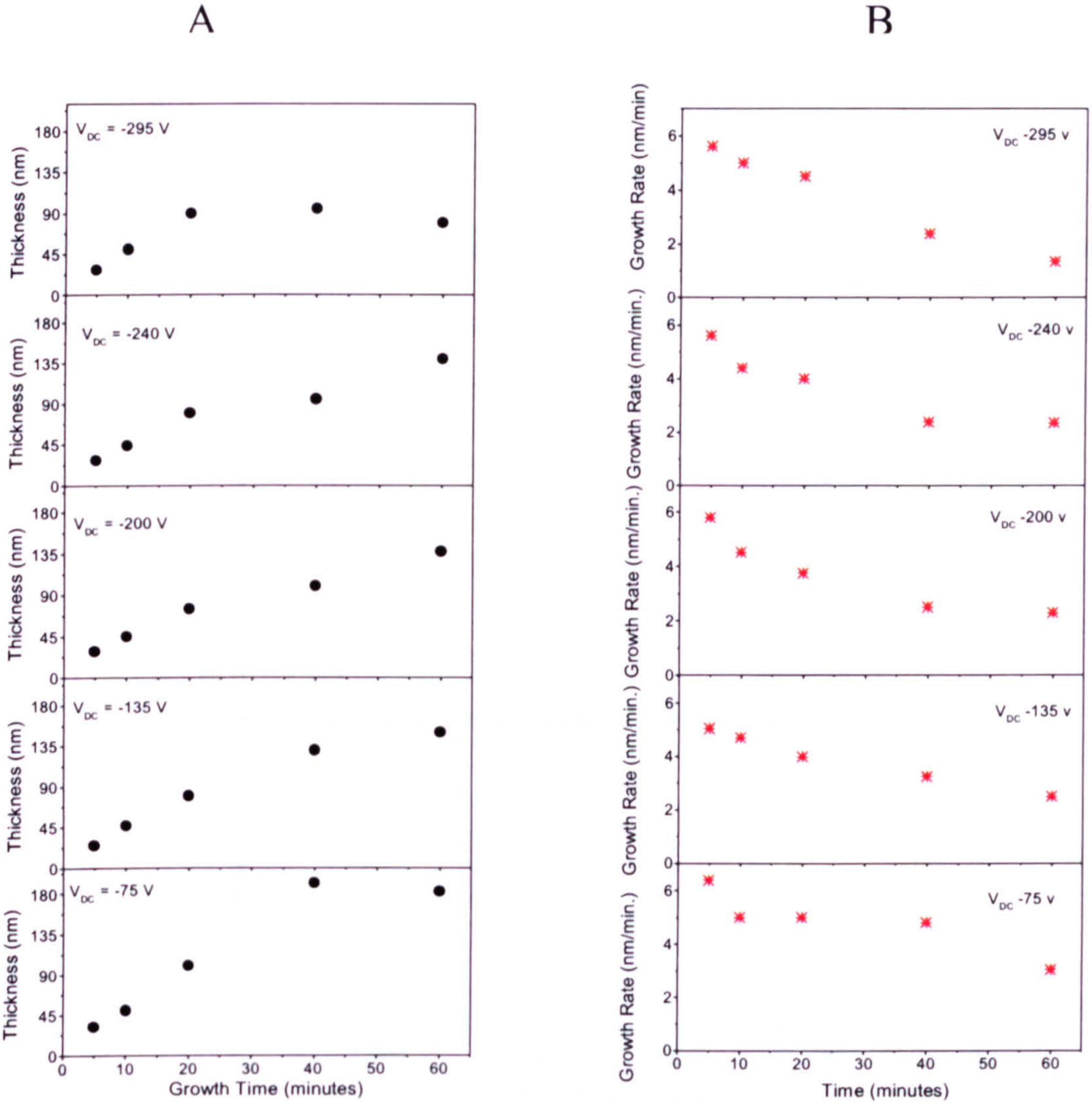

Fig.-4.1 Thickness and growth rate plotted against time at five values of the DC self bias.

It is quite clear from the plot that, in general, the growth rate decreases with increase in the self-bias. At the same time, growth rate falls with increase in the growth time. This means that a simultaneous etch/deposition process is taking place in the rf plasma deposited films [8]. When the deposition time is large, the dominating process is etching. This is clear from Fig.-4.1 (A) which shows that thickness of the film does not change much at high deposition

time. At a higher DC self-bias (≥ -200 V), etching is more dominating than at a lower bias. Thus, by controlling the DC self-bias voltage and deposition time, it is possible in principle, to balance the two competing processes in order to realise films of desired thickness. This is recognised as the *modus-operandi,* that we implemented to control film thickness.

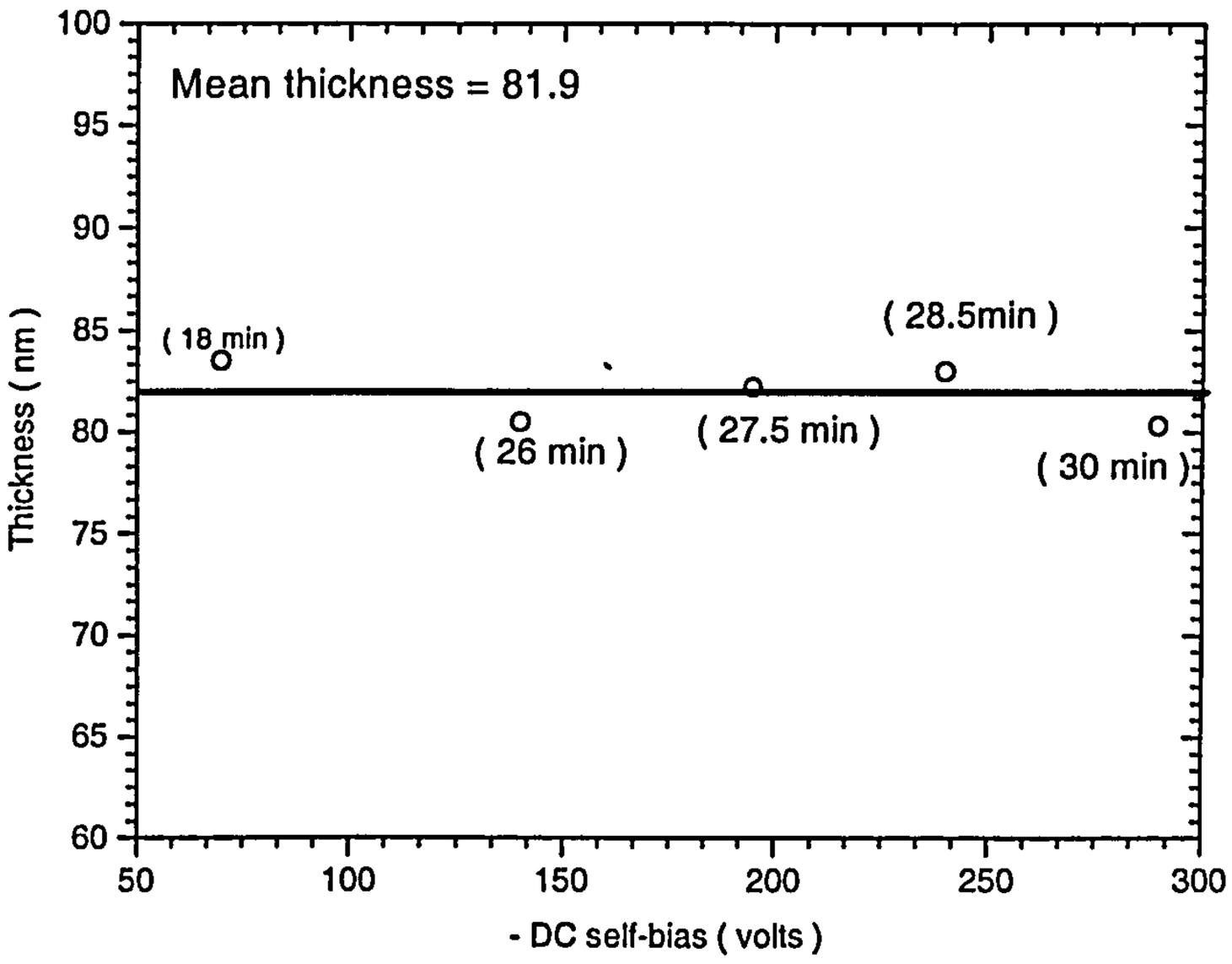

Fig.-4.2 Thickness plotted against DC bias voltage at different growth times.

Now film thickness is a function of DC bias and growth time. However, as was mentioned before, in order to compare properties of films deposited under different bias voltages, the films must be approximately of the same thickness. We achieved roughly the same thickness in the grown films by recording the growth times corresponding to a chosen

thickness, (about 82 nm), at different DC self-bias, (see Fig.-4.1). The growth times corresponding to the standard thickness (~82 nm) at the values of DC bias voltages have been marked in Fig.-4.2.

We hereafter discuss the bias dependence of different film properties, by looking at films of approximate thickness 82 nm. In order to test our thickness optimisation technique, we can compare the measured bias dependence of any material property of such films, with the expected bias dependence of the same property. A favourable comparison will imply that all the films used in the investigation have approximately the same thickness. The results of a test investigation of one important property, namely refractive index (R.I.), is discussed in the next section.

4.2 Refractive Index of the standard thickness film

R.I is an intrinsic material property that represents the compaction of the film. It has been described before, that increasing the bias leads to greater etching of the softer parts of the film, rendering the film harder. Hence, we expect film compaction to increase with increasing bias values. R.I of the films deposited (of same thickness ~82 nm) at different DC bias voltages are shown in Fig.-4.3. The plot shows that there is a gradual increase in the R.I with increase in the bias. The value of R.I of the films deposited in our laboratory, lies between 1.8 to 2.8. Our R.I values are in good agreement with the reported values [9,10] of R.I for a-C:H deposited by PECVD. It is observed that in Fig.-4.3, the R.I drops from 2.70 to 2.56 when the bias is changed from -270 V to –295 V. This is attributed to the very high

energy of the ions that bombard the surface causing the deposited films to be highly stressed. To release this high stress, the film tends to unfurl which leads to its loss of compactness.

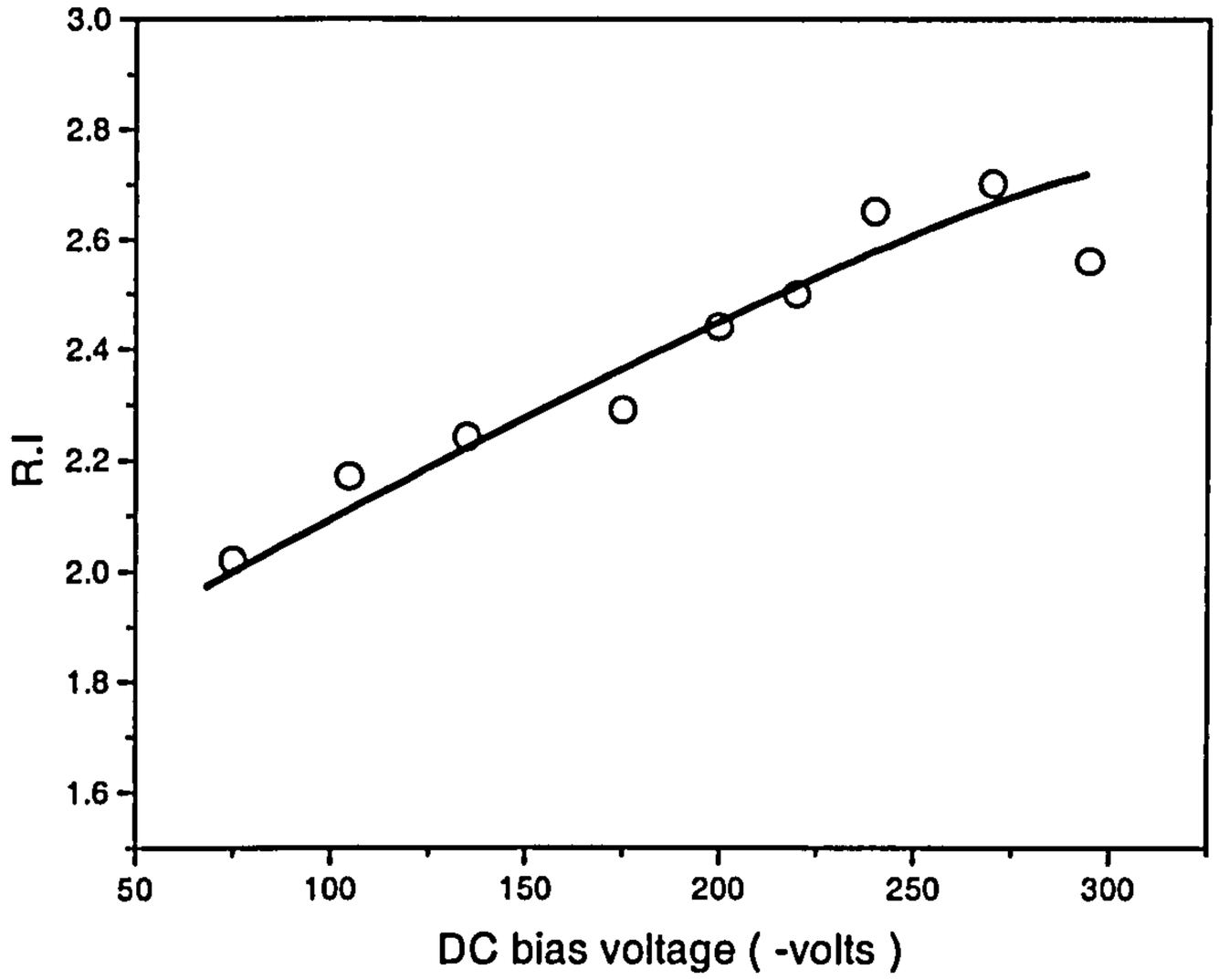

Fig.-4.3 R.I of a-C:H films of ≈ 82 nm thickness, plotted against DC bias

4.3 Effect of Bias on Resistivity of standard films

Film resistivity is an important parameter to realise a device out of any semiconducting material. Generally in crystalline semiconductor materials, the resistivity is invariant under changes in the applied electric field. But in the case of amorphous materials, this is not true [11,12]. This non-linear behaviour of the resistivity is caused by electronic conduction mechanisms within the amorphous semiconductor, (such as, hopping in amorphous silicon, Poole-Frenkel in the amorphous carbon, etc.). In hydrogenated amorphous carbon (except

the polymeric amorphous carbon) the charge transport mechanism is governed by the Poole-Frenkel conduction [12,13,14].

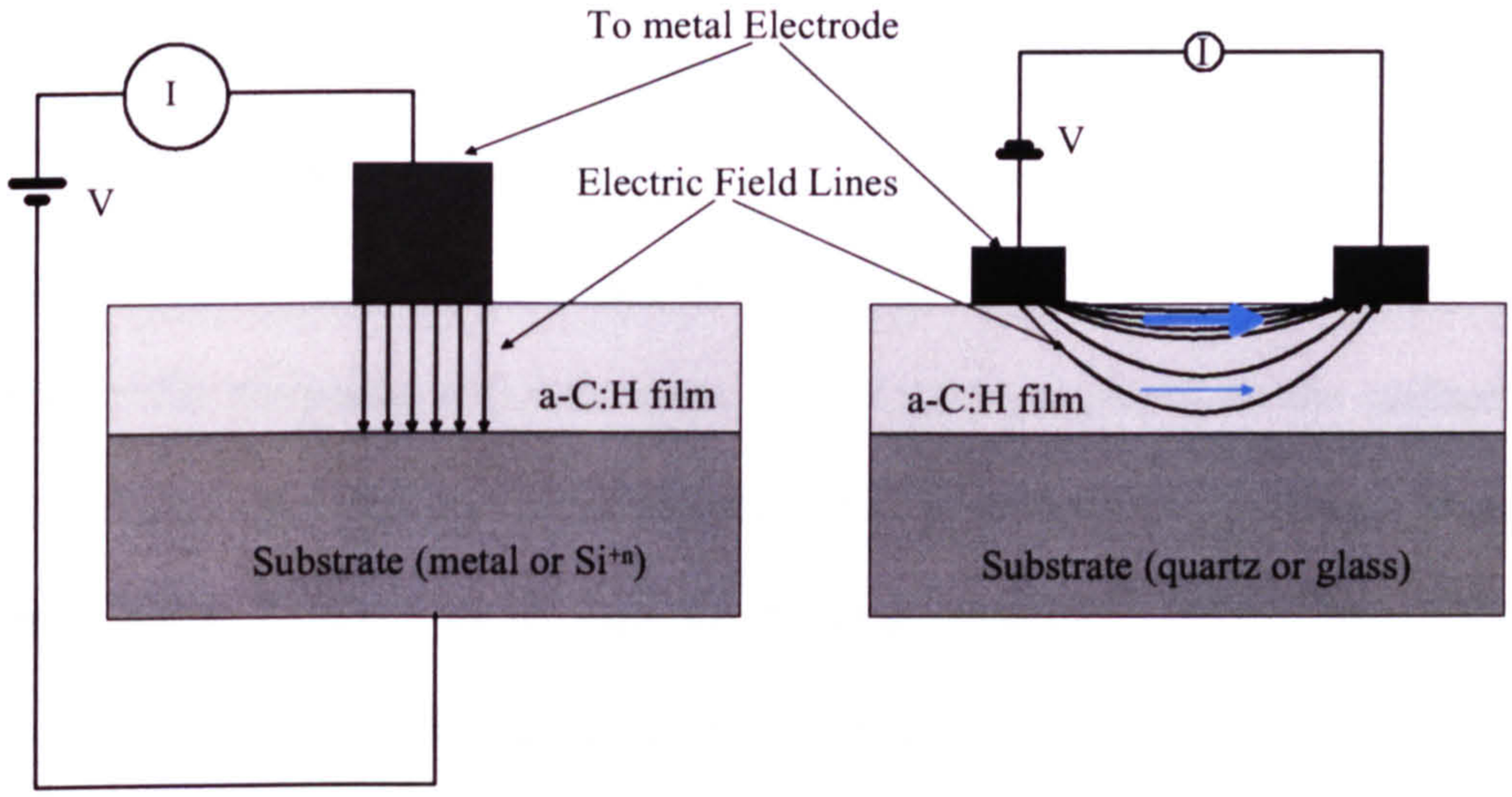

(a) Sandwich Strucutre

(b) Gap Cell Strucutre

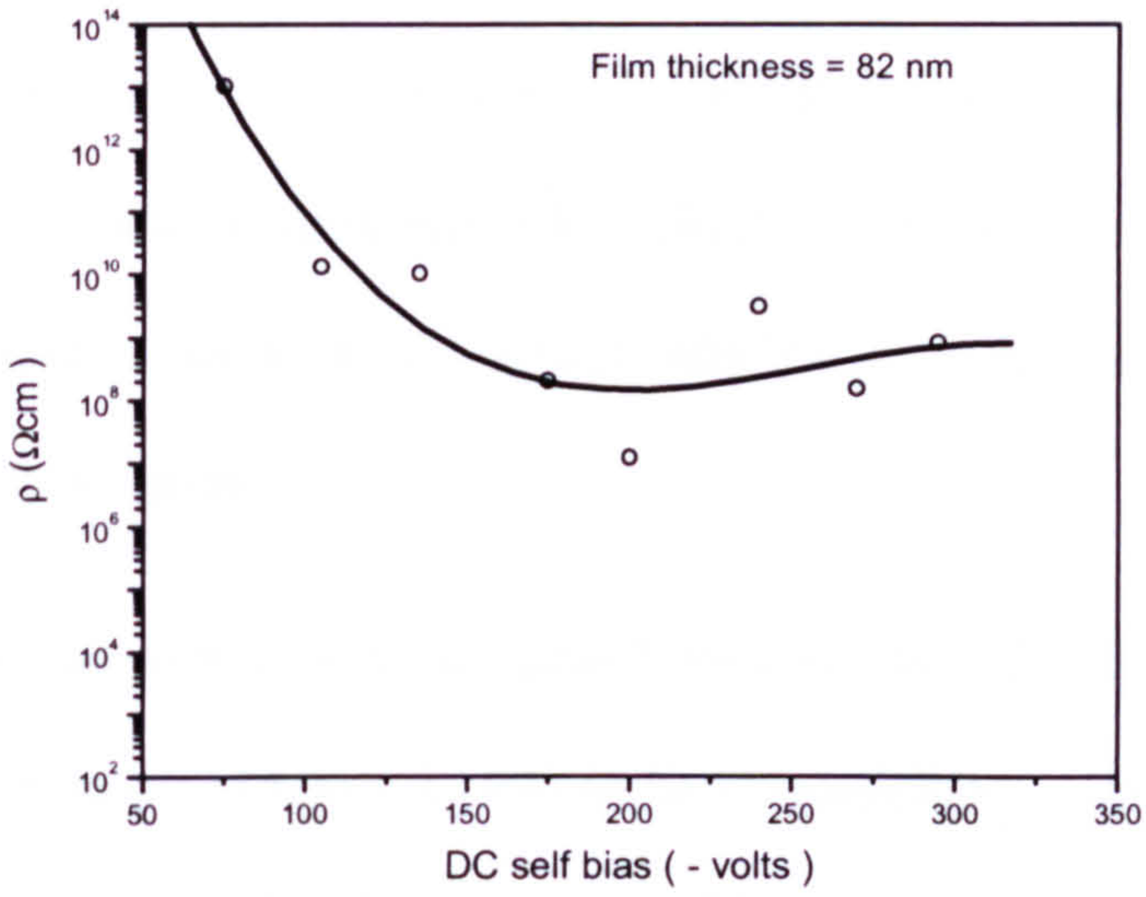

(c)

Fig.-4.4 (a) and (b) Schematic diagrams of sandwich and gap cell measurement arrangement (c) Resistivity of a-C:H films of optimised thickness, plotted against DC self bias.

The recorded value of resistivity can be effected by the measurement techniques. The two techniques commonly used in amorphous materials are the planar structure (gap cell type) or the sandwich structure (Fig.-4.4 (a) & (b)). We preferred the sandwich structure in our experimentation. The sandwich structure measures the resistivity across the depth of the material while the planar structure makes use of contacts placed on the surface of the film. Illie [13] has shown that the resistivity measured perpendicular (sandwich structure) to the substrate is 2 to 3 orders higher than the resistivity measured parallel (gap cell structure) to the substrate in hydrogenated tetrahedral carbon. The difference in the resistivity was explained on the basis of the anisotropic nature of the constituent sp^2 nano clusters.

The resistivity of highly orientated pyrolitic graphite (HRPG) along the c-axis is 10^{-1} Ωcm, while the resistivity in the basal plane is 10^{-4} Ωcm [14]. The lower value of resistivity in the basal plane is due to delocalisation of the π electrons over the whole graphitic sheet and the higher value of resistivity along the c-axis is due to the weak van der Waals bonding between the graphite sheets.

Diamond-like carbon materials are made from a number of different phases and they are inhomogeneous in nature [15,16,17]. The surface of tetrahedral carbon has been investigated extensively and it has been found that it is consists of conductive sp^2-layer [18,19,20]. There are a few investigations which show that there are sp^2 type clusters on the surface of a-C:H films [20,21,22]. Rusman et al [22] extensively investigated the surface of a-C:H films using

scanning electron microscopy/scanning tunnelling spectroscopy. In this investigation, it has been shown that surface of a-C:H films is made up sp^2-like clusters. The sp^2 clusters on the surface can make the surface behave differently from the bulk. In the gap cell measurements electric field lines are crowded near the surface (as shown in Fig.-4.4 (b)) and the measured current is more likely to be from or near the surface. Thus the configuration of the electric field lines in the gap cell measurement and the sp^2-like clusters on the surface, results in a different surface resistivity than the bulk. This justifies our choice of the measurement technique given the multi-faceted nature of carbon.

The plot showing resistivity as a function of DC self-bias is shown in Fig.-4.4 (c). The observed trend is a decrease in resistivity with increase in the bias voltage; the same trend has been observed by other workers in a-C:H layers deposited by PECVD [9,23,24]. This trend is explained on the basis of a decrease in the bandgap of a-C:H. We have also observed the same trend in the bandgap as a function of DC self-bias voltage. This is discussed in greater detail in Section-4.5.

Typically, the resistivity of the films deposited in our laboratory range from 10^6 to 10^{13} Ωcm; this is in agreement with values already published [9]. The extraordinary property that resistivity of amorphous carbon can vary from the semiconductor to the insulator range, can be exploited to utilise the material as an insulator layer as well as an active semiconductor layer in MIS structures.

4.4 Infrared Spectroscopy:

The hydrogen concentration (bound and unbound hydrogen) in an amorphous materials plays an important role in determining the electrical and optical properties of the a-C:H [25,26]. A key parameter in device performance is the density of states (DOS). In hydrogenated amorphous silicon (a-Si:H), the DOS is greatly influenced by the hydrogen concentration in the material [27]. It is believed that the presence of hydrogen reduces dangling bonds and hence the density of states. By extrapolating from studies of amorphous silicon, we can anticipate that the presence of hydrogen in a-C:H may have a significant effect on performance of a-C:H based devices. This section deals with the relative variation in hydrogen with DC self-bias voltage. A commonly used technique to estimate the hydrogen concentration in a-C:H films, is that of Infra Red Spectroscopy [28,29,30]; it has been discussed in details in Chapter-2.

A free-standing film of a-C:H would be an ideal source for any infra-red investigation. Such an investigation can eliminate any effects that the substrate may have in distorting vital information about the film properties. However, it is very difficult to prepare a free standing a-C:H film. In general, low p-type doped Si substrates are used for IR investigation of a-C:H since such a substrate allows a high transparency to infra-red wavelengths. We investigated the IR transmission of four different substrates (corning glass, Si^{+n}, Si^{p} and quartz) in optimising the properties of our amorphous material. The transmission spectra of these substrates are as shown in the Fig.-4.5. It is quite clear from these spectra, that the transmission of IR through the Si^{+n} substrate is very poor. Therefore, it is unwise to use Si^{+n}

for the IR investigation. The corning glass substrate does not offer an extensive IR transmission window which can be employed for the IR investigation of a-C:H.

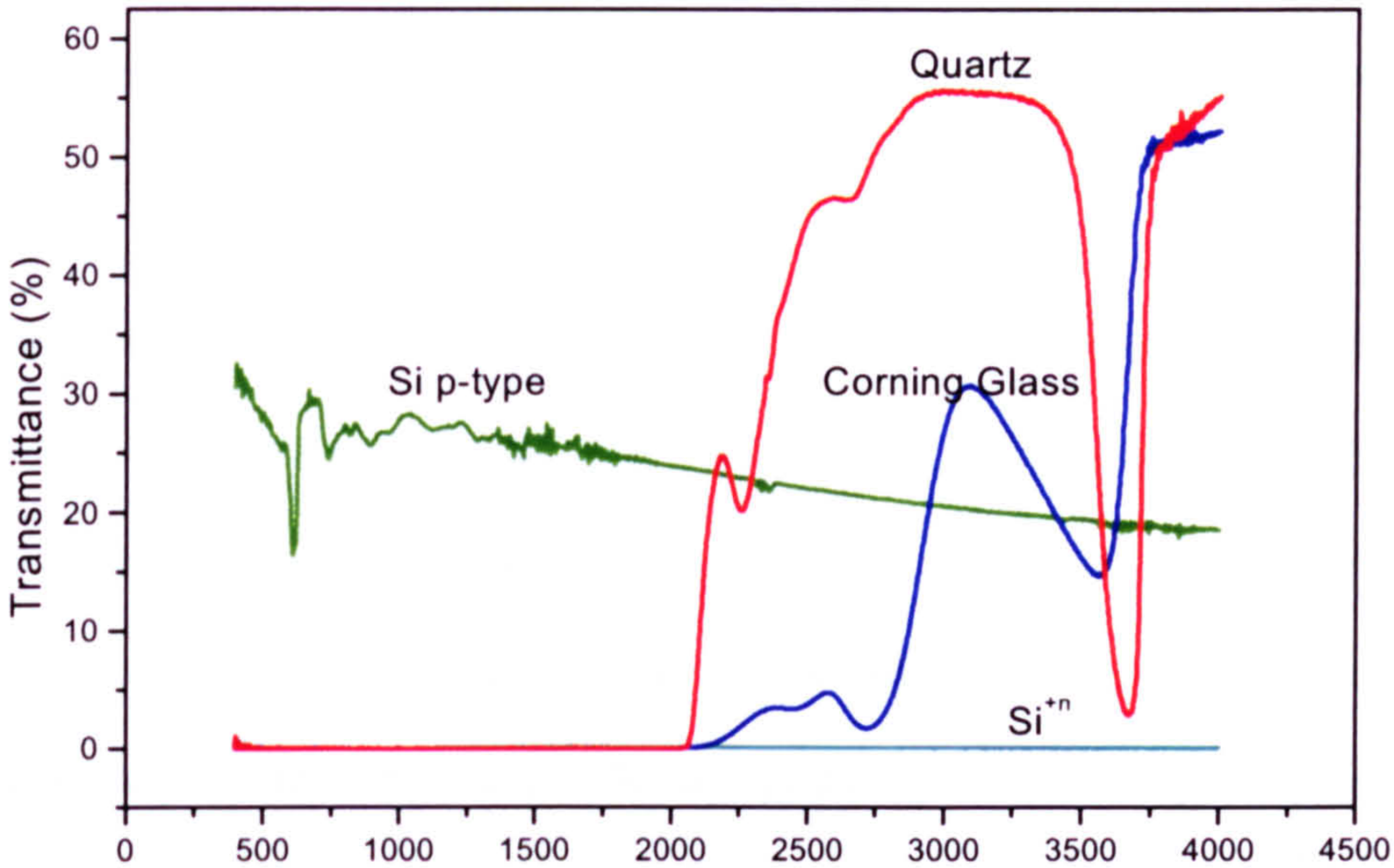

Fig.-4.5 Transparency of various substrates to IR.

The low doped p-type substrate shows an approximately constant transmission, (between 20 - 30%). On the other hand, the quartz substrate shows the highest transparency (55%) to IR, in the range of 2000 cm^{-1} to 3600 cm^{-1} [29,30]. The most significant IR spectra for a-C:H lies within this window. Therefore, quartz may be the right candidate to serve as a substrate for the IR investigation of the a-C:H. However, a-C:H films are commonly deposited on low doped p-type substrates for IR analyses. In view of the study of

transmission spectra discussed above, the arguments in favour of using such a substrate could not be ruled out completely. Hence we deposited a-C:H films on p-type silicon substrate and quartz, at different DC self-bias and made a spectral study of the same in the IR region.. The IR spectra obtained from films deposited on these two types of substrates are shown in Fig.-4.6.

It is evident from Fig.-4.6 that the spectra collected from films deposited on the quartz substrate are less noisy than from the film deposited on the low-doped p-type silicon substrate; the latter spectrum is characterised by multiple crests and dips suggesting less absorption of IR by the quartz substrate in the considered wavelength range than the Si substrate. This merely corroborates the conclusion reached previously, regarding the relative merits of these two substrates, as understood on the basis of transparency of the substrates to IR signal, (Fig.-4.5). On the basis of the results in Fig.-4.6, we decided to deposit our a-C:H films on quartz.

Fig.-4.6(b) displays a wide absorption band of a-C:H films, grown on quartz substrates, centred at about 2900 cm^{-1}. This band is a superposition of absorption peaks of stretching vibration configurations sp^mCH_n, with n,m=1 to 3, [32]. The specific combination of individual peaks that contribute to the 2900 cm^{-1} peak of a-C:H films, depends on the preparatory conditions of the film. With films deposited in our system, we did not see any absorption below a wavenumber of 2400 cm^{-1}. This may be either due to a complete lack of those C-H bonds which absorb IR at lower wavenumbers or very low percentages of these

bonds in our films. The thickness of all these films was maintained to be around 85±5 nm. This was done to ensure correct comparison of the relative concentration of hydrogen in the films.

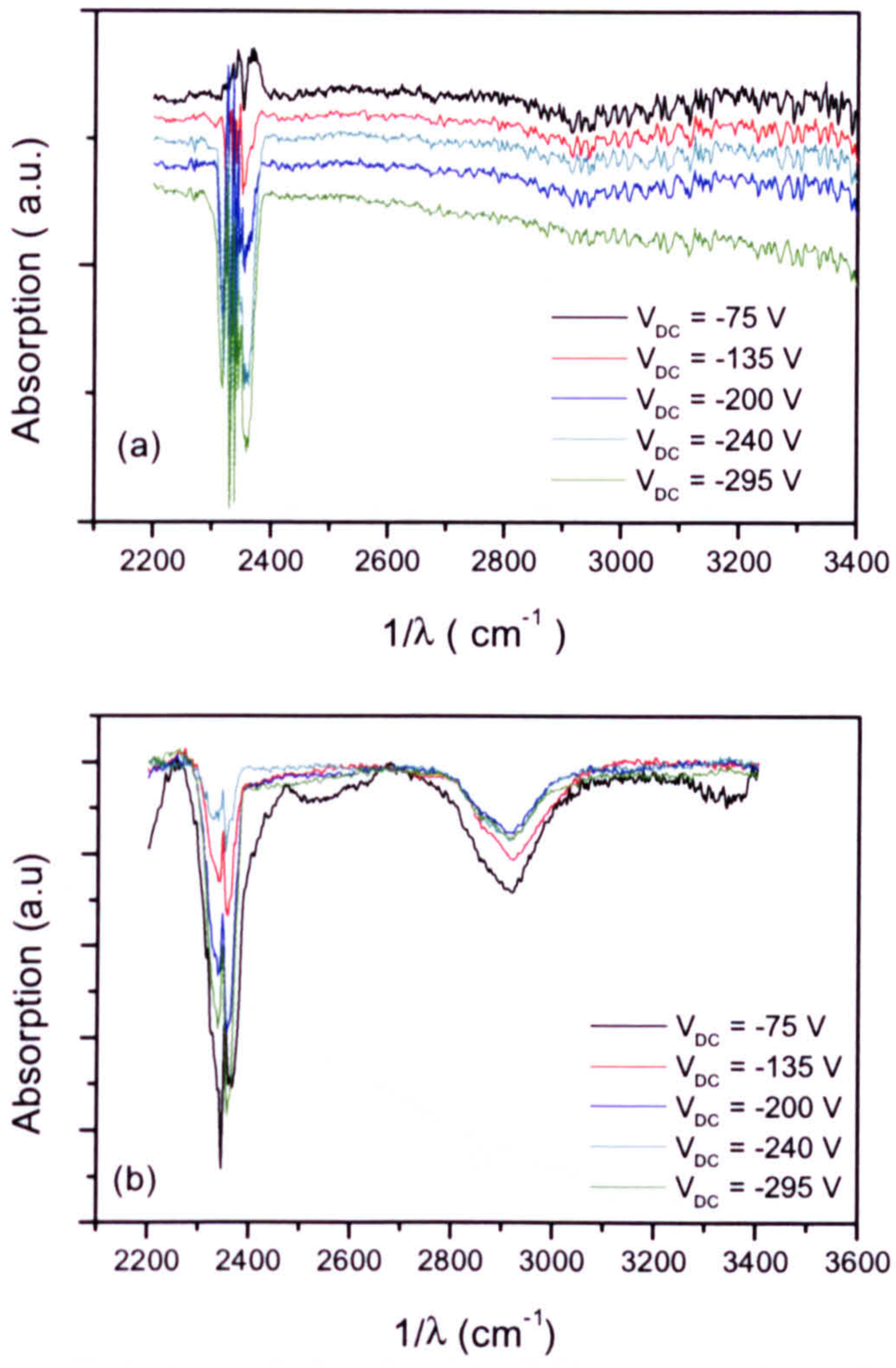

Fig.4-6 IR absorption spectra of a-C:H deposited on (a) low doped p-type Si and (b) quartz substrates, at different DC self-bias voltages.

Typically, in our experimental process, hydrocarbon precursors are used to deposited a-C:H. The precursor(s) and the used deposition technique determine the amount of hydrogen in the film. The content of hydrogen in the film, crucially affects its various properties, such as density of states, resistivity and bandgap. The fractional hydrogen content (C) was estimated by Eqn.-4.2 [31].

$$C = A\int \frac{\alpha}{\omega} d\omega \qquad \ldots\ldots\ldots 4.2$$

Here α is the absorption coefficient of a-C:H, A is a constant and ω is the wavenumber at which the absorption occurs.

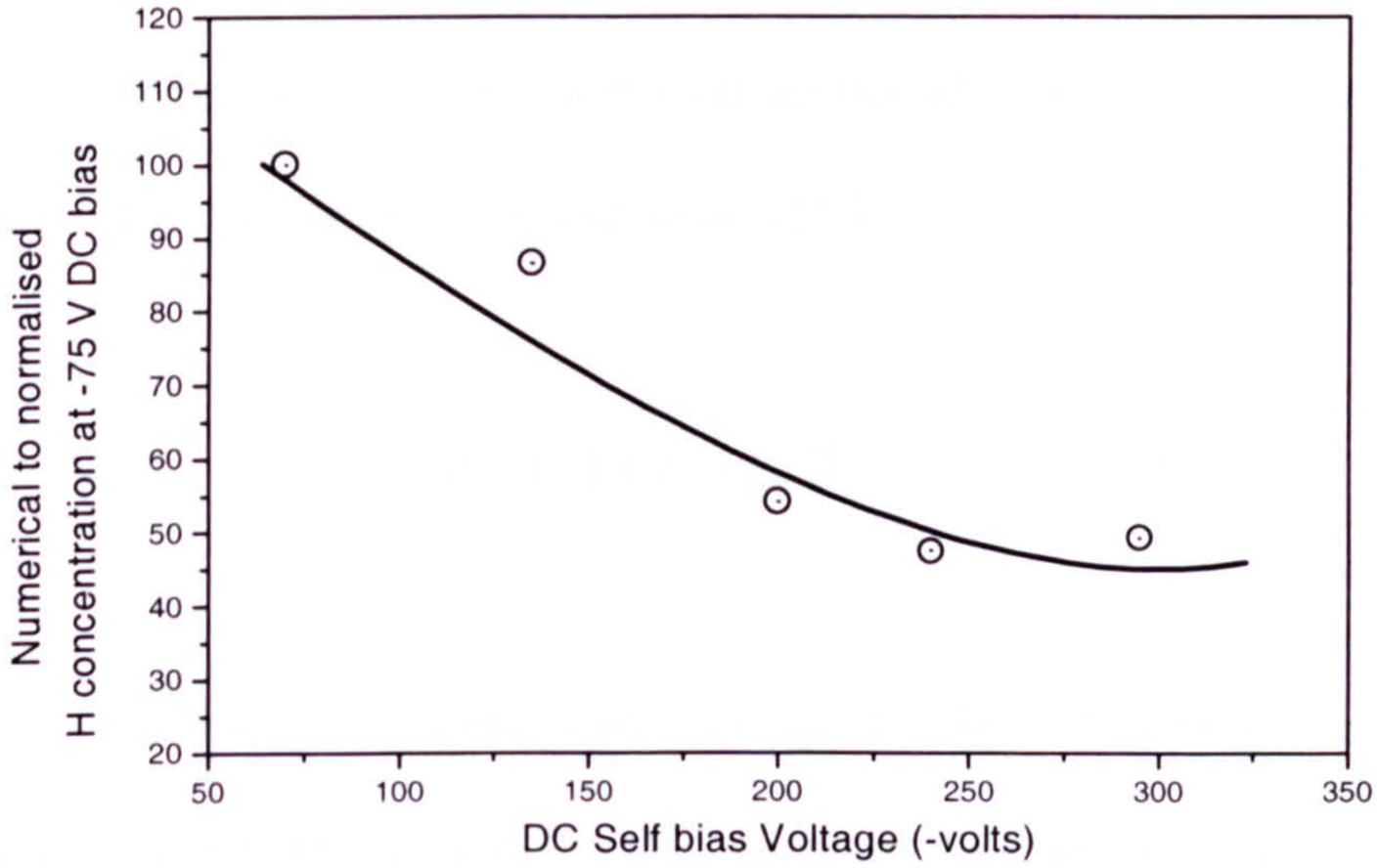

Fig.4.7 Effect of DC-self bias voltage on the hydrogen incorporation in the a-C:H films.

The relative concentration of hydrogen is plotted in Fig.-4.7 as a function of self-bias.

Fig.-4.7 indicates that a decrease in the relative hydrogen concentration is caused by an increase in the DC self-bias [9]. This can be understood on the basis of the changes in the relative fractions of the various phases of carbon with changes in the DC self-bias and more importantly, as a function of the increase in the ion energy with bias. At higher bias voltages the amorphous carbon films are bombarded with ions of higher energies; these high-energy ions can more easily remove any weakly bonded hydrogen from the films.

4.5 UV Spectroscopy

The bandgap of any semiconducting material is an important parameter that helps to realise devices out of the material under consideration. The most commonly used method to determine bandgap in an amorphous semiconductor material is UV/visible spectroscopy. The optical absorption edges of amorphous semiconductors are often analysed with the help of two aides. The first is the Tauc expression [33]:

$$E\alpha(E) = [B(E - E_T)]^2 \qquad (4.3)$$

Here $\alpha(E)$ is the absorption coefficient at energy E; Tauc B parameter; E_T is the optical gap (Tauc gap) of the a-C:H film and E is the energy of the photons used in the spectral analysis. The second tool is the absorption edge of the amorphous material at which the absorption coefficient α equals 10^4; it is referred to as E_{04} [34]. This latter quantity is however of greater

importance in the study of amorphous silicon but not very useful in analysing amorphous carbon. Therefore, we use the Tauc gap to discuss the properties of the amorphous carbon deposited in our laboratory.

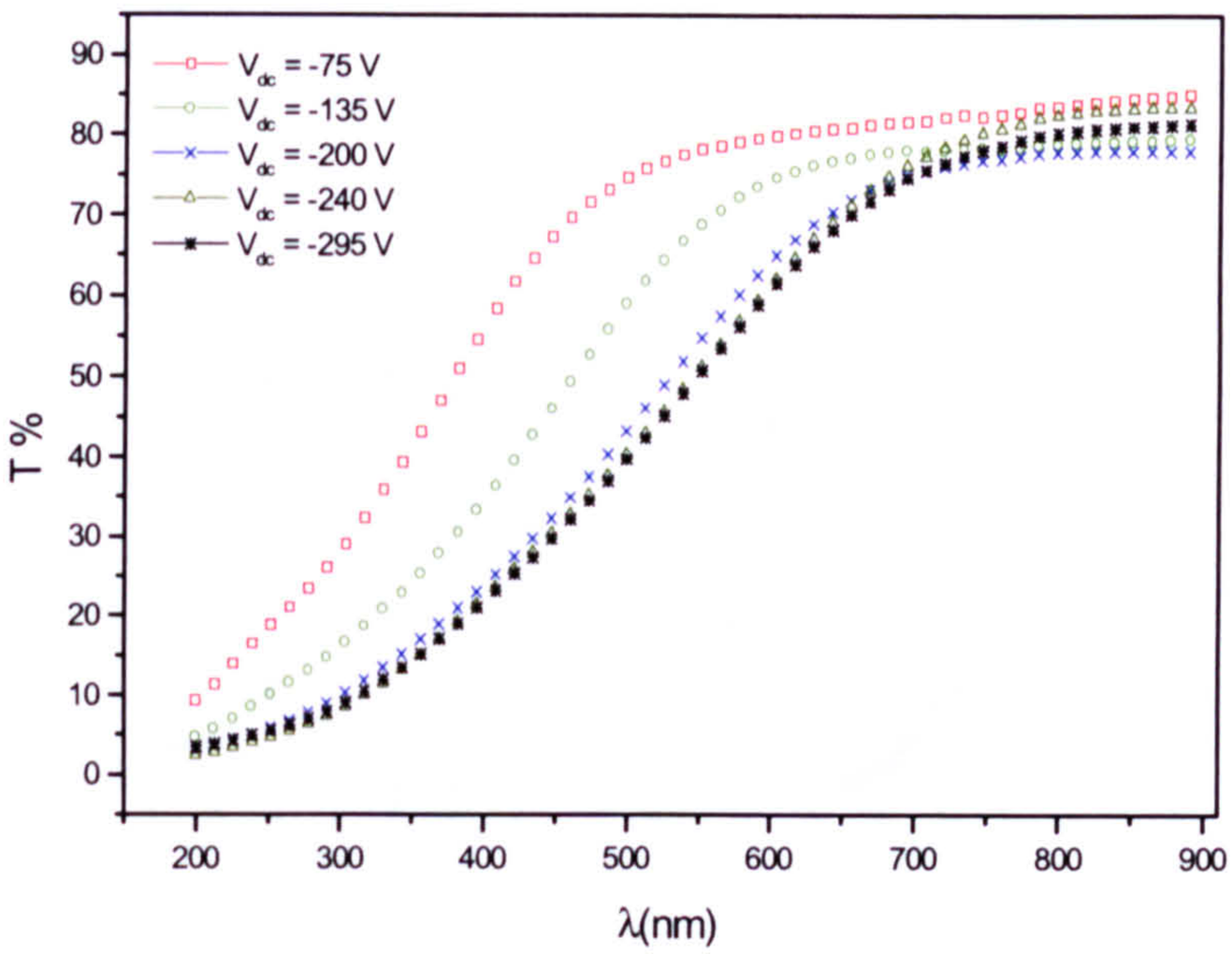

Fig-4.8 Transmittance of UV/visible light through the a-C:H films deposited at different bias.

Fig.-4.8 shows the variation in the transmittance of our a-C:H films with wavelength, in the UV to visible part of the electromagnetic spectrum, at different bias voltages. It is evident from Fig.-4.8 that the DC self-bias voltage has a significant effect on the optical properties of the a-C:H films. The absorption edge shifts towards lower energies, as the DC self-bias voltage increases. This is attributed to a decrease in the bandgap.

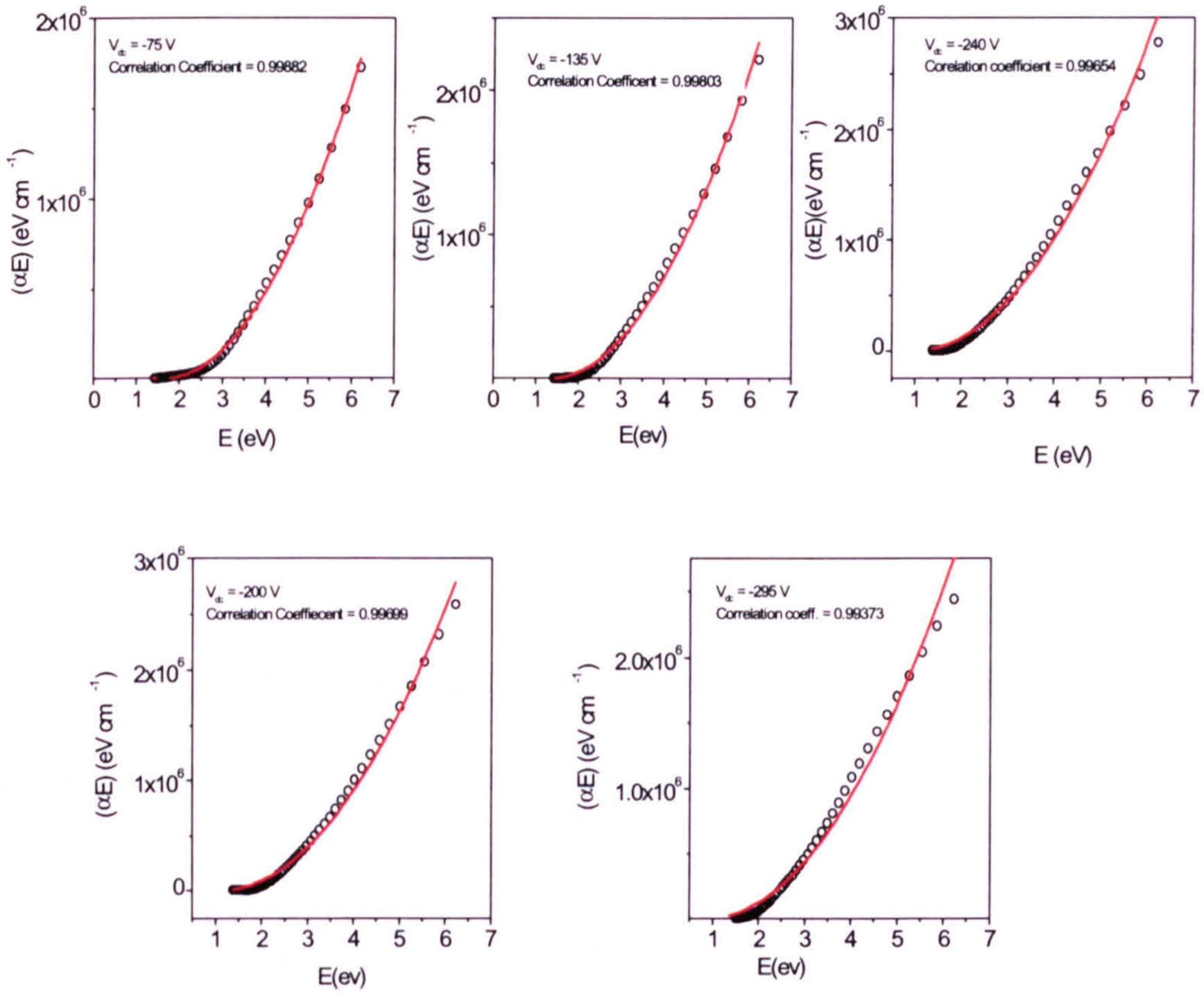

Fig.-4.9 Plots showing fits of the observed data to a second order polynomial in energy.

We plotted experimentally observed values of αE against the energy and fit the data to a second order polynomial in E; the Tauc gap was deduced from the parameters in this fit, using Eqn.-4.3. In a number of publications, determination of the Tauc gap is carried out by correlating the UV data to the logarithm of equation (4.2). Such a method might indicate an

improved correlation, which however could be spurious, resulting in erroneous estimates of the relevant parameters. This motivated us to fit the experimental data directly to the second order polynomial, as suggested by Eqn.-4.3. The results of the fitting exercise, for data collected with various samples deposited at different DC bias voltages are shown in Fig.-4.9. The curves represent the analytical function employed in the fits while the circles represent the experimental data points. We consider all the fits reliable since the correlation coefficient is nearly unity in all cases. The purpose of this fitting exercise is to esitmate the Tauc gap for our a-C:H films.

Table-4.1 Tauc gap and fit parameter *G* of a-C:H films deposited at different bias voltages.

DC bias Voltage (-volts)	Tauc Gap, E_T (eV)	B ($cm^{-1/2} eV^{-1/2}$)
75	1.63	84825.45
135	1.31	97066.72
200	1.07	105718.25
240	0.98	111006.51
295	0.88	96832.25

The material parameters obtained by fitting experimental data to Eqn.-4.3 are listed in Table.-4.1. Firstly, the variation of the Tauc Gap as a function of the self-bias voltage is discussed. The nature of the Tauc gap as a function of the DC self bias is shown in the Fig.-4.10

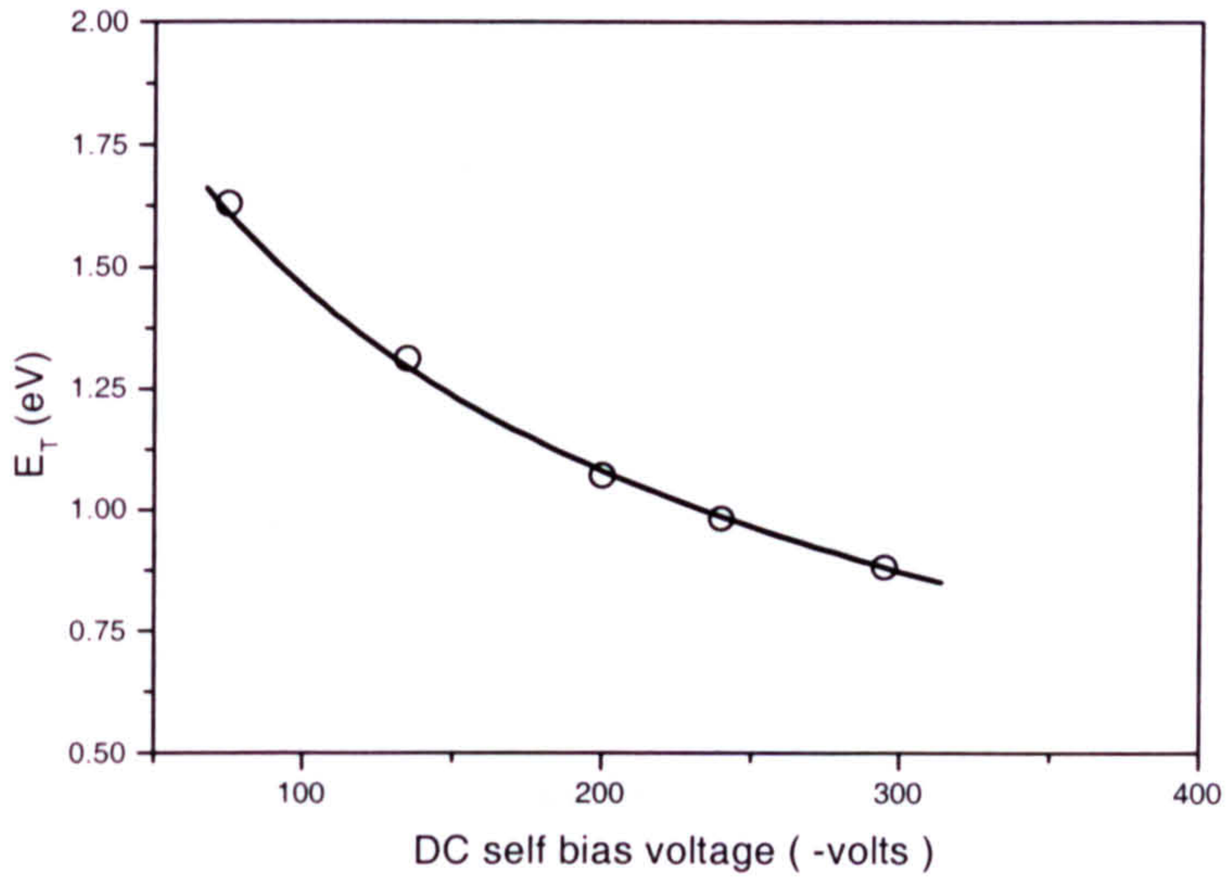

Fig.-4.10 Variation of Tauc gap of a-C:H as a function of DC self-bias.

It is evident from Fig.-4.10 that the Tauc gap decreases monotonically with increase in the DC self-bias. This can be explained on the basis of the model proposed by Robertson and O'Reilly, [35,36]. According to the "cluster model" proposed by Robertson [36], a-C:H contains both sp^2 and sp^3 sites, with sp^2 sites segregated into the clusters embedded within an sp^3 bonded matrix. The optical gap of a-C:H depends on the degree of medium range order [36], rather than just the short range order, as in the case of other amorphous semiconductors. This model suggests that the optical gap is inversely proportional to the size of the sp^2 clusters. Since a-C:H consists of two main components, namely sp^2 and sp^3 species, it seems that the sp^2 species organise themselves in clusters of different sizes. A distribution of the

sizes of clusters implies a distribution of the Tauc gap (E_T) of the clusters. The E_T values obtained from the Tauc equation can at best represent an average value of this distribution. Therefore, the Tauc gap in the sub-micron regions is not a good representation of the optical bandgap of the material.

Fig.-4.10 indicates that the bandgap of a-C:H decreases as the DC self-bias voltage increases. On the basis of Robertson's bandgap model, we can say that the sp^2 clusters control the bandgap. We believe that the size of the sp^2 clusters increases with increase in the self-bias, causing the bandgap to decrease. The effect of DC self bias on sp^2 size is confirmed by the Raman spectroscopy (see later in this Chapter).

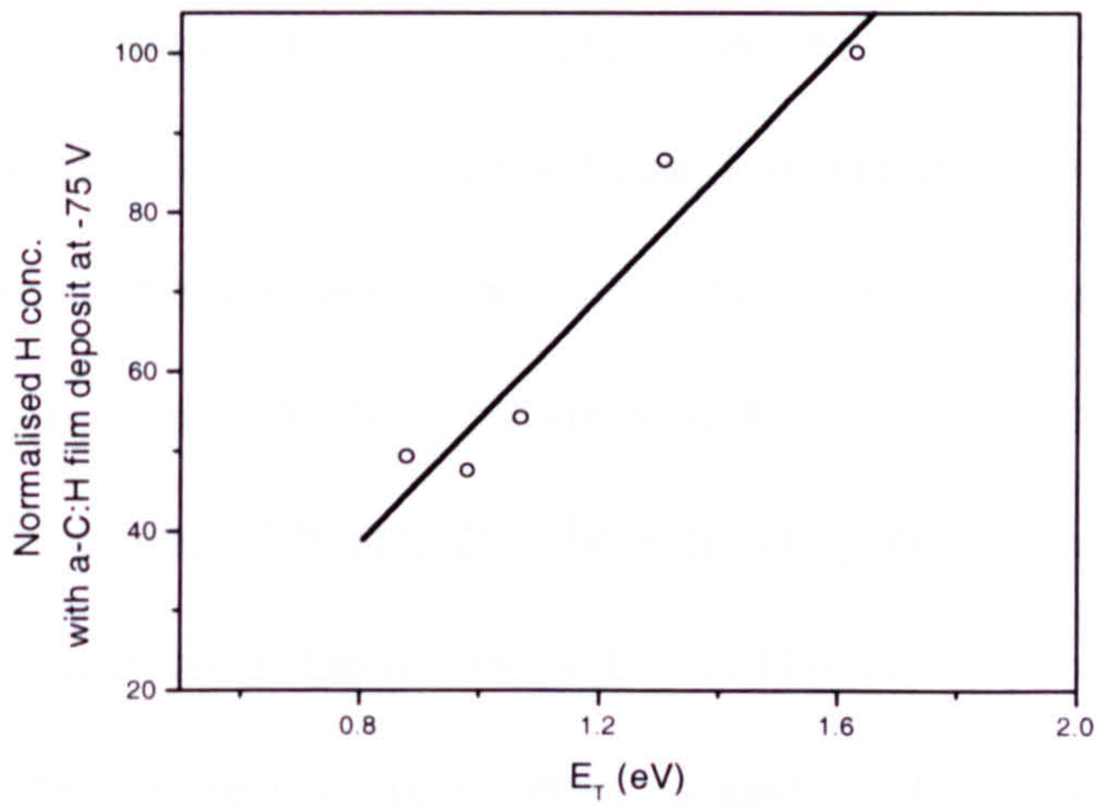

Fig.-4.11 The relationship between the hydrogen present in our films and the Tauc gap is approximately linear.

The other parameter that can affect bandgap is the concentration of hydrogen in the films. From the IR analysis, (Fig.-4.7), it is quite clear that the hydrogen concentration decreases

with an increase in the DC bias voltage. In Fig.-4.11 we show the correlation between hydrogen concentration and E_T. This corroborates the linear relation between E_T and the hydrogen concentration as reported by B. Dischler et al, [32].

4.6 Raman Analysis:

As already stated in Chapter-2, Raman spectroscopy is a key experimental technique used to distinguish between the various allotropes of carbon. To confirm presence of amorphous carbon, we analysed our films deposited at different DC self-bias voltages, using Raman spectroscopy. The Raman spectra collected from various films are shown in Fig.-4.12.

It is clear from Fig.-4.12 (j) that there is a shift in the peaks of the different spectra, towards the smaller wavelengths, with increase in the deposition DC self-bias. This is probably due to a basic restructuring of the films, brought about by the changing bias. The variation in the structural properties of the film as functions of deposition parameters (in our case DC self -bias) can be understood by knowing the nature of the D and G peaks in the Raman spectra [37,38], (see Chapter-2). The Raman spectra from the films deposited at different self-bias were deconvoluted into the D and G peaks. Optimum fitting was achieved by allowing all the fit parameters, (peak positions and widths) to vary. The validity of the final fit was confirmed by reconstructing the initial spectrum from the individual Lorentzians, (obtained via the deconvolution exercise), and ensuring that the final peak positions correlated with the D and G peaks for amorphous carbon.

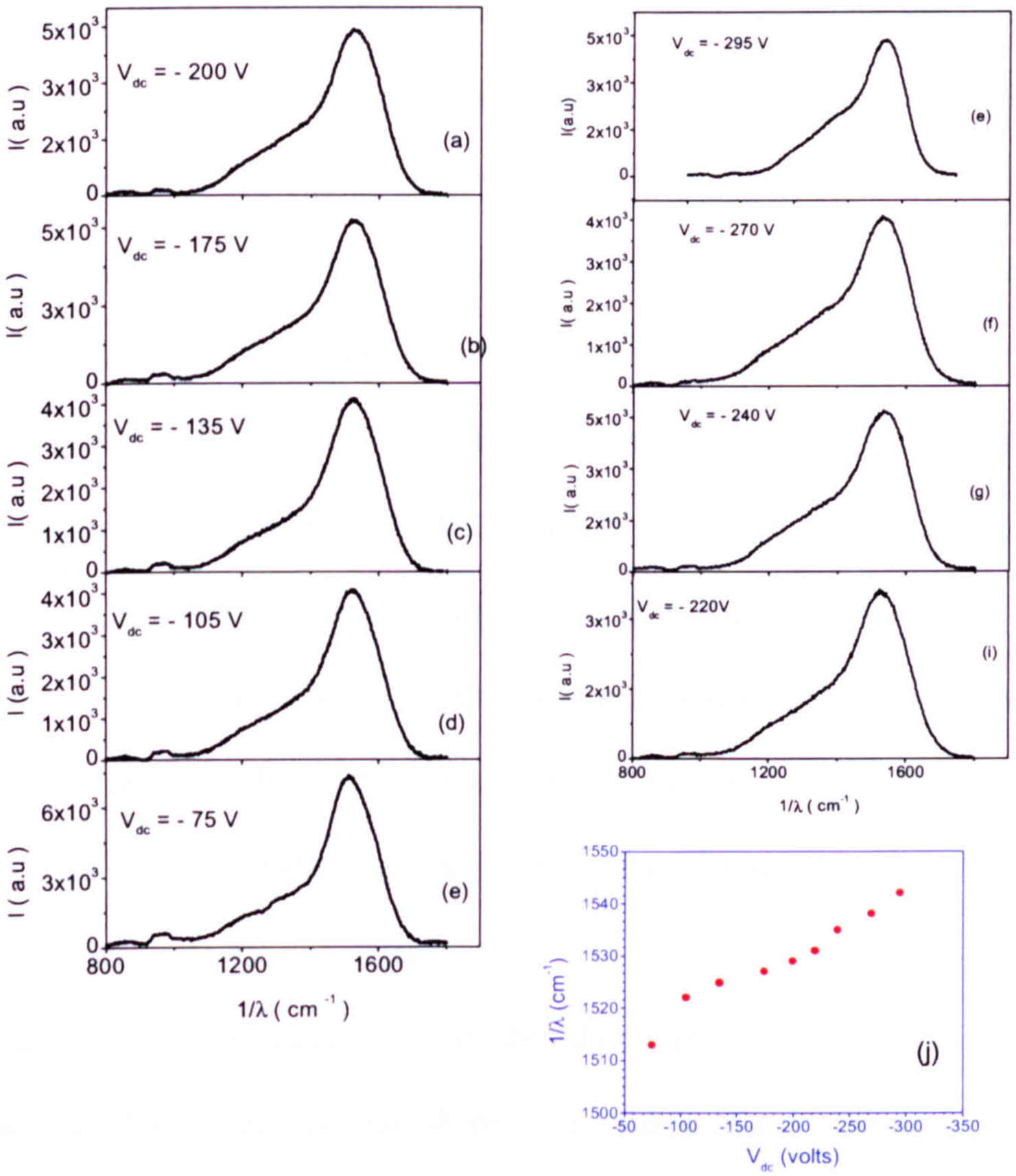

Fig.-4.12 (a-i) Raman Spectra of amorphous carbon deposited at various DC self bias voltage. (J) shows the peak positions at different bias. Films were deposited on Si^{+n} substrate.

Fig.-4.13 shows the ratio of the intensity of the D and G peaks, (I_D/I_G ratio) of the films

deposited at different DC bias. It is observed from the figure that there is an increase in the I_D/I_G ratio with the DC bias voltage. This change can be related to the compositional change in the film properties [39,40]. There are a number reports, [39,40,41], in which the I_D/I_G ratio has been correlated to the sp^3/sp^2 ratio of the films. The higher the value of sp^3/sp^2 ratio, the lower is the value of the I_D/I_G ratio. We have not done any EELS-based investigation to determine the sp^3/sp^2 ratio in our films; however, on the basis of relevant published work [42], we can say that the sp^3/sp^2 ratio decrease in amorphous films with increase in the DC self-bias voltage. This can be explained on the basis of ion energies in the plasma deposition process of a-C:H films. The sp^3 content of the film is controlled by ion energies. The ion energy increases with increase in the DC bias, enhancing the ability of the ions to strike the surface of the substrate. It has been demonstrated by various workers that stress in the films increases with increase in the ion energy. To reduce the stress in the film, it is possible that the sp^3 parts relax into sp^2 rich parts.

The most noticeable characteristic of the films is the variation in the I_D/I_G ratio within the same sample. This suggests that there is a compositional inhomogeneity in the films. Consequently, the electrical characteristics should also differ spatially in the same film when we probe in the submicorn regions. This will be discussed in Chapter-7 of the thesis.

The shift in the G-peak position is shown in Fig.-4.14. The explanation of the variation in the position of this G peak is rather involved. This is because the position of the G-peak depends on the local environment and the size of the graphitic sp^2 clusters. Silva et al demonstrated that there is a shift in the G-peak position to lower wavenumbers, as the

hydrogen content in the films increases. Fig.-4.14 indicates that there is a shift in the G-position towards higher wavenumbers with increasing DC-self bias. We have seen that with increase in the DC-self bias the hydrogen content decreased in the films (see Fig.-4.7). Therefore our observed trend is consistent with the work published in [28]. The other factors which can influence the shift in the peak are the graphite crystallite sizes and their distribution.

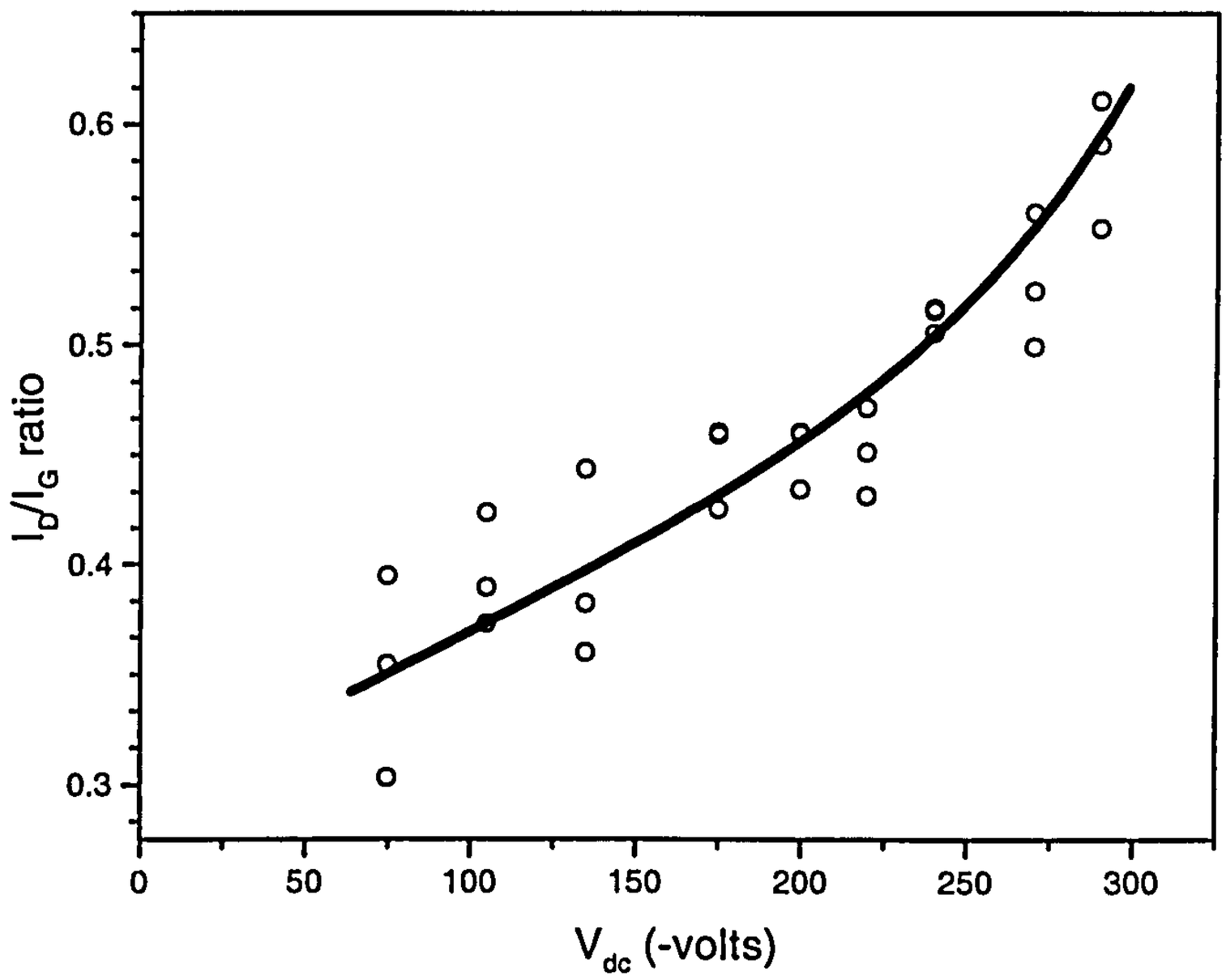

Fig.-4.13 I_D/I_G ratio of our a-C:H films, at different values of the self-bias.

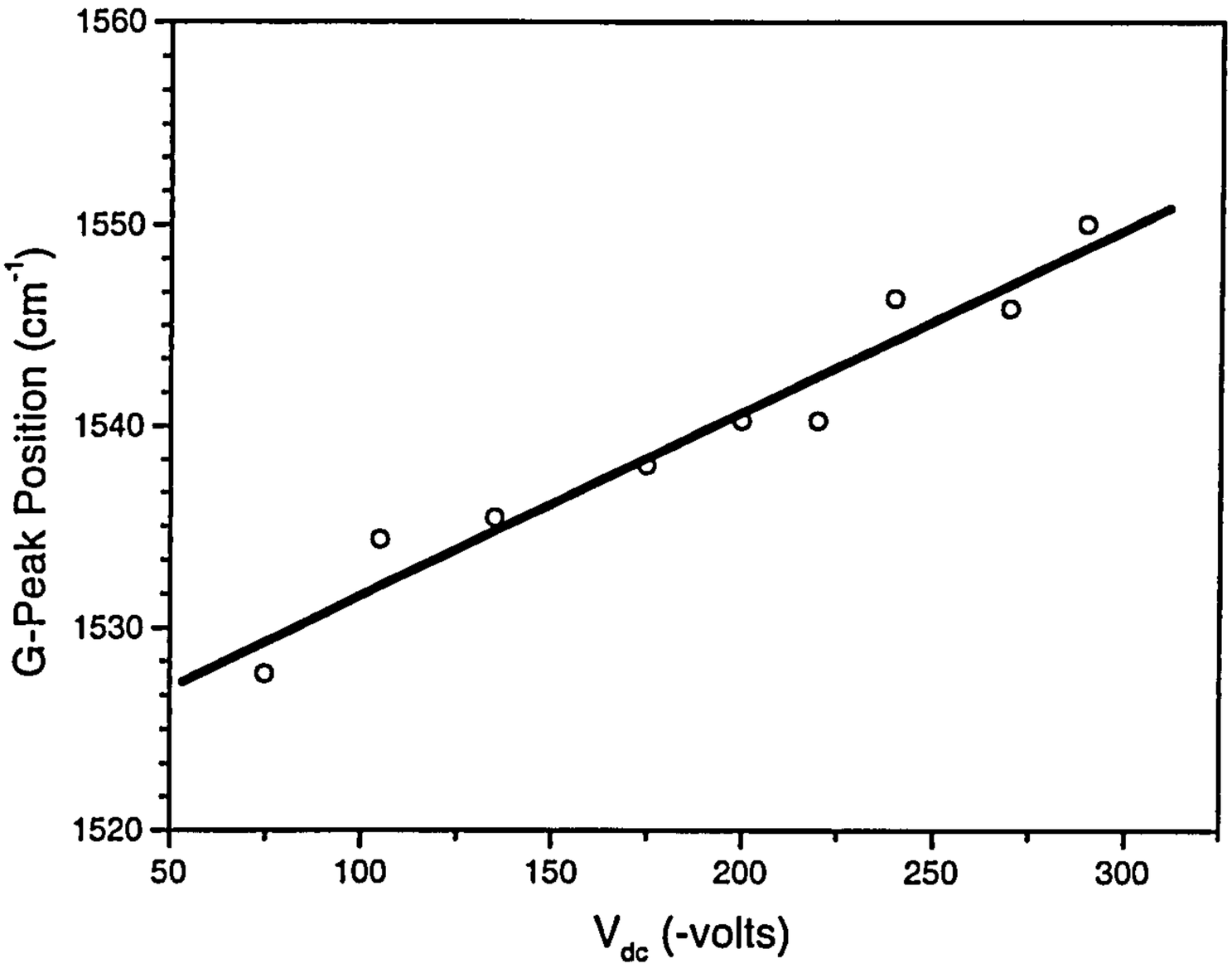

Fig-4.14 Change in the position of the G-peak with change in the DC self-bias voltage.

The width of the G-peak is also very important [43]. Fig.-4.14 shows the change in the width of the G-peak measured as a function of the DC self-bias. The width of the peak is proportional to the angle disorder between adjacent bonds at the sp^2 sites, in the same way that the width of the transverse optical (TO) mode is related to the angle disorder in a-Si [43]. It is clear that with an increase in the DC-self bias there is a decrease in the peak-width. This means that the distortion between adjacent bonds is smaller with increase in the DC bias. This suggests that the sp^2 or the graphitic clusters are arranged parallel to the substrate

surface, (as sheets). Such a stacked up arrangement is referred to by the authors of this cluster model as a good "alignment" of the sp^2 clusters. There have been reports, in which aligned sp^2 clusters have been found to enhance the field emission from tetrahedral carbon [44]. This is achieved by annealing the sample at a high temperature [45]. But the bias based alignment has not been reported previously and we propose from our investigation that this idea can be well-exploited in diamond-like carbon to align the sp^2-clusters during deposition.

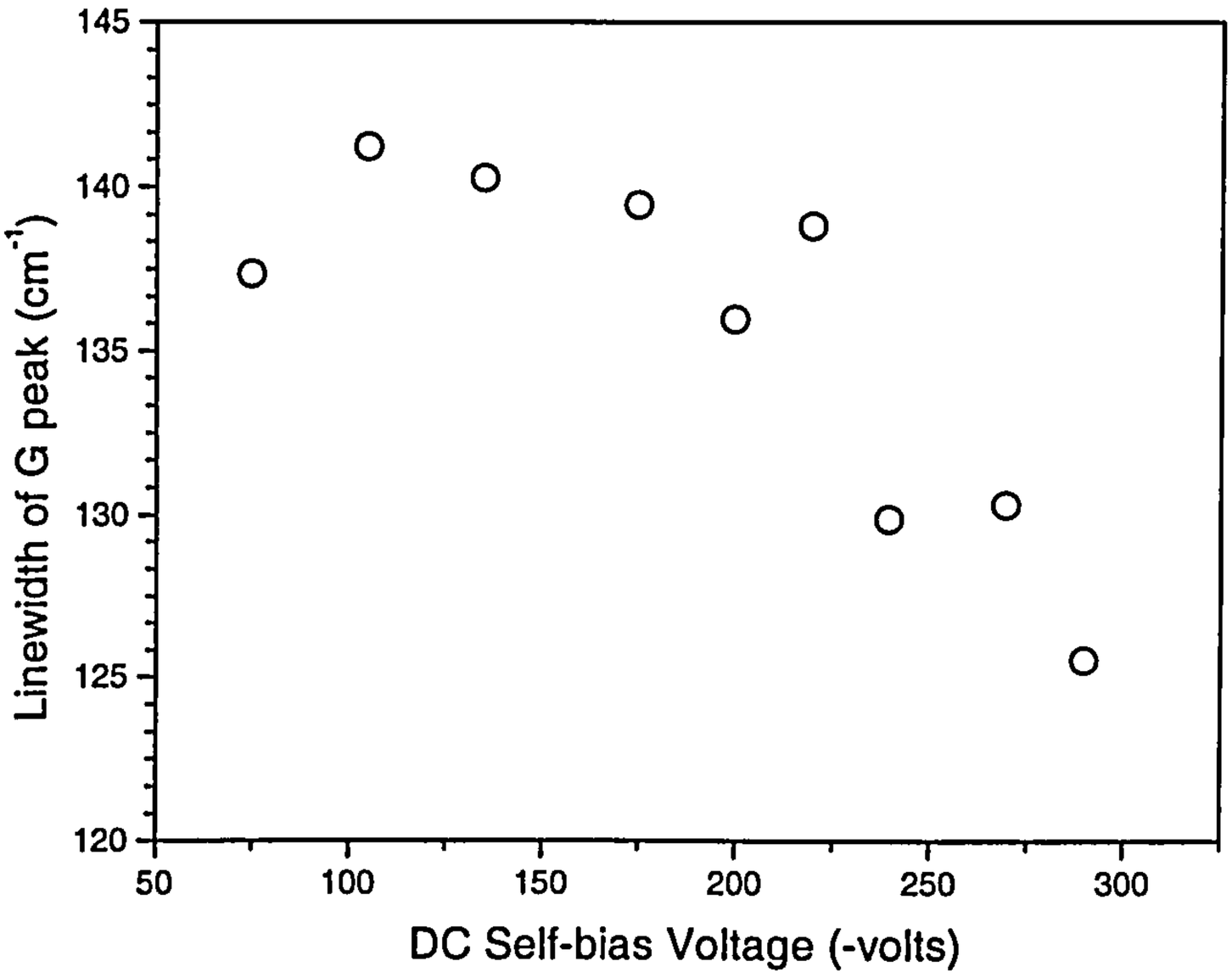

Fig.-4.15 Variation of the width of the G-peak with DC self-bias voltage.

The bandgap of diamond-like carbon is controlled by the sp^2 and sp^3 fractions in the film.

This model was proposed by O'Really and Robertson [35], (discussed above); according to them the optical bandgap is found to vary inversely with sp^2 cluster size. The model suggests that an increase in the sp^2 fraction will tend to increase the average size of the sp^2 clusters and thereby decrease the gap. According to this cluster model, we should expect a decrease in the bandgap with increase in the I_D/I_G ratio. Fig.-4.16 shows the relationship between I_D/I_G ratio and the Tauc gap. It is clear from Fig-4.16 that the Tauc gap decreases with increase in the I_D/I_G ratio.

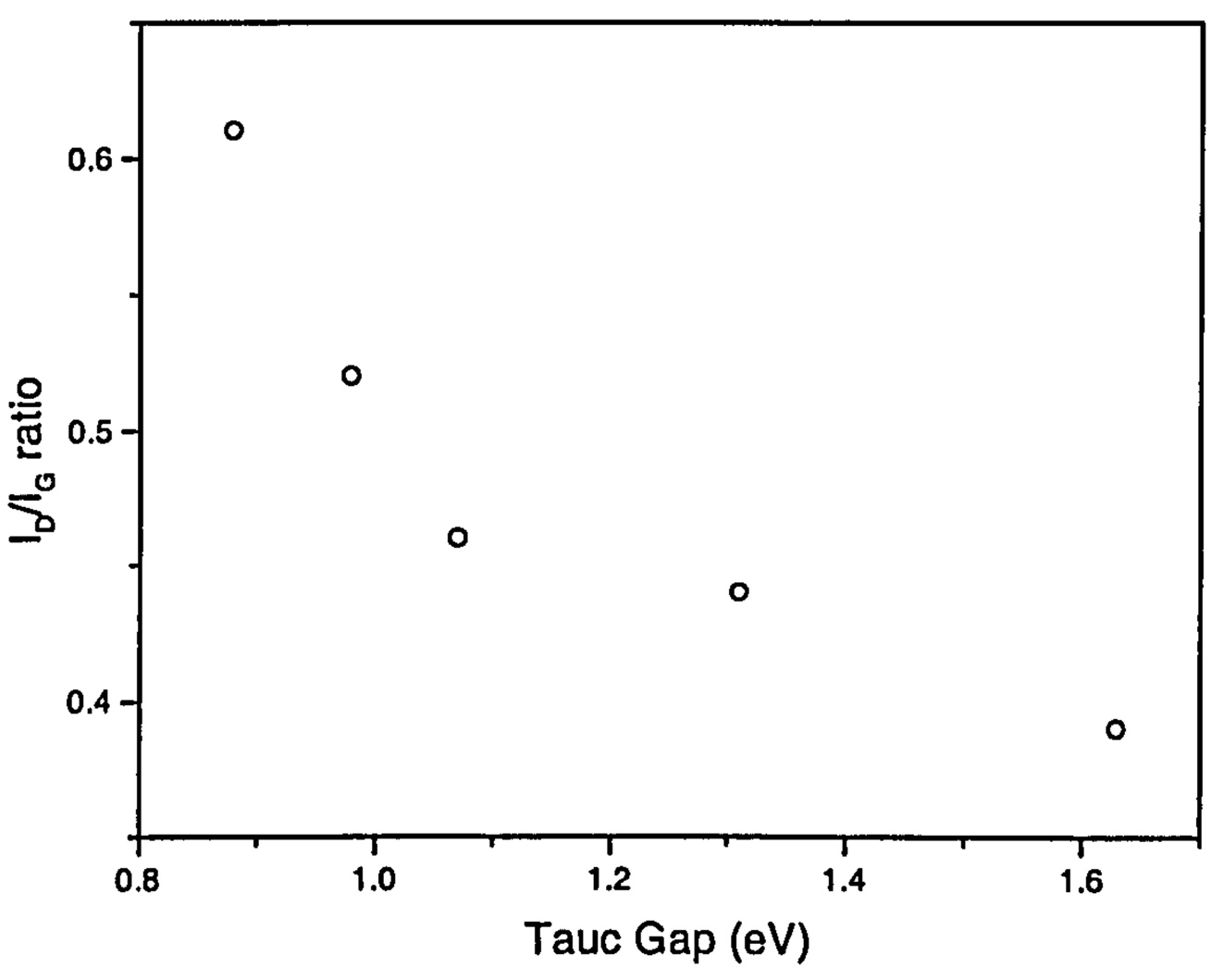

Fig.- 4.16 I_D/I_G ratio against Tauc gap. Plots shows the effect of sp^2 clusters on the Tauc gap.

In conclusion, Raman analysis shows that there is a wide variation in the film properties deposited at different DC self-bias voltages. We can tailor the sp^2 and sp^3 content in the films

by changing the key deposition parameter (the DC self-bias voltage) and hence control the film properties.

4.7 Electron Spin Resonance

Electron spin resonance (ESR) reveals the presence of unpaired electrons in a sample and gives information about the density and properties of the constituent material [46,47]. Though a-C:H films have very interesting properties, so far they have not been used as an active material in electronic applications. This is due to the rather poor understanding of the density of states in amorphous carbon. In this study, we investigated the effect of DC self-bias on the defect centres in the amorphous carbon films.

ESR measurements were performed by placing the sample in a resonant cavity. Electromagnetic radiation of a fixed frequency was used (9.5 GHz) and the resonance was observed by sweeping the external magnetic field. A modulating signal, as represented by a small amplitude magnetic field; its purpose was to achieve phase sensitive detection. For this reason the ESR signal is observed as the first derivative of absorption.

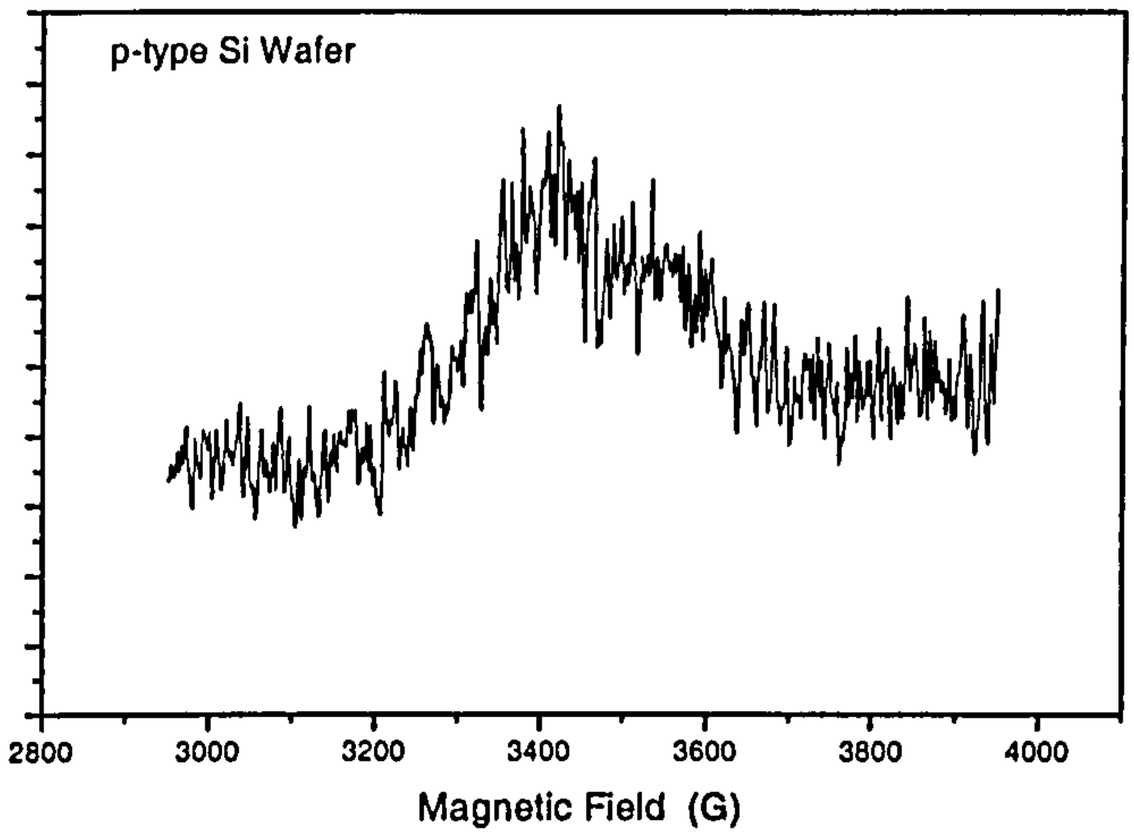

Fig.-4.17 ESR spectrum of p-type high resistivity Si substrate

The selection of a substrate for the ESR study is very important. The chosen substrate should not be ESR active. A suitable choice could be either Pyrex glass or undoped c-Si. We used very highly resistive p-type c-Si substrate and the films deposited on it are approximately 82 nm thick; these films were deposited at five different values of the DC self -bias. To confirm that the substrate does not affect the ESR measurements, we took the ESR spectra of the chosen substrate. Fig.-4.17 does not reveal any ESR activity in the substrate. Therefore, the ESR data collected from the a-C:H deposited on the c-Si substrate is solely due to the amorphous carbon.

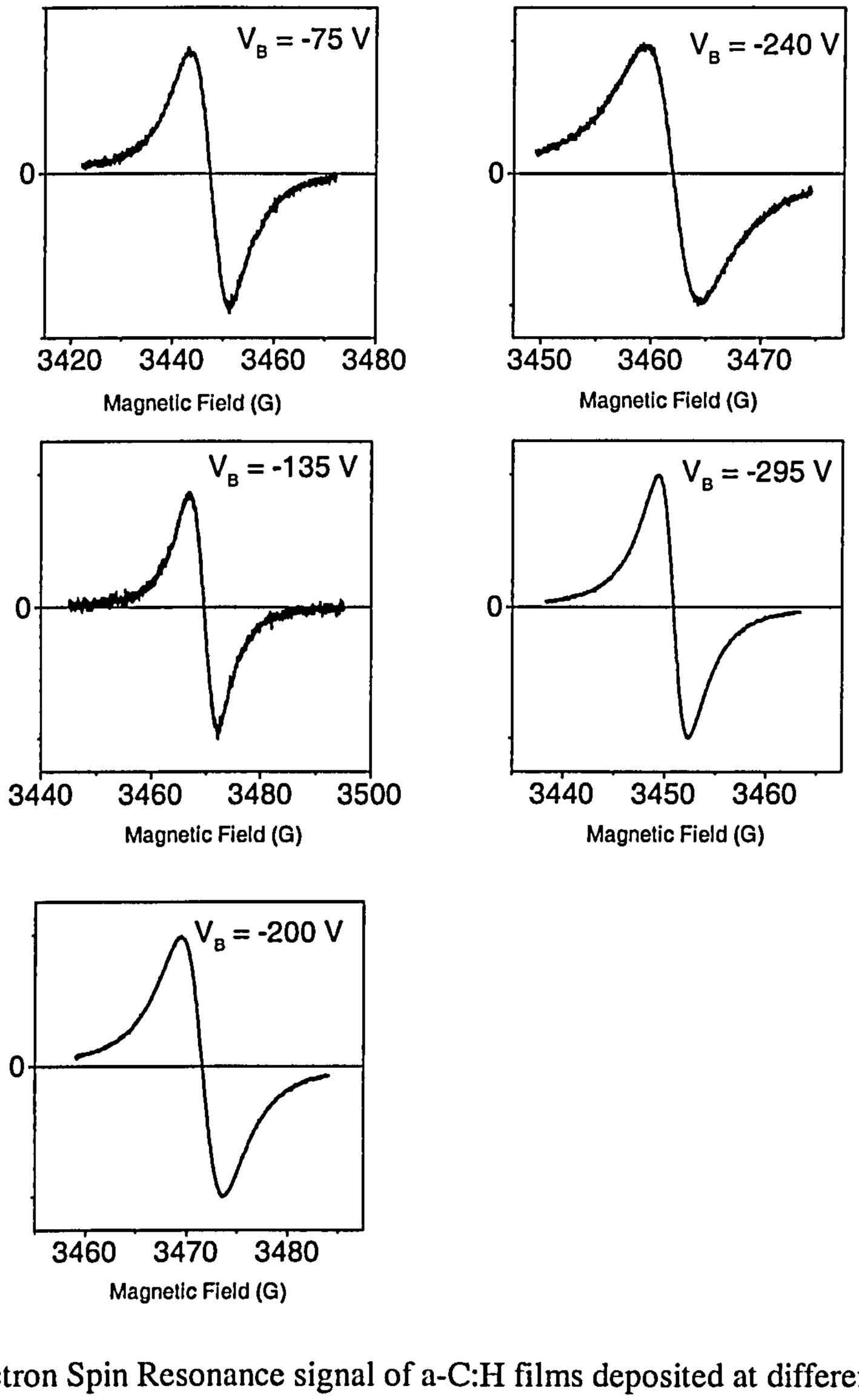

Fig.-4.18 Electron Spin Resonance signal of a-C:H films deposited at different DC self bias.

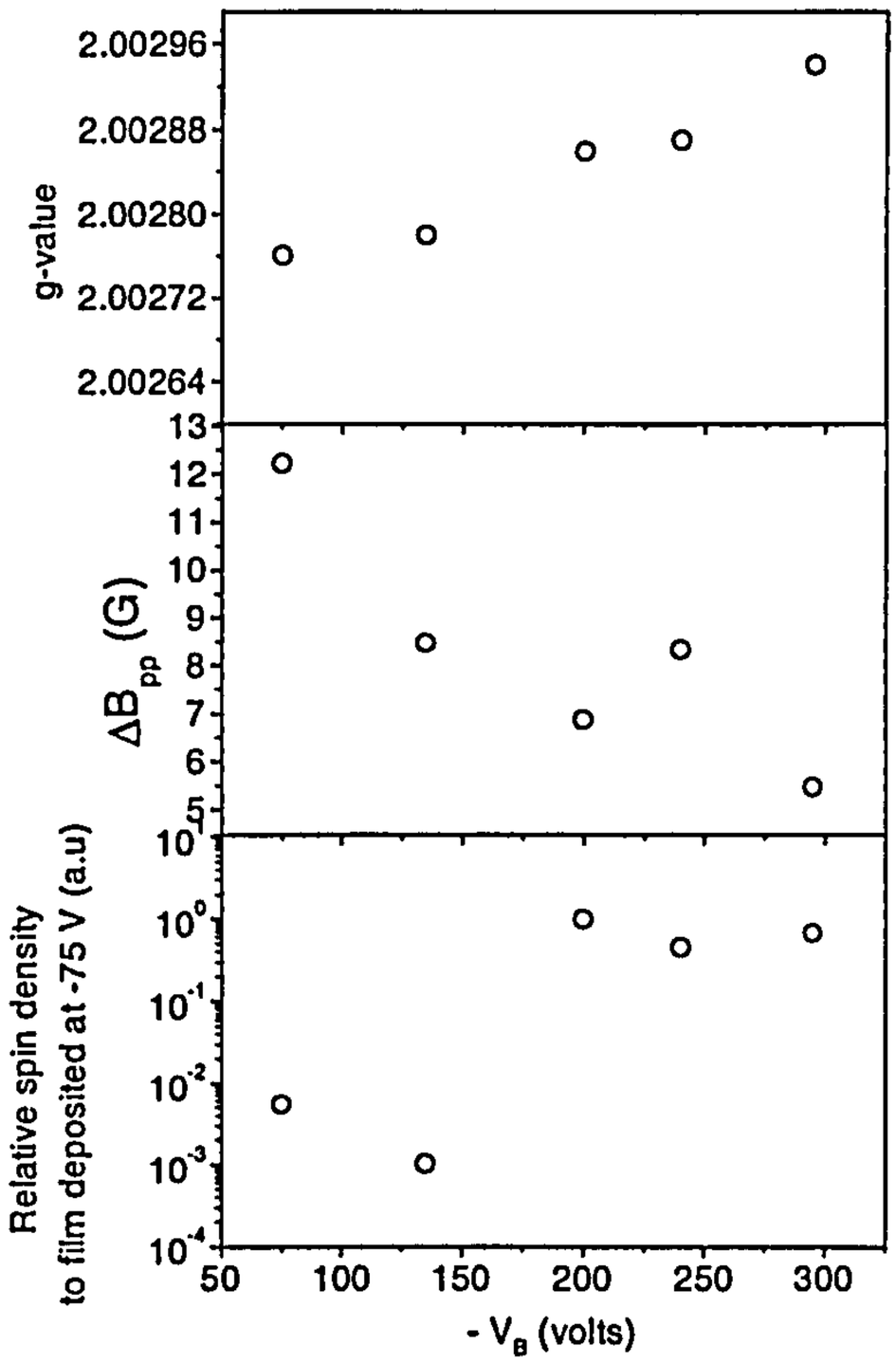

Fig.-4.19 Effect of DC self-bias on the (a) g-value (b) peak to peak width and (c) relative Spin Density of amorphous carbon films.

Typical ESR response of our films deposited at different bias is shown in Fig.-4.18. Fig.-4.18 shows that although there are no discernible changes in the line-shape of the Lorentzian, the peak to peak line-width decreases with an increase in the DC self-bias voltage.

Fig.-4.19 displays the variation in the line-width and the relative spin concentration with change in the DC self-bias. The value of the gyromagnetic ratio, *g*, was determined using Eqn.-2.2 and the relative spin density was determined by numerically integrating the ESR signal twice. *g* varied from 2.00276 to 2.00294, which remains within +0.0002 of 2.0027,

with a bias variation from –75 V to –295 V. The observed *g*-values in our films are consistent with the values reported by various workers [48]. The slight increase in *g* with increase in the DC self-bias is considered constant [51]. The decrease in the line width with increase in the DC bias is explained on the basis of two mechanisms, namely the *dipolar broadening* and *exchange narrowing*.

We know from the basic theory of ESR that resonance occurs when the total magnetic field at an unpaired electron is of a particular value. The total field is made up of the externally applied field and any internal local fields. The local field will contain contributions arising from the magnetic moments of neighbouring unpaired electrons. Since there will be a distribution of distances to these neighbouring electrons there will also be a distribution in the value of the local field indicating a distribution in the external field required for the satisfaction of the resonance. This distribution in the external field values manifests itself as a broadening of the resonance line. This is called dipolar broadening. Abragam [49] has shown that the line width, is related to spin density by the following relation:

$$\Delta B_{pp}^{dipolar} = \frac{4\pi^2}{9} g\mu_B N_s \qquad \ldots\ldots\ldots\ldots \quad 4.4$$

Where, N_s is the spin density and μ_B is the Bohr Magnetron.

At higher bias, the spin density increases and then remains nearly constant (as shown in Fig.-4.19(c)) but there is a significant reduction in the line-width. This is clearly not

predicted from Equ.-4.3 but suggests that another mechanism is at play here. Barklie et al [51] and Carey et al [52] have investigated the effect of DC self bias on the ESR signal of a-C:H films. In these reports, it has been proposed that the exchange-narrowing is more likely be the agent that causes line-width to decrease. This is explained on the basis of size of the sp^2 clusters in the a-C:H films as well as the quantity of such clusters in films. The increase in DC-bias results in larger sp^2 clusters. This consequently promotes electron de-localisation and encourages electron wave functions to overlap. This increases the exchange interaction. Therefore, decrease in the line-width may occur due to the increased exchange interaction between electrons, which grows stronger as the electron de-localises. Since the sp^2 contents as well as sp^2 cluster size in our films increases with increase in the DC self bias, (Section-4.6), as in [50, 51, 52], we can explain the bias dependence of linewidth of our films on the basis of the conclusions reached in [50,51, 52].

The increase in the spin density with increase in the bias may be accounted for partly the loss of hydrogen and partly by the reduction in the π-defect creation energy as the cluster size increases with increased sp^2 content.

Summary

This chapter demonstrates the importance of DC self-bias on the various properties of a-C:H films. We have seen that the resistivity of films can vary from 10^6 to 10^{14} Ωcm, bandgap from 0.8 to 1.7 eV, and R.I from 1.9 to 2.7. Raman analysis shows the effect of self-bias on sp^2 clusters and its correlation with the Tauc gap. We observe, (in agreement with others [9]), that hydrogen concentration falls with increase in the DC self-bias. We have

investigated the film properties of a-C:H extensively and in conclusion, can claim to be able to exploit the growth conditions to realise the desired a-C:H films for a range of device applications. A further crucial factor in determining the suitability of a-C:H films is the density of states, which has not been investigated in this chapter; it will be discussed in Chapter 5.

References:

1. N. Mutsukura and Ken-ichi Akita, *Diamond and Relat. Mat.*, **9**, 761, (2000).
2. L.A Romanko, A.G Gontor, A.M Kutsay, S.I Khamdozko, and V.Yu. Gorokhov, *Diamond and Relat. Mat.*, **9**, 801, (2000).
3. J. Robertson, *Proceedings of the Ist international Specialist Meeting on Amorphous Carbon (SMAC'97)*, pp.32 (1997).
4. P. Koidl, C.Wild, B.Dischler, J. Wagner and M. Ramsteiner, *Mat. Sci. Forum*, **52&53**, 41 (1989).
5. J. Robertson, *Phil. Trans. R. Sco. Lond. A*, **342**, 277 (1993).
6. Y. Lifshitz, S.R. Kasi, J.W. Rabalais, and W. Eckstein, *Phys. Rev. B*, **41**, 10468 (1990).
7. D.R Mckenzie, D. Muller and B.A Pailthorpe, *Phys. Rev. Lett*, **67**, 773 (1991).
8. I.B. Chapman, *Glow Discharge Processes: Sputtering and Plasma Etching*, New York: John Wiley & Sons, 1980.
9. E.Ohta, Y. Kimura, H. Kondo, M. Takahashi, K. Kameyama, K. Yamda and I. Fujimura, *22nd Int. Conf. Sol. Stat. Devices and Materials (SSDM)*, 589, 1990.
10. G.A.J Amaratunga, S.R.P Silva and D. Mckenzie, *J. Appl. Phys.*, **70**, 5374 (1991).

11. A. Grill , V. Patel and S. Cohen, *Diam. and Relat. Mat.*, **3**, 281 (1994).

12. S. Egret, J. Robertson, W.I. Milne and F.J. Clough, Diamond Related. Mater. **6**, 879, (1997).

13. A. Ilie, *Diamond and Relat. Mat.*, **10**, 207 (2001).

14. M.S Dresselhaus and G Dresselhaus, Adv. Phys., 30, 139 (1981).

15. Ph. Komninou, G.Nouet, P.Patsalas, Th. Kehagias, M.Gioti, S.Logothetidis, Th. Karakostas, *Diamond Relat. Mat.*, **9**, 703 (2000).

16. G. Amaratunga, A. Putnis, K. Clay, and W.I Milne, *Appl. Phys. Letts.*, **55**, 634, 1989.

17. S.R.P Silva and G.A.J Amaratunga, *J. Materials Science*, **29**, 4962, 1994.

18. C. Arena, B. Kleinsorge, J. Robertson, W.I Milne and M.E Welland, *J. Appl. Phys.*, **85**, 1609 (1999).

19. P.C Kelires, J. of Non-Crystalline Solids, 1998, **227-30**, PART A, 597 (1998).

20. C.A Davis, K.M Knowles, and G.A.J Amaratunga, *Surf. & Coatings Technol.*, 76-77, 316 (1995).

21. J.D Carey, C.H Poa, R.D Forrest, A.P Burden, S.R.P Silva, *J. of Vac. Sci. & Tech.. B. Microelectronics and nanometer structures. Processing, measurement and phenomena*, **18**, 1051 (2000).

22. I. Rusman, I. Klibanov, L. Burstein, Y. Rosenber, V. Weinstein, E. BenJacob, N. Croitoru, A. Seidman, *Thin solid films*, **287**, 36 (1996)

23. K.J Clay, S.P. Speakman, N.A. Morrison, N. Tomozieu, W.I. Milne and A. Kapoor, *Diamond and Relat. Mat.*, **7**, 1100 (1998).

24. S. Egret, J.Robertson, F.J Clough and W.I Milne, *Diamond and Relat. Mater.*, 6, 879 (1997).

25. F. Jansen, M. Machonkin, S. Kaplan, and S. Hark , J. Vac. Sci. & Tech. A: Vac., Surf. and Films, 3, 605 (1985).

26. J.C. Sánchez-López, C. Donnet, J. Fontaine, M. Belin, A. Grill, V. Patel abd C. Jahnes, *Diam. and Relat. Mater.*, **9**, 638 (2000).

27. R.A Street, *Hydrogenated Amorphous Silicon*, (Cambridge Univeristy Press), 1991.

28. J. Schwan, S.Ulrich, V.Batori, H.Ehrardt and S.R.P.Silva, *J. Appl. Phys.*, **80(1)**, 440 (1996).

29. B.K Kim and T.A Grotjohn, *Diam. and Relat. Mater.*, **9**, 654 (2000).

30. A. Grill and V. Patel, *Appl. Phys. Letts.*, **60**, 2089 (1992).

31. S. Liu, S. Gangopadhyay, G. Sreenivas, S.S. Ang and H.A Naseem, *Phys. Rev. B*, **55**, 13020 (1997).

32. B. Dischler, A. Bubenzer, and P. Koidl, *Appl. Phys. Lett.*, 42, 636 (1983).

33. D.A Anderson, Philos. Mag., **35**, 17 (1977).

34. Rusli, J. Robertson, and G.A.J Amaratunga, *J. Appl. Phys.*, **80**, 2998 (1996).

35. J. Robertson and E.P. O'Reilly, *Phys. Rev. B*, **35**, 2946 (1987)

36. J. Robertson, *Diam. Related Mater.*, **4**, 297 (1995).

37. R. Shuker and R. Gammon, *Phys. Rev. Lett.*, **25**, 222 (1970)

38. F. Li and J.S, Lannin, *Phys. Rev.*, B39, 6220 (1989).

39. A.V Stanishevsky, L.Y. Khriacchtchev, *Diamond Relat. Mater.*, **5**, 1355 (1996).

40. S. Prawer, and K.W Nugent, *Proceeding of the Ist International Specialist Meeting on Amorphous Carbon (SMAC'97)*, eds., S.R.P. Silva, J. Robertson, W.I. Milne, G.A.J Amaratunga, World Scientific Publishing Co. Pte Ltd., pp.199, 1997.

41. S. Prawer, K.W. Nugent, Y. Lifshitz, G.D Lempert, E. Grossman, J. Kulik, I. Avigal and R. Kalish, *Diam. Relat. Mater.*, **5**, 433 (1996).

42. A.C Ferreri and J. Robertson, *Phys. Rev. B*, (2000).

43. 35. J.S Lennin, J. Non-Cryst. Solids, 97, 39 (1987)

44. J. D. Carey, R. D. Forrest, R. U. A. Khan, and S. R. P. Silva, Appl. Phys. Letts., 77, 2006 (2000)

45. A. Illie and J.Robertson, *J. Appl. Phys. (2000).*

46. C.P. Poole, Electron Spin Resonance, (J. Wiley, London; 1983)

47. J.E. Wertz and J.R. Bolton, Electron Spin Resonance, (Chapman & Hall, New York 1986)

48. J. Robertson, Daim. Relat. Mater., 6, 212 (1997) .

49. A. Abragam, Principles of Magnetic Resonance (Clarendon, Oxford, UK, 1996).

50. J.H. Van Vleck, Phys. Rev. B, 74, 1168 (1948).

51. R.C Barklie, M. Collins and S.R.P Silva, *Phys. Rev. B*, **61**, 3546 (2000).

52. J.D Carey, R.D Forrest, R.U.A Khan and S.R.P. Silva, Appl. Phys. Lett., 77, 2006 (2000).

CHAPTER 5

Determination of Density of States in Amorphous Carbon

5.1 Introduction

The distribution of deep density of states in amorphous semiconductors has a determining influence on the electronic and optical properties of the materials [1,2,3]. The performance of devices realised out of amorphous semiconductors, is affected by the recombination centres originating from gap states [4,5]. Therefore, the study of the origin and nature of gap states is crucial to the exploitation of amorphous carbon in the electronic industry. A proper understanding of deep state defects in amorphous carbon is not yet established.

The measurement of DOS as a function of growth conditions, namely the self-bias, is essential for unravelling the origin of the states. The DOS in amorphous materials can be obtained from field effect measurements [6,7], capacitance measurements [8,9], space-charge limited current [10,11] and from deep level transient spectroscopy [12,13]. There are also other methods, which can be exploited to understand the density of states in amorphous carbon [14,15,16,17,18].

Not much work has been reported on the DOS of amorphous carbon. In our investigation, we considered three basic devices using a-C:H from which information about the density of states can be extracted, namely, Schottky diode, a-C:H/Si heterostructues and metal-insulator-semiconductor structures. Firstly I would like to discuss the methodology which used to estimate the DOS from the aforesaid device structures and the associated limitations.

There are a few publications in which estimates of the density of states of diamond-like carbon have been reported [19,20,21,22]. Silva et al [19] reports that the density of state in amorphous carbon deposited by PEVCD is of the order of 10^{19} $cm^{-3}eV^{-1}$ near the centre of the bandgap. In this report, I-V characteristics were used to deduce the density of states. The ESR analysis of amorphous carbon by Zeinert et al. shows that the spin concentration between 3×10^{19} $cm^{-3}eV^{-1}$ and 3×10^{20} $cm^{-3}eV^{-1}$ [20]. A value of spin density lies between 10^{21} cm^{-3} and 10^{17} cm^{-3} as a function of optical bandgap, was reported by Rusli et al [21]. There are no reports on the determination of the density states in a-C:H using capacitance measurements in the literature. We developed mathematical models to extract the density states from capacitance measurements on the following structures:

1. Schottky diodes of a-C:H
2. a-C:H/c-Si heterostructures
3. Metal-Insulator-Semiconductor (MIS) Structures

5.1.1 DOS from the Schottky diode:

In a-Si:H, DOS evaluation is based on the fact that under deep depletion, a linear C^{-2}-V relation is expected regardless of the distribution of states in the gap. Hence, one may use the following well known relationship for the Schottky barrier [23]:

$$C = \left[\frac{qN\varepsilon}{2\left(V_{bi} \pm V - \frac{kT}{q}\right)} \right]^{\frac{1}{2}} \qquad \text{..... 5.1}$$

Here,

C = space charge region capacitance per unit area

Q = the electronic charge,

N = number of all uncompensated gap states per unit volume.

ε = the dielectric constant of semiconducting material

V_{bi} = the zero bias bending,

V = the applied DC bias

kT = the thermal energy (Boltzman constant x Temperature)

Eqn. 5.1 suggests that the slope of a plot of C^{-2} against V will provide an estimate of the trap state density. The contribution of the trap states to the effective capacitance is very much determined by the frequency of the ac signal used in the C-V measurement. The frequency is indirectly proportional to the response time of the deep states. If there are deep states at the energy level E, one has to consider their response time, τ. The strong dependence of τ on E-E_c can be assumed to yield a sharp cut-off in the energy of the states that can respond to the test signal frequency ω. This cut-off energy can easily be shown to be[24]:

$$E_\omega = E_c + kT \ln(\omega \tau_o) \qquad 5.2$$

Where τ_o is the electron emission rate constant.

It is quite clear from Eqn.-5.2 that the trap states are sensitive functions of the signal frequency at a given temperature. The lower the frequency, the deeper the states that can be probed. Therefore, plots of C^{-2} against V at different frequencies yield different values

of N. If the number density of uncompensated trap states, thus found, is used to construct a E_ω - E_r vs N plot and a function is fit to the resulting curve, (say $f(E)$), the derivative of this analytical function $f(E)$ will be the density of states, at the corresponding energy.

5.1.2 Determination of Density of States from Si/DLC heterostructure

During our investigation, we have observed that the deposition of DLC on a Si substrate is easier than on many others, (especially metallic substrates). The films deposited on Si-substrates are much smoother and display a good sticking quality. DLC/Si structures are therefore easy to manufacture. There are reports of the determination of the density of states in DLC using this structure. One can estimate the density of states using the following relationship for Si/DLC heterostructure diode by solving Poisson's equation [23]:

$$\frac{d\left(1/C^2\right)}{dV} = \frac{2\left(\varepsilon_{Si}N_{Si} + \varepsilon_{dlc}N_{dlc}\right)}{\left(a^2 q \varepsilon_{Si} N_{Si} \varepsilon_{dlc} N_{dlc}\right)} \qquad \text{..... 5. 3}$$

Where,

C = space charge region capacitance per unit area

ε_{Si} = dielectric constant of Si

N_{Si} = doping concentration in Si substrate

ε_{dlc} = dielectric constant of DLC

N_{dlc} = number trap states per unit volume

a = device area

Since undoped DLC is always p-type, n-type Si substrate can be used to form Si/DLC diodes, which can be subsequently used to the deduce density of states from capacitance-

voltage-frequency (*C-V-f*) measurements. It is again obvious from Eqn.5.2 that participation of the states in the measured capacitance, is a function of the ac signal frequency. Therefore, plots of C^{-2} against *V*, at different frequencies will have different slopes (as dictated by Eqn.5.3), which will give us the number density of states at E_ω. Now, if the plot of E_ω against *N* is fit to a polynomial say *f(E)*, the first order derivative of this function will give the distribution of density of states in DLC.

$$DOS = \frac{d(f(E))}{dE} \qquad \text{.....5.4}$$

5.1.3 Discussion on determining the density of states from Schottky diode and Si/DLC heterostructure:

An investigation to measure the density of states of DLC from Schottky behaviour, was reported by Racine et. al., [25]. This Schottky contact was reported to be characterised by a diameter of 1 mm. Such a large diameter device stands in contradiction to our experience. In our investigation, it has been demonstrated [26], that it is possible to form a Schottky contact on amorphous carbon only if the metal contact diameter is less than about 1μm. Further, the work published by Racine et al does not include any discussion on the rectification ratio, thus rendering it difficult to determine the extent of the observed Schottky behaviour, with such a large area of contact. In the work reported in [26] we used metal tips of tip areas that were only approximately known, to form Schottky contacts on DLC. When the metal-tip of a known area is brought in contact with the a-C:H film, the contact area changes, depending upon the hardness and the pressure. The exact value of the contact diameter is therefore difficult to obtain. However, a detailed

examination, (with an SEM), of a number samples, revealed that only when the contact area is less than about 1μm, the rectification ratio is good enough to claim the formation of a Schottky barrier at the metal-semiconductor interface, (see Chapter 7 for more detail). Thus, we do not agree with Racine et. al; nevertheless, it is also true that the determination of the density of states from Schottky contacts with unknown contact area, is not a reliable procedure. Therefore the theory developed in Sec.-5.1.1, for using Schotky diodes to estimate the density of states of a-C:H, cannot be applied owing to this uncertainty in the contact area. Some other approach is required.

There is a report in which capacitance measurements of DLC/Si structures have been used to find the density of states [27]. Such an approach needs to be supplemented by a thorough scrutiny of the conclusion that the measured capacitance is solely due to the density of states of the DLC. If we recall Eqn.-5.3, we observe that if $N_{DLC} >> N_{Si}$, the equation can be reduced to the following form:

$$\frac{d(1/C^2)}{dV} = \frac{2}{(a^2 q \varepsilon_{Si} N_{Si})} \qquad 5.5$$

It is quite clear from the above equation that in this limiting case, the measured density of states is due to the Si and definitely not the DLC. To demonstrate this notion, we deduced the slope of $C^2.V$ curves for different doping concentrations in the silicon substrates and plotted these slopes against the number of states. It is clear from the Fig.-5.1 that if the Si substrate concentration is orders of magnitude lower than the density of states of the DLC, the slope is constant. The value of the density of states in DLC is typically

estimated to be higher than about $1x10^{18}$ cm^{-3}. Hence only for n-type Si substrates with doping concentrations of the order of this value, can the measured capacitance be attributed to the DLC. However, such highly doped Si-substrates will merely act like a metal due to the degeneracy of the electrons in the conduction band. This will result in a leaky p-n junction rendering the capacitance measurements unreliable.

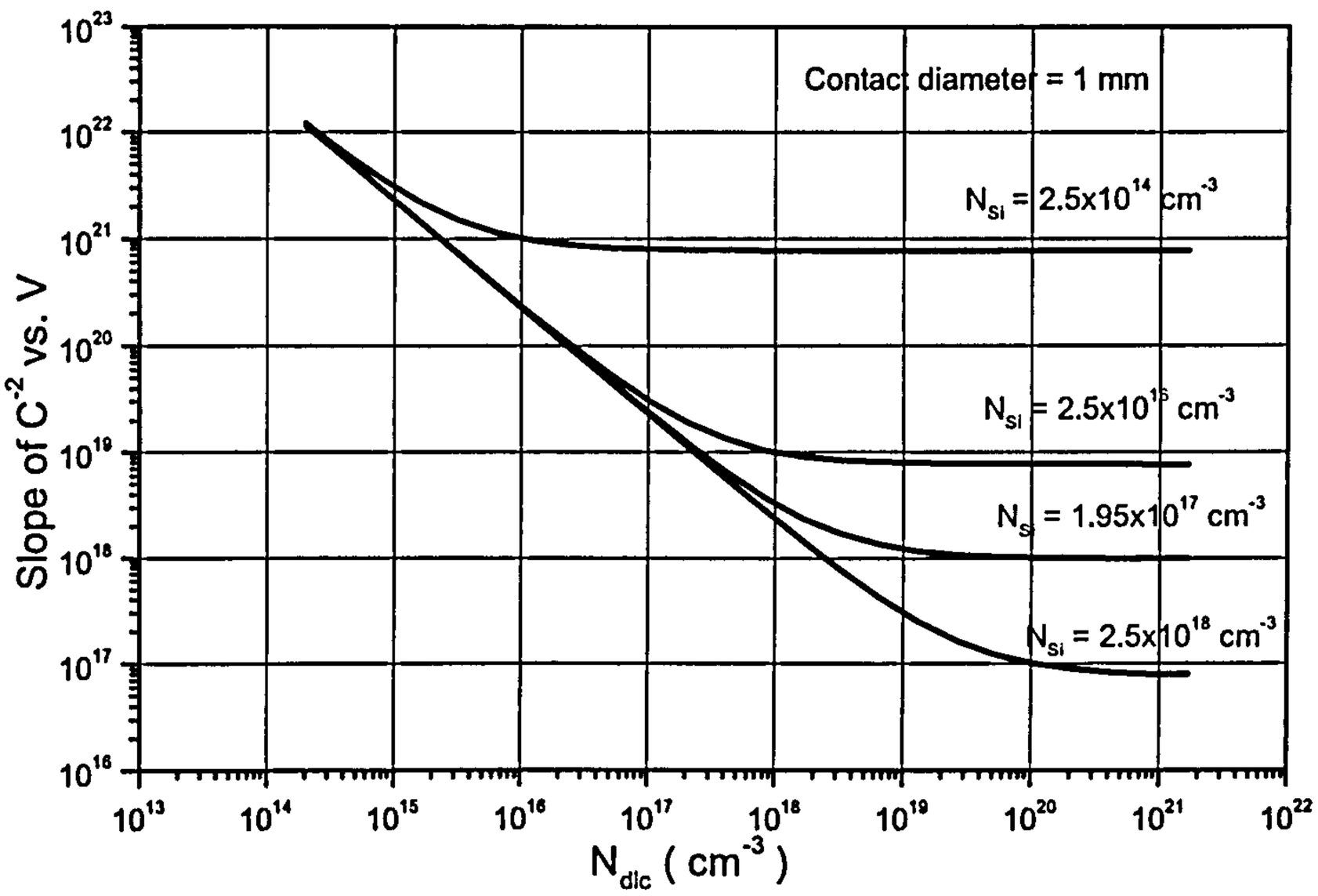

Fig.-5.1 $\frac{d(1/C^2)}{dV}$ plotted against the number of states (per unit cc) of Si/DLC heterostructures at different doping concentration in Si substrate.

5.2 Density of States from Metal-Insulator-Semiconductor diode

In view of the above discussion, it appears that it is not possible to deduce meaningful DOS data from either a Schottky diode or a DLC/Si heterostructure. To get around this

problem, we decided to look into another family of structures; the metal-insulator-semiconductor type of device. The schematic diagram of this structure is presented in Fig.5.2. A thermal oxide (SiO_2) of thickness 120 nm was grown on Si(100) substrate of resistivity 0.002 Ωcm. The resistivity of this Si substrate is so low that we can consider the Si substrate as a metal. The silicon substrate acts like a bottom gate. The amorphous hydrogenated carbon was deposited on the SiO_2 at different DC self-bias voltages, while all other growth parameters were maintained as constants. The Cr top contact was evaporated on to the a-C:H through a metal shadow mask in a vacuum chamber (pressure ~$1x10^{-6}$ Torr). The diameters of the evaporated holes were 2 mm, 1.5mm, 1 mm, and 0.5 mm.

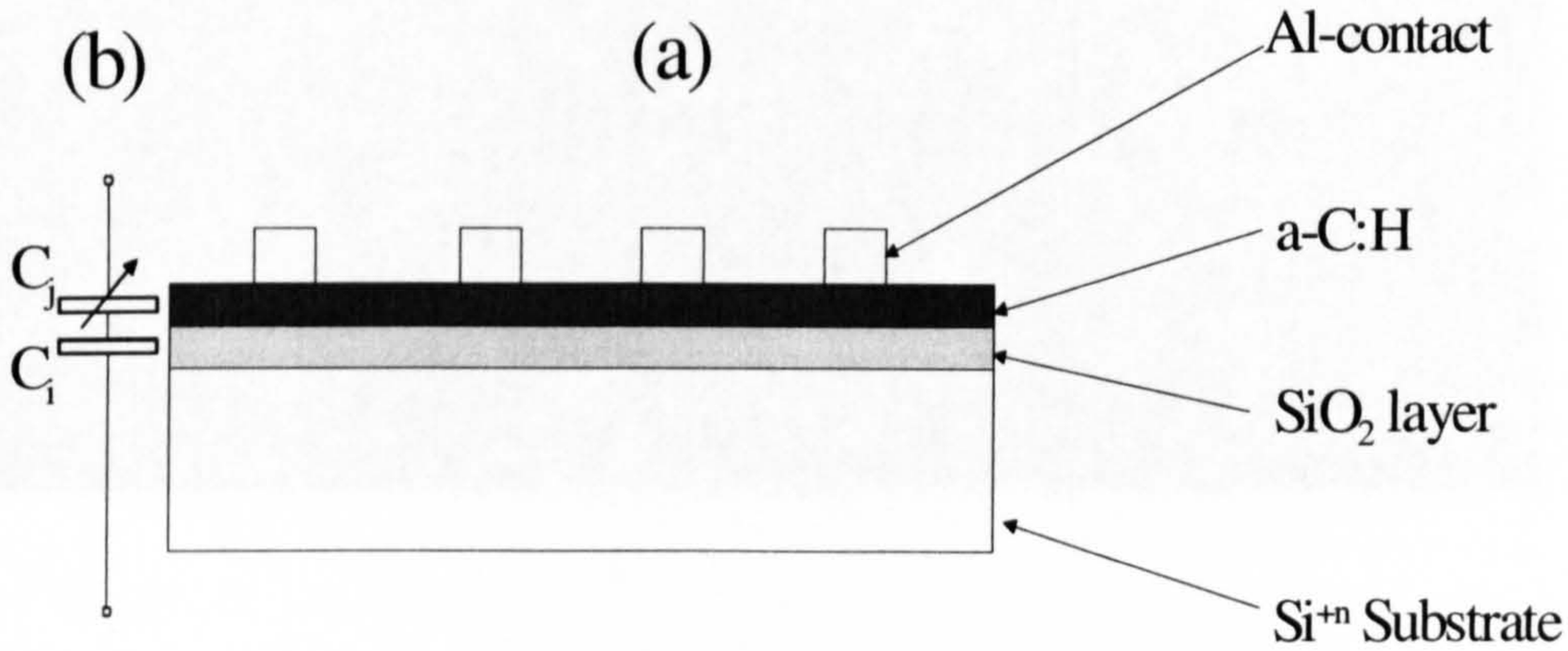

Fig.-5.2 (a) Structure of MIS diode fabricated in our laboratory in our laboratory to deduce the density of states in a-C:H. The Si^{n+} substrate, is highly conductive. (b) Equivalent circuit of MIS diode.

The discussion of the determination of the density of states in DLC using this structure, begins with a note on the mathematical model, developed to determine the density of states from MIS structures.

We investigated the voltage and frequency dependent capacitance of the MIS structures grown in our laboratory. Such measurements will help us to estimate the density of states of the amorphous hydrogenated carbon. The theory (which we developed) to determine the density of states is as follows.

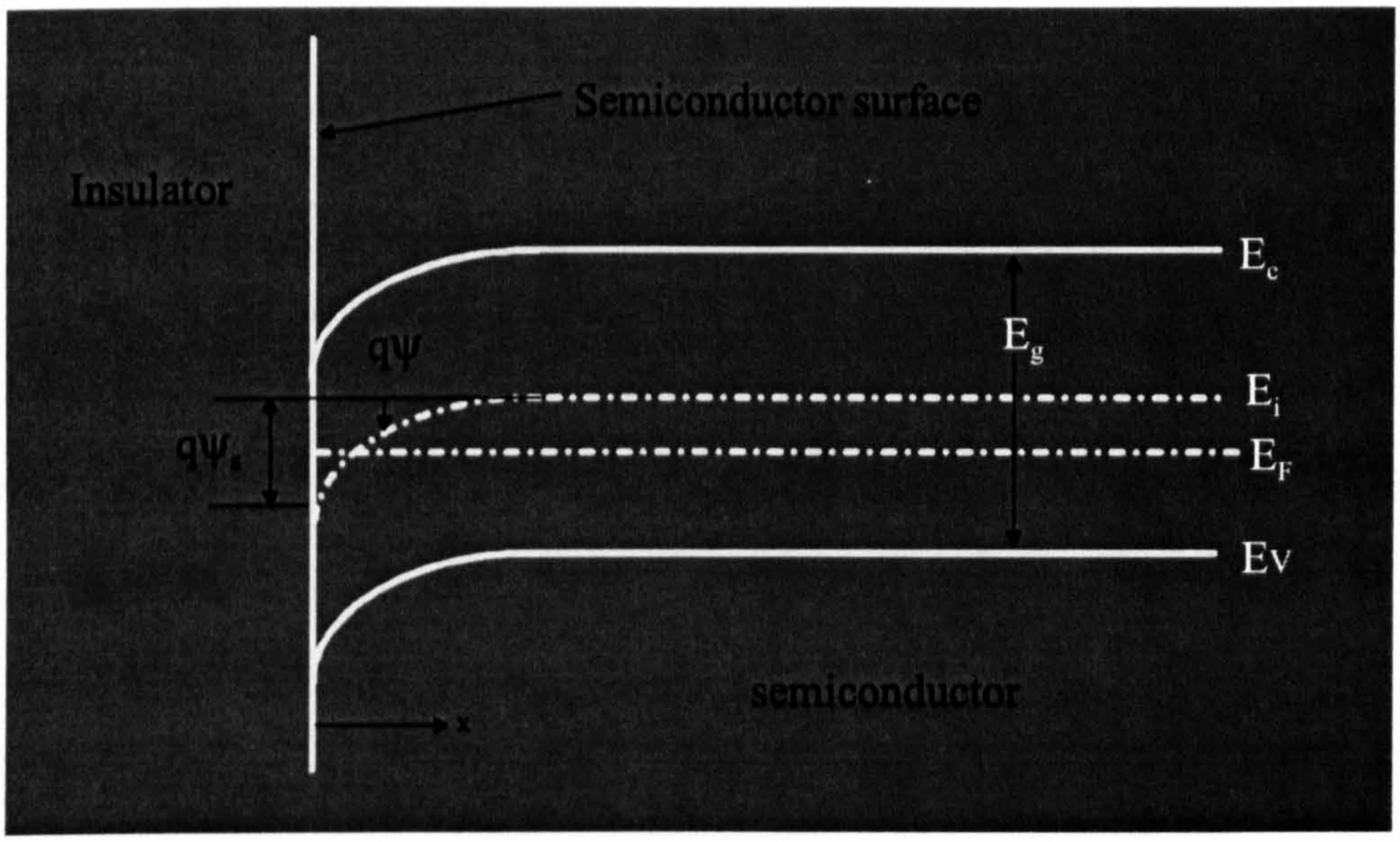

Fig.-5. 2 Energy –band diagram for ideal MIS diodes at the surface of p-type a-C:H.

The capacitance associated with the deep states is related to the density of such states.

If we have *n* number of states (per unit volume per unit energy) and their respective

ionised densities are $N_1, N_2, N_3, \ldots\ldots\ldots\ldots\ldots N_n$, then the Poisson equation [23] is expressed as:

$$\frac{d^2\Phi(x)}{dx^2} = \frac{q\left(\sum_1^n N_i\right)\Phi(x)}{\varepsilon_o \varepsilon_r} \qquad \ldots\ldots\ldots\ldots\ldots\ldots 5.6$$

Where, $\Phi(x)$ is a potential which is a function of the spatial co-ordinate x and ε_o and ε_r are the permittivity of free space and the relative permittivity of the semiconductor. Using proper boundary conditions, one can obtain the following solution to Eqn.(5.6)

$$\Phi(x) = \Phi_s \exp\left(-\frac{x}{x_o}\right) \qquad \ldots\ldots\ldots 5.7$$

Where, $x_o = \sqrt{\frac{\varepsilon_o \varepsilon_r}{q\left(\sum_1^n N_i\right)}}$ and Φ_s denotes the surface potential.

Since the space charge density is equal to $-qN\Phi(x)$, the space charge due to the traps is expressed by:

$$Q_j = -\int_0^d qN_j\Phi(x)dx \qquad \ldots\ldots\ldots\ldots\ldots 5.8$$

Since the differential capacitance equals $\left|\frac{dQ}{d\Phi_s}\right|$, the capacitance due to m of the total number, N_j of the trap states is:

$$\sum_1^m C_j = \left(\frac{q\varepsilon_r\varepsilon_o}{\sum_1^n N_i}\right)^{\frac{1}{2}} \sum_1^m N_j \qquad \ldots\ldots\ldots\ldots\ldots (5.9)$$

Here, $\sum_1^n N_i$ is the total ionised density. The value of m depends upon the frequency, i.e. the measured capacitance will be due only to a subset of the total number of states,

depending on the value of the ac frequency used. At low frequencies, almost all the states will contribute to the measured capacitance C, leading to the following situation:

$$\sum_1^n N_i = \sum_1^m N_j \qquad \text{..... 5. 10}$$

Therefore, one can obtain the following relationship from the above equations:

$$\sum_1^m N_j = \left(\frac{C}{q\varepsilon_o\varepsilon_r}\right)\sum_1^m C_j \qquad \text{..... 5. 11}$$

The density of states, N_m, corresponding to the m^{th} trap state, can be calculated at a given frequency, from the following expression:

$$N_m = \left(\frac{C}{q\varepsilon_o\varepsilon_r}\right)\left(\sum_1^m C_j - \sum_1^{m-1} C_j\right) \qquad \text{..... 5. 12}$$

The corresponding trap energy can be calculated using Eqn.-5.2. The value of τ_o in amorphous silicon is generally taken to be 10^{-13}s [24,33] and in amorphous carbon to be 10^{-12}s [34]. By substituting the value of temperature (T=300 K), τ_o and Boltzmann's constant in Eqn.-5.2, the range of energies from a frequency of 20 Hz to 1MHz (which is the available range of the HP4284A LCR bridge), is -0.56 eV to -0.3 eV with respect to the conduction band. Thus the lower is the frequency, the deeper are the states that we can probe.

5.2.1 Equivalent circuit for MIS diodes.

To get the correct information from the capacitance measurements it is important to know the equivalent circuit of the MIS diode. Fig.-5.2(b) shows capacitor-based

equivalent circuit of the MIS diode. The total capacitance C of the system is a series combination of the insulator capacitance C_i and the frequency-dependant, semiconductor depletion layer capacitance C_j. Therefore, the capacitance measured by the HP LCR bridge is given by the following relationship:

$$\frac{1}{C_{measured}} = \frac{1}{C_i} + \frac{1}{C_j} \qquad \text{.....(5. 13)}$$

The density of states can only be determined if we know the exact capacitance that is contributed by C_j (which can be calculated from Eqn.-5.13 at each frequency). A numerical code has been formulated to automate the process of obtaining *Cj* and the density of states with the variation in the frequency, (see Appendix-I).

5.3 Electrical Behaviour Of MIS diodes:

Not much has been published in the field of determination of the DOS in a-C:H from MIS diodes. It would be gratifying to check our theory to determine the DOS in a-C:H. This inspired us to undertake the following experimental investigation. Films of a-C:H were grown under conditions tabulated in Table-5.1. A-C:H films were deposited on a layer of thermally grown Silicon Dioxide (SiO_2) of thickness 120 nm, which itself was sitting on a 0.002 Ωcm n-type c-Si substrate. The highly conductive Si substrate again served as a bottom contact. The key parameter which influences various properties of diamond like carbon [20,29], including the DOS, is DC self-bias. Hence the deposition was carried out at 5 different DC-self bias voltages.

Table-5. 1 Growth parameters at which various MIS structures were fabricated.

Dc Self Bias Voltage (volts)	CH_4 Flow Rate (sccm)	Argon Flow Rate (sccm)	Film Thickness (nm)
-70	10	100	83.5
-140	10	100	80.5
-195	10	100	82.2
-240	10	100	83.0
-290	10	100	80.3

5.3.1 *I-V* Characteristics of MIS diode

A typical *I-V* characteristic for the MIS diodes is shown in the Fig.-5.4. These measurements were carried out to check leakage current through the gate. The value of current is quite low (<3pA) and hence the device quality is concluded to be very good. This confirms that there is hardly any leakage current which can affect the capacitance measurements. Therefore, we can say that the quality of the oxide layer (insulator) is quite good and that no defect or process-based damage has been introduced to the MIS diodes.

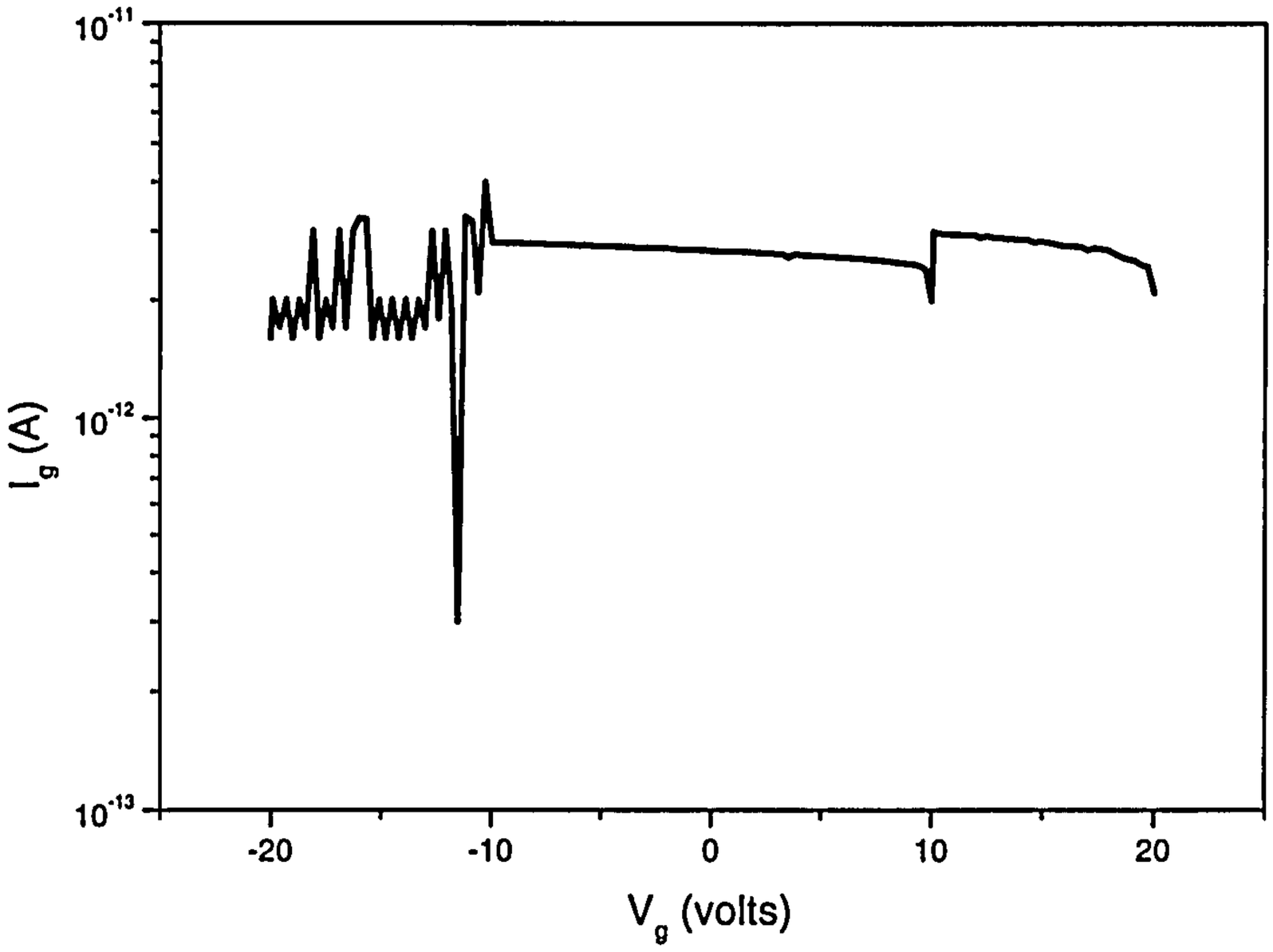

Fig.-5. 3 Leakage current through MIS diode. The current was measured between the top metal and the bottom gate electrode.

5.3.2 *C-V* measurements of MIS diode

Typical Capacitance-Voltage data obtained for MIS diodes manufactured at different DC self bias voltages is shown in Fig.-5.5. *C-V* measurements were carried at room temperature. The positive polarity probe of the HP 4284A LCR bridge was connected to the bottom contact (silicon wafer) while the negative polarity was connected to the top metal. It has been observed by a number of workers that as-deposited a-C:H films are p-type in nature [28,29]. It is evident from the *C-V* plots that the semiconductor material is indeed p-type in nature.

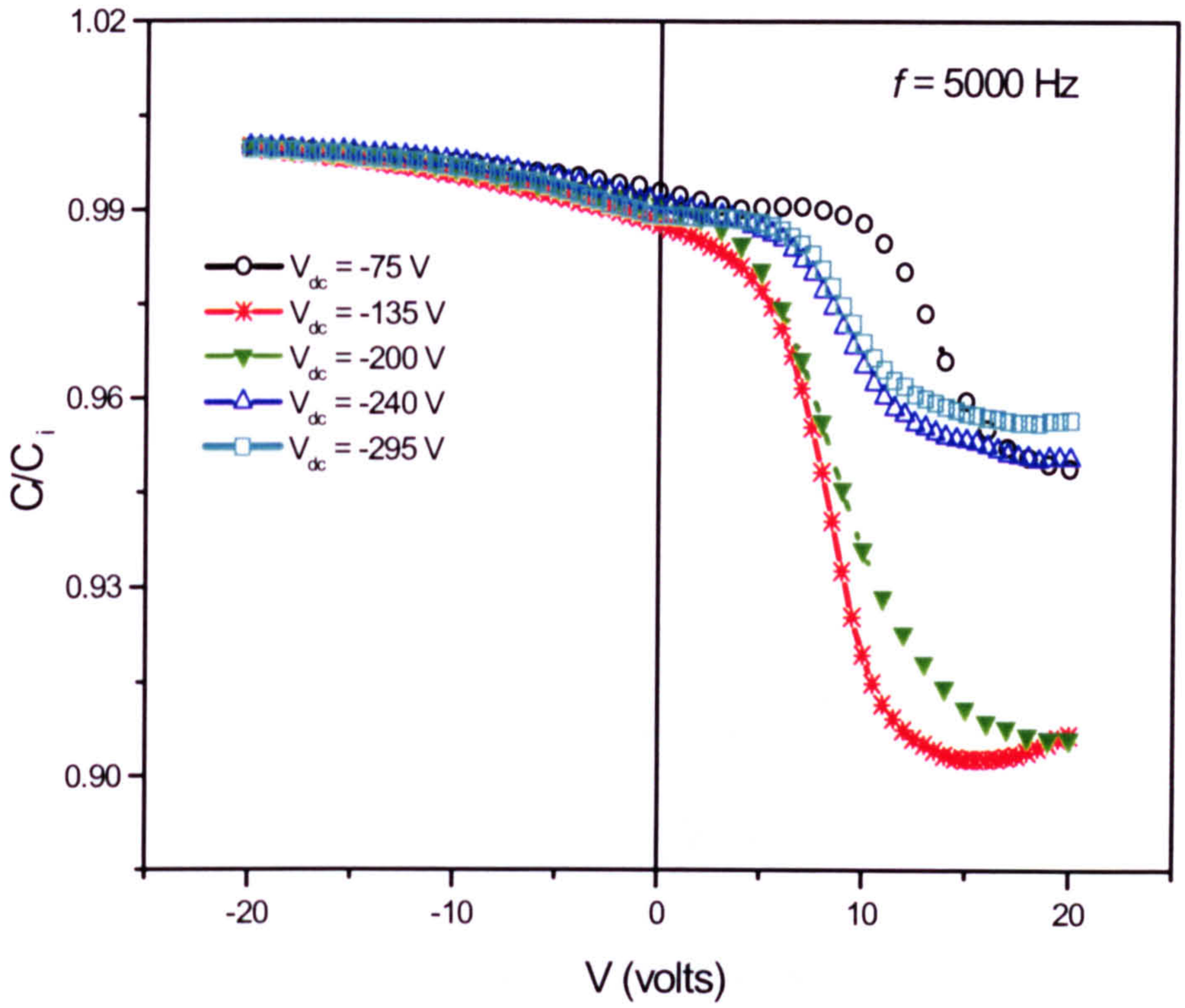

Fig.-5.5 *C-V* curves of MIS diodes fabricated at different DC self bias.

In describing these curves, I begin from the left hand side (negative voltage), where we have an accumulation of holes and therefore a relatively high differential capacitance of the semiconductor. As a result the total capacitance is close to the insulator capacitance. As the negative voltage is reduced, a depletion region forms near the semiconductor surface, and the total capacitance decreases.

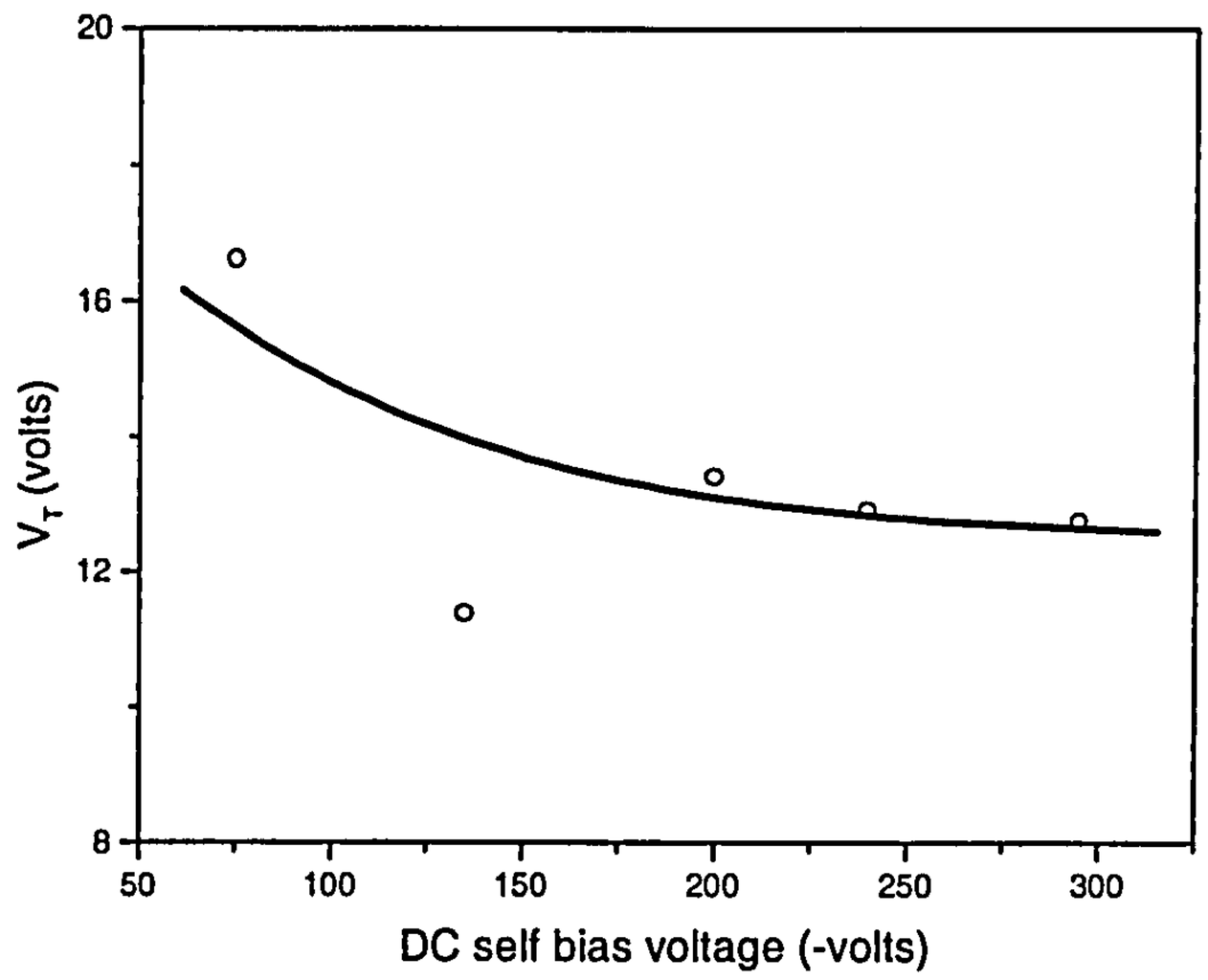

Fig.-5.6 Threshold Voltage of MIS diodes deposited at different DC self-bias voltage.

It should be noted that the flat band capacitance (where V= 0) for all the devices is nearly the same. The threshold voltage (or turn voltage) is an another quantity, which will crucially describe the *turn-on-state* of a transistor. At this voltage strong inversion takes place. Fig.-5.6 shows the effect of DC self bias on the threshold voltage. It is clear from Fig.-5.6 that the general trend is for the turn on voltage to flatten off with increase in the DC self-bias. This could be due to a reduction in the built in potential with decrease in the bandgap. The threshold voltage lies between 11.4 V and 16.6 V. These values are nearly the same as reported in [30,31] for ta-c based TFTs. It has also been observed from Fig.-5.5 that the change in the capacitance of MIS devices is minimal (around 10%) when the voltage sweeps from -20 V to 20 V. This may be due to the large width density of states around midgap and there is therefore little change in the depletion layer width when that

voltage sweep is done. Clough et al [30] have shown that in ta-C TFTs there is only one order of change in the magnitude of the drain current during the measurements of gate-transfer characteristics. Similar behaviour can be observed from our devices in the *C-V* plots.

5.3.3 Capacitance Frequency Measurements

The capacitance of PECVD a-C:H MIS diodes was measured by the LCR bridge at an ac signal of amplitude 25 mV over the frequency range 1MHz to 20 Hz. The measurements were carried out at different DC biases and at room temperature. Typical frequency dependence of the capacitance of the MIS diodes on the bias voltage is shown in Fig.-5.7. Films deposited at different DC self-bias voltages show different *C-f* behaviour. The measured capacitance is a function of the density of states and their distribution in the energy gap. This suggests that the DC self bias (which is a key parameter in determining the various properties of a-C:H films) can affect the nature of defects (distribution of deep states or profile of DOS).

Fig-5.7 (a) shows the *C-f* behaviour of MIS diode in which a-C:H was deposited at -70 V DC self-bias. The change in the capacitance with change in the gate bias and frequency is minimal. This may be due to a reduction in the accumulation of charge carriers near the interface of a-C:H/SiO_2. The film deposited at -70 V DC self bias has a Tauc Bandgap around 1.63 eV and resistivity of about 10^{14} Ωcm. Therefore the material behaves like an another insulator in the structure, hence the observed behaviour. The film deposited at higher DC bias shows distinct changes in the capacitance with changes in the frequency.

This is due to revised in the structural properties of the a-C:H film. The resistivity and bandgap fall with increase in the DC self –bias voltages. *C-f* plots show that there is an increase in the capacitance with decrease in the measurement frequency. This is because at relatively lower frequencies, even the deeper states starts responding to the ac signal. Thus a greater number of charges start to take part in forming the accumulation layer, causing the capacitance to be larger at lower frequencies.

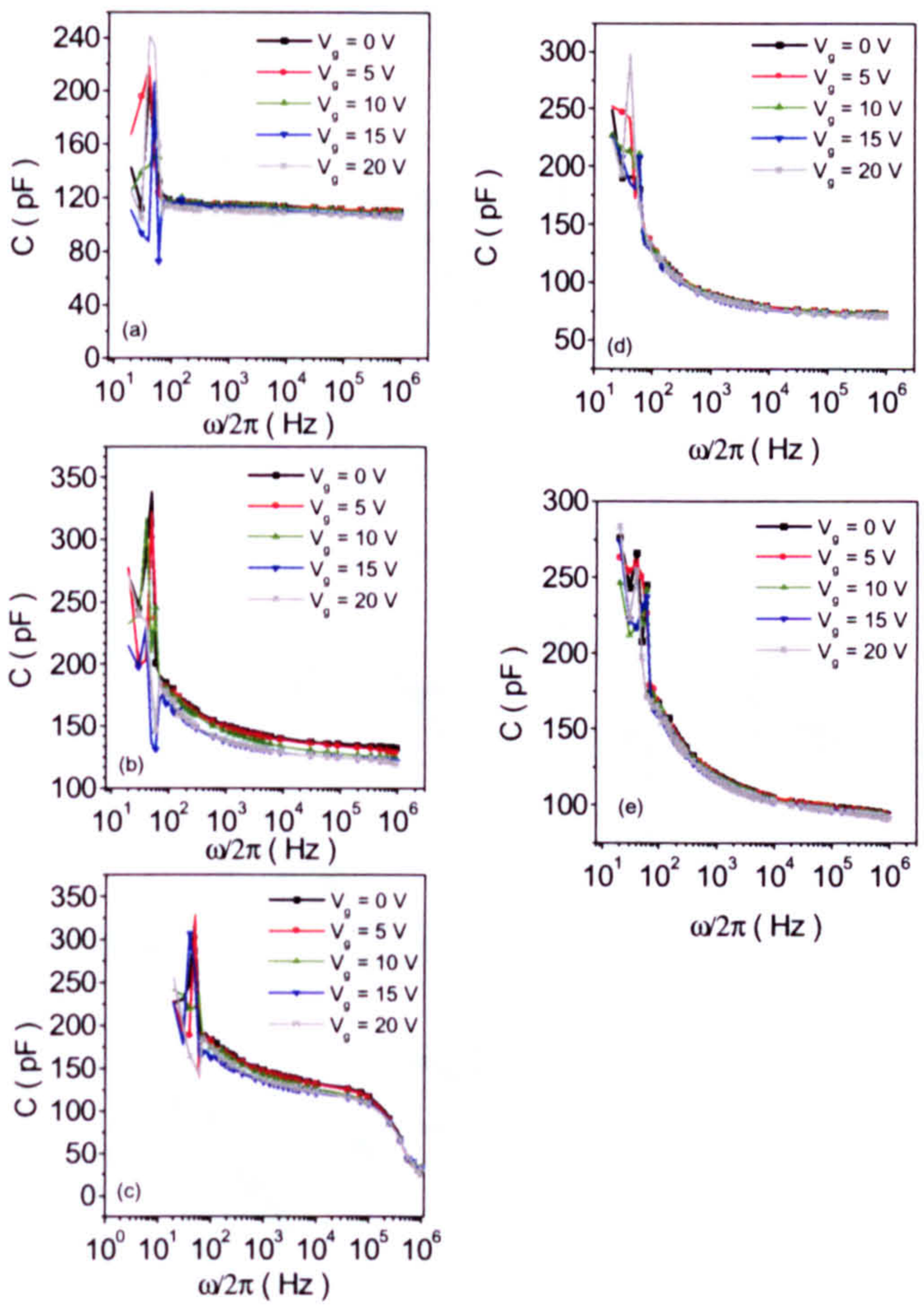

Fig.-5. 7 Capacitance-frequency characteristics of MIS diodes fabricated at different DC-self bias voltage. a-C:H films were deposited at (a) –70 V, (b) –135 V, (c) –200, (d) –245 V and (e) –295 V.

5.4 Deduction of density of states from *C-f* data

The density of states deduced from the *C-f* plots at a gate voltage of zero. This was done with the help of a computer programme. Estimation of the DOS was achieved using Eqn.-5.12.

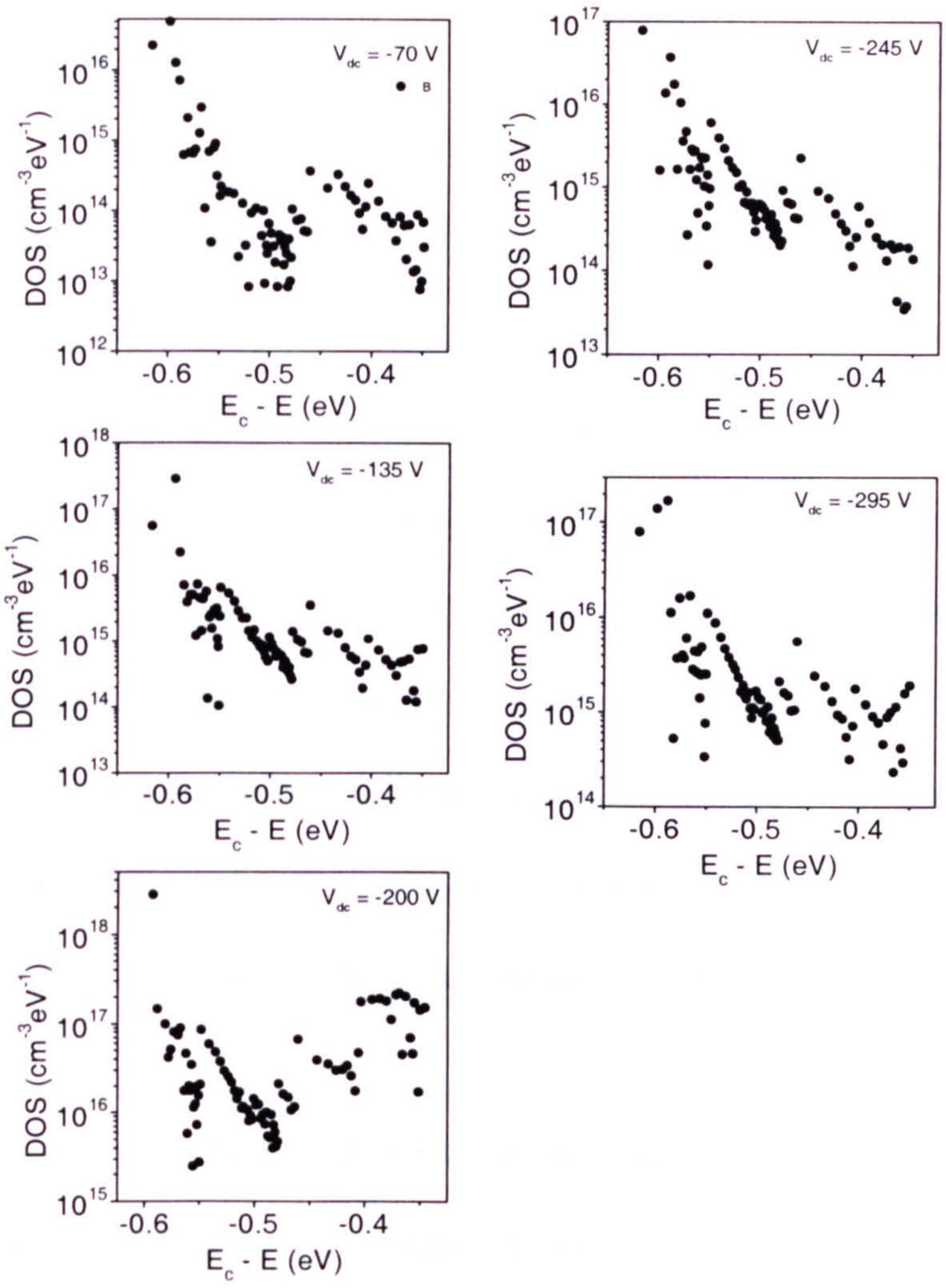

Fig.-5.8 Distribution of density of state in a-C:H deposited at different DC self bias.

Fig.-5.8 shows the distribution of DOS in the midgap region. It is quite clear from these plots that there is some change in the distribution of the DOS with change in the DC self bias. The value of the density of states lies between 10^{18} cm^{-3} eV^{-1} and 10^{15} cm^{-3} eV^{-1} on average. The value is one order lower than the measured value in a-C:H [32]. This may due to the technique we used to measure the density of states. It has also been shown by [32] that the ESR DOS is a few orders of magnitude different from the DOS measured from photoluminescence (PL) investigations.

In the amorphous carbon a number of forms of carbon are present and each has a different electronic configuration. Therefore, the density states in a-C:H is rather complex to interpret. But it can certainly be stated that the distribution of the DOS is not very smooth. DOS distribution is uneven in the midgap. The density of states does not follow any particular mathematical function. This may be due to different phases of carbon which constitute the electronic structure of amorphous carbon. Therefore, their distribution in the amorphous matrix of carbon effects the distribution of DOS. It has been reported by various workers that the distribution of various phases of carbon is not uniform in the amorphous material [35,36,37,38,39]. Hence, as the local structure varies so will the DOS.

Summary

Chapter 5 reports the structures and techniques have been used to investigate the density of states in a-C:H. The distribution of states in the gap is affected by the DC self-bias voltage. The threshold–voltage lies in the range 11-16 V, which agrees with reported values on the ta-C thin film transistor. *C-V* measurements show that the a-C:H films are p-type in nature. *C-f* measurements are as expected by Eqn-5.12. This suggests that the mathematical

model developed is correct and can be used to deduce the density of states. The DOS lies between 10^{15} to 10^{18} cm^{-3} eV^{-1}, which indicates that the quality of films is good. Films of this quality can be achieved by a proper selection of growth parameters.

References:

1. M. J. Powell, C. van Berkel, and A. R. Franklin and S. C. Deane and W.I. Milne, *Phys. Rev. B*, **45**, 4160 (1992)
2. G. H. Döhler, G. H. Döhler, *Phys. Rev. B*, **19**, 2083 (1971)
3. Stephen K. O'Leary, S. R. Johnson and P. K. Lim, *J. Appl. Phys.*,**82**, 3334 (1997).
4. P. Chatterjee, R. Vanderhaghen and B. Equer, *J. Appl. Phys.*, **87**, 1874 (2000).
5. M. J. Powell and J. W. Orton, *Appl. Phys. Letts.*, **45**, 171 (1984).
6. Hoe Sup Soh, Choochon Lee, Jin Jang, Moon Youn Jung, and Soon Sung, *Appl. Phys. Lett.*, **63**, 779 (1993).
7. S. C. Deane and M. J. Powell, *J. Appl. Phys.*, **74**, 6655 (1993).
8. P. Kleider,C. Longeaud, M. Gauthier and P. Rocai Cabarrocas, *Appl. Phys. Lett.*, **75**, 3351 (1999).
9. Fan Zhong and J. David Cohen, *Phys. Rev. Lett.*, **71**, 597 (1993).
10. S. Nespurek and J. Sworakowski, *J. Appl. Phys.*, **51**, 2098 (1980).
11. K.D McKenzie, P.G Lecomber and W.E Spear, *Phys. Rev. Lett.*, **46**, 377 (1982).
12. Carol E. Michelson and J. David Cohen, *Phys. Rev. B*, **41**, 1529 (1990).
13. C.-Y. Huang, S. Guha, S. Hudgens, *Phys. Rev. B*, **27**, 7460 (1983).
14. J. Robertson, *Diamond and Relat. Mater.*, **6**, 212 (1997).

15. J.H. Van Vleck, *Phys. Rev. B*, **74**, 1168 (1948).

16. G. Fusco, A. Tagliaffero, W.I. Milne, M. Fanciulli, *Diamond and Relat. Mater,* **3**, 844 (1994).

17. C.P. Pole, *Electron Spin Resonance*, John-Wiley, London, 1983.

18. Balberg and D.E Carlson, *Phys. Rev. Lett.*, **43**, 58 (1979).

19. S.R.P Silva, *Thesis*, Dept. of Engineering Cambridge Univeristy. Cambridge, UK (1993).

20. A. Zeinert, H.-J. von Bardeleben, and R. Bouzerar, *Diamond and Relat. Mater.*, **9**, 728 (2000).

21. Rusli, J.Robertson and G.A.J Amaratunga, *J. Appl. Phys.*, **80**, 2998 (1996).

22. J. Reistin, J. Schafer, and L. Ley, *Diam. Relat. Mater.*, **4**, 508 (1995).

23. S.M. Sze, Physics of semiconductor Devices, (Wiley Interscience), 1987.

24. D.V lang, J.D Cohen and J.P Harbison, *Phys. Rev. B*, **25**, 5285 (1982).

25. B. Racine, *Ph.D Thesis*, University of Amiens, France, (1999).

26. S. Paul and F.J. Clough, *Diamond Related Materials*, **7**, 1734, (1998).

27. K.C Palinginis, Y. Lubianiker, J.D. Cohen, A.Ilie, B.Kleinsorge, W.I Milne, *Appl. Phys. Letts.*, 74, 371 (1999).

28. S. Egret, J. Robertson, W.I. Milne and F.J. Clough, Diamond Related. Mater. **6**, 879, (1997).

29. E.Ohta, Y. Kimura, H. Kondo, M. Takahashi, K. Kameyama, K. Yamda and I. Fujimura, *22nd Int. Conf. Sol. Stat. Devices and Materials (SSDM)*, 589, 1990.

30. F.J Clough, W.I. Milne, B. Kleinsorge, J. Robertson, G.A.J Amaratunga and B.N. Roy, *Electronics Letters*, 32, 498 (1996).

31. S.L Maeng, S. Uchikoga, F.J Clough, A. Tagliaferro, A.J Flewitt, J. Robertson and W.I Milne, *Diam. and Relat. Mater.*, **9**, 805 (2000).

32. F. Giorgis, F. Giuliani, C.F Pirri, A. Tagliaferro and E. Tresso, *Appl. Phys. Letts.*, **72**, 2520 (1998).

33. A.J Snell, K.D Mackenzie, P.G LeComber and W.E Spear, *Phil. Mag.*, **40**, 1 (1979).

34. L. Klibanov, M.Allon-Alaluf, N.Croitoru and A. Seidman, *Diamond and Relat. Mater.*, **5**, 1414 (1996).

35. Ph. Komninou, G.Nouet, P.Patsalas, Th. Kehagias, M.Gioti, S.Logothetidis, Th. Karakostas, *Diamond Relat. Mat.*, **9**, 703 (2000).

36. G. Amaratunga, A. Putnis, K. Clay, and W.I Milne, *Appl. Phys. Letts.*, **55**, 634, 1989.

37. S.R.P Silva and G.A.J Amaratunga, *J. Materials Science*, **29**, 4962, 1994.

38. I. Rusman, I. Klibanov, L. Burstein, Y. Rosenber, V. Weinstein, E. BenJacob, N. Croitoru, A. Seidman, *Thin solid films*, **287**, 36 (1996).

39. S. Paul and F.J Clough, *Diamond and Related Materials*, 1998, Vol .7, pp.1734-1738.

CHAPTER 6

Development of SEM/Micro Tip Instrument

6.1 Introduction

Material properties are often dictated by the resolution at which the instrument analyses the sample. There are a number of materials, which reveal information about their intrinsic properties in the sub-micron or the nano-scale [1,2,3,4], which remains obscured by studies at larger dimensions, [5,6]. We have already published reports on the contrasting behaviour of a-C:H in the sub-micron region compared to the observed nature of the material over larger areas [5]. We intend to investigate these properties in even greater detail.

Typically such investigations have been undertaken in experimental set-ups in which Scanning Tunnelling Microscopes, (STM) are placed in the Scanning Electron Microscope (SEM) chamber and the material properties of interest have been measured [8,9,10]. The fraction of the sample under local investigation through an STM is not representative of the entire surface. In the SEM/STM combination, panning and zooming with the SEM, along with a coarse positioning by the STM, provide extensive access to the whole surface. The combination is necessary for examining polycrystalline materials characterised by microscopically varying geometric and electronic properties. A combined STM/SEM device also allows the study of the properties at the interface of two grains (e.g. segregation and phase separation). Without an SEM, it is virtually impossible to distinguish between a grain boundary and a scratch caused by polishing or a naturally occurring line defect. These and

other advantages of the SEM/STM combined system encouraged various workers and resulted in three distinct categories of SEM/STM combination:

1. High-vacuum (HV) SEM/STM [11,12]
2. UHV SEM/STM without simultaneous imaging [13,14]
3. UHV SEM/STM with simultaneous imaging [15,16].

The instruments presented above are highly expensive and can have unaffordable. To understand the properties of diamond-like carbon in the sub-micron scale we introduced a simple *tip-holding arm* to an existing SEM in our laboratory. A schematic diagram of this instrument is shown in the Fig.-6.1. The advantage of this instrument is that one can make electrical contact (*C-V* and *I-V*) measurements with it. The spurious currents caused by any superficial impurity, recorded during non-contact electrical measurements (such as when an STM is being used alone) can be eliminated by using our instrument. Another significant advantage of this instrument is that the electrical characteristics of insulator materials can also be easily measured; it is difficult to use an STM for that purpose.

6.2 Instrument Details

We designed a mechanical arm (shown in Fig-6.2), which is incorporated in the SEM. The sub-micron tip (similar to tips used in STM analysis) can be attached to the end of this arm. Considering the direction of impingement of the electron beam to be the $\vec{z}$ direction, we conclude that the tip can be moved manually in the *X-Y* plane. The tip can be used to measure

the contact electrical characteristics. The electrical connections to the tip and the sample are made via the feed-through, which is attached to the ultra-high (UH) vacuum chamber of the SEM. A picoammter or an LCR bridge was connected to the outer terminal of a feed-through. The development of this instrument allows us to connect any electrical meter to the SEM/tip arrangement; thus enabling the utilisation of the picoammter (HP 4140B), LCR bridge (HP 4248A), etc (which are the commonly available measuring devices in semiconductor laboratories).

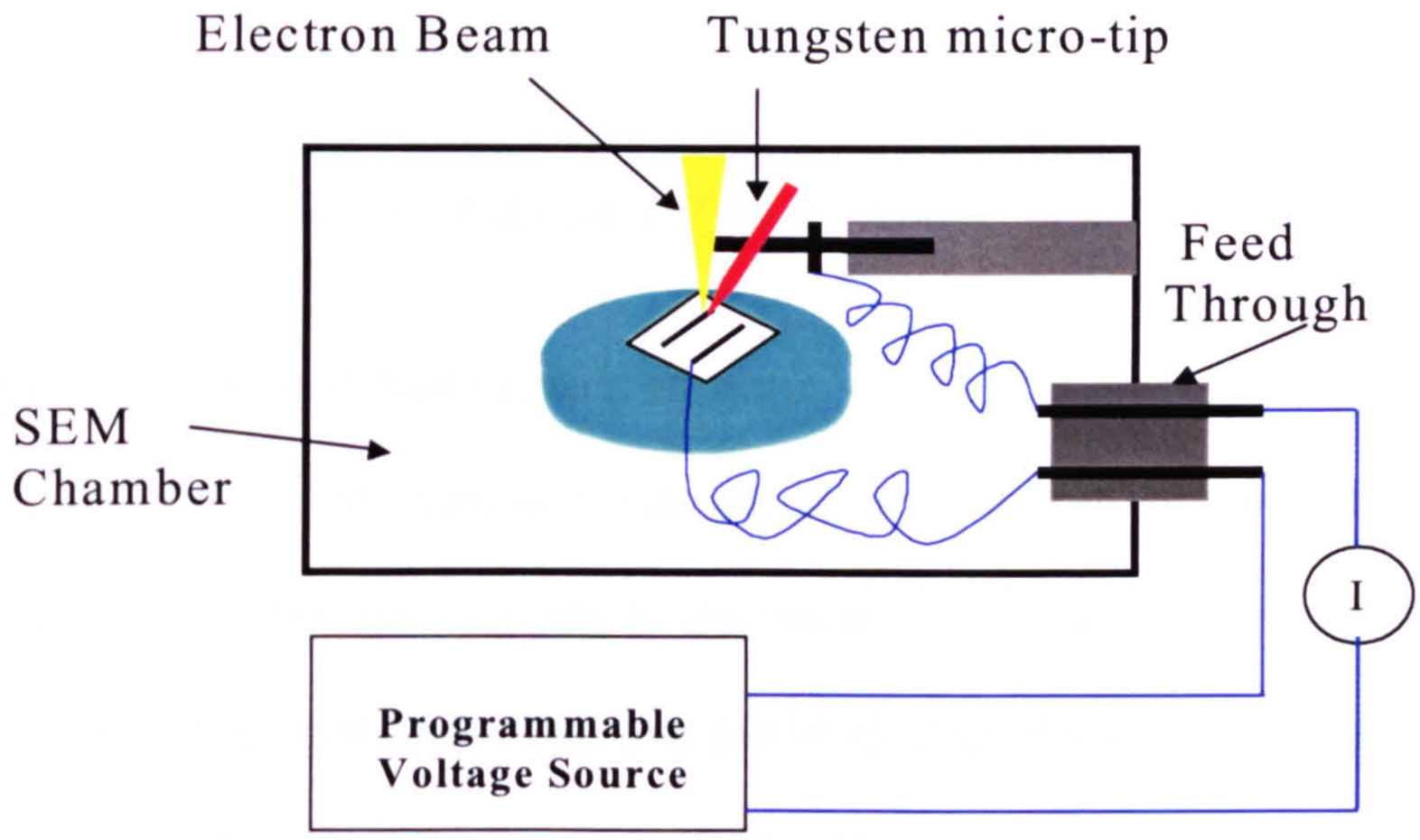

Fig.- 6.1 Schematic diagram of the SEM/micro-tip instrument used in the analysis of the properties of a-C:H in the sub-micron scale.

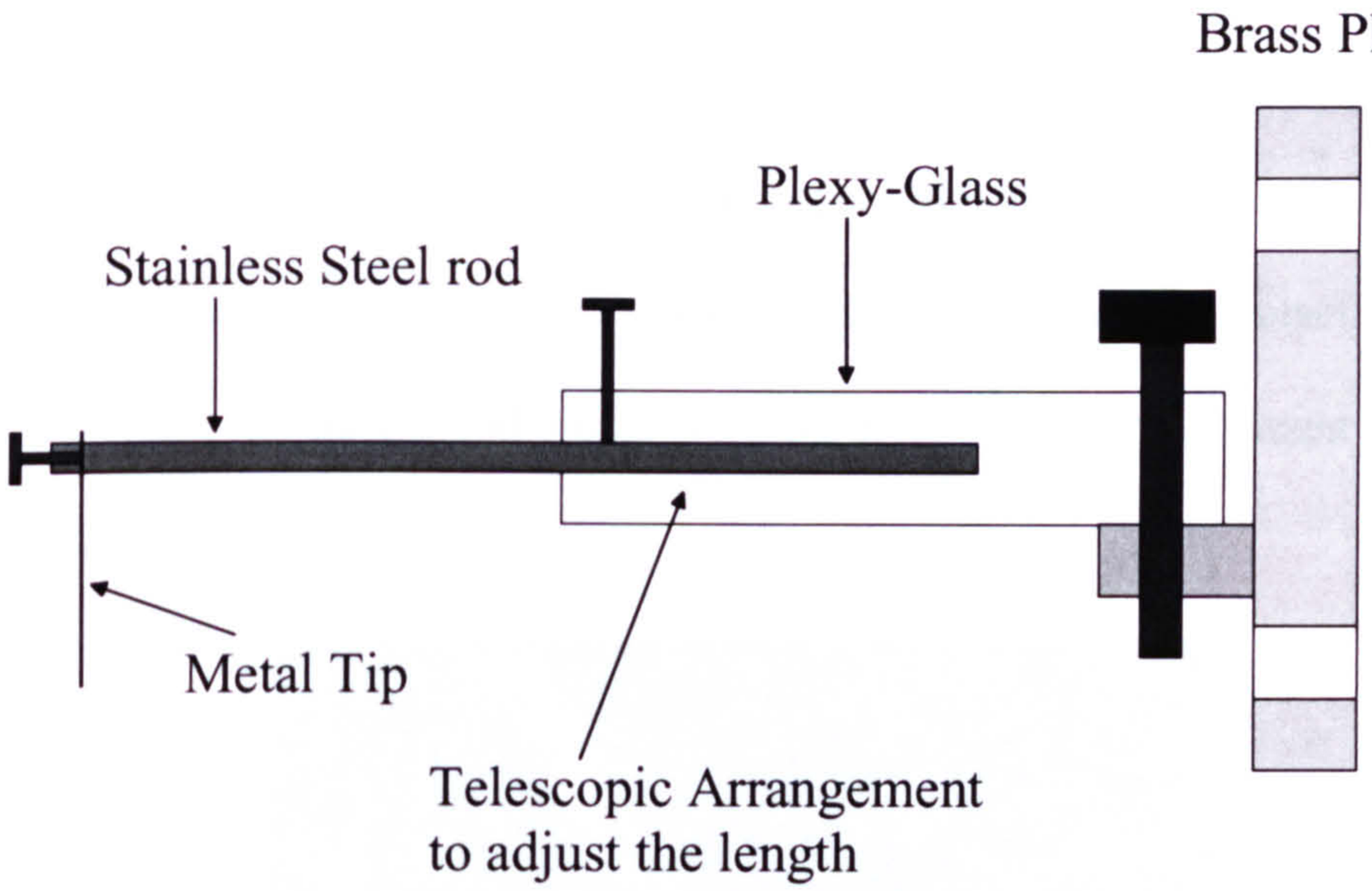

Fig.-6.2 Schematic diagram of the *tip-holding arm*.

6.2.1 Aligning tip to the Optical Axis of electron beam

Once we have closed the SEM chamber we do not have to control the movement of the arm that holds the tip, since the arm can only be moved in the *X-Y* plane manually. But we need the tip to be coincident with the optical axis of the electron beam. This is essential to ensure that the contact of the tip to the sample is visible. The optical alignment of the tip was carried out in two steps; firstly we loaded a cross-shaped metal stub, shown in Fig.-6.3, into the SEM chamber. With the help of **X**, **Y** and **Z** stage controllers, we focused the electron beam at the centre of the *cross-stub* to get highest magnification while retaining the alignment

between the centre of cross and the middle of computer screen. The SEM chamber was opened without disturbing the *crossed-stub*. The end of the tip was aligned to the centre of the *crossed-stub* with the help of an optical microscope. Maximum care was taken during this step to ensure that the end of the tip and the crossed-stub were not in contact. Fig-6.3 shows the tip at the centre of the crossed-stub. With the help of this arrangement we obtained a resolution upto 50 nm.

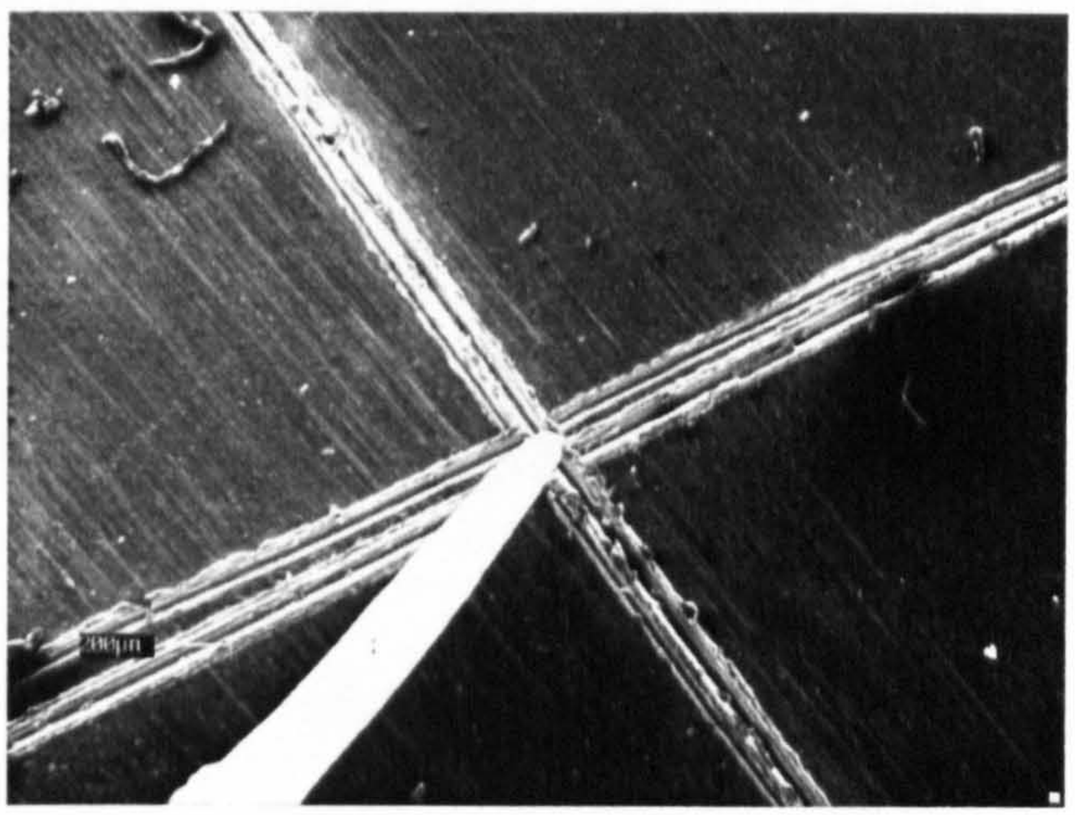

Fig-6.3 SEM micrograph of micro-tip aligned to the centre of the crossed-stub. The alignment helps us to see the material-tip contact upto a scale of 50 nm.

6.2.2 Electrical connection to the sample

The positive terminal is connected to the tip which is completely isolated (electrically) as some portions of the arm are made of plexy glass. This was done to avoid any short-circuiting of the electrical signal to the chamber. The negative terminal of the instrument is connected

to the sample by the use of silver paste. The sample under investigation is glued to the insulating stub to avoid any short-circuiting. The other end of both wires (coming from the sample and tip) are connected to the feedthrough.

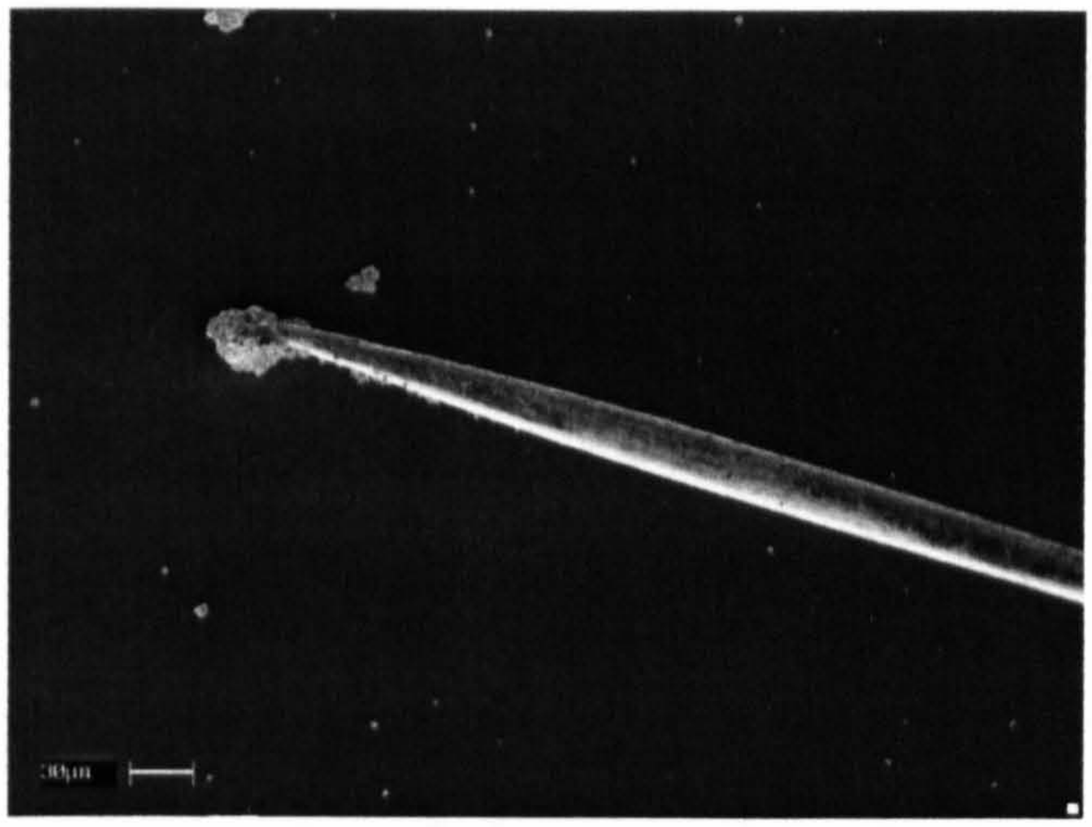

Fig-6.4 Tungsten tip making a contact with a chromium cluster, which lies on the surface of the a-C:H film.

6.3 Electrical Measurements

As already mentioned, the advantage of this instrument is that it offers contact measurements. To make a contact with the surface of any material at the point of interest, the **X**,**Y** and **Z** stage controllers of the SEM were used. Fig.-6.4 shows contact to the Cr cluster that lies on the surface of an amorphous carbon film. During the process of focusing, there may be accumulation of electrons on the surface of the sample. This is because the sample is

placed on the insulating stub. To discharge this accumulation we grounded the wire coming out from the sample. At this stage electrical meters were not connected to the outer terminal of the feedthrough. After focusing the electron beam to the desired point on the surface of the film, the contact between the tip and the sample is established with the help of the stage controllers of the SEM. The electron beam is switched off to avoid any effects of the impinging e-beam on the electrical measurements. A piccoammeter (HP 4140 B) and an LCR bridge (HP 4248 A)were interfaced to a computer and data was collected with the help of HP-VEE programmes.

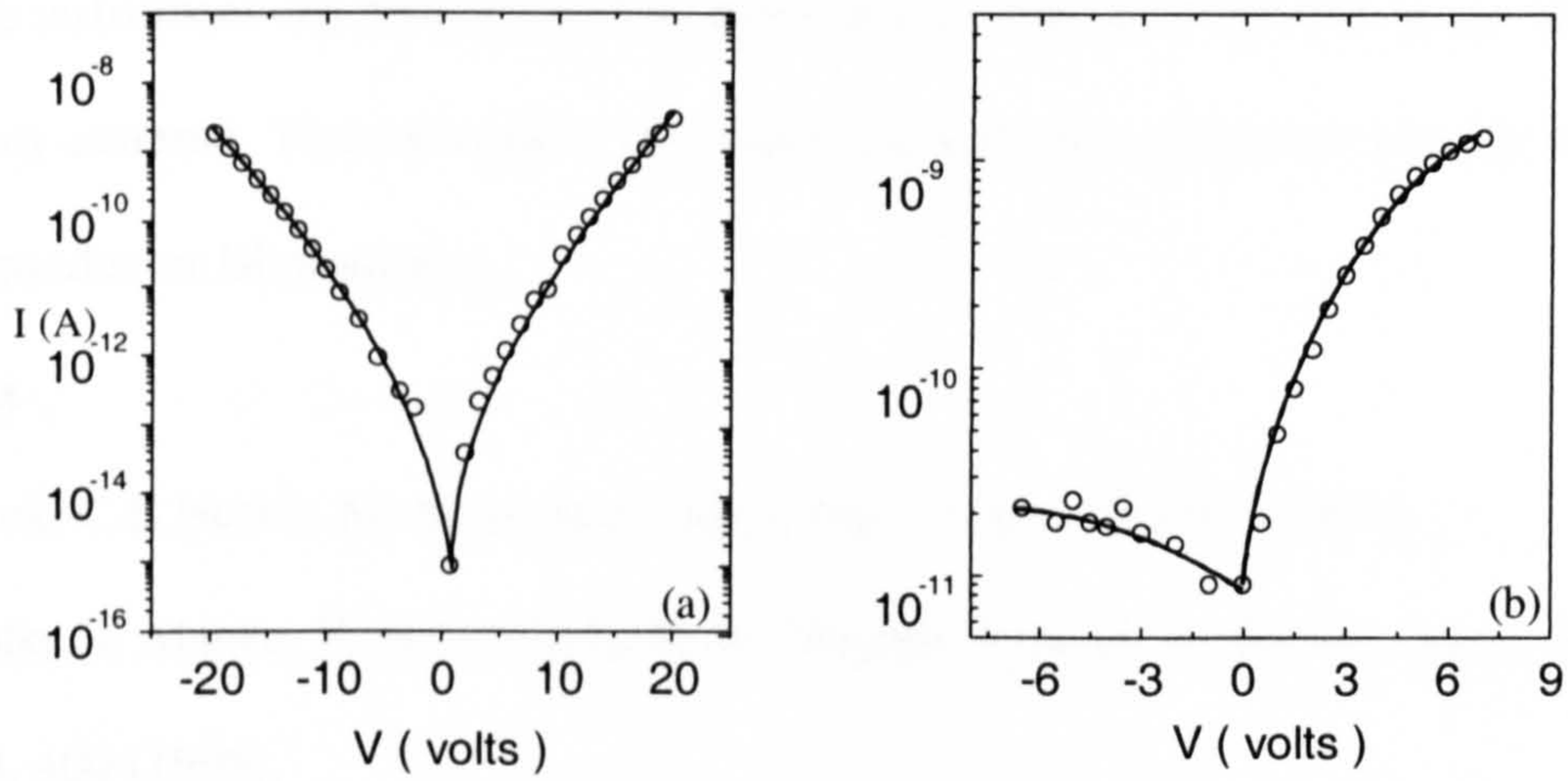

Fig. 6.5 (a) A typical symmetrical *I-V* characteristic for a 'micro-tip' MSM structure in the middle of a Cr strip (b) A typical asymmetrical *I-V* characteristics from a 'micro-tip' MSM structure at the edge of a Cr strip.

We have measured electrical characteristics of various samples of crystalline Si, amorphous silicon and amorphous hydrogenated carbon. This was done to check the performance of the instrument. The electrical characteristics of amorphous carbon deposited on metal strips are shown in the Fig.-6.5. The *I-V* characteristics measured at the middle of strip are symmetrical while the plots are asymmetrical when measured at the edge of the strip. *I-V* characteristics measured for this system are interesting and throw light on the PECVD process. The details of these measurements are discussed in Chapter 7.

We used this instrument extensively to understand the properties of amorphous carbon. This simple instrument can be employed to measure the electrical properties in the sub-micron range of any material. This instrument is economical and uses appliances already existing in most semiconductor laboratories.

References

1. B. Rezek, C.E Nebel, M. Stutzmann, *Appl. Phys. Letts.*, **75**,1742 (1999)
2. D. Pahlke, I. Manke, F. Heinrichsdorff, M. Daehne Prietsch, W. Richter, *Appl. Surf. Sci.*, **123-24**, 400 (1998).
3. K.J Koivusaari, T.T Tantala, J. Levoska and S. Leppävouri, *Appl. Phys. Letts.*, **76**, 2794 (2000).
4. Y. Zhen, H.W.C Postma, L. Balents, C. Dekker, *Nature*, **402**, 273 (1999)
5. S.Paul and F.J Clough, *Diamond Related Mater.*, **7**, 1734 (1998).

6. S.Paul and F.J Clough, *Materials Research Society Proceeding* , **Vol. 558**, pp.149-154, (2000)

7. R. Heiderhoff, R.M. Cramer, L.J Balk, *34th IEEE int. Reliability Physics Symp*, Proc. (IRPS 96). P.336 (1996).

8. Ch. Gerber, G. Binning, H. Fuchs, O. Marti, and H. Rohrer, *Rev. Sci. Instrum.*, **57**, 221 (1986)

9. S. Maruno, N. Nakahara, S. Fujita, H. Waranabe, Y. Kusmi, and M. Ichikawa, *Rev. Sci. Instrum.*, **68,** 116 (1997).

10. A.V. Ermakov an d E.L Garfunkel, *Rev. Sci. Instrum.*, **65,** 2853 (1994)

11. M. Troyon, H.N Lei, and A Bourhettar, *Ultramicroscopy*, **42-44**, 1564 (1992).

12. K.Takata, S. Hosoki, S. Hosaka, and T. Tajima, *Rev. Sci. Instrum.*, **60**, 789 (1989).

13. S. Chiang and R.J Wilson, *IBM J.Res. Dev.*, **30**, 515 (1986).

14. R. Weisendanger, D. Buergler, G. Trrach, D. Anselmetti, H.R. Hidber, and H.J. Guntherdot, *J. Vac. Sci. Technol.*, **A8**, 339 (1990).

15. G.C. Rosolen and M.E. Wellan, *Rev. Sci. Instrum.*, **63**, 4041 (1992)

16. E.E. Ehrichs, W.F. Smith, and A.L. deLozanne, *J. Vac. Sci. Technol.*, **B 9**, 1380 (1991).

CHAPTER 7

Metal-Semiconductor-Metal Switches and Schottky diodes

7.1 Review of Metal-Semiconductor-Metal switches

Metal-semiconductor-metal and metal-insulator devices form a class of highly novel devices that find use as switches in flat panel technologies and in the determination of various intrinsic properties of materials [1,2,3,4]. The dominant flat panel technology (FPT) at present is the active matrix liquid crystal display (AMLCD) in which each pixel incorporates a switching element to regulate the electro-optic response to the liquid-crystal (LC) cell [1]. Three-terminal thin film transistors (TFT) are commonly used as control switches in flat panel displays (FPD); these devices are generally made of either hydrogenated amorphous silicon (a-Si:H) [2] or polycrystalline silicon [3]. However, there has been a recent upsurge in the development of simpler and cheaper diode-based switching technologies, [4] owing to the high number of mask levels in current TFT technology. The rather stringent alignment conditions required to manufacture TFT structures with high yields over large areas, has also challenged the monopoly of TFTs. The comparatively small size of two terminal devices also increases the pixel aperture ratio, thereby improving LCD brightness and power efficiency. The wide usage of a-Si:H diodes and TFTs owes to extensive investigations of this material and these devices. Inspite of comprehensive studies of a-Si:H based TFT technology, full control over the stability of these devices is yet to be achieved. The instability of these devices arises from

the creation of defect states within the a-Si:H layer during device operation [5,6]. Defect creation results in threshold voltage instability and leads to fluctuations in the pixel switching speed.

Two terminal devices such as varistors, [7], and metal-insulator-metal (MIM) or metal-semiconductor-metal (MSM) structures have been developed. The most commonly used materials in these structures are tantalum pentoxide (Ta_2O_5) [8,9,10,11] and the silicon-rich silicon nitride (a-SiN_x:H) [12,13,14] .

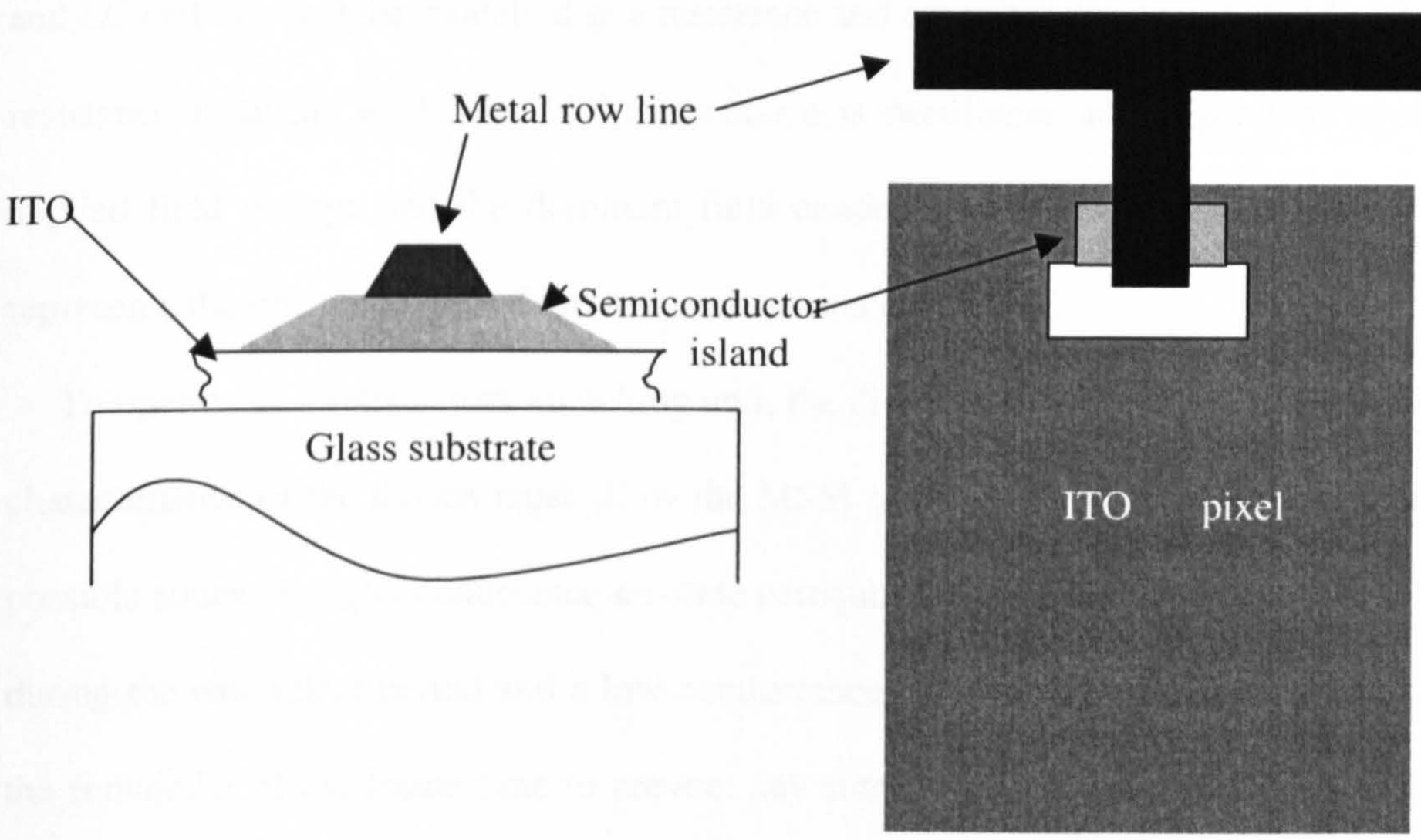

Fig.-7.1 Cross-section of an MSM structure and its integration into an LCD pixel.

The schematic diagram of an MSM sandwich structure and its integration into an LCD pixel is shown in Fig-7.1. MSM fabrication requires a maximum of only three masks, to

define the semiconductor-island and the top and bottom contacts. Significantly, any minute misalignment between the row metal and the ITO bottom contact has no effect on the current density within the device and hence the device characteristics are unaffected. The opaque metal contact also acts as a light shield to the MSM semiconductor layer.

The row and column connections to an MSM addressed LCD pixel and the corresponding equivalent circuit are shown in Fig.-7.2. Each pixel comprises an MSM and an LC cell connected in series between the row and column electrodes. The MSM and LC cell can each be modelled as a resistance and capacitance in parallel [18]. The LC resistance is linear while the MSM resistance is non-linear and dependent upon the applied field voltage and the dominant field conduction mechanism. The resistor R_{line} represents the line resistance of the row and column electrodes.

To operate as a satisfactory switching unit, the display drive scheme and the electrical characteristics of the device must allow the MSM to be configured to either one of two possible states. A high conductance *on*-state is required to enable charging of the LC cell during the row select period and a low conductance *off*-state must be maintained during the remainder of the frame time to prevent any significant leakage of the pixel voltage. Rapid switching between the *off* and *on* states is also important to achieve a small operating voltage range for the device (i.e. from $-V_{ON}$ to $+V_{ON}$).

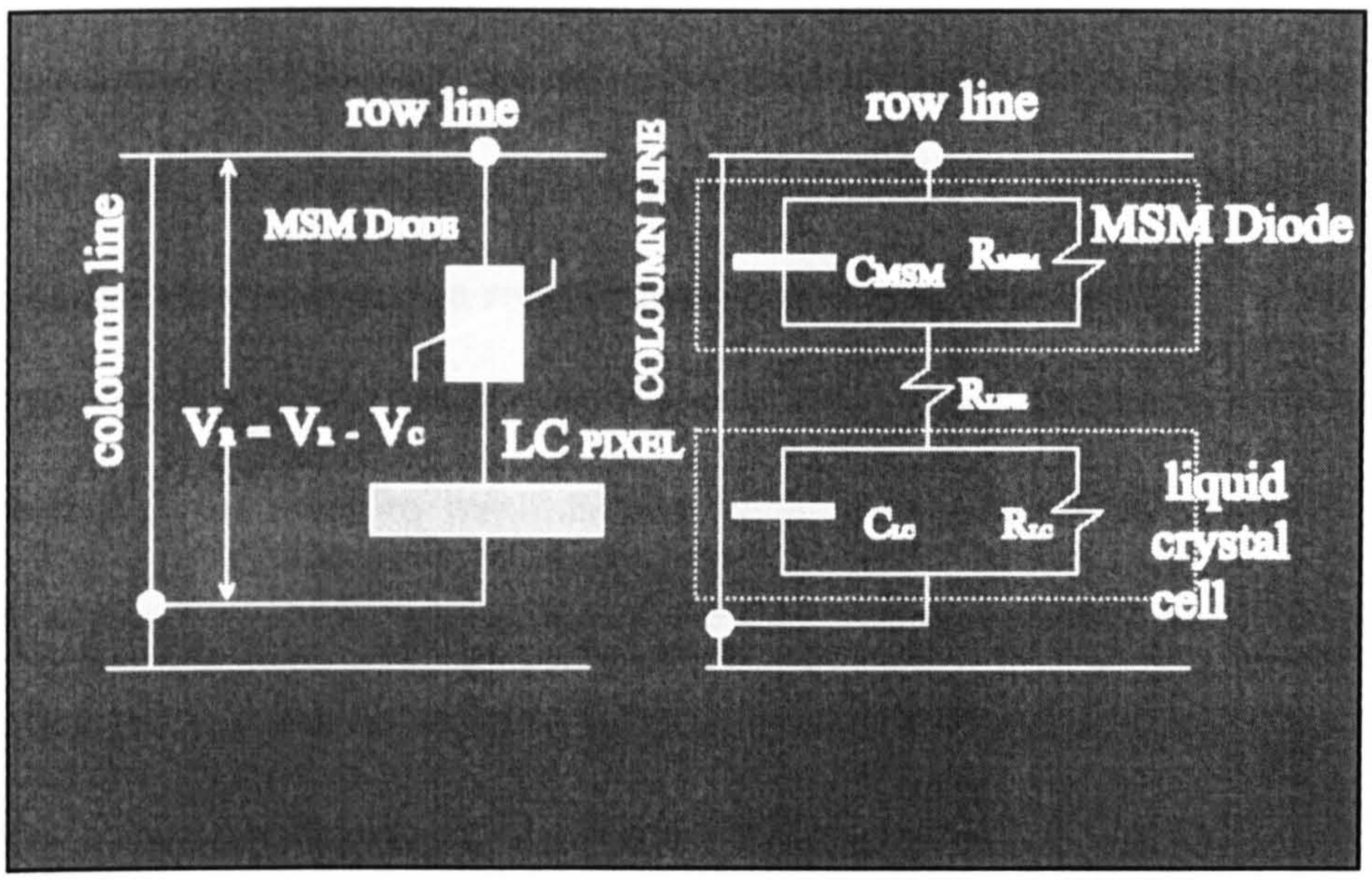

Fig.-7. 2 MSM addressed LCD pixel and equivalent circuit.

The current –voltage (*I-V*) characteristic required from a two terminal MSM switch is shown in Fig.-7.3 [18]. A symmetrical *I-V* characteristic is preferred to an asymmetrical one, since it allows standard ac driving of the LC cell to be achieved more easily. Simple calculations show that for a VGA resolution, graphic display requires *on*-currents exceeding 0.1μA and *off*-currents as high as a maximum of 1pA, [15]. Assuming the surface area of the MSM switch to be 10 μm x 10 μm, these constraints on currents translate to current densities in the range of 10^{-6} to 0.1 Acm^{-2}.

Two terminal, MSM-based displays require a more complex addressing scheme than TFTs. The simplest addressing scheme uses the 4-level row drive waveform shown in Fig.-7.4[9]. In both the positive and negative address half cycles there are two distinct regions. In the *select*-period the row voltage is raised to the SELECT level (V_s) and the MSM is turned *on*. In the *hold*-period the row voltage is set to the HOLD level (V_H) which is chosen, in order to minimise the potential appearing across the MSM and maintain it in the *off* state, irrespective of the data voltages applied to the column line. More complicated reset drive schemes have also been developed to counter the effects of device non-uniformity and threshold voltage drift [16].

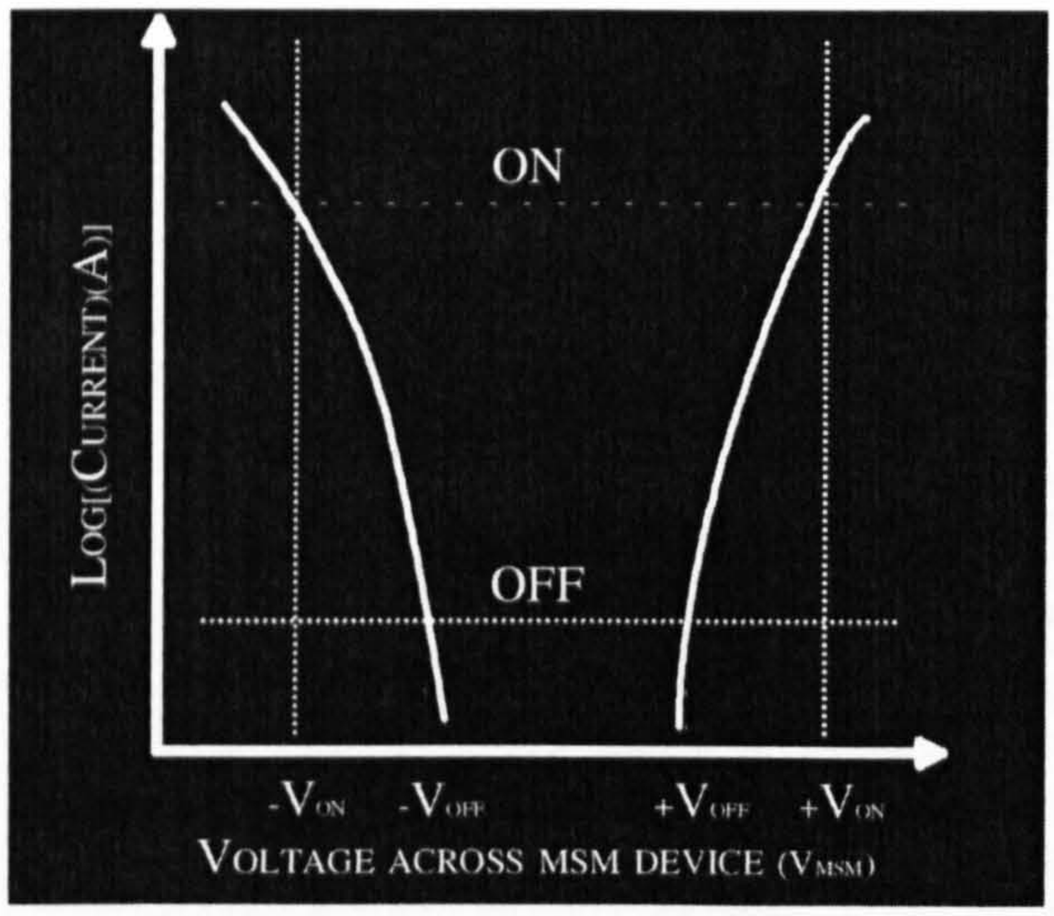

Fig.-7.3 Optimum MSM *I-V* characteristics for AMLCD applications.

The LC voltage (V_{LC}) across a full cycle of the drive-voltage is also shown in Fig.-7.4. During select periods, the LC pixel capacitance (C_{LC}) is charged and V_{LC} increases

from $V_1(\pm)$ to $V_2(\pm)$. This is known as "kickback" [15]. During the *hold* periods the LC voltage slowly changes from $V_2(\pm)$ to $V_3(\pm)$ as a result of changes in the LC capacitance and the MSM capacitance (C_{MSM}), caused by leakage in the LC and MSM. To minimise capacitance coupling and the "kickback" effect it is essential that $C_{LC} >> C_{MSM}$. This ensures that more of the pixel voltage (V_p) is correctly applied to the LC cell. In real displays this condition can be satisfied for $C_{LC} \approx 3$ to 10 times C_{MSM} [4]. This effectively establishes a lower limit on the pixel size and thereby the display resolution. To realise low capacitance MSMs, for high resolution and/or large aperture-ratio displays, low dielectric constant materials are required.

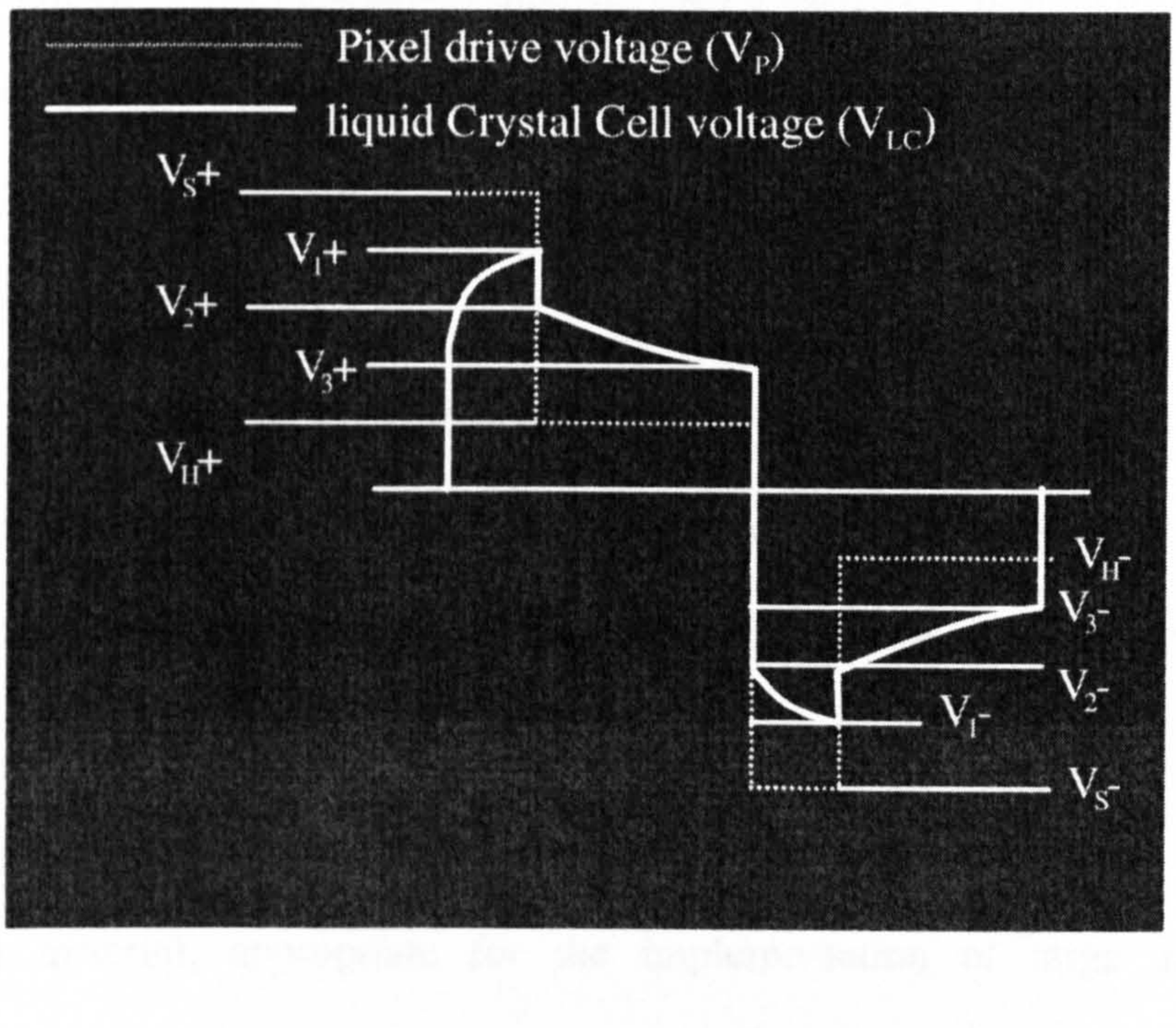

Fig.-7.4 Four Level MSM derive scheme and LC cell voltage.

7.1.1 Comparison of MSM technologies and current status

Of all materials that have been investigated for MIM and MSM applications, Ta_2O_5 and a-SiN_x:H have received greatest attention to date. Ta_2O_5 MIM can be fabricated at a relatively low cost because no CVD process is required; they have been successfully used to active-matrix address a full colour 14″ LCD [10]. However, the high dielectric constant of Ta_2O_5 results in a comparatively high C_{MSM} and a low switching speed [4].

The dominant MSM technology is therefore currently based on plasma deposited a-SiN_x:H. MSM diodes have been used to manufacture a high definition projection display with a 56″ diagonal [17]. As-deposited a-SiN_x:H has a much lower trap density than DLC. As a result, electrical conduction in unstressed a-SiN_x:H is limited by thermionic emission over the reverse biased metal-semiconductor Schottky barrier [14]. This leads to an exponential dependence of the current density (J) on the electric field strength (E), (described by Eqn.-7.1, [1] later).

The relative performance of bulk-limited DLC MSMs and contact limited a-SiN_x:H MSM have been compared by other workers, [18]. By comparing device characteristics, it has been concluded that switching speed increases with decrease in the bandgap.

7.2 Benefits of DLC for MSM devices

More recently, diamond-like carbon has been shown to be a very promising semiconducting material, appropriate for the implementation of large area MSM structures [18,19]. DLC offers a number of advantages for FPD switches. DLC films are

mechanically strong, very smooth and free of pin-hole defects. The films can be deposited by the existing plasma deposition techniques over large area substrates at room temperature. The other advantage of DLC is that by varying the deposition conditions the electrical properties of DLC can be varied from those of a semiconductor to a highly insulating film [19]. This allows the MSM characteristics to be tailored for AMLCD applications.

However, the key advantage of DLC is the opportunity that it offers for an electronic grade material to be deposited at room temperatures. DLC-based pixel switches are therefore fully compatible with the ambition of FPD technology to manufacture on plastic substrates; a process which will bring down the maximum process temperature to around 100°C. The dielectric constant of the DLC films is quite low [18], which is another advantage since this reduces the delay during the LCD operation.

7.3 Properties of MSM devices fabricated in our laboratory

MSM devices are simple to fabricate, however, the substrate can significantly characteristics of the device. The Metal/DLC/Si^{+n} structure fabricated in our laboratory shows rectifying behaviour while the Metal/DLC/Metal structure does not show any traces of such behaviour. The rectifying behaviour in the former structure (Metal/DLC/Si^{+n}) is due to the barrier formation between DLC and Si^{+n} substrate. Therefore, it is vitally important to deposit DLC on metal-coated glass or metal-coated Si

substrates, in order to determine the exact conduction mechanism in the films. For this investigation we deposited the a-C:H films on Al and Cr coated corning glass and Si substrates.

7.3.1 Electrical behaviour of MSM devices:

Sandwich-type metal-semiconductor-metal (MSM) devices were fabricated by depositing a thin layer (0.1-0.15 μm) of a-C:H on Cr covered C7059 corning glass substrates. The films a-C:H were deposited from CH_4/He and CH_4/Ar gas mixtures at a pressure of 100 mTorr and a temperature of 20° . The a-C:H films used in this study had an optical bandgap of about 1.7 eV. Top contacts (contact diameters 1.5,1,0.5, 0.38 mm) were manufactured by the thermal evaporation of metal through a shadow mask at high vacuum. The *I-V* characteristics of the MSM structures were measured using a HP 4140B picoammeter that was interfaced with a computer. Typical symmetrical *I-V* characteristics of the Al/DLC/Cr MSM structures are shown in Fig.-7.5. The devices with the different contact areas exhibit symmetrical *I-V* characteristics for negative and positive applied voltages. The symmetrical *I-V* characteristics are typical of a bulk-limited mechanism. The metal/a-C:H interface does not play any significant role in determining the electrical behaviour these devices.

Knowledge of the electrical conduction mechanism that operates in amorphous carbon MSMs sandwich structures, is fundamental to the understanding of the operation

of MSM. In insulators and high bandgap semiconductors, high field conduction can occur by a number of mechanisms which are dependent upon the trap density, the trap depth below the conduction band (Φ) and the size of any Schottky barrier at the metal-semiconductor contacts, [20,21,22].

If the Schottky barrier conduction mechanism is predominant, then current is limited by thermionic emission over the barrier. This yields an exponentially varying current density (J_{SB}) of the form [18]:

$$J_{SB} = A^{*}.T^{2}\exp\left(-\frac{e\Phi_{B}-\alpha eE}{kT}\right) \quad \ldots. \quad 7.1$$

Where A^{*} is the Richardson constant, e is the electronic charge and α is the tunnelling constant for the material (about 4 nm for a-SiN_x:H, [14]), E is the electric field, T is the temperature and Φ_B is the barrier height. Conduction will be contact limited and dependent on the metal used to manufacture the MSM structure and the polarity of the bias.

If the Schottky barrier is very large, (for example if a wide bandgap insulator is used), the rate-limiting step becomes high enough to induce Fowler-Nordheim tunnelling [22], which implies that the current density (J_{FN}) is of the form [23]:

$$\log\left(\frac{J_{FN}}{V^{2}}\right) = C_{1} + C_{2}\frac{\Phi_{B}}{V^{3/2}} \quad \ldots. \quad 7.2$$

Here C_1 and C_2 are constants.

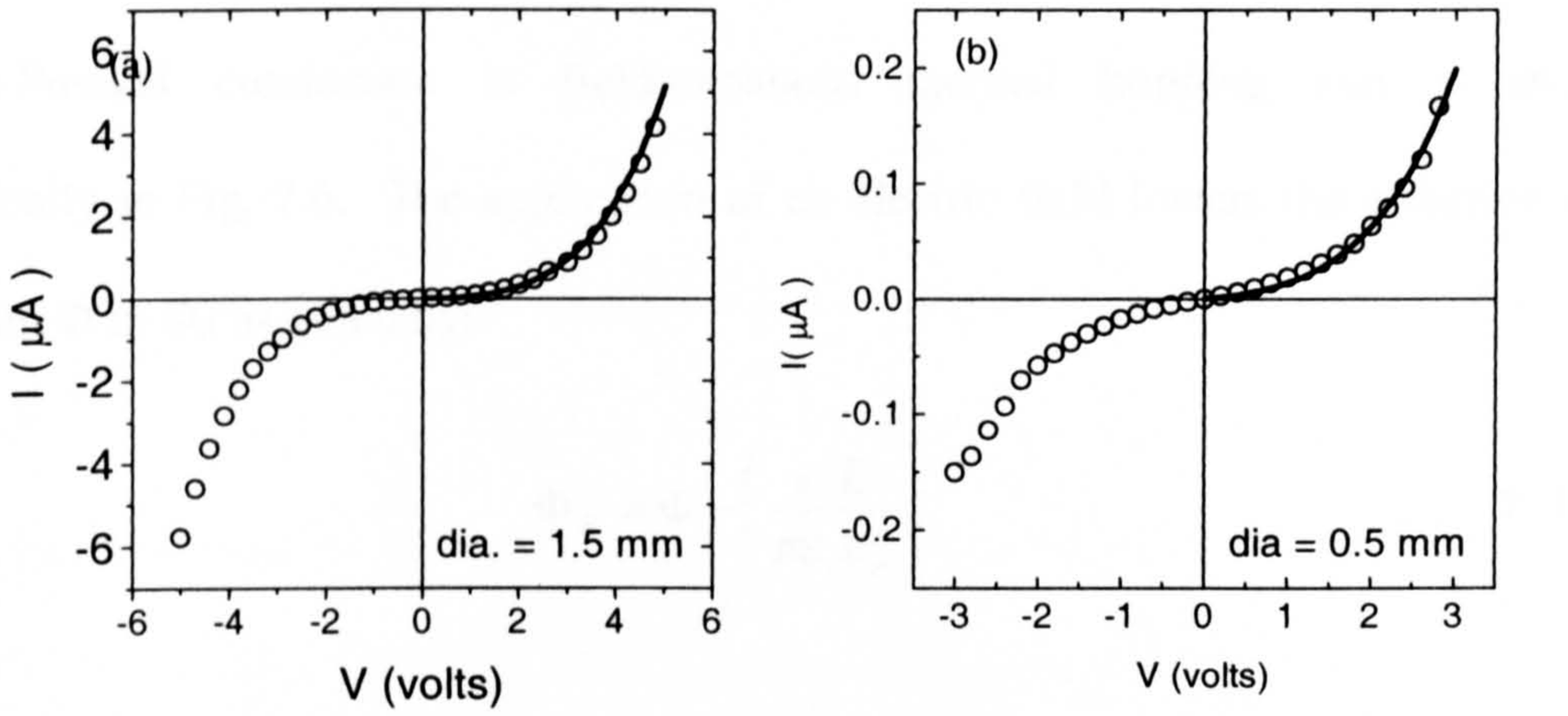

Fig.-7.5 *I-V* characterisitcs of MSM switches of different areas. The solid solid lines represent "best fit" characterisitics assuming Poole-Frankel conduction. Film was depostited at DC self bais = -200 V.

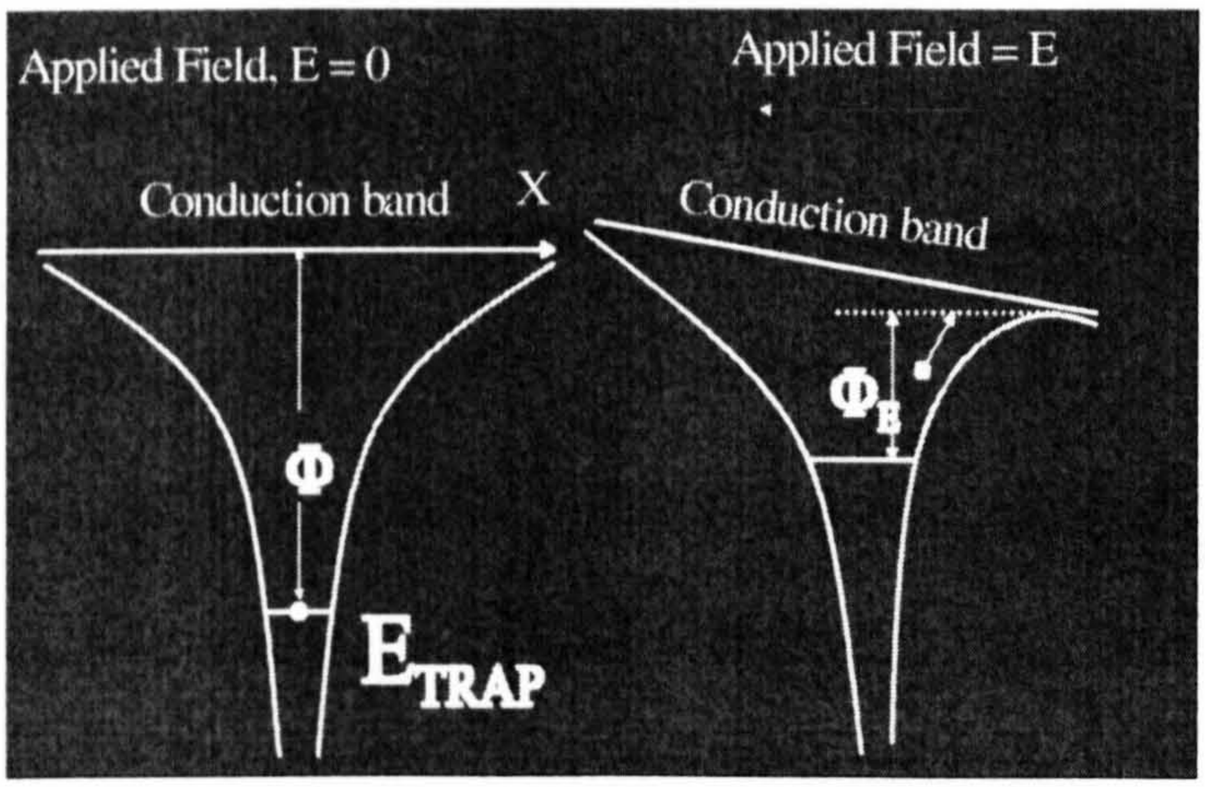

Fig.-7.6 Poole-Frenkel conduction mechanism

Alternatively, if the trap density dominates, the bulk conduction mechanism the current density is likely to be bulk-limited by the Poole-Frenkel effect.

Poole-Frenkel conduction is field-enhanced thermal hopping and is shown schematically in Fig.-7.6. The application of an electric field lowers the effective trap depth from Φ to Φ_E as given by:

$$\Phi_E = \Phi - \left(\frac{e^3 E}{\pi \varepsilon_r \varepsilon_o} \right) \qquad \ldots. \quad 7.3$$

Where E is the applied field, ε_o is the permeability of vacuum and ε_r is the relative permeability of the semiconductor material.

This leads to an expression for Poole-Frenkel conduction of the form []:

$$J_{PF} = Ne\mu E \exp\left(\frac{\Phi_E}{kT} \right) \qquad \ldots. \quad 7.4$$

$$= Ne\mu \left(\frac{V}{d} \right) \exp\left(-\frac{\Phi}{kT} \right) \exp\left(\frac{e^3 V}{\pi n^2 \varepsilon_o k^2 T^2 d} \right)^{1/2}$$

Eqn.7.4 can be more generically expressed in the following form:

$$J_{PF} = C_0 V \exp\left(\beta . V^{1/2}\right) \qquad \ldots. 7.5$$

$$\text{where, } C_o = \frac{Ne\mu}{d}\exp\left(\frac{\Phi}{kT}\right) \quad \ldots \quad 7.6$$

$$\text{and} \qquad \beta = \frac{1}{kT}\left(\frac{e^3}{\pi n^2 \varepsilon_o d}\right)^{1/2} \quad \ldots . \quad 7.7$$

Here V is the applied voltage, N is the band edge density of states, μ is the mobility, d is the film thickness and n is the refractive index (where $n^2 = \varepsilon_r$). Thus Eqns.-7.1, 7.2 and 7.4 give current densities corresponding to all the dominant conduction mechanisms which are likely in MSM devices. With the help of these equations and current and the measured *I-V* characteristics, the dominant conduction mechanism responsible for the observed electrical behaviour can be determined.

Upon inspection, the symmetrical *I-V* characteristics (shown in Fig.-7.5) are typical of bulk limited conduction by the Poole-Frenkel mechanism. This was confirmed by fitting the symmetrical *I-V* plots to a Poole-Frenkel characteristic (shown by the solid lines in Fig-7.5)

7.4 Capacitance Measurements of large area MSM devices

One of the simplest ways to gain an insight into the dynamic response of an amorphous material is to measure the capacitance as a function of frequency or voltage, at a constant temperature. We have investigated capacitance-voltage (*C-V*) and capacitance-frequency (*C-f*) characteristics of a number of MSM devices. Cr/a-C:H/Cr

MSM devices were used in this investigation and the diameter of the upper electrodes was 1 mm. Typical *C-V* characteristics at fixed frequencies are shown in the Fig.-7.7. The *C-V* data is nearly symmetrical for both negative and positive applied bias voltages at a given frequency. This indicates that there is no barrier formation at the a-C:H/Cr interface. This is in line with the previous observation of symmetrical *I-V* characteristics. The effect of frequency in the *C-V* measurements is quite clear. With decrease in the signal frequency the measured capacitance increases. The increase in the capacitance can be explained on the basis of the trap states in the material. The involvement of the trap states is very much determined by the frequency of the ac signal used in the measurement of *C-V*, (ω). The frequency dependence of the energy of deep states has been explained in Section 5.1.1.

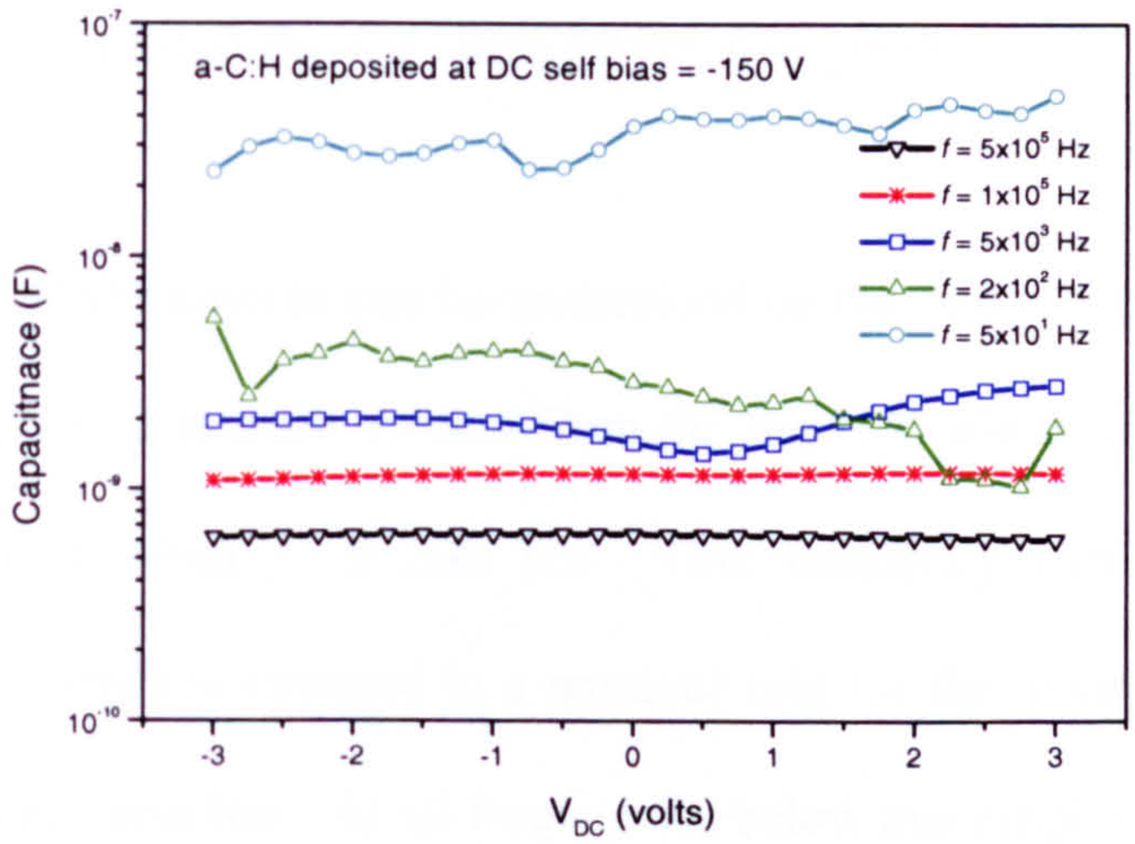

Fig-7.7 *C-V* plot of MSM devices at different frequencies.

It is quite clear from the Equ.5.2 that contributing trap states are strong functions of the signal frequency at a given temperature. The lower the frequency, the deeper the states that are being probed by *C-V* measurements. The enhancement in the number of deep states accessed implies an increase in charge which consequently causes the capacitance to increase with any decrease in the signal frequency. This is indicated by undulating *C-V* curves at lower frequencies while the curves get much smoother as the frequency increases.

7.4.1 Capacitance-Frequency

A typical *C-f* characteristic of an MSM devices are as shown in Fig.-7.8. A dominant feature of capacitance-frequency plots is the sharp rise in the capacitance at low frequencies. Investigations of *C-f* characteristics of MSM devices have been reported before, [25]. We have investigated the *C-f* characteristics in greater depth than reported in Klibanov et. al [25].

The *C-f* behaviour of MSM devices can be understood on the basis of the interaction of trap states with frequency. It is quite evident from the Fig.-7.8 that there is an abrupt increase in the capacitance when $f \leq 500$ Hz. This frequency corresponds to a demarcation between an active (as opposed to a passive) role for the amorphous carbon film in a sandwich-structure capacitor. At all frequencies below this cusp, a film behaves like a passive dielectric medium that is not polarisable on the time scale of the

measurement frequency. At high frequencies (>500Hz) the plot represents the geometrical capacitance, given by the following equation:

$$C_{HF} = \varepsilon \frac{A}{t} \qquad 7.8$$

Where, ε , A and t are the dielectric constant, area and thickness of the amorphous carbon film under investigation.

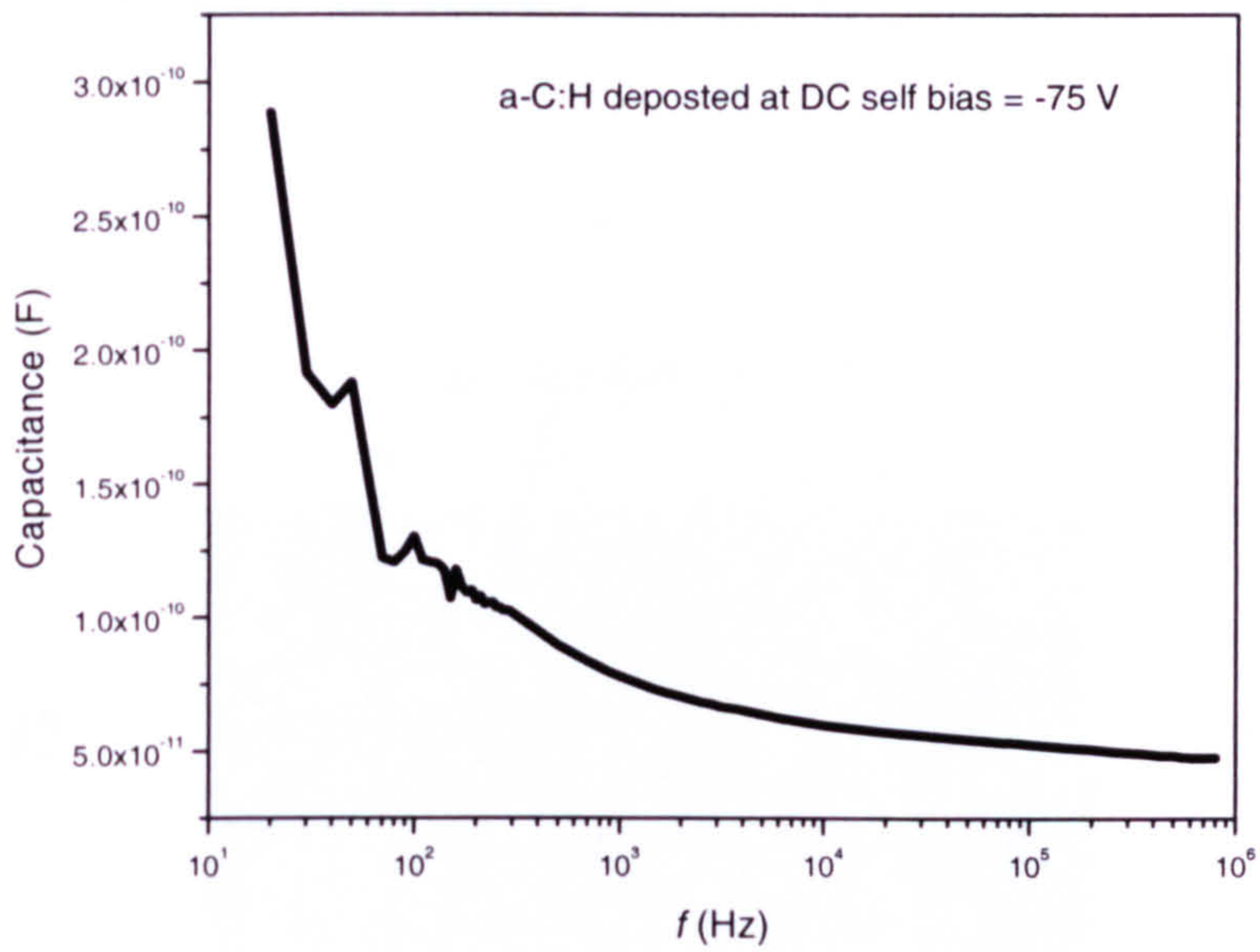

Fig.-7.8 Typical capacitance against frequency plot of an MSM device fabricated in our laboratory (*C-f* measurement were carried out at zero dc bias).

As the frequency decreases below this demarcation frequency a progressively greater number of deep states start participate in the net capacitance and a higher charge accumulates at the metal/a-C:H interfaces, as shown in the Fig.-7.8. The equivalent

circuit of such a sandwich structure after the *turn-on* occurs in the capacitance, is shown in Fig.-7.9. The *RC* time constant of the structure is short enough to be of the order of the frequency of the ac voltage used in the measurement causing the dielectric layer to be polarised. In other words, one could also describe the capacitance *"turn-on"* by saying that the dielectric response time of the film is short enough so that the film can behave as a polarised dielectric on the time-scale of the measurement frequency. This cusp in the capacitance is also sometimes referred to as *"freeze-out"*, when observed during a scan from low to high frequency. The zero bias capacitance at the *"freeze out"* is:

$$C = \varepsilon \frac{A}{2W} \qquad 7.9$$

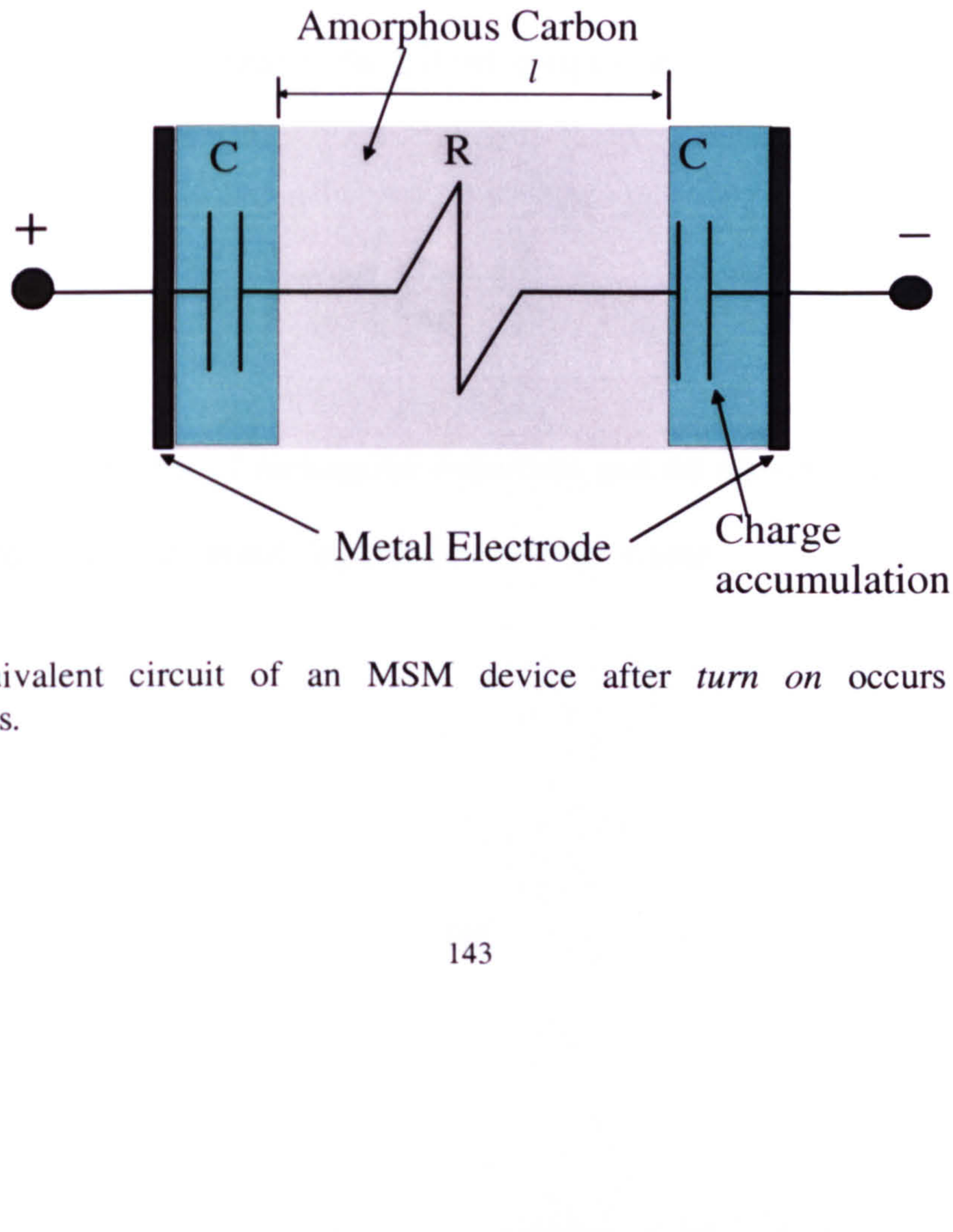

Fig.-7.9 Equivalent circuit of an MSM device after *turn on* occurs in the *C-f* characteristics.

Here, W is the thickness and A is the cross-sectional area of the charge-accumulated layers on each side of the film. The resistance of the bulk material in the interior of the film is then:

$$R = \rho \frac{l - 2W}{A} \qquad 7.10$$

Here, ρ is the bulk resistivity and l is the length of the resistive part of the film (see Fig.-7.9). The *turn-on* criterion is that the response time equals the time constant. The response time can be obtained by multiplying Eqn.-7.9 and 7.10:

$$\tau = \rho\varepsilon\left(\frac{C}{C_{HF}} - 1\right) \qquad 7.11$$

We know that $\tau = \frac{1}{f}$; this leads to the following equation:

$$\frac{1}{f} = \rho\varepsilon\left(\frac{C}{C_{HF}} - 1\right) \qquad 7.12$$

The above equation is that of rectangular hyperbola and the observed *C-f* characteristics (Fig.-7.9) of MSM devices gratifyingly follow this behaviour.

7.4.2 Estimation of resistivity of a-C:H films from *C-f* characteristics of MSM devices

Eqn.7.12 can be used to estimate resistivity of the a-C:H film. The experimental data for the resistivity-voltage (ρ-V) and *C-f* plots for the MSM devices are shown in Fig.-7.10. *C-f* data plotted in Fig.-7.10 (a), is collected for MSM structures at zero DC bias.

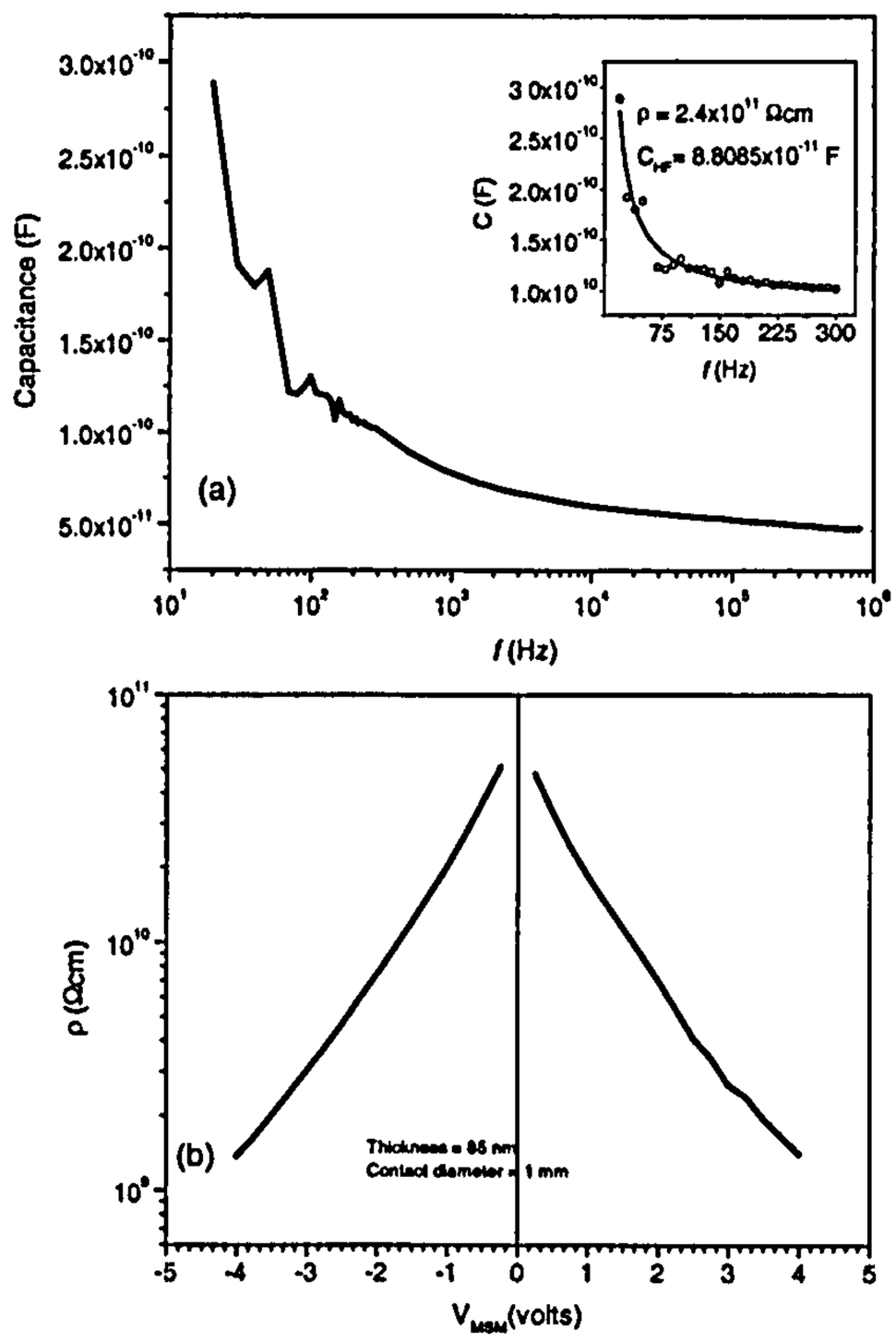

Fig.-7.10 Electrical characteristics of an MSM device (a) capacitance against frequency (b) resistivity against voltage. Diameter of the upper electrode is 1mm and the thickness of the a-C:H film is 85 nm. Film was deposited at DC self bias = -95 V.

To estimate the resistivity we fit the experimentally obtained *C-f* data to Eqn.7.12. The fit to the data is shown in the inset of Fig.-7.10(a). The correlation coefficient is 0.97, which suggests a satisfactory fit. The parameter obtained by this fitting exercise the resistivity (ρ). Typical value of resistivity (for different deposition conditions) obtained with a number devices are listed in Table-7.1. To compare the resistivity the values corresponding to both the types of the measurements are listed in Table-7.1. It is clear from this table the both *I-V* and *C-f* measurements yield approximately the same values. Therefore we conclude that the theory developed to estimate the resistivity of MSM devices is reliable and can be confidently used to deduce the dielectric constant of the material (from estimates of geometrical capacitance and resistivity).

Table-7.1 Calculated resistivity and geometrical capacitance of MSM devices fabricated at two different DC self-bias voltages.

DC-self bias Voltage (volts)	**Resistivity from *I-V* measurements (Ωcm)**	**Resistivity from *C-f* measurements (Ωcm)**
-95	$7x10^{10}$	$2.4x10^{11}$
-135	$2x10^{9}$	$4.1x10^{9}$

7.5 An attempt to realise metal/a-C:H Schottky diode

The MSM devices fabricated from amorphous carbon, when the contact area is large, always show symmetrical behaviour. The fabrication of a rectifying, Schottky barrier-type, metal/a-C:H contact has proved difficult. This has been attributed to the existence of an sp^2-rich interfacial layer [26]. The graphitic surface layer results in the pinning of the Fermi level at the surface and the formation of ohmic metallic contacts. We have carried out an extensive investigation to realise Schottky contacts to a-C:H.

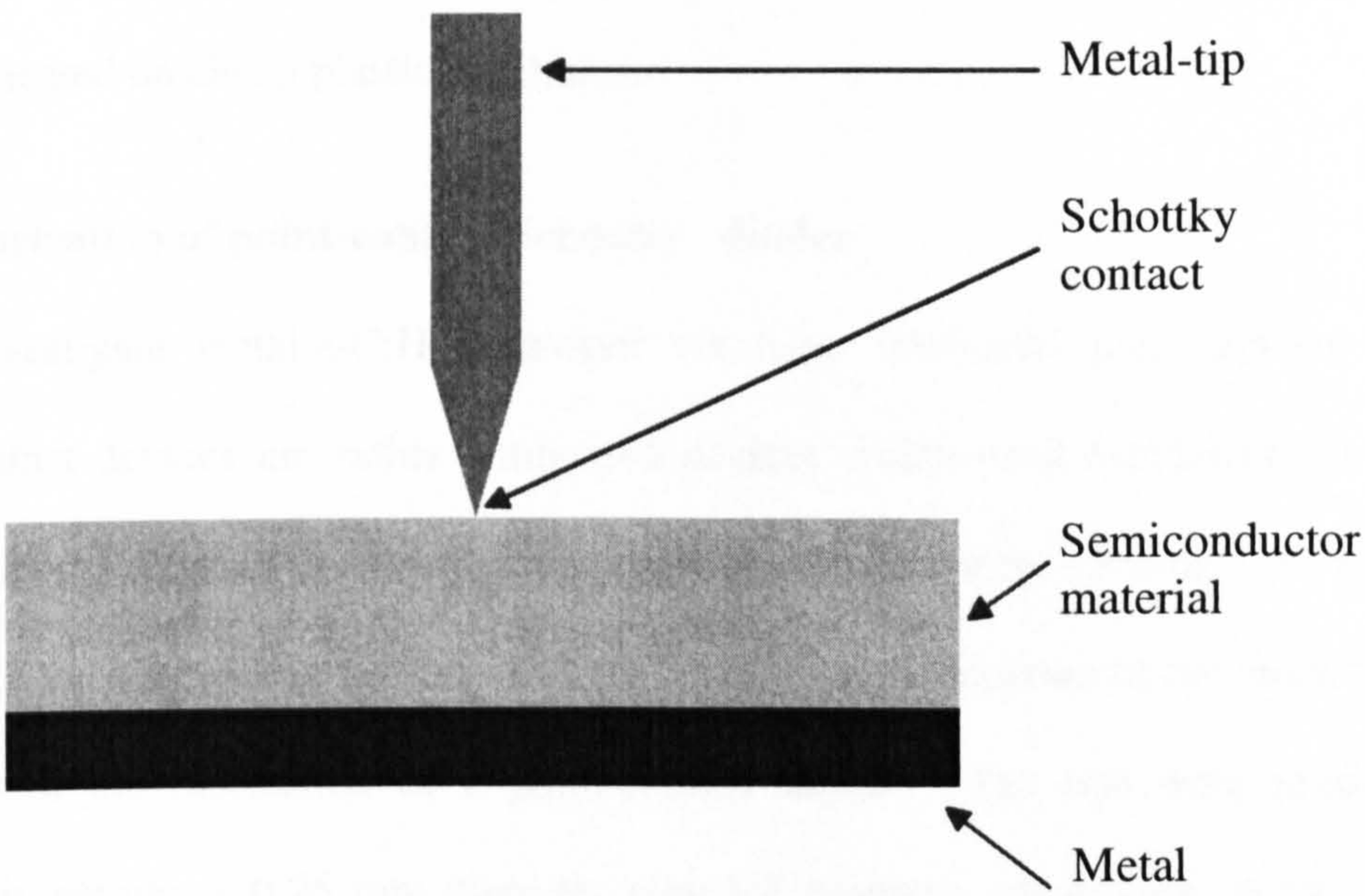

Fig.-7.11 Schematic diagram of point-contact diode

There are numerous advantages to fabricating Schottky contacts to a semiconductor material. Metal-semiconductor barrier structures have been used as simple and effective

characterisation tools to study the electronic properties of both crystalline, [23], and amorphous [27] semiconductors. *I-V* analysis can be used to extract information about the dominant conduction mechanism and estimate the height of any barrier at the metal/a-C:H junction [23]. *C-V* analysis can be used to investigate the density of states of a-C:H. Schottky barrier structures have the added advantage over other structures in that they are simpler to fabricate. Moreover, formation of a Schottky barrier is the first step towards the fabrication of a Metal Semiconductor Field Effect Transistors (MESFET) using a-C:H. The deposition of a-C:H at room temperature, would allow the MESFETs to be fabricated on cheap plastic substrates.

7.5.1 Fabrication of point-contact Schottky diodes

To investigate metal/a-C:H behaviour we have fabricated point-contact devices. Point-contact devices are rather antiquated devices which used extensively during the Second World War as a demodulator in RADAR detection systems. A schematic diagram of such a devices is shown in Fig.-7.11. The manufacture of the metal tip is the first step in the fabrication of a point-contact device. The tips were produced by electrically etching a 0.25 mm diameter wire (of tungsten, aluminium, nickel or gold) [28,29]. The etching of the metal wire was carried out in a 1 M KOH solution; 15 V ac was used for electrical etching. To create the uniform electric field around the tip, when placed in the etching solution, a circular copper electrode is placed in the solution which

is connected to the neutral terminal. This was done to manufacture a metal-tip with the required conical structure. An ac signal of frequency 50 Hz was applied to the metal. The whole process takes 25-30 minutes to produce a tip, a typical example of which is shown in Fig.-7.12. The initial diameters of all the tips used in this work were estimated by a scanning electron microscope to be <1 μm.

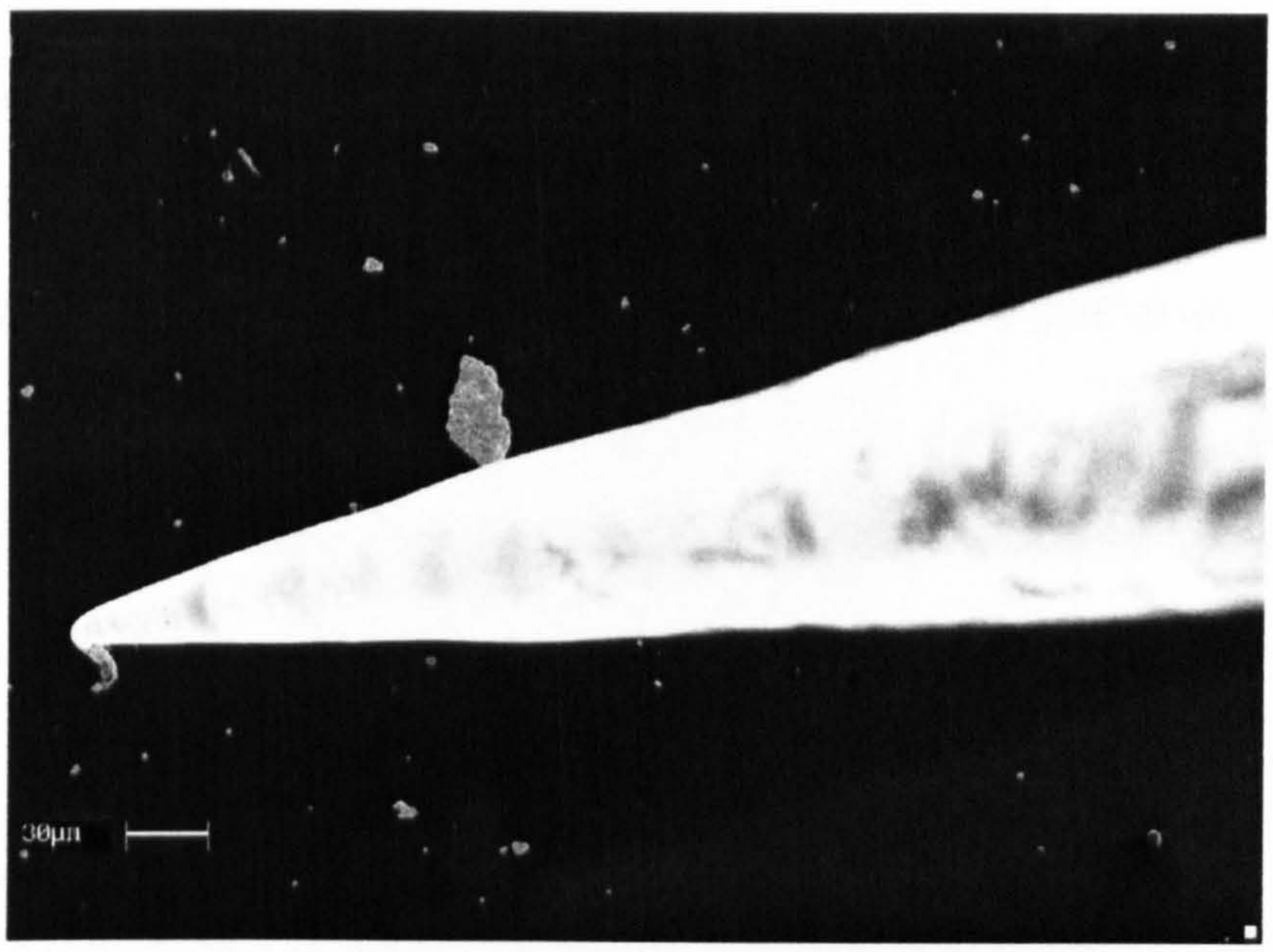

Fig.-7.12 The tungsten tip making in contact with the a-C:H surface.

7.5.1.1 Contact Formation of the Metal tip to a-C:H

The purpose of electrically forming a contact is to guarantee the stability of the *I-V* characteristics and to obtain an enhancement of performance [28,30]. The formation

process can be carried out in many different ways with similar results. A few ways of forming Schottky contacts to semiconductor materials are [28]:

- Passing high DC for a short interval of time.
- Passing a large ac current with a load in series.
- Use of an ac or DC pulse signal.

Using our probe system, we formed a metal contact to the surface of an a-C:H film without damaging the surface. Then we passed a high DC for a short time interval to form the metal/semiconductor contact. During the microcomputer-controlled forming process, a forward current of approximately 10 mA is passed for a period of 1-50 ms. The contact is formed due to the dissipation of electrical power at the metal/a-C:H interface, giving rise to metal/a-C:H weld. After forming the metal/semiconductor contact, *I-V* and *C-V* characteristics of these devices were investigated.

7.5.2 Electrical Characteristics of Point Contact Diodes:

The *I-V* characteristics of the metal/a-C:H diodes were measured using a PC-driven HP-4140B picoammeter. Capacitance-Voltage (C-V) measurements were made over the frequency range 20 Hz to 1 MHz using an HP 4284A LCR bridge.

The *I-V* characteristics of many of the micro-tip/a-C:H/metal structures showed a significant and reproducible asymmetry, indicative of barrier formation at the micro-tip/a-C:H interface. Typical asymmetrical *I-V* characteristics for the range of metal

micro-tips investigated in our study, are shown in Fig.-7.13. Rectification ratios upto three orders of magnitude have been observed. In addition to the observed asymmetrical behaviour, parts of the same sample were found to exhibit symmetrical *I-V* behaviour.

Typical C^{-2} - V behaviour (at 2 kHz) for an asymmetrical contact is shown in Fig.-7.14. The linear fit to the characteristic in the depletion region further corroborates the formation of the Schottky barrier, [23].

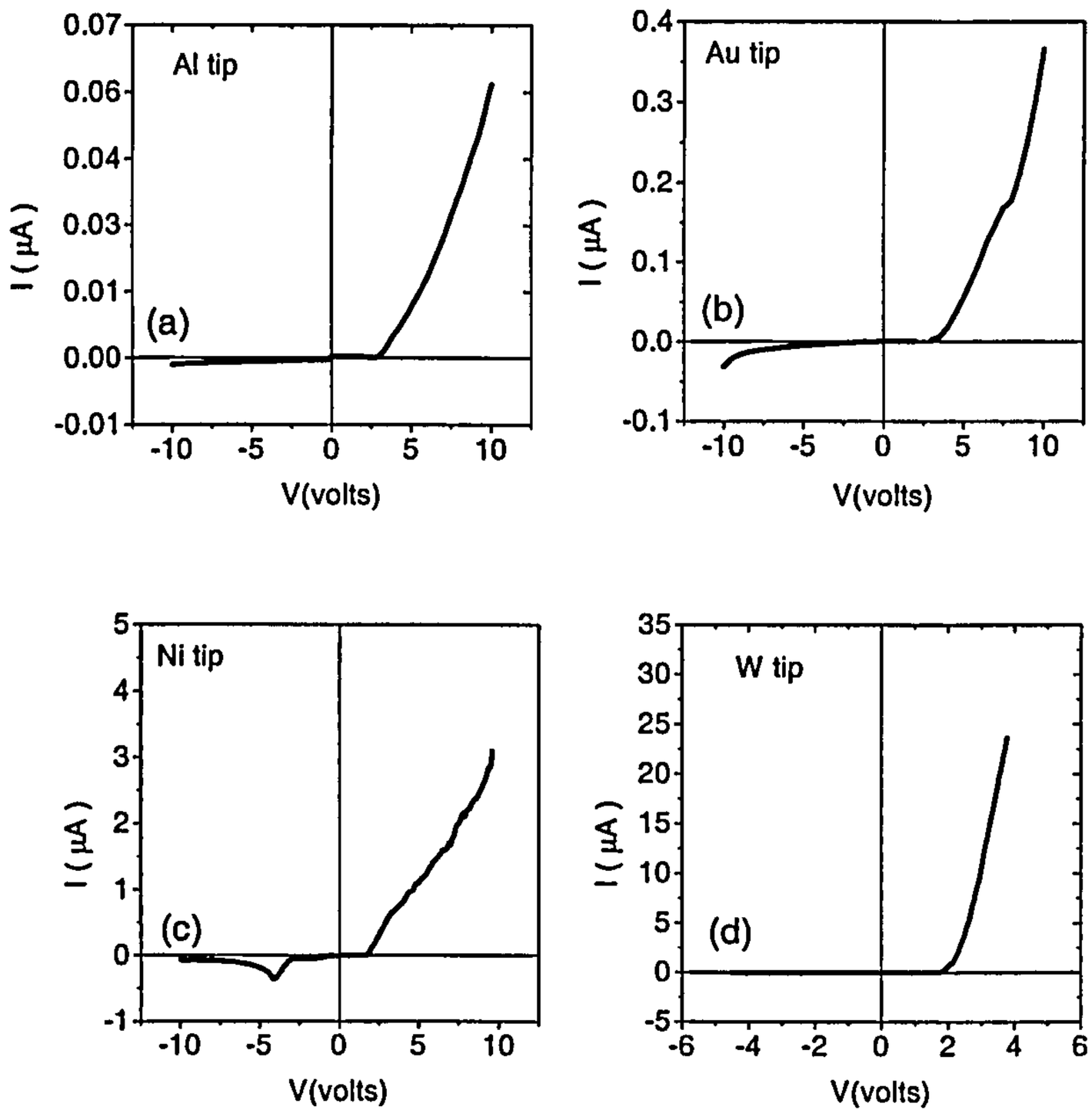

Fig.-7.13 Typical *I-V* characteristics of micro-tip/a-C:H/Cr structure using different metals for top contacts. A-C:H films was deposited with DC self voltage –200 V.

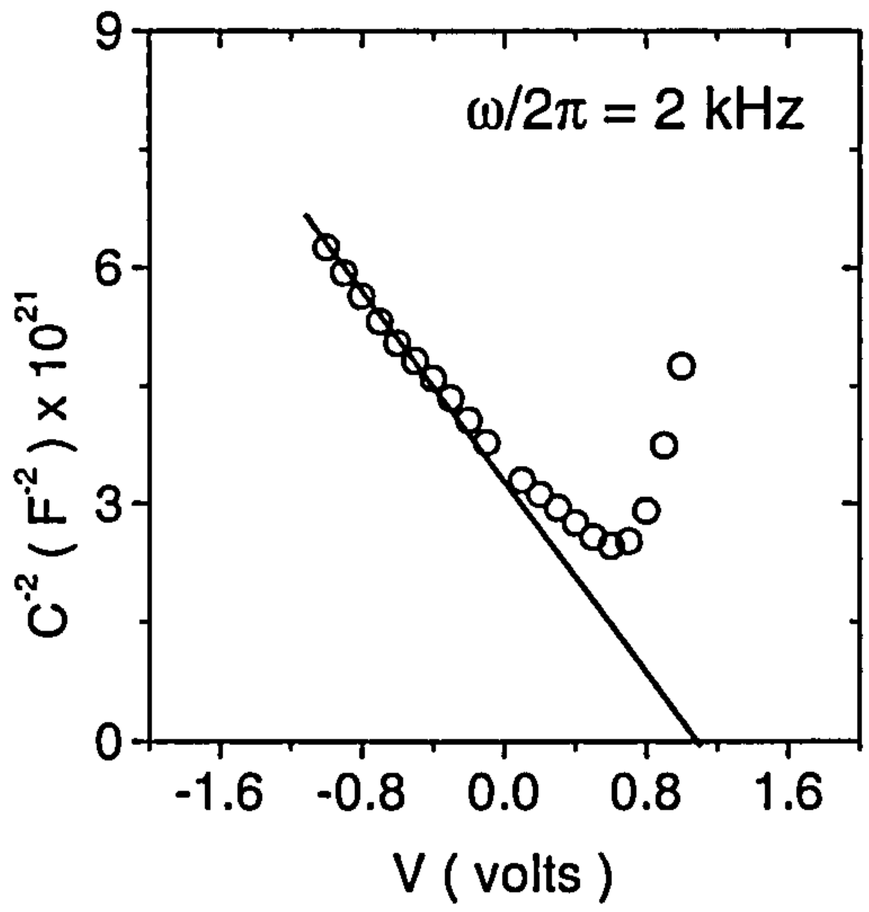

Fig-7.14 Typical C^{-2}-V plot for a W/a-C:H/Cr structure.

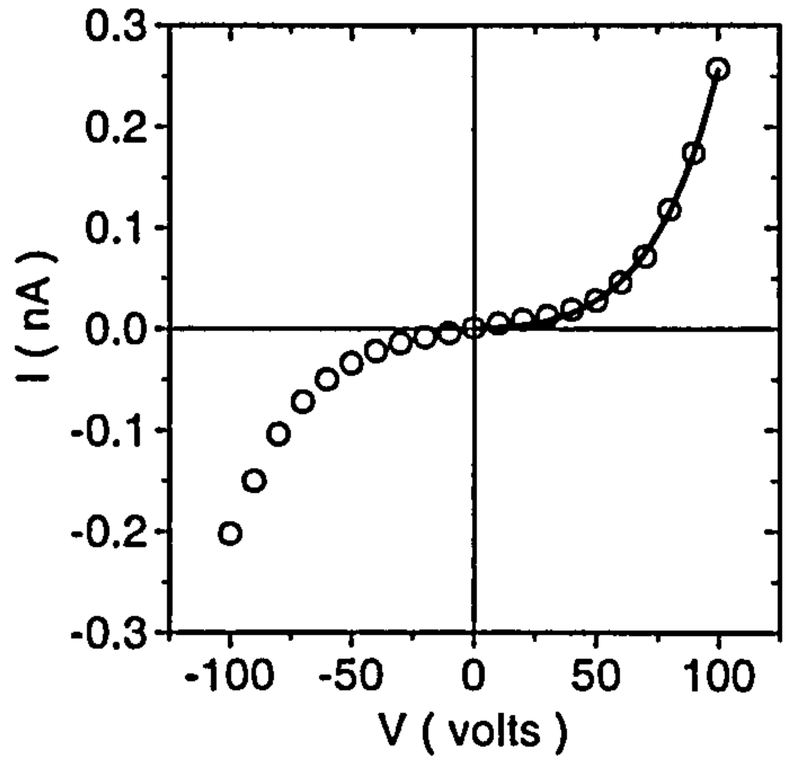

Fig.-7.15 Typical characteristics of W-micro-tip/a-C:H/Cr structure. The solid lines represent "best fit" characteristics assuming Poole-Frenkel conduction. The symmetry factor is 1.06, which indicated that the *I-V* characteristics are highly symmetrical.

Of primary importance to our study was the ability to confirm Schottky barrier formation at the micro-tip/a-C:H interface. A variety of alternative mechanisms were investigated as possible causes of the observed rectification. Metal-carbide formation was considered. Studies on metal/polycrystalline diamond structures, undertaken by other workers, have suggested that metal-carbide formation results in a highly conducting interfacial layer that destroys barrier formation [31]. To ascertain if metal-carbide formation was indeed occurring in our devices, we fabricated point-contact devices at room temperature, to minimise the thermal energy available for metal-carbide formation. Local heating during the electrical forming process was also ruled out. EDAX analysis of the microtip as well as the a-C:H films did not reveal any evidence of segregation or diffusion of the metallic constituent of the tip into the a-C:H surface during the forming process or during the subsequent *I-V* analysis. The sensitivity of EDAX analyses is around 0.1%, if the amount of metal induced into the a-C:H films that is lower than it. Then it is not possible to detect it. As already stated, metal carbide formation destroy the barrier. Thus if there is amount of metal induced into the a-C:H, we should not see the asymmetrical behaviour. To confirm further, one should use the Secondary Ions Mass Spectroscopy and it can detect any impurities in the material to the *ppm* level. When Au micro-tips were used, Schottky behaviour was again observed; this test safely eliminated the possibility of oxide formation as a cause of the asymmetrical behaviour.

We have also observed symmetrical *I-V* characteristics at a number of locations using micro-tip contacts (Fig.-7.15). The observed variation in the electrical properties of sub-micron metal contacts may be indicative of significant inhomogeneity in the a-C:H surface. The structure and properties of PECVD grown a-C:H are primarily controlled by the self-bias voltage, (discussed in Chapter 3), which determines the kinetic energy of the carbon ions impinging on the growing film surface. In such a process, diamond crystallites, embedded in an amorphous carbon matrix, have been reported [32,33]. Recently, Transmission Electron Microscopy (TEM) investigation of amorphous carbon, has shown large inclusions of crystalline forms of carbon embedded in an amorphous carbon matrix, [34]. Silva et al [33] have reported hexagonal diamond grains approximately 30 nm size, within an amorphous carbon matrix. Amaratunga et al [32] have observed single-crystals of diamond up to about 0.2 μm in size, in PECVD materials. It is evident from these reports that diamond crystallites can be present in PECVD amorphous carbon with sizes that can vary from the nanometer to the micrometer scale. Our observations of both symmetric and asymmetric *I-V* characteristics on the same sample suggests inhomogeneity in the material surface, which is consistent with the presence of contactable crystallites in r.f-PECVD DLC. In the following section we discuss the method that we have developed to predict the locations where Schottky contacts to the a-C:H film are more likely to occur by the point contact method.

7.5.3 Schottky contact on a-C:H- a more reliable approach.

In this section, we present a novel way of confining the semiconductor-like parts of a-C:H to particular regions of the films. Thus, the location and formation of Schottky contacts to a-C:H, become more predictable. This was achieved by depositing a-C:H on to metal patterned Si substrates. Test structures were prepared by thermally evaporating 20nm thick films of Cr on crystalline silicon (c-Si) and C7059 glass substrates [35]. Thin Cr layers were used to minimise step coverage induced stress effects in the deposited layers. In addition, thin metallic "strip-and-pad" structures, with feature sizes up to several mm, were patterned on selected substrates using shadow masks during the thermal evaporation stage. A typical SEM image of a film deposited over metallic "strip-and-pad" structures is shown in the Fig-7.16. All substrates were subjected to an *in-situ* Ar plasma pre-cleaning for 30s prior to the deposition of the a-C:H layer. The films were deposited at different DC self bias voltages.

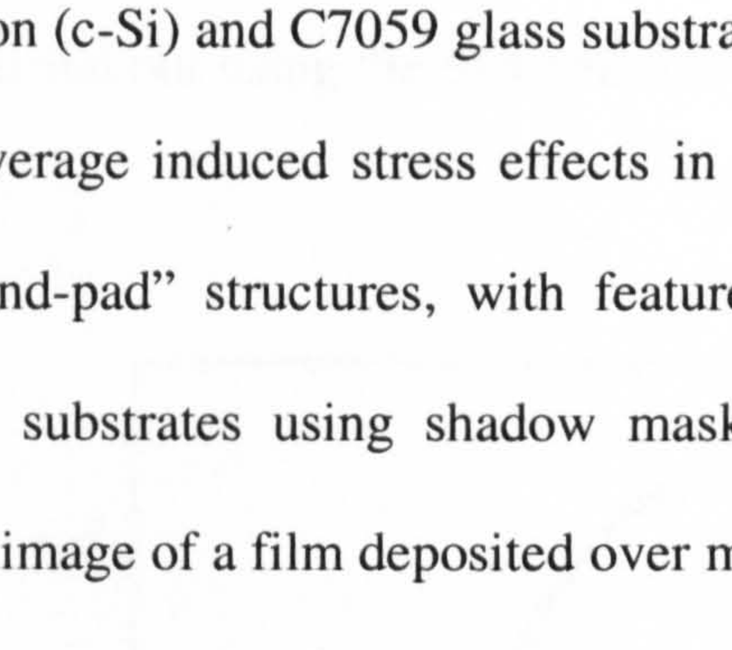

Fig.- 7.16 SEM image of an a-C:H layer covering adjacent c-Si and Cr coated regions.

The current-voltage (*I-V*) characteristics for the a-C:H layer were measured using micro-tip system described previously, connected to a PC-driven HP4140B pico-ammeter/voltage source. The micro-tip arrangement allowed the surface morphology and local electrical properties to be probed with a high spatial precision (see Chapter 6). Large area MSM structures were also produced for electrical characterisation by thermally evaporating circular metal dots of 1mm diameter each, on top of the a-C:H layer. Micro-Raman measurements were carried out using the 514.5nm line of an Ar ion laser with a 2μm spot size.

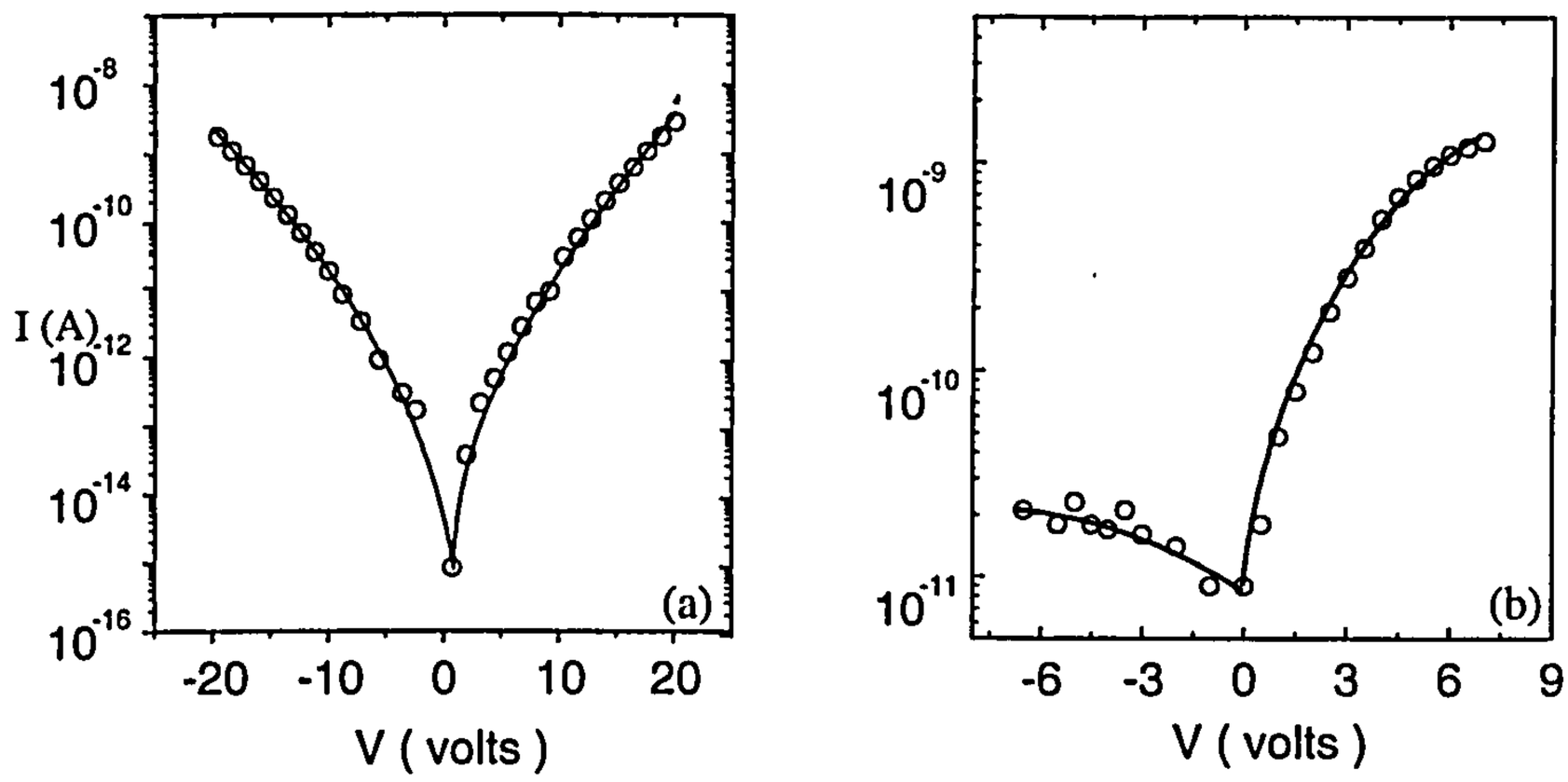

Fig.- 7.17 (a) A typical symmetrical *I-V* characteristic for a 'micro-tip' MSM structure in the middle of a Cr strip (b) A typical asymmetrical *I-V* characteristics from a 'micro-tip' MSM structure at the edge of a Cr strip.

The micro-tip technique was used to investigate the electrical properties of a-C:H layers at a variety of locations in the vicinity of the Cr tracks. Typical *I-V* characteristics of an a-C:H film deposited at a DC bias of -150V are shown in Fig.-7.17. Fig.-7.17(a) shows an *I-V* characteristic of an MSM structure formed in the middle of the strip, with a W tip. The *I-V* characteristic is symmetrical for all applied voltages which is indicative of a bulk-limited Poole-Frenkel conduction mechanism [23]. Fig.-7.17(b) shows the typical asymmetrical *I-V* characteristic for a tip/a-C:H structure, formed near the edge of the Cr Strip. Most of the contacts that we measured near the edge showed Schottky type behaviour.

We have previously reported similar inhomogeneities in the *I-V* characteristics of micro-tip/a-C:H/metal structures formed at different locations on a continuous metal coated corning glass substrate, [30]. The observation of asymmetrical *I-V* behaviour was attributed to Schottky barrier formation at sp^3 rich regions of the film. Of key significance in the this work, is the frequent occurrence of asymmetric *I-V* characteristics near the strip edge (suggesting high sp^3 content) and symmetrical *I-V* characteristic in the centre of the strip (high sp^2 content). This observation is a clear indication that properties of the a-C:H layers vary from the middle to the edge of the Cr strip. In step with the findings of [30], here again we propose that the observed spatial variation in material properties is associated with a higher "local" DC field in the vicinity of the strip edge. More importantly, during the deposition process, the space rate of change of the bias

voltage at the edge, is higher than the same at the centre of the strip. This is synonimous with a higher local electric flux at the edge than the centre during the deposition.

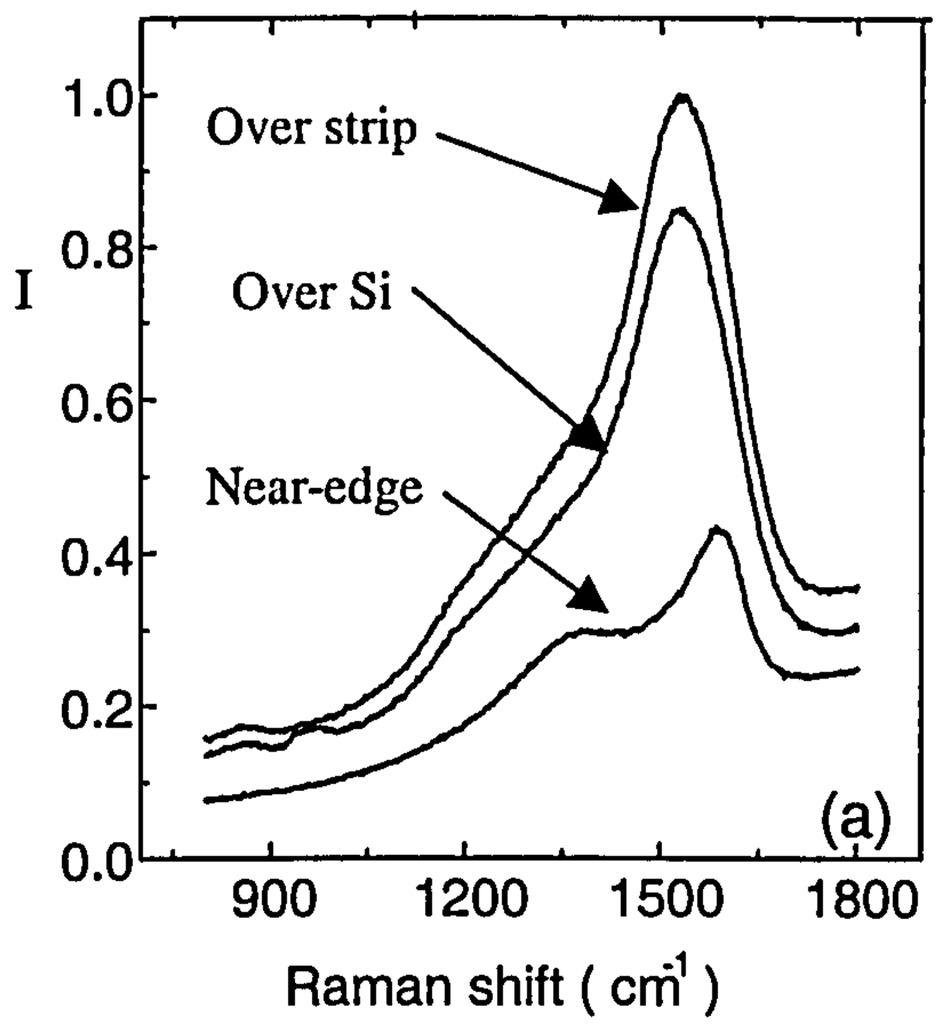

Fig.- 7.18 Typical Raman spectra of an a-C:H at three different regions in the film.

Micro-Raman spectroscopy has been carried out to confirm the compositional variation in the a-C:H film across the metal tracks. Typical Raman spectra at different locations on the same a-C:H layer, namely the region near the edge of a metal-strip, in the centre of a metal strip and over the c-Si substrate, are shown in Fig.-7.18. The Raman spectrum at the edge of the metal strip is clearly (and reproducibly) different from the same at the other locations. Determination of the composition of sp^3-rich regions with visible Raman spectroscopy is rather dubious. This is because visible Raman

spectroscopy is more sensitive to sp^2 rich sites (50 to 230 times) than the sp^3 sites, [37,38]. We believe that there are more sp^3 enriched regions near the edges of the film step and therefore there is a higher probability of Schottky contact formation at these parts of the film.

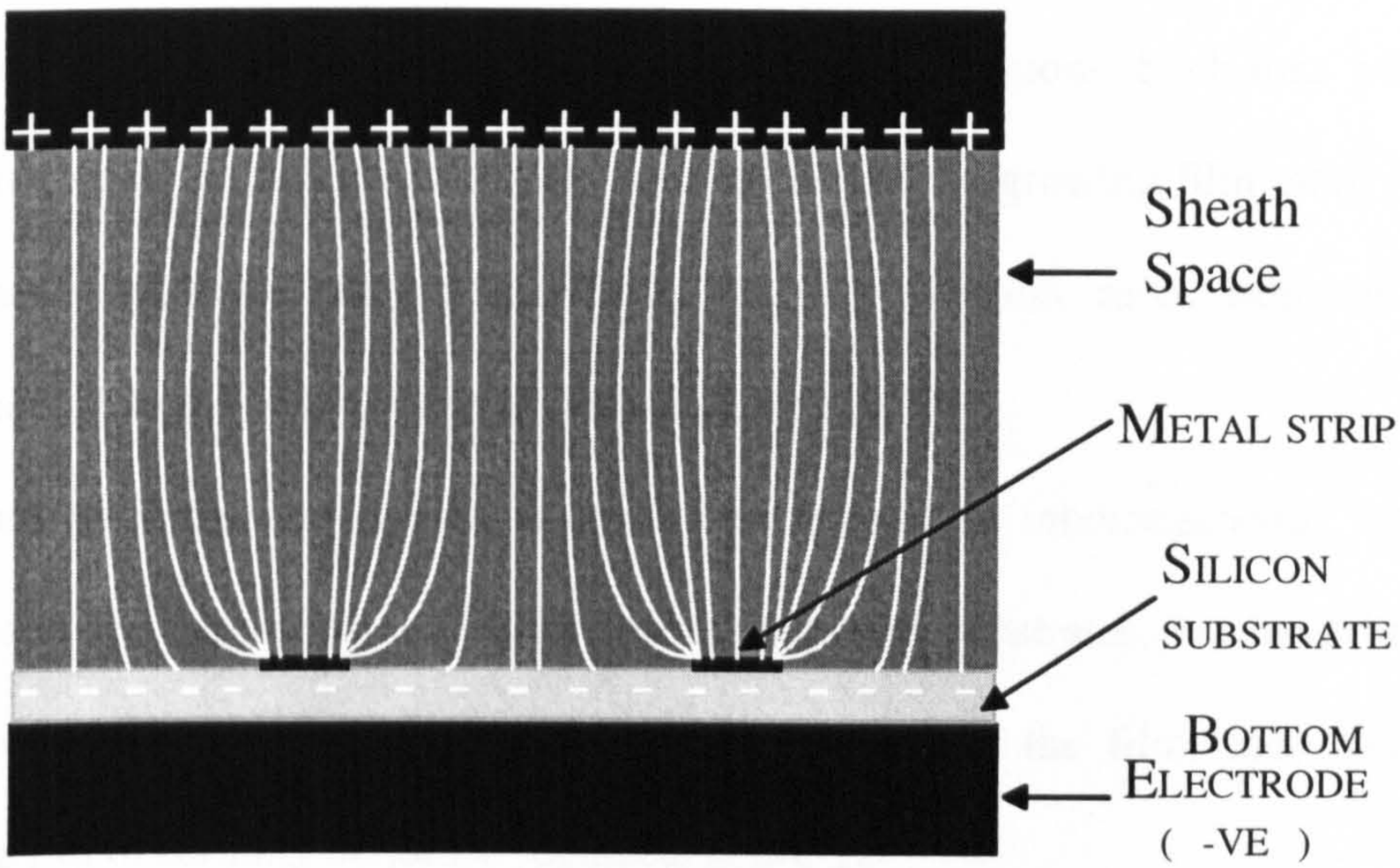

Fig.-7.19 Geometry of electric field lines when a metal-patterned substrate is placed in the PECVD reactor.

These results can be explained on the basis of the PECVD process and the electrical field distribution during the deposition. Fig.-7.19 shows the distribution of electric field lines in the sheath space when a metal-patterned substrate is placed in it. The properties of amorphous carbon films are mainly dependent on the energies of the impinging ions during the deposition process. The ion energy in the rf-PECVD system is determined by

the DC self-bias developed across the sheath space and the inelastic collisions that occur in the acceleration process across the sheath. When highly energetic ions strike the substrate surface, they combine together resulting in small clusters (sp^1, sp^2 and sp^3) of sizes a few nanometers or less. The DC bias is strongest at the edges of steps in the film; hence the ions impinging on the edges of the films will have the highest energies, which may be the key to the formation of diamond-like rich regions. Such ions will also etch away the softer portions (sp^1 and sp^2 rich regions) of the growing film more readily than the harder (diamond-like) parts. Thus the edges exhibit more semiconductor like behaviour than the central parts in the a-C:H films.

Both electrical and Raman analyses corroborate the inhomogeneous nature of the material. By depositing a-C:H on metal patterned substrates, we have been able to concentrate the sp^3 rich clusters in specific regions in the film, thus increasing the certainty in of forming Schottky contacts in a-C:H.

7.5.4 Current Transport Mechanism in Schottky diodes

The current transport mechanism is the key to understand the device behaviour. In metal-semiconductor contacts the current transport is mainly due to the majority carrier, in contrast to pn junction, where the minority carriers are responsible. To describe the current transport in the schottky diodes; the thermionic emission theory proposed by Bethe [39] and the diffusion theory proposed by Schottky [40]. Crowell and Sze [41] analysed both the theories and proposed that the current mechanism in most GaAs, Ge

and Si Schottky barrier diodes. The following expression is commonly used to describe the current-voltage characteristics of these diodes:-

$$J = J_s\left[\exp\left(\frac{eV}{\eta kT}\right)-1\right]$$

where, $J_s = A^{**}T^2\exp\left(-\frac{e\phi}{kT}\right)$, A^{**} is the Richardson constant, T is the Temperature, e is the electronic charge, k is the Boltzman's constant, η is the ideality factor and ϕ is the barrier height.

The above expression can be reduced to the following equation in the forward bias ($V >> \frac{kT}{e}$) and $\eta \approx 1$;

$$J_F \approx A^{**}T^2\exp\left(\frac{e(V-\phi)}{kT}\right)$$

To find the activation energy ($e(V-\phi)$)at given value of a forward voltage (V), the above expression can be written as:

$$\ln\left(\frac{J_F}{T^2}\right) = \ln(A^{**}) + \frac{e(V-\phi)}{kT}$$

Thus for a given forward bias (V), the slope of a plot of $\ln\left(\frac{J_F}{T^2}\right)$ versus $\frac{1}{T}$ straight line and the slope will yield the activation energy. Such investigation is important to ensure current transport mechanism in the schottky devices. Due to lack of time, we could not perform such investigation. But care should be taken in interpreting the result at higher temperature (> room temperature) that diamond-like carbon is a multi-phase material. It may be possible that some phases may not stable at higher temperature and therefore the may change to another form of carbon, which can lead wrong interpretation of the observed results.

References

1. B.J Lechner, F.J. Marlowe, E.O. Nester and Tults, *Proc. IEEE*, **59**, 1566 (1971).
2. M.J Powell, *IEEE Trans. Electron. Devices*, **36**, 2753 (1989).
3. M.G. Clark, *IEE Proc. Circuits Devices and System*, **141**, 3 (1994).
4. E. Lueder, *MRS Symp. Proc.*, **373**, (1995).
5. C. Van Berkel, M.J. Powell, and S.C. Deane, *J. Non-Cryst. Solids*, **164**, 653 (1993).
6. K.J.B.M. Nieuwesteeg, J. Boogaard and G. Oversluizen, *MRS Symp. Proc.*, **164**, 379 (1993).
7. D.E. Castleberry, *IEEE Trans. Electron. Devices*, **ED-26**, 423 (1979).
8. D.R. Baraff, J.R.Long, B.K. Maclaurin, C.J.Miner and R.W. Streater, *IEEE Trans. Electron. Devices*, **ED-28**, 736 (1981).

9. S. Togashi, *Optoelectronics – Devices and Technology*, **7**, 271 (1992).

10. V. Hochholzer, E. Lueder, T. Kallfass and H.U Lauer, *SID Digest*, 423 (1994).

11. S. Zhang and J.K.O Sin, *IEEE Electron. Device Letts.*, **19**, 192 (1998).

12. M.Susuki, M. Toyama, T. Harajiri, T. Maeda and T. Yamazaki, *Proc. SID*, **28**, 101 (1987).

13. E. Mizobata, K. Yoshida, Y. Hirai, H. Uchida and S. Kaneko, SID Digest, 226, (1991).

14. J.M. Shannon, J.N. Sandoe, I.D. French and A.D. Annis, *MRS Symp. Proc.*, **297**, 987 (1993).

15. A.G. Knapp, R.A.Hartman, Proc. IDRC, Monterey, CA, USA, pp.14-19 (1994).

16. A.G.Knapp, J,N, Sandoe, J.M. Shannon, P.B.A Wolfs, J.H.W Kuntzel and A.J. Van Roosmalen, SID International Symp. Digest, **24**, 379 (1993).

17. J.A. Chapman, D.S. George, J.A. Clark, J.R. Hughes, A.D. Pearson, R.V. Winkle and N.K Wright, *Proc. 13th IDRC (SID, Strasbourg)*, pp.-275-278 (1993).

18. S. Egret, J. Robertson, W.I. Milne and F.J. Clough, Diamond Related. Mater. **6**, 879, (1997).

19. E.Ohta, Y. Kimura, H. Kondo, M. Takahashi, K. Kameyama, K. Yamda and I. Fujimura, *22nd Int. Conf. Sol. Stat. Devices and Materials (SSDM)*, 589, 1990.

20. J. Frenkel, *Phys. Rev.*, **54**, 647 (1955).

21. D.R. Lamb, Electrical Conduction Mechanism in Thin Film Insulators, (Metheum, London, 1967).

22. R.M. Hill, *Phil. Mag.*, **23**, 59, 1971.

23. S.M. Sze, Physics of semiconductor Devices, (Wiley Interscience), 1987.

24. D.V lang, J.D Cohen and J.P Harbison, *Phys. Rev. B*, **25**, 5285 (1982).

25. L. Klibanov, M.Allon-Alaluf, N.Croitoru and A. Seidman, *Diamond and Relat. Mater.*, **5**, 1414 (1996).

26. F.J Clough, B. Kleinsorge, W.I. Milne, J.Robertson, G.A.J Amaratunga and B.N Roy, *Electronics Letters*, **32**, 498, 1996.

27. R.A Street, Hyrdrogenated Amorphous Silicon (Cambridge University Press), 1991.

28. H.K Henisch, *Rectifying Semiconductor contacts*, (Oxford University Press), 1957.

29. G.Bradely and G. Whitford, IEEE J. Quantum Electron., QE-18, 428,

30. S. Paul and F.J Clough, *Diamond and Relat. Mat.*, **7**, 1734, (1998).

31. Y. Koide, M. Yokoba, A. Otsuki, F. Ako, T. Oku, M. Murakami, *Diamond Films Technol.*, **6**, 61 (1996).

32. G. Amaratunga, A. Putnis, K. Clay, and W.I Milne, *Appl. Phys. Letts.*, **55**, 634, 1989.

33. S.R.P Silva and G.A.J Amaratunga, *J. Materials Science*, **29**, 4962, 1994.

34. Ph. Komninou, G.Nouet, P.Patsalas, Th. Kehagias, M.Gioti, S.Logothetidis, Th. Karakostas, *Diamond Relat. Mat.*, **9**, 703 (2000).

35. S.Paul and F.J Clough, *MRS Symp. Proc.*, **558**, 149 , (1999).

36. S.Paul and F.J Clough, Submitted to *Review of Scientific Instruments.*

37. N.Wada, P.J. Gaczi and A.Solin, *J. Non-Cryst. Solids*, **35&35,** 543 (1980).

38. S.R. Salis, D.J Gardiner, M.Bowden, J.Savage, and D.Rodway, *Diamond Relat. Mater.* **5**, 589 (1996).

39. H.A Bethe, *Theory of the Boundary Layer of Crystal Rectifiers*, MIT Radiat. Lab. Rep., 43-12 (1942).

40. W. Schottky, Halbleitertheorie der Sperrschicht, *Naturwissenschaften,* **26**, 843 (1938).

41. C.R Crowell and S.M. Sze, *Solid State Electron.*, **9**, 1035 (1966).

CHAPTER 8

Amorphous Carbon as a Low-k Insulator Inter-layer Dielectric for VLSI/ULSI

8. 1 Introduction

A number of materials have been reported as potential low-k dielectrics in the back end of line (BEOL) interconnect structures in VLSI/ULSI circuits [1,2,3,4]. The continuing shrinkage of electrical device and wiring dimensions in ULSI circuits result in enhancements of resistance of the BEOL metallisation and capacitance, (both at the inter and the intra levels), thus increasing signal delays. This renders low-k dielectrics particularly suitbale for BEOL applications. Reduction of these capacitances and improvement in the switching performances of future ULSI circuits can be brought about by low dielectric constant materials, with k significantly lower than that of the SiO_2. Dielectrics with low k values are available, (e.g. polytetrafluoroethylene (PTFE) with k=2.0) [5]; however these materials are not stable at temperatures above 300-350^{0}C while integration of the dielectric in ULSI chips requires thermal stability at temperatures at least as low as 400^{0}C[6].

8. 2 Use of amorphous carbon as an interlayer dielectric material

Diamond-like carbon (DLC) and fluorinated DLC (F-DLC) have also attracted much attention for use as an interlayer isolation material [7,8,9,10]. The delay time associated with

an integrated circuit is a key measure of performance. "Low-k" dielectric (i.e. materials with a dielectric constant lower than that of SiO_2) are needed to minimise parasitic capacitance in the ULSI circuitry. The combination of low dielectric constant, smoothness, mechanical strength and chemical inertness, renders diamond-like carbon an ideal candidate for such application.

The critical growth parameter when depositing a layer of rf-PECVD is the DC bias (which is explained in Chapter-4). The potential for the "effective" DC bias to be influenced by the electrical properties of the substrate and the conductivity and topography of additional layers on the substrate surface is clear but, to date, no extensive investigation has been carried out in this field. We have investigated such effects [9,11] very rigorously. Such effects are likely to be particularly relevant when optimising layers of a-C:H meant to be utilised as an interlayer dielectric. The requirement to deposit layers of electronic grade a-C:H directly on top of narrow metallic lines (e.g. gate, source/drain or interconnection tracks) will make these applications sensitive to such effects.

A number of metals are used in the multilevel process in VLSI/ULSI. Aluminium [12,13,14], copper, tungsten, tantalum, and chromium are some of the most commonly used metals. The interaction of DLC with track-materials (Al, Cu, Cr, Ta, etc.) has not been established yet. It will be interesting to study the interaction of these metal(s) with DLC under a constant electric stress. This investigation is important to select metals suitable for use in multilayer metallisation processes, in which DLC is used as an interlayer dielectric material. In particular, we have examined the behaviour of Al since it is the most commonly

used metal in electrical connection in ICs. No such investigation was found reported in the literature.

In this chapter, the presented discussion covers investigation of the adhesion, morphology and electrical and structural properties of a-C:H films, grown on C-Si and C8059 corning glass substrates which were either with or without predefined metallic patterns. The film properties were also investigated for various electrode metals under time dependent electrical stress.

8. 3 Preparation of a test structure

The films of a-C:H were deposited at room temperature from CH_4/Ar gas mixtures using a capacitvely coupled rf-PECVD (as described in chapter-3) system at a pressure of 100 mTorr. A nominal a-C:H film thickness of 90 nm was maintained for all samples. The plasma power was varied to develop a DC self-bias of -70V to -295 V. Test structures were prepared by thermally evaporating 20 nm thick films of Cr on to c-SI and C8059 corning glass substrates. The schematic diagram of such a structure is shown in the Fig-8.1.

Thin Cr layers ware used to minimise the step coverage induced stress effects in the deposited layers. Substrates (2cm x 2 cm) with a continuous metal coating were also used to investigate the properties of a-C:H films deposited on to large area metallic substrates. In addition, thin metal strip and pad of structures, with feature sizes up to several mm, were patterned on to selected substrates using shadow masks during the thermal evaporation stage

as well as lift-off lithography to the smaller sizes. Fig.-8.2 shows the Si-patterned substrate with Cr strips.

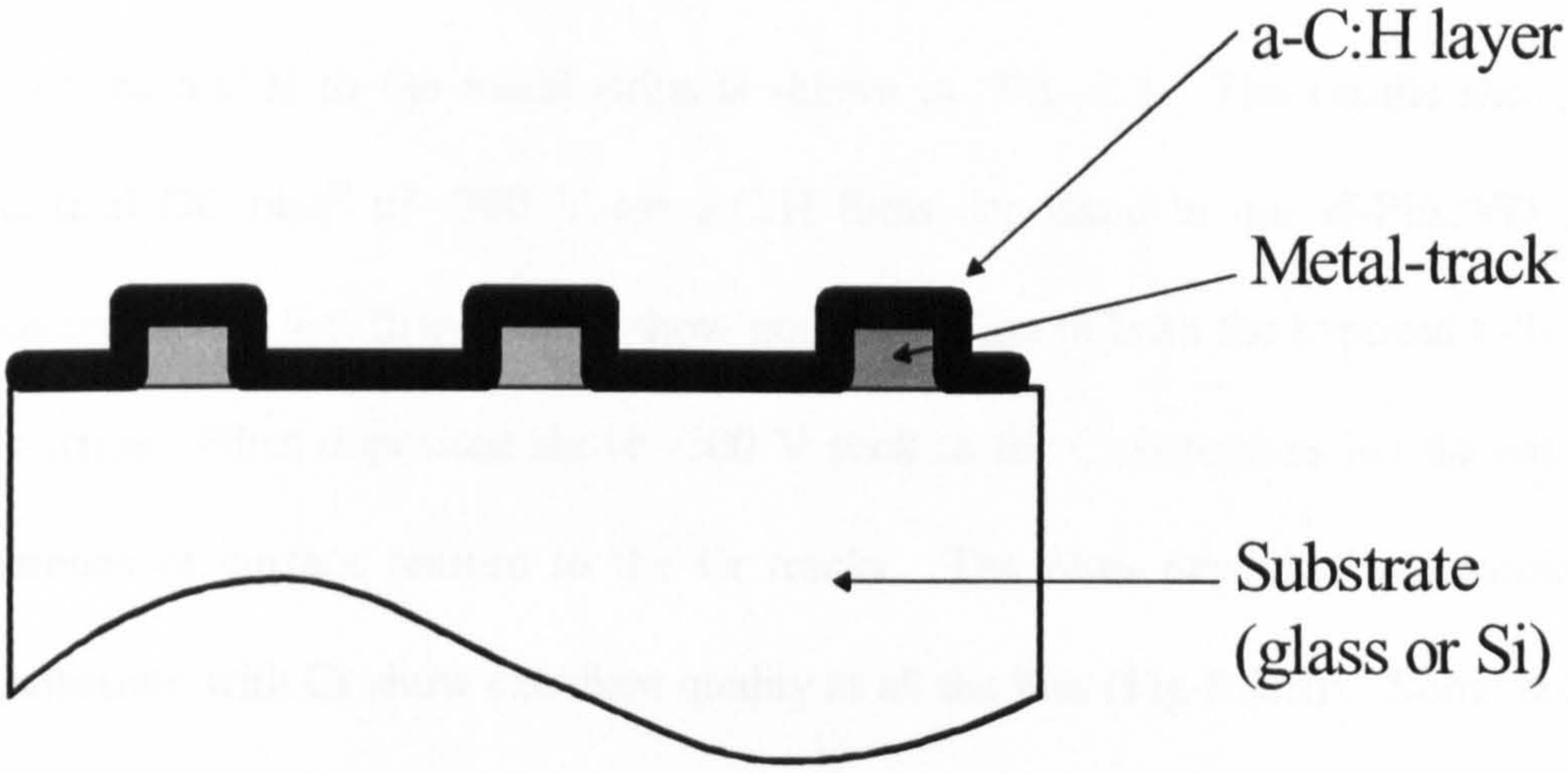

Fig.- 8. 1 Schematic diagram of deposition of DLC on the metal patterned substrate.

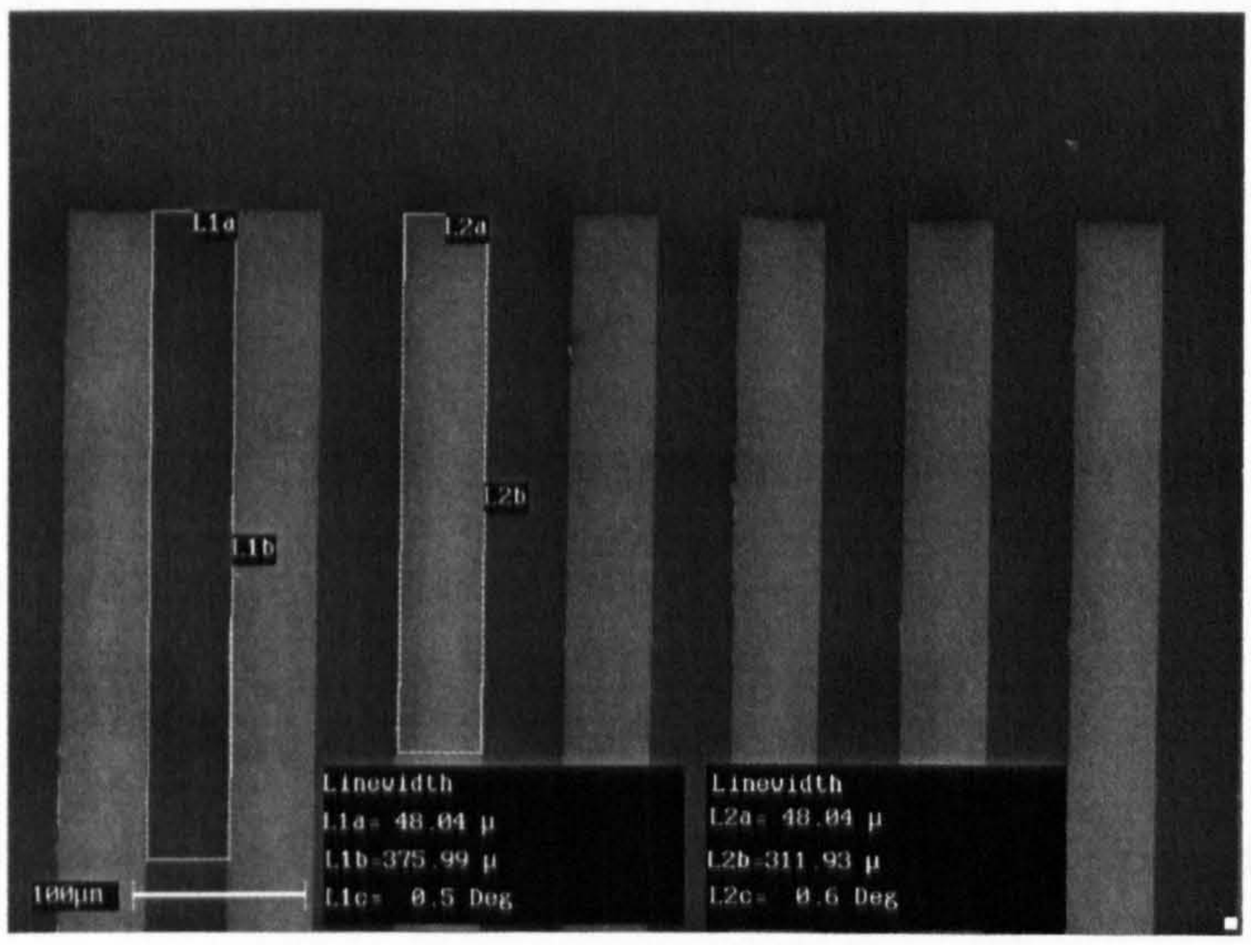

Fig.-8. 2 SEM micrograph of Cr patterned Si Substrate.

We systematically investigated the adherence of a-C:H across c-Si substrates with pre-defined Cr strips, at different values of the DC self-bias. The effect of DC bias on the adherence of the a-C:H to the metal strips is shown in Fig.-8.3. The results show a well defined "critical DC bias" of -200 V for a-C:H films deposited in our rf-PECVD system. Films deposited at bias less than -200 V show good adhesion to both the exposed c-Si surface and the Cr-strips. Films deposited above -200 V stick to the C-Si regions but do not exhibit good adherence or surface texture to the Cr tracks. The films deposited on continuously coated Si substrate with Cr show excellent quality at all the bias (Fig-8.3(d)). Some reduction in the film adhesion is predictable at the edge of the Cr pad, where there is a significant change in the surface topography which causes enhancement in film stress. However, this does not explain the general observation of excellent film adherence to Cr strips below -200 V DC self bias and poor adherence above that value. Also, films show good adherence to the C-Si substrate while very poor adherence to the Cr strip, under same the growth conditions.

Adhesion is closely related to film stress (which is a function of the presence of sp^2 and sp^3 constituents in the film) and dependence of film stress on the DC bias is well documented for rf-PECVD by Silva et el [15]. Within the DC bias range which results in 'hard' a-C:H films, an increase in the bias voltage results in a corresponding increase in the film stress. It is suggested that the observed reduction in film adhesion on the metallic tracks can be attributed to electric field enhancement in the region around the metallic patterns arising from their high conductivity (relative to the surrounding c-Si substrate). Field enhancement results in a 'local'

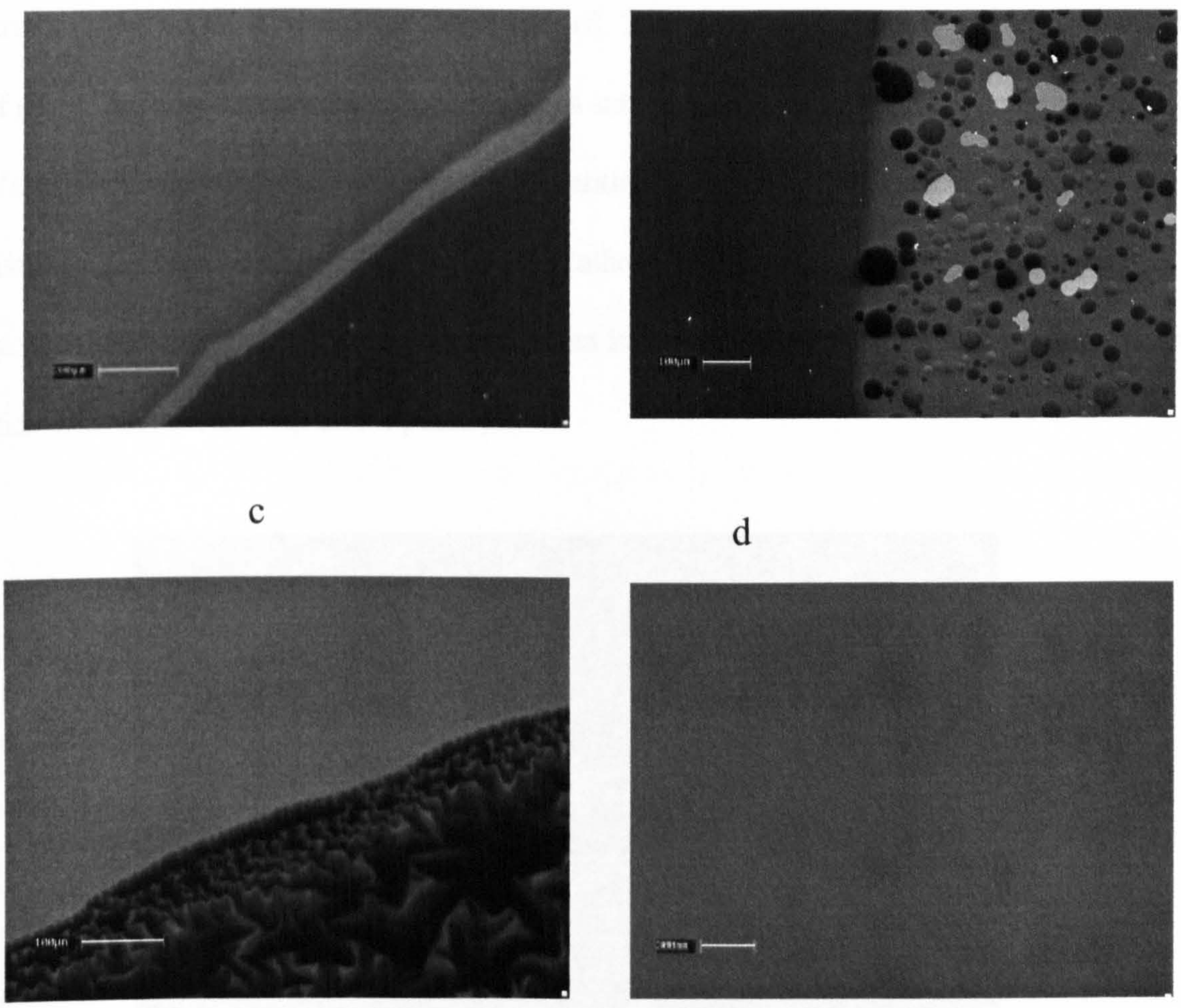

Fig.-8. 3 SEM micrographs of an a-C;H film deposited on to a C-Si substrate with pre-defined Cr strip at different DC self-bias., (a) –175 V (b) –200 (c) –240 (d) fully-cover Si substrate with Cr at –240 V.

DC bias which can exceed the 'average' bias set by the process controller. The corresponding increase in the film stress is then sufficient to overcome the cohesive force between the metal strip and the a-C:H film and the film peels off. This rationale is supported by the observation of good film adhesion on fully Cr coated c-Si substrates at higher 'average' applied DC biases. We try to understand this behaviour by quantitative analysis of the change in the electric field distribution associated with a surface metallic pattern. Therefore, after the electric field exceeds the critical value, the stress in the film is so high that the film will no longer be able to stick with the metal strip and it peels off.

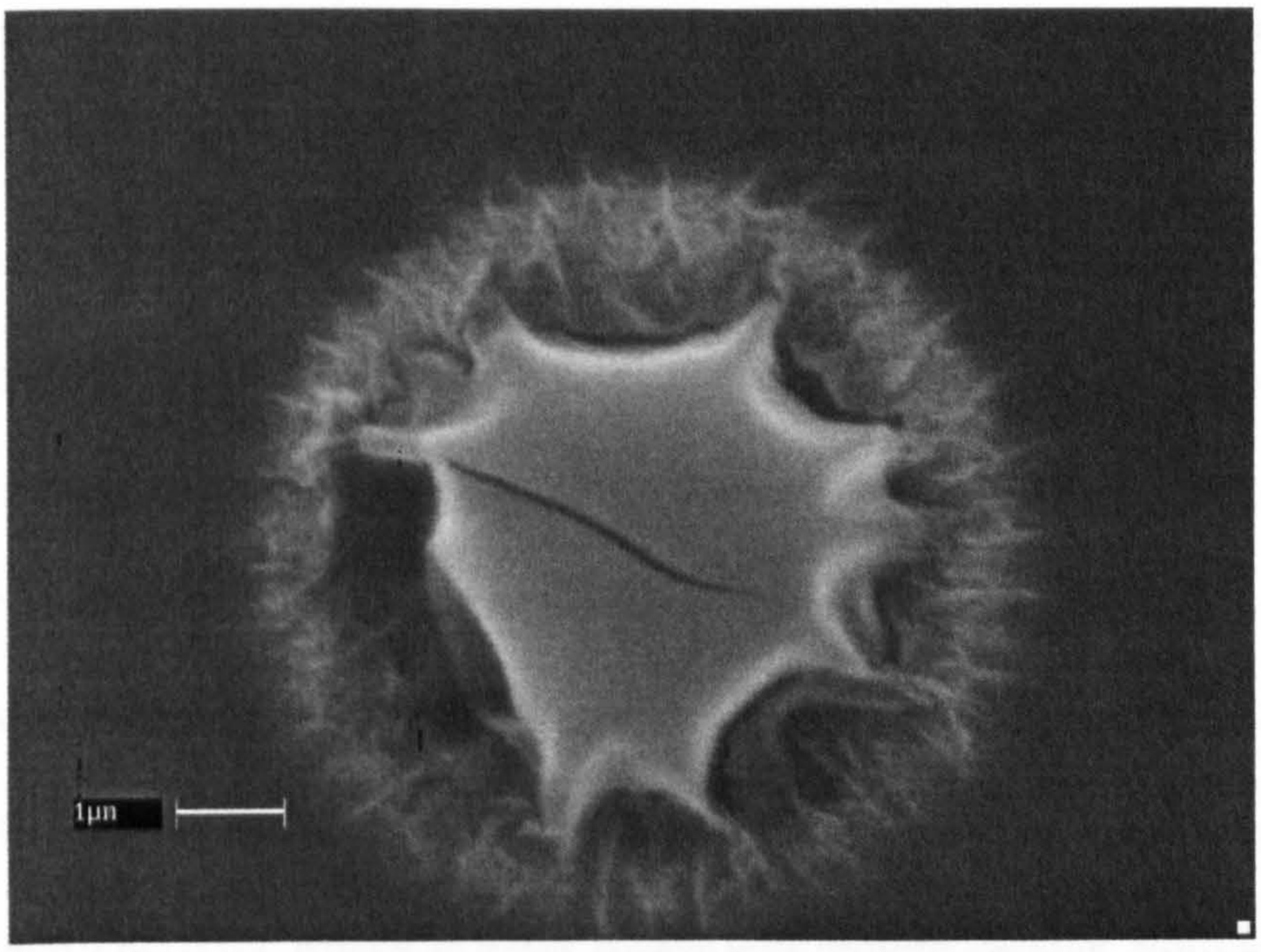

Fig.-8.4 Blister formation in a-C:H films over the Cr-strip when DC self-bias just above –200 volts.

Fig.-8.4 shows the blister formation in the a-C:H films just above the critical bias (-200V). This shows that the film is highly stressed and peels off wherever the localised stress is very high.

There is yet another important property to check -- the inhomogeneity in the film properties on the metal strip, due to non-uniform electric field distribution on the metal strip. Fig.-7.18 shows that the field is more concentrated near the edges. We have observed different electrical behaviour at the different locations of a-C:H deposited on metal-strips. Both symmetrical and asymmetrical behaviour have been observed on the metal strips. These results are explained on the basis of the PECVD process and the electrical field involved with the deposition in Chapter 7.

On the basis of the above investigation, we can confidently conclude that the properties of a-C:H deposited on metal-strips are electrically and morphologically different from that of films deposited on the large area substrates. Therefore, the observed properties on the large substrates cannot be extended to small area metal-strips. The adhesion and material properties of thin films of rf-PECVD a-C:H film can be significantly affected by the substrate material on which the film is deposited and the substrate topography. For applications in large area electronics and interlayer isolation these issues will require serious consideration. We have investigated the material variations associated with metallic films of a relatively small aspect ratio (20 nm thick and 1 mm wide). In real applications the metal tracks may be considerably thicker (up to a few microns) and narrower (down to a few microns). This will result in more extreme variations in the 'local' electric field and hence the material properties. A better

understanding of the substrate dependence of the 'local' DC bias and the microscopic properties of a-C:H is therefore important if these materials are to be reliably integrated into large area electronic and 'low-k' dielectric applications.

8.4 Reliability of different metal contacts with amophous carbon

A number metals have been used in fabricating top and bottom metal contacts in MSM, MIM devices and multi-level metallisation [16,17]. There is no single report on the interaction between the metal and a-C:H films. On the basis of basic interface physics, different metals interact differently with a material. For example, Si can diffuse into Al and form a metal-silicide at the Al/Si interface [18]. This deteriorates the device properties. The migration of atoms from one material to another is generally governed by the diffusion process. Therefore, the interaction of a metal with the semiconductor material is both time and temperature dependent. During MSM or VLSI operation, temperature of the device remains nearly constant and therefore it is only the dynamics of the interaction of a-C:H with the metal, that is of concern. The understanding of such an interaction is important, as this will help to estimate the life time of the devices and will direct us to the choice of the most suitable metal that should be used to fabricate any devices out of a-C:H.

To carry out such investigations we deposited a-C:H films on the Si^{+n} substrate of size $2"x2"$ and resistivity 0.025 Ωcm. The top metallic contacts were deposited by the thermal evaporation of metal through a shadow mask at high vacuum ($1x10^{-6}$ Torr). Cu, Al, and Cr

metals dots of 1 mm diameter were deposited on the same sample. This was done to compare results obtained from each metal contact.

The time dependence of the reaction (if any) of a-C:H with the metallic dot was monitored by the change in the capacitance. If we recall Eqn.-7.8, the capacitance measured at 1 MHz provides the value of the geometrical capacitance. The thickness (d) and contact area (A) are unaltered during the measurements. The time dependence of reaction was monitored by capacitance change. The capacitance of unaltered a-C:H layer is characterised by the capacitance of the layer. Any changes in the capacitance can be safely attributed to a change in the dielectric constant of the material. To carry out such investigations, we applied a constant voltage of 10 V between the lower and upper electrodes of the metal/a-C:H/Si^{+n} structures and measured the time dependent capacitance at 1 MHz. Diffusion of metal atoms into the a-C:H film or carbon atoms into the metal will certainly be reflected in the capacitance.

Typical Capacitance-Time (C-t) plots observed for Al, Cu, and Cr have been presented in Fig.-8.5. It is quite clear from the plot that after a certain time, the capacitance of the Al contact to the a-C:H film exhibits rather irregular behaviour while the C-t behaviour corresponding to the Cu and Cr contacts, is quite smooth. We investigated a number of devices for the sake of reproducibility in the observed behaviour. The results were similar.

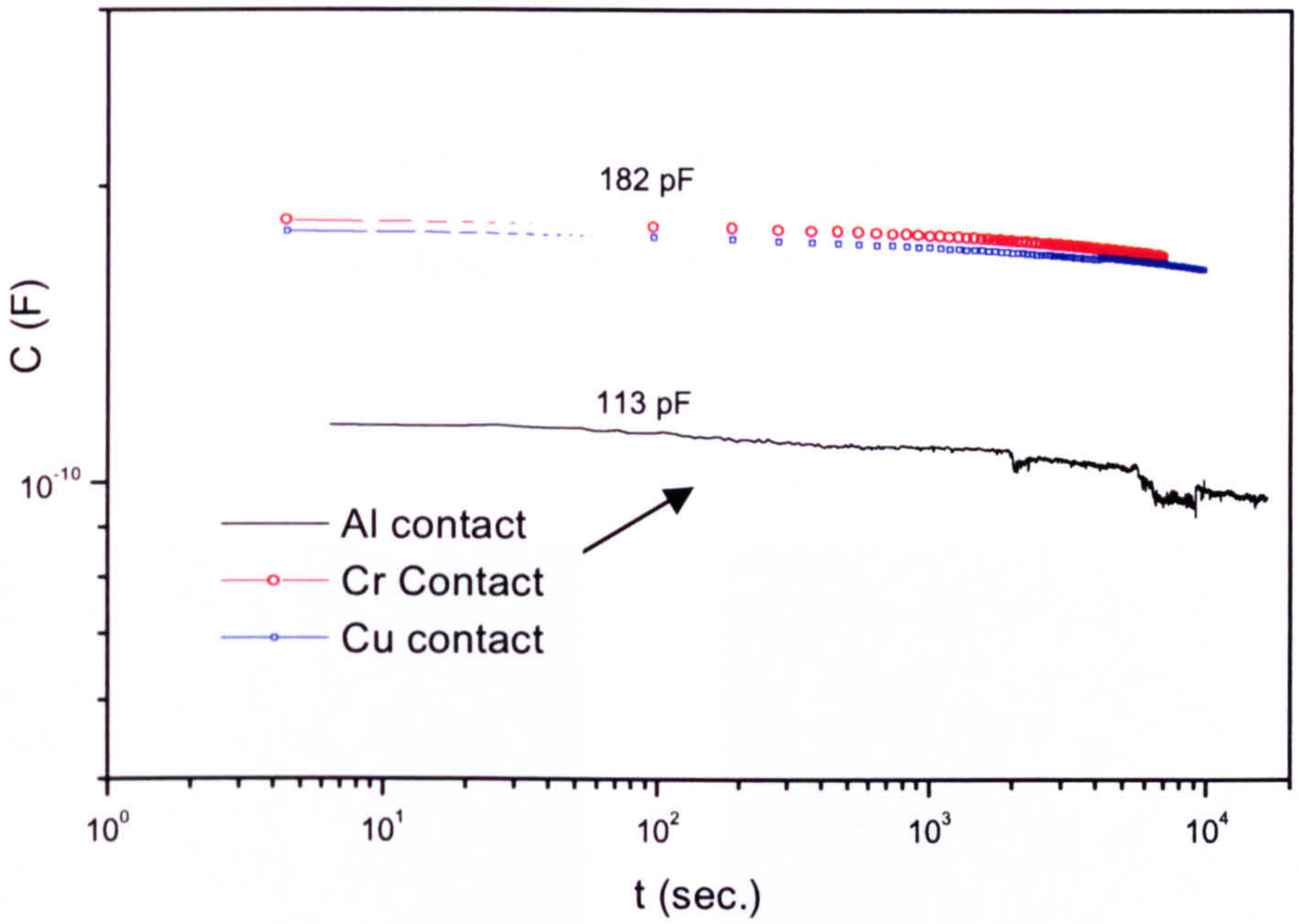

Fig-8.5 C-t characteristics of metal/a-C:H/Si devices, where metal is Cr, Cu and Al.

For further understanding, we carried out surface study of metal contacts before and after imposition of the electrical stress. Fig. –8.6 shows the micrographs taken before and after the electrical stress was applied. It is quite clear from the Fig.-8.6 that there is hardly any change caused to the morphology of the Cr and Cu contacts by the introduction of the stress, while there is a drastic change in the look of the Al contact. We investigated the relative percentage of Al at three different locations in the film and found inconsistencies in the percentage of Al on the a-C:H surface. On the basis of EDAX analysis, we can say that there is a loss of Al during the duration of the electrical stress. The change in the capacitance and EDAX analysis

suggest the Al has diffused into the a-C:H films, while Cu and Cr did not diffuse into the a-C:H film under similar electric stress conditions. It has been shown by Lacerda et al [19] that nitrogen doped a-C:H is a good barrier material as for as diffusion of Cu into them in concerned. We have observed similar behaviour in case of Cu in our investigation.

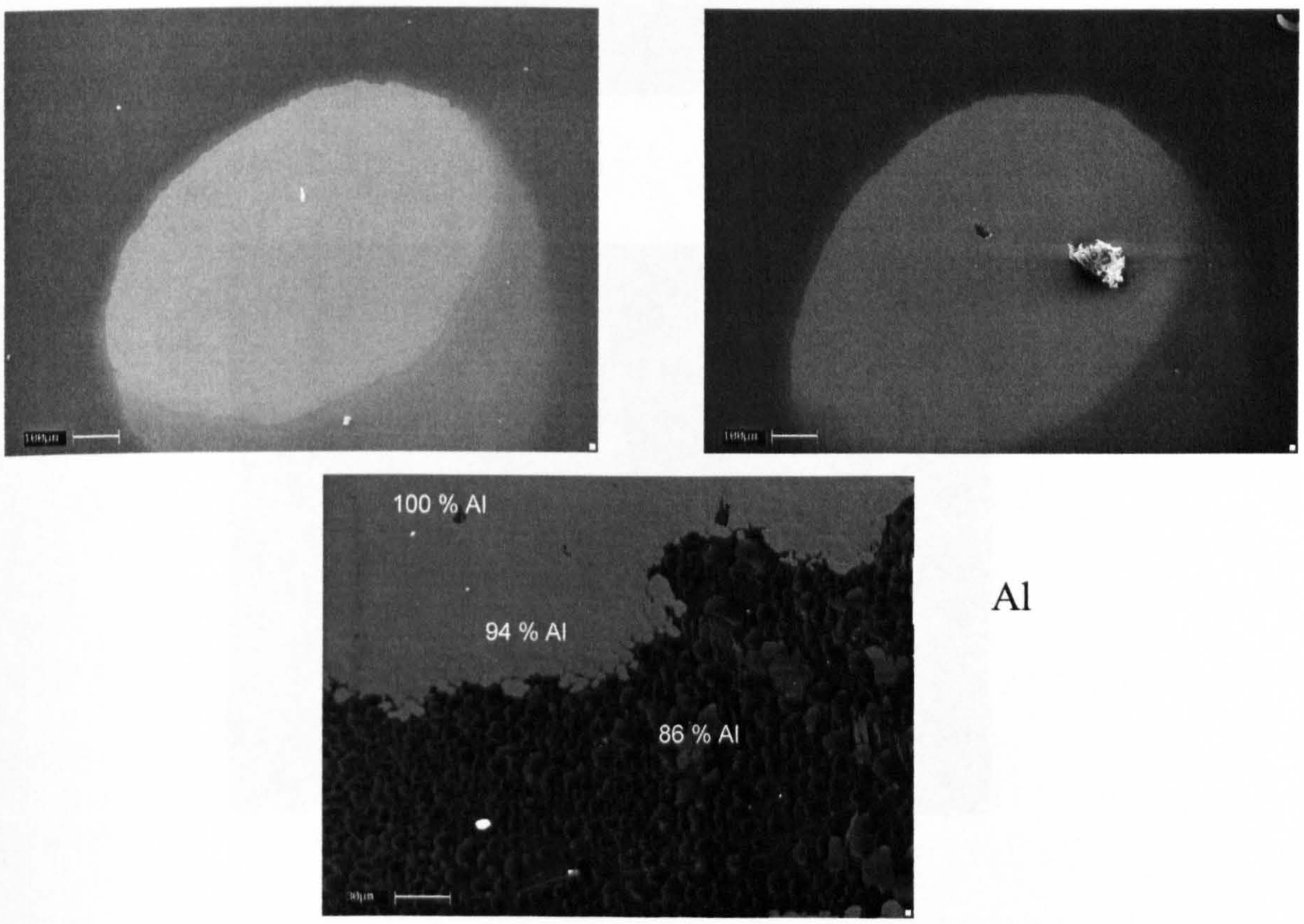

Fig.-8.6 SEM micro-graph of different metal contacts before and after the imposition of electrical stress for similar stress time.

(a)

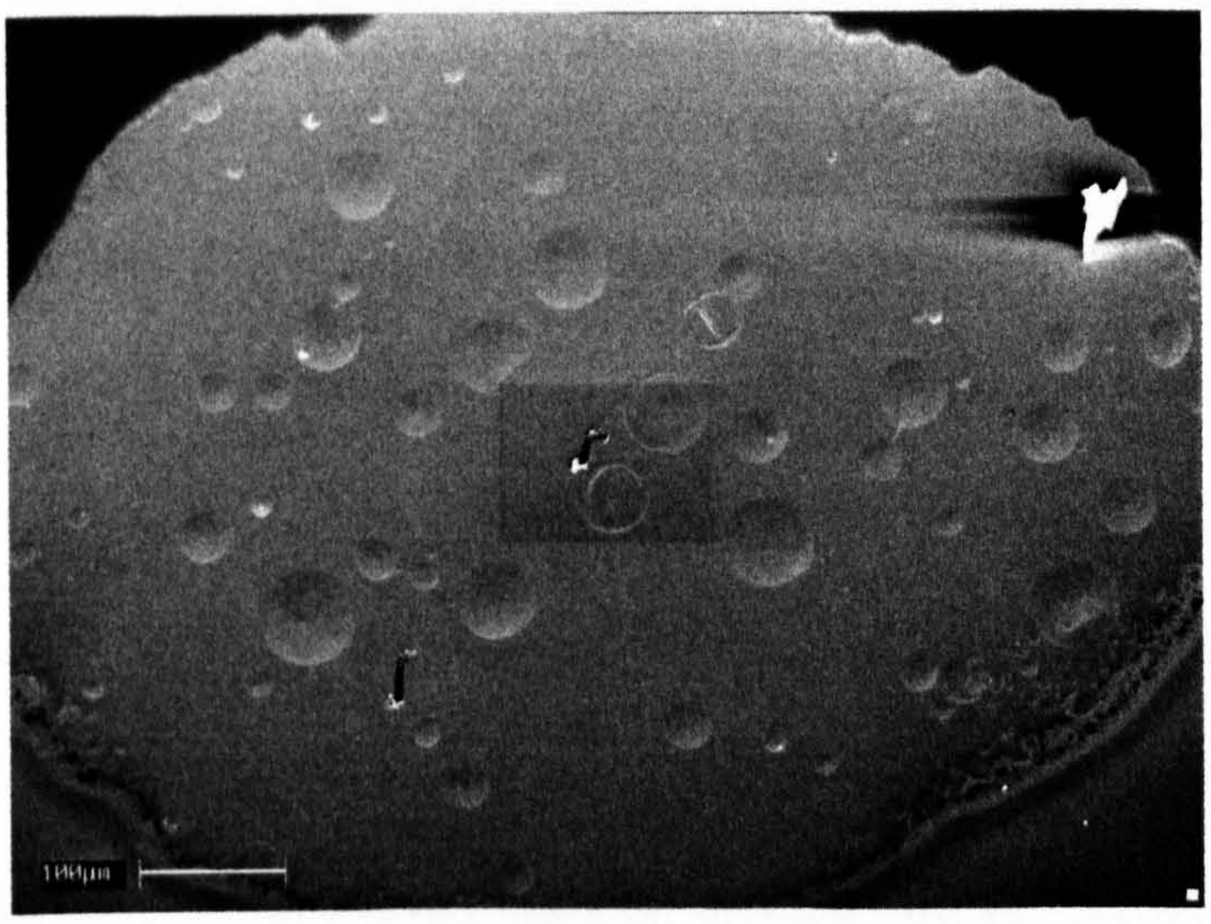

(b)

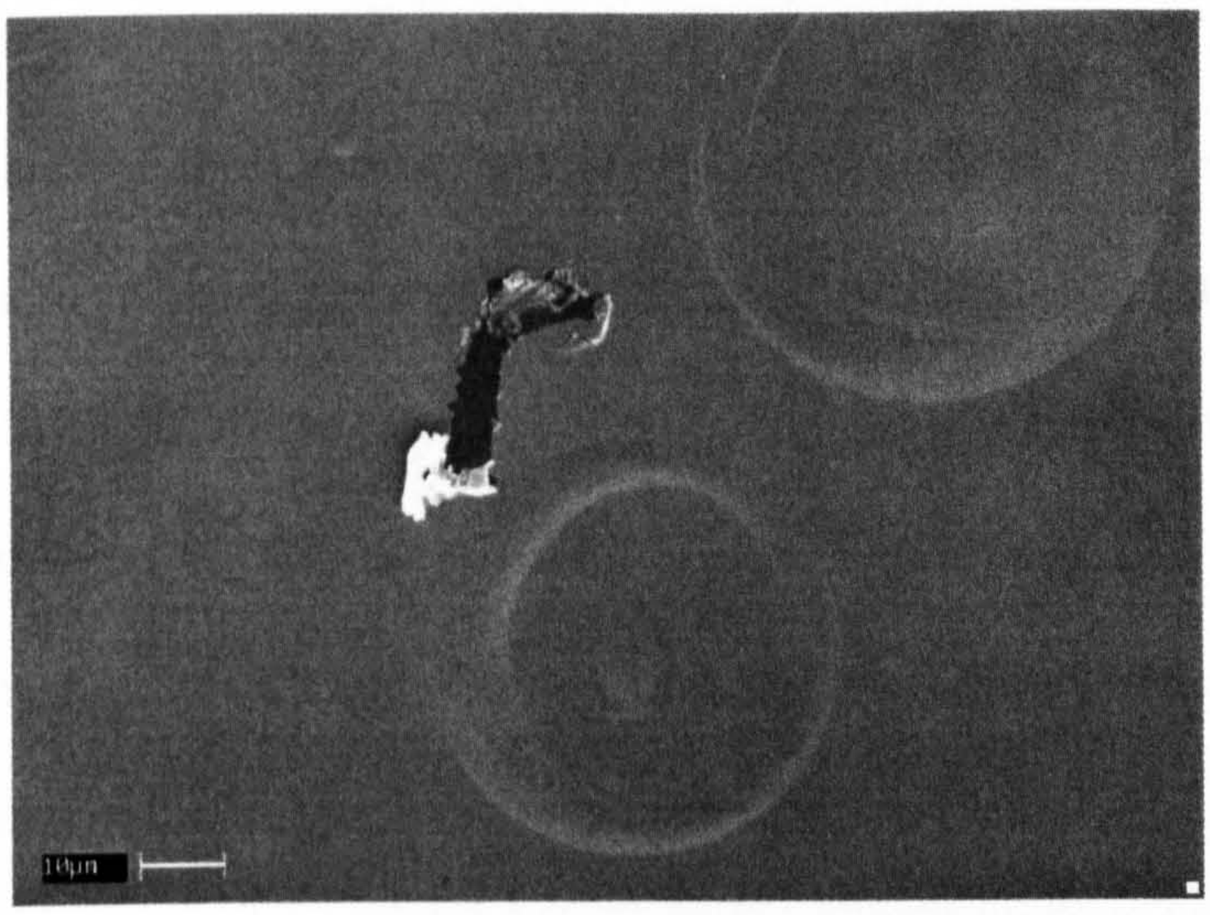

Fig.-8.7 Crater created with electrical stress on the Al contacts to a-C:H (a) shows the whole contact area (b) zooms in at the crater in (a).

To investigate the behaviour of Al, we stressed Al/a-C:H/Si^{+n} structures for different time intervals. We stopped the *C-t* measurements when the capacitance start to change from a constant value. Subsequently, a number of contacts were examined using SEM. Typical behaviour of contacts is shown in Fig.-8.7. It is clear from the micrograph in Fig.-8.7 that Al diffuses into the a-C:H films. The nature of diffusion can be understood on the basis of the diffusion coefficient of different metals to a-C:H. On the basis of our investigation, we can say that Al has much higher diffusibvity than Cr and Cu into the a-C:H Therefore, Al is not a right candidate (but it is commonly used in most laboratories), for forming metal contacts in a-C:H films. On the other hand, interfaces of Cu and Cr with a-C:H show high diffusion barriers and therefore these metals are much better candidates for metal contacts in a-C:H device fabrication. If we desire to exploit diamond-like materials (DLC, FDLC) as a low-k material in VLSI/ULSI, the correct selection of the metal for contact formation is vital. The commonly used metal for this purpose, Al, is most unsuitable, since we have proved that it diffuses into the a-C:H. Cr and Cu could be the interconnect material. But recently, the interconnect copper has turned out to be a viable candidate to address both issues. The feasibility of the copper metallisation was shown by confirmation of the achievable low resistivity and improved reliability compared to the standard Aluminium based metallisation. Therefore, copper as an interconnect material and diamond-like carbon as a low dielectric material promise new technologies of VLSI/ULSI to reduce delay time and electromigration.

Summary

The adhesion and material properties of thin films of rf-PECVD a-C:H film can be significantly affected by the substrate material on which the film is deposited and the substrate topography. For applications in large area electronics and interlayer isolation these issues will require serious consideration. Aluminium is not good as a contact material while copper and chromium show high diffusion barriers. This investigation suggests that copper metallisation along with a-C:H as an interlayer dielectric material, is a promising combination for future VLSI/ULSI circuitry.

Reference

1. T. Usami, H. Ishikawa, and H. Gomi, *Mater. Res. Soc. Symp. Proc.*, **476**, 69 (1997).
2. M.A. Plano, D. Kumar, and T.J Cleary, *Mater. Res. Soc. Symp. Proc.*, **476**, 213 (1997).
3. K.R Carter, *Mater. Res. Soc. Symp. Proc.*, **476**, 87 (1997)
4. J.P. Sulivan, T.A. Friedmann, C.A. Apblett, M.P. Siegal, N. Missert, M.L. Lovejoy, P.B. Mirkarimi, and K.F. McCarty, MRS Symp. Proc., **381**, 273, (1995).
5. Wu Shaoyu, E.T. Kang, K.G. Neoh, C.O Cui, B.M. Thiam, *IEEE trans. on Adv. Pack.*, **23**, 538 (2000).
6. P. Singer, *Semicond. Internat.*, **18(2)**, 88 (1996)
7. A. Grill, V. Patel, C. Jahnes, *J of the Electrochem. Soceity*, **145**, 1649, (1998).
8. K. Endo, *European Patent Application*, EP 0 701 283 A2, (1995).

9. S. Paul and F.J Clough, *MRS Symp. Proc.*, **558**, 149 , (1999).

10. J.A Theil, *J. Vac. Sci. Technol.*, **B 17(6)**, 2397 (1997).

11. S.Paul and F.J Clough, *App. Phys. Letts.*, (accepted for publication).

12. S.P Muraka, S.W Hymes, *Crit. Rev. Solid State Mater. Sci.*, **20**, 87 (1995).

13. J.T. Clemens, *Bell Labs technical journal*, **2**, 76, 1997.

14. S.P. Murarka, *Microelectronic Engineering*, **37**, 29, (1997)

15. S.R.P Ravi, *Ph.D Thesis*, Dept. of Engg., Cambridge University, Cambridge, UK

16. E. Liu, X. Shi, L.K. Cheah, Y.H. Hu, H.S. Tan, J.R Shi and B.K Tay, *Solid-State Electronics:An International Journal*, **43** , 427 (1999).

17. M. Nakayama, J. Yanagisawa, F. Wakaya, K. Gamo, *Jap. J. of App. Phys, Part I*, **38**, 7151 (1999).

18. Gillot_B, Weber_G, Souha_H, Zenkouar_M : *Journal of alloys and compounds*, 270, 275 (1998).

19. R.G. Lacerda and F.C. Marques, *Appl. Phys. Lett.*, **73**, 617 (1998).

CHAPTER 9

Use of Amorphous Carbon as a Gate Insulator for GaAs and Related Compounds.

The development of a metal-insulator field effect transistor (MESFET) technology using the III-V compounds semiconductors requires a gate insulator which is highly resistive, mechanically strong and electronically stable. Oxides grown on III-V semiconductors have not yet demonstrated these attributes. For example, arsenic and phosphorus oxides are thermodynamically unstable in the presence of GaAs and InAs [1]. The failure of the grown oxides to provide a suitable gate insulator dictates the use of the deposited insulators. The other problem in regard to the deposition of gate insulator on III-As based compounds is that the high temperature deposition ($\geq 350^{\circ}C$) destroys the stoichiometery in the III-As compounds. For example, heating of GaAs above $350^{\circ}C$ results in As segregation near the surface which leads to a large number of defect formation in GaAs [2,3,4]. The creation of defects reduces the mobility (both holes and electrons) in GaAs; thus use of GaAs as a high electron mobility material is throttled. To use an insulator material in the GaAs MISFET structure, the insulator material can be deposited at low temperatures. This suggests the use of amorphous carbon as a gate insulator in the GaAs MISFET, since it can be deposited at room temperature.

9. 1 Choice of Insulator

To use any material as an insulator for deposition on a III-As compound semiconductor, consideration of the following bulk properties is important:

- Mechanical, chemical, and physical stability
- Electrical Resistivity
- Dielectric constant
- Breakdown strength
- Bulk traps

These requirements are now considered in greater details. The deposited insulator needs to adhere well to the semiconductor substrate, be relatively scratch resistant and be compatible with further integrated circuit processing. The insulator should also be in-sensitive to environmental effects, (such as moisture) and be capable of withstanding appropriate thermal and electrical stressing. Low DC leakage is an extremely important requirement for an insulator and is one consideration, which has often been overlooked. If the leakage current is large, electron or hole accumulation may be impossible since these carriers will be drained from semiconductor surface into the insulator. This requires that the insulator resistivity be very high ($\geq 10^{14}$ Ωcm). The switching speed of MISFET is determined by various factors, though dielectric constant of the insulator is the most important among them. Lower the dielectric constant, higher is the switching speed. High breakdown strength of the insulator material allow MISFET to operate at higher voltages. The final bulk property of importance is bulk traps. Traps provide a mechanism for electrical conduction and can thus influence the

leakage current, which is not desirable from the point of view of device reliability and performance.

9.2 A Review of Insulators Used in GaAs MISFET Devices

AlGaAs/GaAs heterostructure FET's with high mobility two-dimensional electron gas have attracted increasing attention because they are promising devices for high speed and low power integrated circuit applications [5]. A number of gate insulators have been suggested to improve the performance of MISFET devices [6,7,8]. However, many attempts to realise GaAs MISFET's have shown that conventional dielectric materials, such as SiO_2 and Si_3N_4, are not suitable [8]. This is due to the high interface state density caused by the native oxide, contamination and various kinds of intrinsic defects, found in dielectric/GaAs interfaces. To minimise such effects, new materials are attempted to be used as gate insulators. Such materials are, crystalline CaF_2 at 600°C [8], Germanium nitride (Ge_3N_4) [7], and Al_2O_3 deposited by wet oxidation. The deposition of these materials are either carried out at higher temperatures (>350°C) or the technique which is used for their deposition is not very economical. Here, we suggest diamond-like carbon as a gate insulator in GaAs based MISFET. The key advantages of DLC as a gate insulator are that it can be deposited at room temperature and it has high electric breakdown strength. In the next section, I will discuss advantages of using DLC as a gate insulator in GaAs based MISFET devices.

9.3 Merits of DLC as a Gate Insulator in GaAs

The key advantage of DLC is that it permits deposition on GaAs at room temperature by the

plasma-enhanced chemical vapour deposition technique [9,10]. Deposition of DLC on GaAs substrate at room temperature will help to avoid any stoichiometeric changes. This reduces the defect density in GaAs caused by the high temperature deposition of gate insulators.

DLC also has high mechanical strength [11,12]. High mechanical strength makes DLC a scratch free material and hence the incorporation of any mechanical damage during device fabrication can be reduced by the very use of DLC as a gate insulator. The inert nature of DLC stops the formation of an interfacial layer between metal contact and DLC, which could potentially deteriorate the performance of the final device.

A high resistivity material for gate insulators is an imperative requirement. The resistivity against DC self bias plot shown in Chapter 4 depicts that highly resistive DLC can be deposited at relatively lower DC self-bias voltage, i.e. by relatively low energy incoming ions. The low energy ions are benign in that they do not cause any interfacial damage that can be caused by the bombardment of the ions on the surface of the substrate during the deposition.

The switching speed of MISFET devices is determined by various factors. Dielectric constant is one of them. Higher the dielectric constant more will be the delay. The DLC films has been reported with a low dielectric constant thus justifying implementation as an interlayer dielectric material in the multilevel metalisation in VLSI/ULSI [13,14,15]. Use of DLC films as a gate insulator in GaAs MISFET technologies reduces the signal delay time.

Diamond-like carbon has a remarkably high dielectric breakdown strength (10^7 V/cm) [16]. This allows its use at high gate voltages. The higher the gate voltage, the GaAs MISFET will

have higher power.

9.4 Leakage Current Behaviour of a-C:H

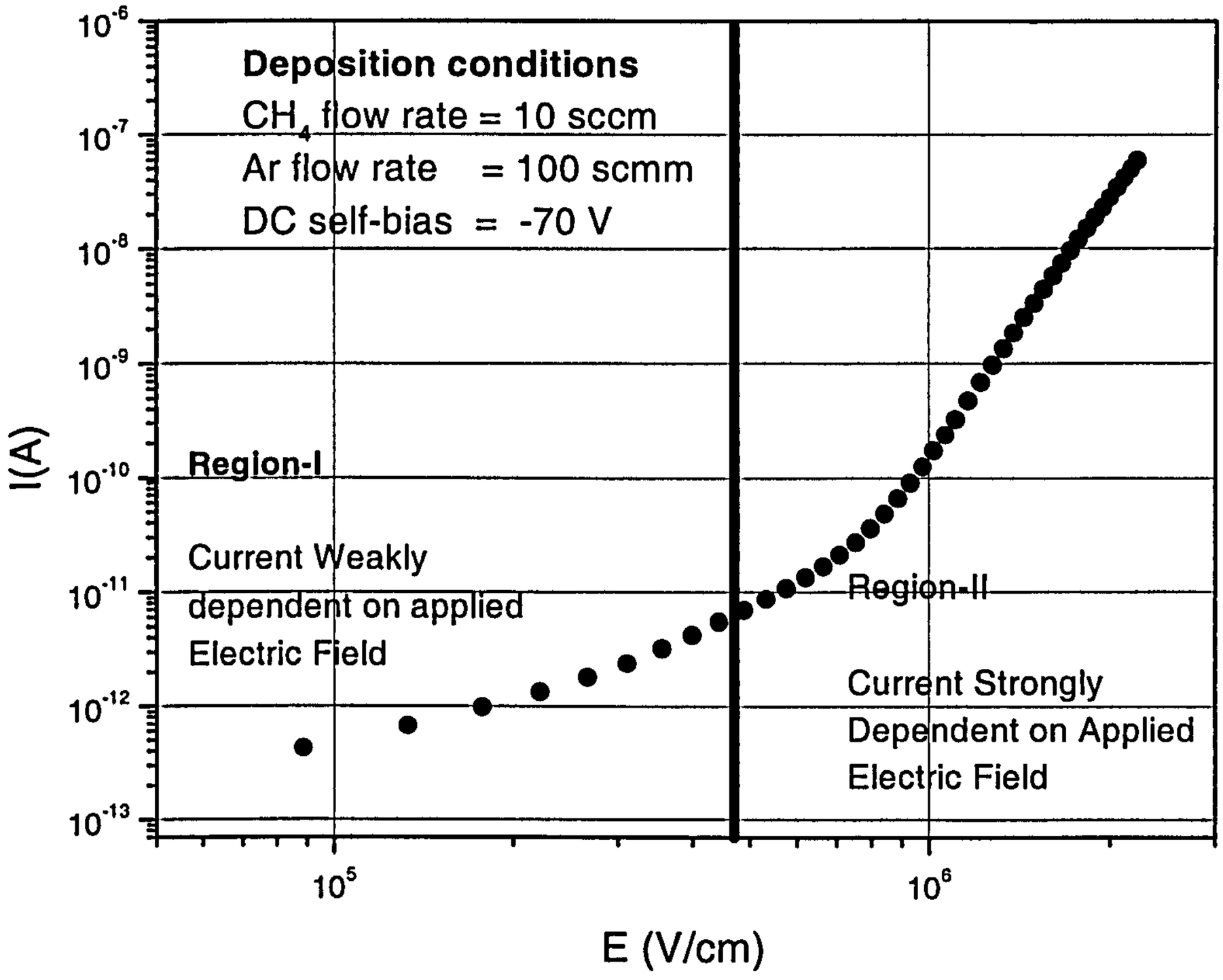

Fig.-9.1 Typical Current against Electric Field of Cr/a-C:H/Si^{+n} structures.

The conductance of insulator materials is assumed to be zero in the ideal case. But real insulators display conducting properties at high electric fields or high temperatures [16]. There are a number of conduction mechanisms which take place in the insulator material, for example, Frenkel-Poole conduction in Si_3N_3. This mechanism is a strong function of the

electric field. This material has been extensively used in the field of large area thin film transistor. But if the electric field is very high (>1MV/cm), then the leakage current will be high too (from nA to μA, depending upon the quality of the film). Therefore, it is very important to check the leakage current as a function of electric field in order to estimate the field above which an insulator cannot be used in the transistors. Fig.-9.1 shows a typical current against electric field plot of a Cr/a-C:H/Si^{+n} structure. It is clear from the picture that there are two regions, **I** and **II**. Region **II** is characterised by a very strong dependence (Frenkel-Poole conduction) on the electric field, while region **I** corresponds to a weak dependence on the field. The leakage current in region **I** is a few pA. This implies that if we would design a device in a way so that we confined the electrical characteristics of the film to Region **I**, then we could use a-C:H as an insulator material in the GaAs MISFET devices

9.5 Fabrication and Characterisation of Cu/a-C:H/GaAs structures

To investigate the electrical behaviour and the surface morphology of a-C:H and GaAs substrates, we deposited a-C:H from the gas mixture of Methane and Argon at –70 V DC self-bias voltage at room temperature on GaAs(100) n-type substrate. The bottom contact to the GaAs substrate metal was prepared by diffusing Indium at 170^{0}C in hydrogen ambience. The back contact metallisation was done prior to the deposition of a-C:H on GaAs. The top Cu metal dots of 1 mm diameter were made through the metal shadow mask in the high vacuum evaporator chamber. The electrical characteristics of MIS diodes were measured using a picoammter HP4142 B and an LCR bridge HP4284. The SEM investigated the

surface morphology of the layer deposited on GaAs.

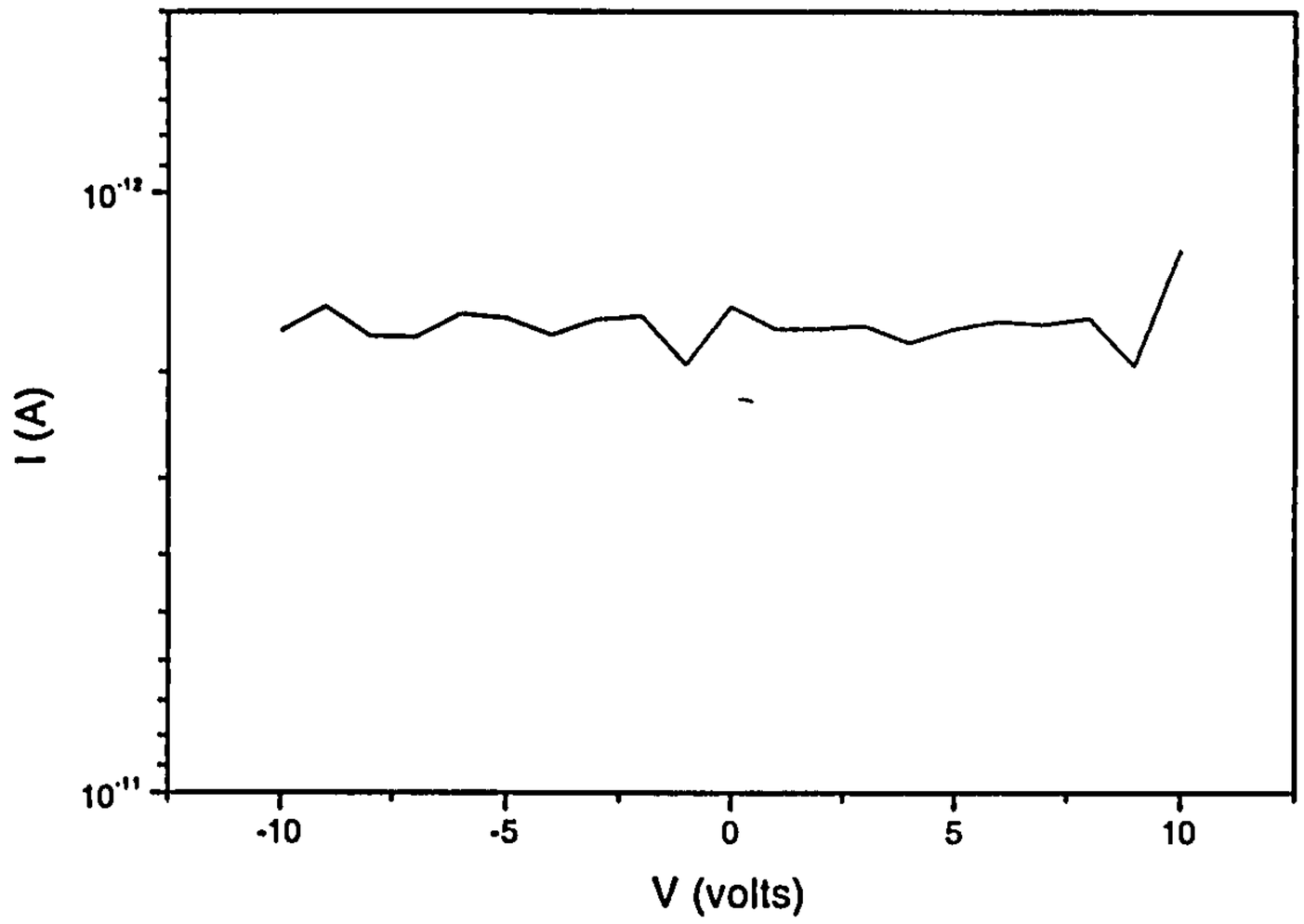

Fig.-9.2 *I V* characteristics of Cu/a-C:H/GaAs diodes brings out the good quality of the insulator layer.

Typical *I-V* characteristics between the bottom gate and the top metal contact of MIS diodes are shown in the Fig.-9.2. These measurements were carried out to check leakage current through the gate. The value of current is quite low (~1.5 pA) and hence the device quality is concluded to be very good. Therefore, we can say that the quality of the a-C:H layer (insulator) is quite good and that no defect or process-based damage has been introduced to the MIS diodes.

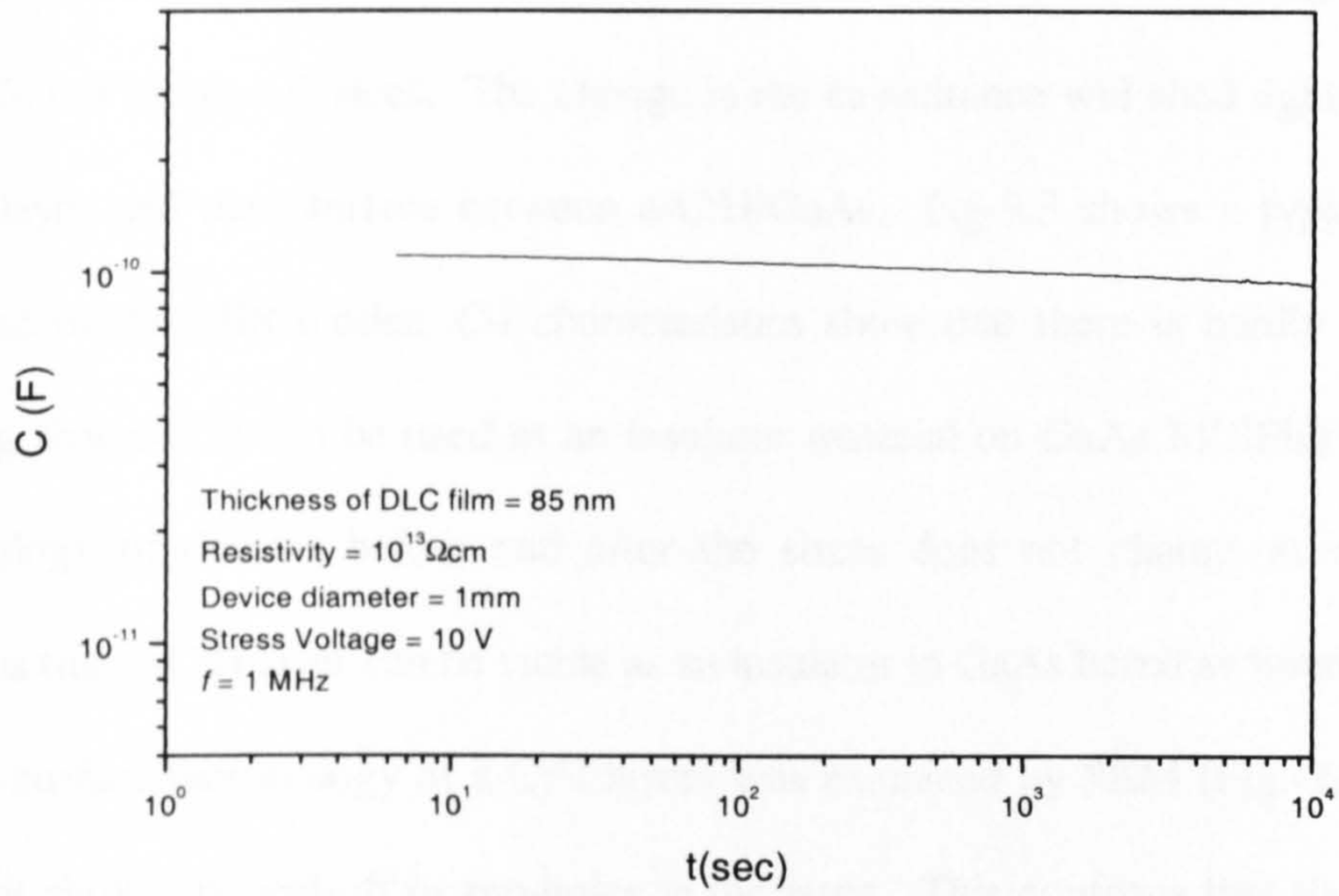

Fig.-9.3 *C-t* behaviour of Cu/a-C:H/GaAs diode at constant frequency and voltage.

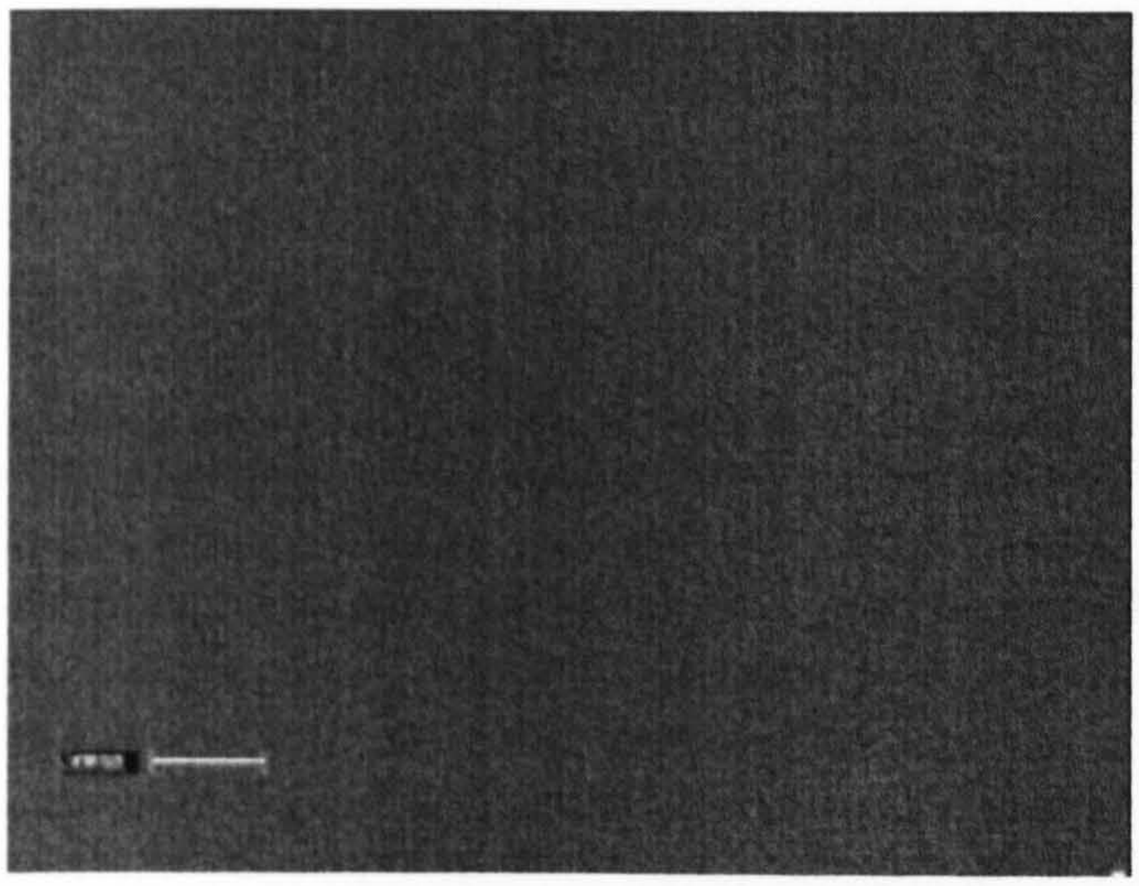

Fig.-9.4 SEM micrograph of a-C:H film on GaAs (100) n-type substrate. The deposited a-C:H film is uniform and free from pin-holes.

To check the interfacial damage due to the electric stress, we investigated Capacitance-time (*C-t*) of number devices. The change in the capacitance will shed light on the quality of a-C:H layer and the interface between a-C:H/GaAs. Fig-9.3 shows a typical *C-t* behaviour observed of the MIS diodes. *C-t* characteristics show that there is hardly any change, thus assuring that a-C:H can be used as an insulator material on GaAs MISFET devices. Surface morphology of devices before and after the stress does not change at all. This further confirms that a-C:H layer can be viable as an insulator in GaAs based switching technologies.

The surface morphology of a-C:H layers was examined by SEM (Fig.-9.4) and this study does not show any peel-off or pin-holes in the layer. This confirms that the adherence of a-C:H to the GaAs substrate is good.

Summary

a-C:H films show good adherence to GaAs substrates. The measured electrical characteristics qualify a-C:H as a good insulator for GaAs-based MISFET technologies. The main advantage of the a-C:H layer is that it allows deposition at room temperature. The room temperature deposition stops segregation of As near the surface. Therefore, the quality of GaAs layer will not be affected by the highly volatile As species in GaAs.

References

1. C.W. Wilsen, Ed., *Physics and Chemistry of III-V Compound Semiconductors Interfaces*, New York, Plenum, 1985.
2. K. Mahalingam, N. Otsuka, M.R. Melloch, J.M. Woodall and A.C. Warren, *J. of Vac. Sci. and Tech. B: Microelect. And nanomter strucutres*, **9**, 2328 (1991).
3. N. Chand, R.C. Miller, A.M.Segent, S.K. Sputz and D.V Lang, *Appl. Phys. Letts.*, **52**, 1721 (1981).
4. M.N. Chang, J.W Pan, J.I Chyi, K.C. Hsieh and T.E Nee, *Appl. Phys. Letts.*, **72**, 587 (1998).
5. T. Mizutani, M.Harinao, S. Fujita, and K. Maezawa, *IEDM Tech. Dig.*, 603 (1987).
6. T. Waho and F. Yanagawa, IEEE Elect. Dev. Lett., **9**, 548 (1988)
7. R.V.V.V.J Rao, T.C. Chong, W.S. Lau, L.S. Tan and N. Lim, *Elect. Lett.*, **33**, 1258 (1997)
8. G.A Johnson, V.J Kapoor, *J. Appl. Phys.*, **69**, 3616 (1991).
9. S. Egret, J. Robertson, W.I. Milne and F.J. Clough, *Diamond Related. Mater.*, **6**, 879, (1997).
10. S. Paul and F.J Clough, *MRS Symp. Proc.*, **558**, 149 , (1999).
11. K.V Ravi, *Proc. 2nd Int. Conf. on the application of Diamond Films and Related Materials*, MY, Tokyo, 13 (1993).
12. A.H. Lettington, *SPIE*, **1120**, 175 (1989).

13. J.P. Sulivan, T.A. Friedmann, C.A. Apblett, M.P. Siegal, N. Missert, M.L. Lovejoy, P.B. Mirkarimi, and K.F. McCarty, *MRS Symp. Proc.*, **381**, 273, (1995).

14. A. Grill, V. Patel, C. Jahnes, *J of the Electrochem. Soceity*, **145**, 1649, (1998).

15. K. Endo, *European Patent Application*, EP 0 701 283 A2, (1995).

16. S.M.Sze, *Physics of Semiconductor Devices*, Wiley Eastern Limited, 1991.

CHAPTER 10

Properties of a-C:H/Si Diodes

10.1 Introduction

The applications of hydrogenated amorphous carbon (a-C:H) films to electronic devices have been of considerable interest in recent years [1-4]. An interesting property of these films is their high breakdown strength (10^7 Vcm^{-1}). Properties such as a low dielectric constant (which implies higher switching speed), high breakdown strength and deposition at room temperature, make this material useful for cheap, glass compatible technologies and for power electronics. One very widely used class of device that could benefit from these properties is the p-n diode. The electrical characteristics of p-n junctions are fundamental to the electronics industry. Rectification, isolation, amplification and switching are key operations that involve the use of p-n junctions in electronic circuits. Therefore, fabrication of p-n junction diodes is an appropriate starting point in the development of a semiconductor technology based on amorphous carbon. In order to implement a-C:H films (deposited by rf-PECVD) in heterostructure junctions, it is vital to understand the electrical behaviour of a p-n heterojunction as a function of the growth parameters. The plasma deposition of a-C:H proceeds by ion bombardment which is activated by the negative DC self-bias (V_{DC}) of the driven electrode on which the substrate is placed (as explained in Chapter 5). The film properties are therefore strongly influenced by the magnitude of the DC self-bias, which is in

turn dependant on the applied rf power and the operating pressure. The effects of DC self-bias on resistivity, activation energy, optical bandgap, hydrogen content, have been discussed in Chapter 4. But the effect of the DC self-bias on electronic devices such heterostructures, is not available in literature. Therefore, understanding the a-C:H/Si junction as a function DC self -bias will shed light on its electrical behaviour.

This chapter of the thesis investigates the rectification ratio of a-C:H/Si heterostructure as a function of DC self-bias. Also to be discussed in this chapter are the effects of the interface between the a-C:H and Si on the device characteristic. I will further discuss fabrication of high reverse breakdown diodes out of a-C:H.

10.2 Fabrication of a-C:H/Si Diodes

Thin films of a-C:H were deposited at room temperature from CH_4/Ar gas mixture using a capacitively coupled rf-PECVD (13.56 MHz) system at a pressure of 100 mTorr. The plasma power was varied to develop DC self-bias voltages ranging from -70 V to -295 V. A nominal a-C:H thickness of 90 nm was maintained for all samples to investigate the rectification as a function DC self -bias voltage. The heterojunction diodes were manufactured by depositing a-C:H on to n-type and p-type Si substrates, of resisivities 1-2 Ωcm and 200-220 Ωcm respectively. The upper contact was formed by evaporating Al through a shadow mask with a circular aperture of diameter 1 mm. The bottom contact was formed by blanket

evaporation of an Al layer on to the back of the Si substrate followed by annealing at 450°C for 30 minutes prior to the deposition of a-C:H. This was done to ensure the ohmic nature of the bottom contact.

Current-voltage (I-V) characteristics for the a-C:H/Si structures were measured using a pc-driven picoammeter (HP4140B) and a high voltage source (HP4284A). During the measurements of the I-V characteristics, the DC voltage was applied to the upper contact while the back contact was earthed.

10.3 I-V behaviour of a-C:H/Si diodes manufactured at different DC bias.

The I-V behaviour of a-C:H/Si heterostructures manufactured on to 1-2 ohm-cm n-type substrates, at different bias, is shown in Fig.-10.1. The rectification ratios (R.R) measured at 10 V for these devices are as shown in Fig.-10.2. An increase in the DC self bias voltage shows an increase in the R.R till V_{DC} = -200 V. After that the DC self bias R.R starts decreasing. The highest rectification ratio of 10^5 is achieved at V_{DC} = -200 V in this investigation. To understand the effect of V_{DC} on device behaviour we plotted the rectification ratio of the films as functions of V_{DC} in Fig.-10.2. The resistivity of the films falls from $2x10^{12}$ to 10^6 Ωcm as the DC self-bias is varied from –70 V to -220 V (see section 4.3.2).

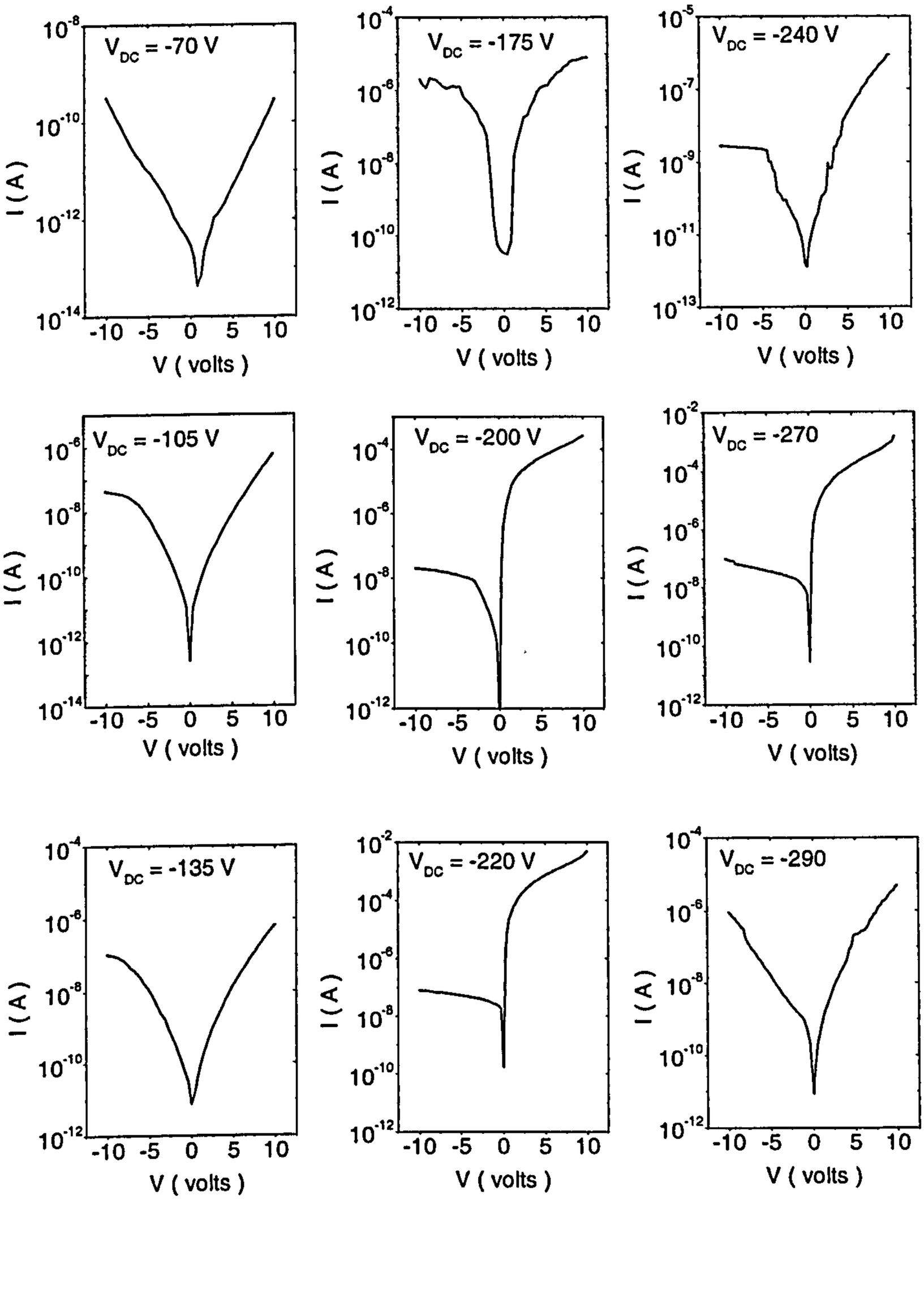

Fig.- 10.1 Variation in I-V behaviour of a-C:H/Si heterostructures diodes as a function of DC self-bias.

The decrease in the resistivity can be explained on the basis of structural changes arising from the change in the DC self-bias [6]. This was confirmed by Raman-spectroscopy and optical band gap analysis (as we have discussed in Chapter 4). The explanation of the symmetrical I-V behaviour at lower bias is given by the fact that the corresponding resistivity of the films is very high (10^{13} Ωcm) and the devices behave like MIS structures. As the resistivity starts falling and the semiconducting regime is approached (resistivity < 10^7 Ωcm) the increase in the rectification behaviour is obvious. This novel investigation shows how a single parameter, namely the DC self-bias, changes the device properties strongly (from the MIS to the heterostructure configuration).

Interestingly, it is also observed that rectification ratio again starts falling after V_{DC} = -220 V. It becomes nearly unity at V_{DC} = -290 V. This behaviour can be explained on the basis of the change of the interface between a-C:H and Si substrate. Raman analysis shows (Fig-4.15, Chapter4) that there is an increase in the I_D/I_G (with DC self bias). This suggests that graphitic-like clusters in the a-C:H films become more active in the determination of the properties. We believe that once the critical bias is crossed i.e –220 V, the surface of a-C:H is dominated by sp^2 clusters and hence there is a large number of dangling states at the surface. These surface states pin the Fermi-level and then start destroying the built-in potential [7]. At V_{DC} = -290 V the barrier is nearly destroyed and hence there is any hardly rectification.

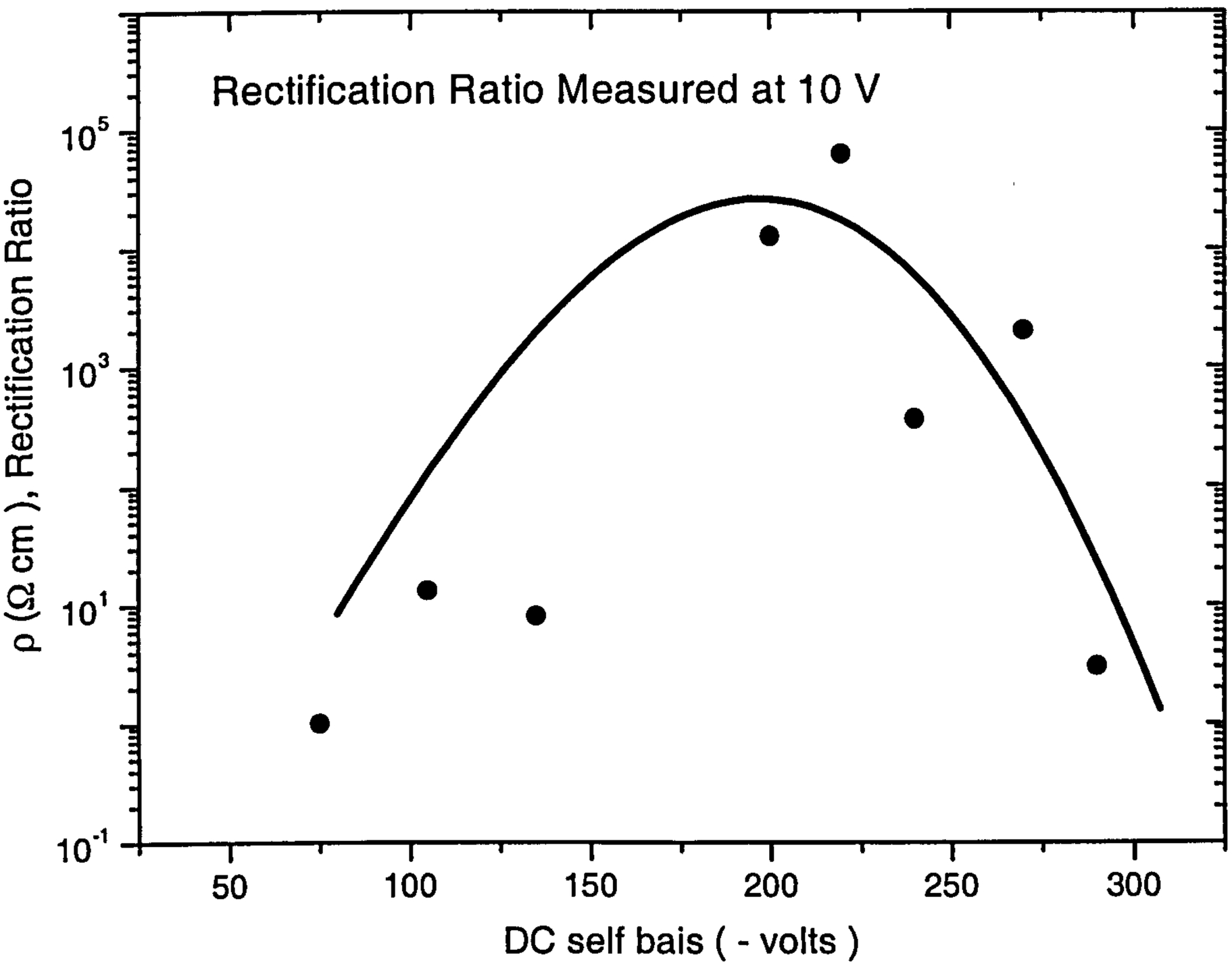

Fig.-10.2 Variation the rectification ratio with DC self bias.

With the help of this investigation, information of the diode behaviour with DC self-bias voltage is established. This investigation, will help us to exploit the high breakdown strength of a-C:H to fabricate diodes which can be withstand at very high voltage,

10.4 Fabrication and characterisation of high reverse breakdown diodes

On the basis of above investigation, we selected the growth conditions (V_{DC} = -220 V) which corresponded to the highest rectification ratio. This was done to realise the high reverse breakdown diode. To realise the high reverse breakdown voltage, a-C:H/Si diodes were prepared with two different thicknesses, 90 nm and 200 nm.

Scanning Electron Microscopy (SEM) was used to determine the surface quality of the deposited films. The heterojunction diodes were also exposed to prolonged electrical stress (upto 2 hours) to investigate charge trapping either at the Al/a-C:H interface or in the bulk. Significant charge trapping is expected to result in poor reproducibility in the I-V characteristics [7].

The I-V behaviour of an a-C:H/Si heterostructure is shown in Fig-10.3. The asymmetrical (at positive and negative applied bias) I-V curves are clearly indicative of diode behaviour. These devices were manufactured to obtain high reverse breakdown voltages by depositing a-C:H on to 200-220 Ωcm p-type Si substrates. Fig.-10.3 shows the typical I-V behaviour of diodes produced by depositing a 90 nm thick film of a-C:H. The reverse breakdown voltage and rectification ratio of these diodes were 400 V and 10^4 (measured at 50 V) respectively. The reproducibility of these characteristics was studied by keeping these devices continually under increasing electrical stress (from - 200 V to 350 V for 2 hours). From Fig.-10.3 we can see that there is no change in the electrical behaviour of these devices arising from the application of this continuous electrical stress. Diodes of higher reverse breakdown strengths

were achieved by fabricating heterostructures with a 200 nm a-C:H layer. Typical I-V behaviour of such diodes is as shown in Fig. 10.4 . The reverse breakdown voltage of such diodes was typically 850 V. The electrical characteristics of such diodes were again unaltered following the application of prolonged electrical stress (Fig.-10.4).

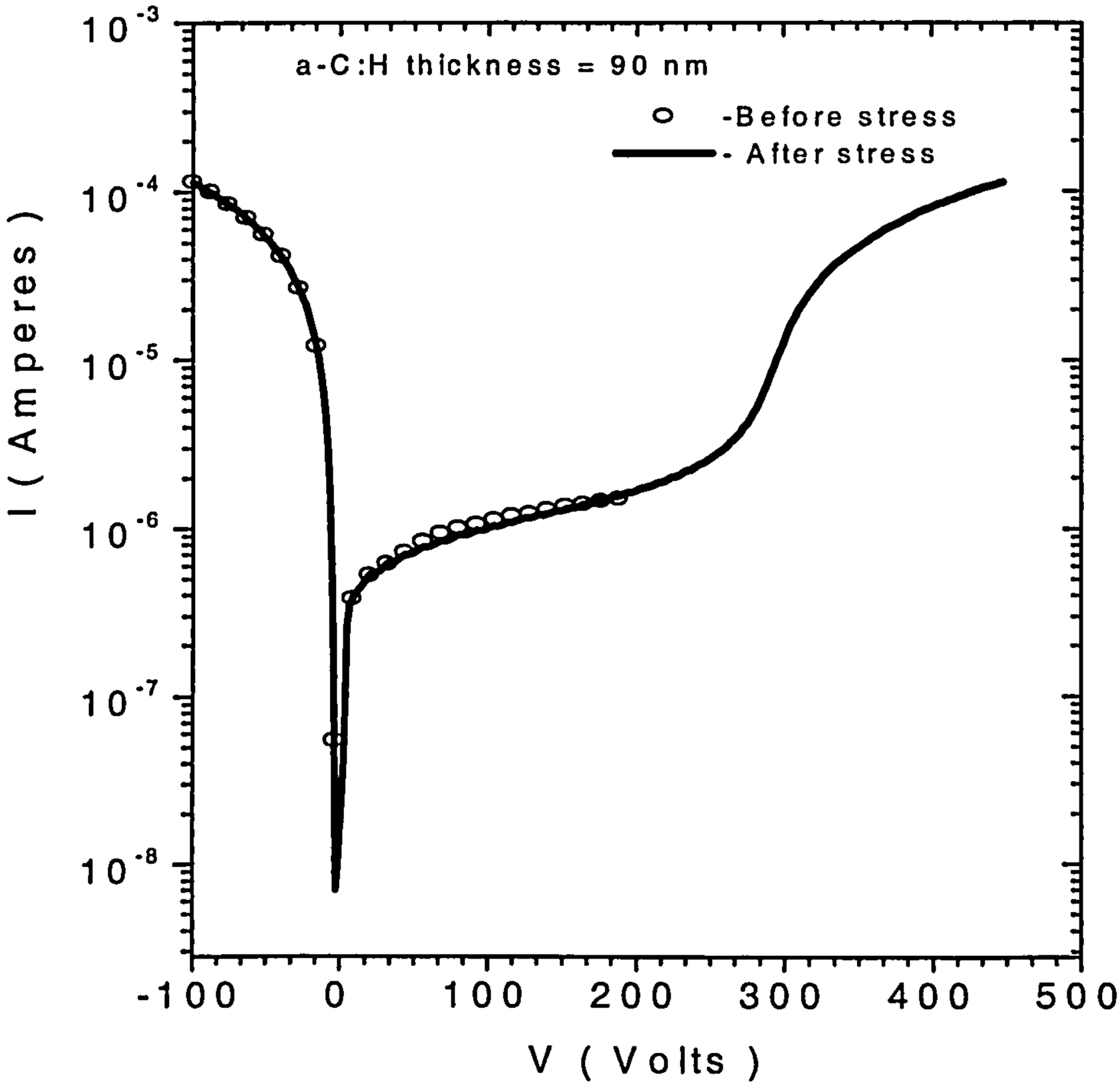

Fig.-10.3 The circles show the I-V behaviour measured before the application of electrical stress, while the line shows after the application (for a-C:H thickness = 90 nm)

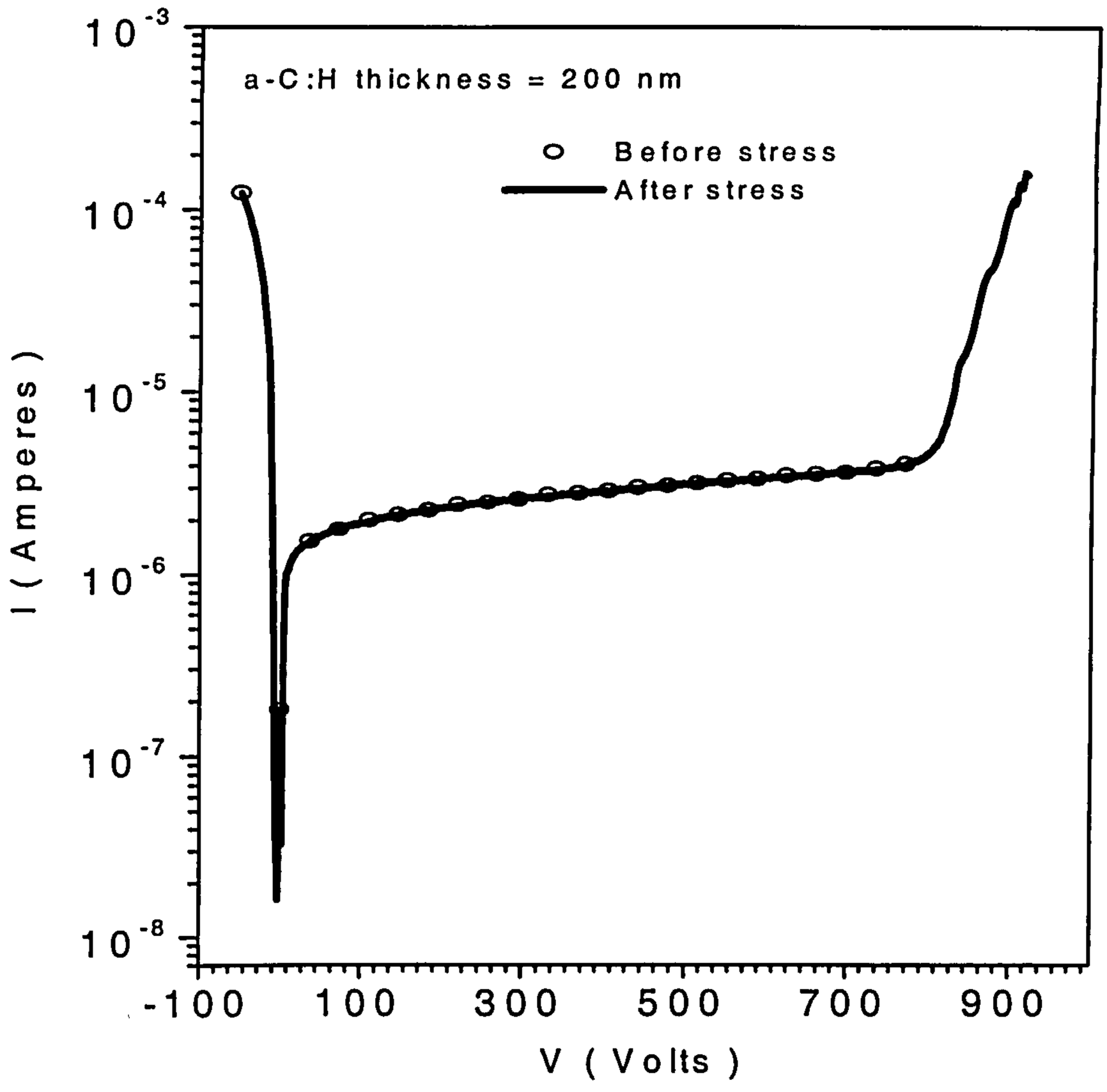

Fig.-10.4 The circles show the I-V behaviour measured before the application of electrical stress, while the line shows after the application (Film thickness = 200 nm).

An earlier attempt to investigate the high-voltage performance of a-C:H/Si diodes by Amaratunga *et al* [8] resulted in poor reproducibility after the application of high voltage. In this report it was suggested that this was due to an excessive increase in the barrier height as

a result of fixed negative charges at the Al/a-C:H interface and in the bulk of a-C:H. Trapped charges would be indicated by hystersis in the I-V or C-V characteristics of the devices that we studied. If the explanation given in [8] is true then we can say that the trapped charge densities in our devices, both at the interface and in the bulk, are negligibly small and have no significant influence on device behaviour. Production of a-C:H/Si diodes (for high voltage operation) using the technique of photochemical vapour deposition has also been reported [9]. This technique does not expose the growing film to ion bombardment and, it is suggested, results in reduced trapped charge densities. The authors of [9] have successfully demonstrated that high voltage diodes prepared by this technique can withstand reverse bias voltages upto 400 V.

Through optimisation of the growth conditions using detailed investigation of the film properties a more robust diode has been realised by rf-PECVD. In their report [8], a number of large crystallites of diamond, of size between 100 nm and 200 nm, were observed in the amorphous carbon matrix. The crystallites in the material will lead to preferred conduction paths through the amorphous carbon layer or less resistive paths around the diamond crystallites and, ultimately, premature breakdown. To check for large crystallites and pin-holes in our films we extensively investigated the a-C:H films used in these devices using SEM. Fig-10.4 shows the homogenous and smooth surface of the a-C:H films deposited in our laboratory. The films were uniform and free from pinholes. Therefore, to achieve high breakdown voltage a-C:H/Si diodes the important factors appear to be uniformity of the a-

C:H films and low trap states. These can be achieved by detailed optimisation of the PECVD growth conditions.

SUMMARY

In summary, effect of DC self bias on the rectification ratio of a-C:H/Si heterostructure diodes has been observed. A high reverse breakdown voltage a-C:H/Si diode has been successfully fabricated by rf-PECVD for the first time. The trap states (both at the interface and in the bulk) can be reduced by selecting the growth conditions carefully. Optimum films were free from pinholes.

References:

1. J.Robertson, Adv. Phys. 35 (1986) 317.
2. F.J. Clough, B.Kleinsorge, W.I.Milne, J.Robertson, G.A.J. Amaratunga, B.N.Roy, Electron. Lett. 32 (1996) 498-499,
3. S.Egret, J.Robertson, W.I.Milne, F.J.Clough, Diamond Relat. Mater., 6 (1997) 879-883.
4. S Paul and F.J Clough, Diamond Relat. Mater., 7 (1998) 1734-1738.
5. K.Kohler, J.W.Coburn, D.E Horne, E.Kay and J.H Keller, J. Appl. Phys. 57, 59 (1985).
6. E. Ohta, Y.Kimura, H.Kondo, M.Takahashi, K.Kameyama, K.Yamada and I.Fujimura, 22nd Int. Conf. Sol. Stat. Devices and Materials (SSDM), 589 (1990).

7. Y. Koide, M. Yokoba, A. Otsuki, F. Ako, T. Oku, M. Murakami, *Diamond Films Technol.*, **6**, 61 (1996)

8. G. Amaratunga, W. Milne, A. Putnis, IEEE EDL 11 (1990) 33.

9. S.B. Hwang, Y.K Fang, K.H Chen. C.R Liu, and L.C Kuo, Electronics Letters, 27 (1991) 2043

CHAPTER 11

Conclusions of my Research Work and Future Work

Enough of Science and of Art;
Close up those barren leaves;
Come forth, and bring you a heart
That watches and receives.

--William Wordsworth
from The Tables Turned

This chapter concludes the work of my thesis and suggests future research that can be based on the investigations mentioned in the earlier chapters.

11.0 Conclusions

My postgraduate research involved the growth and characterisation of hydrogenated amorphous carbon films and fabrication of devices using the same. Since such an investigation lacked precedence in the Emerging Technologies Research Centre, we needed to optimise properties of a-C:H films over large substrate areas, before embarking on analysing these films. We advocate a novel and simple idea, involving the refractive index and the resistivity of the grown films, to achieve this requirement. The pre-requisite of high dielectric strengths of the grown a-C:H films, was confirmed by *I-V* characteristics of MSM devices realised out of the grown films. The smoothness of the grown films was confirmed by SEM studies.

DC self-bias was concluded to be a key parameter that influences various properties of the films. This is in line with work already published. We found that in our system, DC bias can be varied from -70 V to -290 V at 100 mtorr pressure and flow rates of 100 sccm and 10 sccm for argon and methane respectively. With these growth parameters, the resistivity of the films was found to vary between 10^{13} to 10^{6} Ωcm, bandgap between 1.7 to 0.8 eV and R.I was observed to vary from 2 to 2.7.

It was intuitively felt that such wide-ranging changes in film properties were accompanied, (rather caused by) compositional variation in the films with the bias. Since the material under consideration was marked by multiple types of hybridisation, such variation would imply a change in the ratio of the sp^2 to the sp^3 content in the films, as the bias voltage was changed. We could be confident of such a conjecture only when a full-proof analysis of the films were made. Raman spectroscopy was identified as an apposite tool for this purpose; Raman spectroscopic based studies corroborated the expected systematic structural variation in the film properties with DC self-bias.

One of the most important by-products of my doctoral thesis is certainly the mathematical formulation that we developed to estimate the density of states in a-C:H. The methodology is simple and easily calculable. When I started my research, the density of states in a-C:H films was poorly understood. Various methods have been proposed by other workers to deduce the density of states. Our investigations show that capacitance measurements of MIS structure is

a more appropriate way to deduce the density of states. In this regard, we have developed a formulation, which is an agreement with the experimental data.

Our attempts to understand many of the behavioural patterns of a-C:H, in terms of the physical characteristics of the films, led us to develop a simple and elegant instrument in which a micro-tip was incorporated into an SEM set-up. This system was employed in the detection of inhomogeneities (to 50nm in length scale) in the grown films.

Diamond-like carbon is a low-k material and can be deposited at room temperature. Therefore, MSM switches can be fabricated at room temperature on plastic substrates. We have extensively investigated the properties of MSM device, by *I-V*, and *C-V-f* measurement. Our *I-V* investigation shows that the conduction mechanism in DLC film is of Poole-Frenkel type. The reliability of MSM devices is important. Electrical stress investigation confirms that Al is not a good metal to make contacts with a-C:H films, while Cu and Cr are quite stable as a metal contact to a-C:H. It was believed that the schottky contacts to diamond-like carbon were not possible due to a conducting superficial layer on the DLC. We investigated this problem thoroughly and found that Schottky contacts are possible to a-C:H when the contact area is less than 1 μm. To improve the predictability of the schottky contacts, we deposited DLC on metal strips and found that there are high chances of forming contacts near the edges of these strips while the film deposited at the centre of the strips exhibited symmetric electrical behaviour.

We decided to examine the of-suggested idea that DLC is appropriate as an interlayer dielectric material in VLSI/ULSI. This was motivated by the low dielectric constant of the material. However, the conclusion from our SEM study is that our a-C:H films exhibit a significant degree of inhomogeneity, rendering some parts of the film semiconductor-like while the others maintain their insulator status. Such films would be leaky and therefore unsuitable for dielectric purposes. We carried out a number of capacitance-time measurements on our films, deposited on different metals, to infer that the most commonly used metal substrate for a-C:H films, is also the most unsuitable. Cu and Cr were judged to the best candidates for this purpose.

We challenged the notion of depositing insulating materials, (like Si_3N_4, CaF_2, Al_2O_3, etc.) on GaAs substrates to produce MISFET structures, on the basis of the realisation that the As in the substrate often segregates on the surface at the high temperatures required for the deposition of these insulators on GaAs. As an alternative, we suggest a-C:H films, which can be deposited at room temperature, on GaAs.

We have manufactured a-C:H/Si heterostructure diodes and found their rectification ratio to be DC bias dependent. The exceptional dielectric breakdown strength of DLC was exploited for the first time, to produce a-C:H/Si heterostructure diodes, which was found to be able to withstand voltages upto –900V.

11.1 Future work

Diamond-like carbon is a very complex material. A number phases of carbon constitute this material. Small variations in these phases on nanometer scales can have drastic effects on some of the material properties. Therefore, a detailed investigation in the submicron scale is an important step in further understanding of this material. If we managed to control the occurrence of multiple phases in the nano scale then the inconsistency in results, between different working conditions, can be eliminated. As this material shows random variations in composition and therefore properties, the physics of complexity could be invoked to understand it; the currently used approach of taking statistical averages is not really adequate.

The technique which we developed in Chapter 6, to investigate the in-homogeneity in the material, can be further improved using X, Y, Z controllers, which can be attached to the tip. This can help to achieve maximum resolution of the SEM without the painstaking efforts that are presently required.

We have also proposed that a-C:H can be used as a dielectric material in GaAs MISFET technology. We have shown the films to have good adherence to the GaAs substrate and the electrical characteristics imply that films are not leaky. Further work is required to make workable devices with a-C:H as the insulator in the GaAs MISFETs.

We have proposed a theory to determine the density of states and the results should be checked with other techniques to consolidate our formulation.

We have investigated contacts of various metals with a-C:H. The interaction of other metals, such as, Ti, W, Ta, Au remain unchecked yet. This is important in the implementation of DLC-based materials as an interlayer dielectric.

Appendix -I

```
REM PROGRAMME TO DEDUCE THE DENSITY OF STATES FROM C-f DATA

REM f$ is the input data file (frequency, capacitance)
REM O$ is the output data file (Trap Energy, DOS)

INPUT "ENTER INPUT DATA FILE NAME ", f$
PRINT " "
INPUT "ENTER OUPUT DATA FILE NMAE ", O$
PRINT " "
INPUT "AREA OF DEVICE (cmXcm) = ", A
PRINT ""
INPUT " RELATIVE DIELECTRIC CONSTANT = ", k
PRINT " "
INPUT "THICKNESS OF FILM(in cm) = ", L
PRINT " "
INPUT " Capacitance at 1 MHz =  ", c
INPUT " Capacitance at 20 Hz =  ", cc
INPUT "TEMPERATURE (K) = ", T

REM THERMAL ENERGY  M(eV)

       M= 8.34e-5*T

INPUT "Highest frequency (HZ) = ", f1

INPUT "Capacitance of SiO2 (F)", Ci

cq = (Ci * cc) / (ABS(Ci - cc))

cm = (Ci * c) / (ABS(Ci - c))

PRINT cq, cm

q = 1.6 * 10 ^ -19

REM e = dielectric constant
```

```
REM f0 = phonon frequency in a given material

e1 = 8.85E-14

e = e1 * k

REM HERE f0 is the phonon frequency

f0 = 10 ^ 12

r = e1 * q

OPEN f$ FOR INPUT AS #1
OPEN O$ FOR OUTPUT AS #2

C2 = cm / A


c0 = cq / A


REM f = frequency of the ac signal
REM ET = trap energy (eV)

DO UNTIL EOF(1)
INPUT #1, f, c1
c1 = c1 / A
ET = M* LOG(f / f0)

N = (c0 / r) * ABS(c1 - C2)

PRINT #2, ET, N

C2 = c1

LOOP
END
```